THE INFLUENCE OF CHEMICAL COMPOSITION AND NUCLEATION ON ALIPHATIC-AROMATIC COPOLYESTERS' CRYSTALLIZATION

Małgorzata Wojtczak-Michalska
PhD Thesis

Supervisor: prof. dr hab. Andrzej Gałęski

Polymer Physics Department
Centre of Molecular and Macromolecular Studies,
Polish Academy of Sciences

Łódź, 2015

Abstract

With the growing awareness of environmental problems induced by plastic waste, great interest has been given to biodegradable polymeric materials. Until now, aliphatic polyesters have been found to be the most attractive biodegradable polymers. Those polymers are susceptible to microbial attack due to the specific ester structures in the main chain. Although the aliphatic polyesters are available on the market, their thermal and mechanical properties do not favor their usage in many applications. Thus the improvement of thermal and mechanical properties has become an important task.

Aromatic polyesters such as poly(ethylene terephthalate) or poly(butylene terephthalate) possess better thermal and mechanical properties in comparison to aliphatic polyesters. Therefore the incorporation of aromatic units along aliphatic polyester chains appeared to be a good concept to merge biodegradability characteristic for aliphatic polyesters and good thermal and mechanical properties typical for aromatic polyesters. However, aliphatic-aromatic copolyesters (AAC) are biodegradable under condition of sufficiently short sequences of aromatic units which was shown by Witt et al [1]. Moreover, Witt et al. [2] drew a conclusion that AAC remain biodegradable provided the population of aromatic ester comonomers does not exceed 60 mol%. Up to now, there have been reports about copolyesters possessing from one up to three aliphatic units and one aromatic. However, none of them focused on the influence of chemical composition on nucleation of crystallization and on crystallization of AAC, especially that too short sequences of crystallizable units can significantly decrease crystallizability.

One of the aims of our studies, was to specify the chemical composition of AAC, that would optimally combine ability to biodegradation and good physical performance. The technology of polymerization of nearly random aliphatic-aromatic copolyesters based on polycondensation was developed some time ago at the Institute of Biopolymers and Man-Made Fibers, Łódź, Poland [3]. The technology differs from other technologies by the use of three aliphatic esters instead of the usual one. Therefore, Dr. Sławomir Dutkiewicz of that institute, was kindly asked to synthesize a range of aliphatic-aromatic copolyesters containing: butylene adipate, butylene succinate, butylene glutarate and butylene terephthalate esters (PBASGT), differing in composition. Obtained PBASGTs were characterized by ^{1}H NMR spectroscopy. Using the assignment of proton resonance due to homogeneous and heterogeneous dyads [4, 5, 6], the average block length and the degree of randomness were investigated over the range of copolymer composition.

New aliphatic-aromatic copolyesters differing in composition have been characterized by differential scanning calorimetry (DSC), wide- and small-angle X-ray scattering (WAXS, SAXS) and their molecular characteristic was studies using size exclusion chromatography (SEC), crystallization aptitude and morphology were examined by other various techniques including atomic force microscopy (AFM), polarized light microscopy with hot stage (PLM), light depolarization technique (PLD).

Using the assignment of ^{1}H NMR resonances due to homogeneous and heterogeneous dyads, the fraction of dyads f, molar content of aliphfatic and aromatic units P, mean length of aliphatic and aromatic sequences $\bar{L}_n$ and the randomess index R were investigated for all copolyesters. All of the synthesized copolyesters having the content of aromatic component from 10% to 90% were nearly random copolymers. Surprisingly, it appeared that almost all PBASGTs are able to crystallize. It turned out also that in all the crystallizable copolyesters only butylene terephthalate (**BT**) blocks are able to crystallize in the crystallographic form characteristic of homo poly(butylene terephthalate). The increase of aromatic units' contents did not change the crystallographic structure, in contrary to the results obtained by Li et. al [7] for similar systems, however, with only one aliphatic ester, succinate. It is worth to underline that there are slight differences in several X-ray diffraction peak positions (not all) of synthesized copolyesters and aromatic homopolymer discussed in more details in the thesis.

On the DSC heating traces for copolyesters with aromatic content less than 60% a broad peak of melting is observed, which becomes narrower and shifter to higher temperatures with the increase of aromatic units. The same phenomena is observed for the crystallization peak. The changes of glass transition temperature together with the increase of aromatic units content was also observed.

Mechanical properties of aliphatic-aromatic copolyesters in a range of compositions from 10 to 90% of aromatic component were studied by tensile deformation. Copolyesters with aromatic unit content below 60% deformed in an uniform manner characteristic for rubbers. With increasing aromatic units content the yield stress point becomes well-defined and the deformation manner changes. For copolyester with 80% of aromatic content a rubber deformation manner becomes stress-oscillating (or self-oscillating) due to jumping from uniform stable necking to neck propagation form of deformation and reverse. With further increase of aromatic content to 90% the deformation proceeds in a manner characteristic for semicrystalline thermoplastics with highly localized yielding, and formation of a well-defined neck or by simple brittle breaking, which is characteristic for aromatic homopolymer.

From the synthesized copolyesters the most promising composition with respect to biodegradability, thermal and mechanical properties was selected for further investigation of crystallization. The spectroscopy and X-ray methods were complemented by small angle light scattering (SALS). It revealed that PBASGT crystals form spherulitic aggregates filling the entire volume of the material with spherulites of average radius above 7 μm, which are formed from few nanometers thick fibrous crystals while the crystallinity reached 20%. Fibrous crystals thickness appeared as the main factor influencing the depression of PBASGT melting temperature.

The studies showed that the crystallization behavior of PBASGTs is strongly driven by the presence of self-nucleation. Self-nuclei can survive the temperature up to 160°C. Self-nucleation studies evidenced the existence of three self-nucleating domains determined by the temperature at which PBASGT was melted.

The chemical structure, morphology and crystallization behavior of PBASGT were compared with commercial aliphatic-aromatic copolyester of butylene terephthalate and butylene adipate (PBAT), Ecoflex®.

It was expected that butylene adipate crystalline sequences in a random copolymer with butylene terephthalate would show much lower crystallization and melting temperatures than those of homopolymer. In order to check the possibility of crystallization of aliphatic component, samples of the copolymers were cooled down to 4°C and kept at this temperature for 24 h. On both heating thermograms melting endotherms were presented. Melting of crystals of aromatic components was observed at 110°C and 121°C for PBASGT and PBAT, respectively. In addition, a small endothermic peak at 39°C was seen on the thermogram of PBAT that is identified as melting of crystals of aliphatic sequences. No such peak can be detected for similarly treated PBASGT sample. Thus it appeared that, in contrast to aliphatic part of PBAT, aliphatic part of PBASGT is unable to crystallize, when annealed below room temperature.

Comparison of correlation function evolution of PBASGT and PBAT showed that the crystalline structure of aromatic component forms quickly in the case of PBAT, not in a step-wise manner as the structure of PBASGT. However, the final average thickness of crystals of PBASGT and PBAT is nearly identical (3.5 nm). The measured average crystal thickness closely corresponds to the length of 3 butylene terephthalate repeat units (3.48 nm) in the PBT crystal structure. Two, three or four aromatic units in a row are the most probable in a macromolecule of PBAGST.

Strong and distinct self-nucleation phenomena led us to a conclusion that crystallization of PBASGT can be accelerated by introduction of nucleating agents. It was found that the nucleating agents that are effective for PBT are also effective for PBASGT. Two types of phthalocyanine and talk were found to be effective. For example, a nucleation of PBASGT with green phthalocyanine shifted the nonisothermal crystallization peak from 70°C to 84°C during cooling at the rate of $10^{\circ}\mathrm{C}\cdot\mathrm{min}^{-1}$. However, the crystallization peak temperature shift for most effective nucleating agent was significantly smaller than that for a sample with active self-nuclei (90°C).

Streszczenie

Ze względu na powiększającą się ilość odpadów komunalnych składających się z tworzyw sztucznych wzrosło zainteresowanie materiałami biodegradowalnymi. Główną rolę pośród tworzyw biodegradowalnych odgrywają poliestry alifatyczne ze względu na wiązania estrowe podatne na atak mikroorganizmów. Wyróżnić wśród nich można polihydroksymaślan pochodzenia biologicznego oraz polilaktyd pochodzenia syntetycznego. Jednakże do wad wymienionych materiałów należą np.: słabe właściwości mechaniczne. Dlatego też podjęto wysiłki prowadzące do poprawienia tych właściwości poprzez wytworzenie kopoliestrów alifatyczno-aromatycznych.

Proces otrzymywania prawie bezładnych kopoliestrów alifatyczno-aromatycznych oparty o polikondesację został rozwinięty pewien czas temu w Instytucie Biopolimerów i Włókien Chemicznych (IBWCh) w Łodzi [3]. Proces technologiczny prowadzony w IBWCh różni się od innych znanych procesów tym, że używa się trzech estrów alifatycznych w zamian standardowo używanego jednego estru. Na potrzeby tej pracy została wytworzona seria kopoliestrów alifatyczno-aromatycznych (PBASGT) o zróżnicowanym składzie chemicznym zawierających od 10% do 90% składnika aromatycznego tereftalanu butylenu (synteza, dr S. Dutkiewicz, IBWCh). Kopolimery zawierały mieszaninę estrów alifatycznych: adypinianu butylenu, bursztynianu butylenu oraz glutaranu butylenu. W ramach rozprawy doktorskiej, otrzymane kopolimery PBASGT zostały scharakteryzowane za pomocą spektroskopii protonowego rezonansu magnetycznego (^{1}H NMR). Korzystając z wodorowych pasm rezonansowych odpowiadających homogenicznym i heterogenicznym diadom, wyznaczono zawartość frakcji diad f, zawartość molową jednostek alifatycznych i aromatycznych P, średnie długości bloków $\bar{L}_n$ oraz stopień losowości R dla wszystkich otrzymanych kompozycji kopoliestrów.

Nowe kopoliestry alifatyczno-aromatyczne o zróżnicowanym składzie chemicznym zostały scharakteryzowane również za pomocą różnicowej kalorymetrii skaningowej (DSC), rozpraszania promieniowania rentgenowskiego pod dużymi (WAXS) i małymi kątami
(SAXS), a masy cząsteczkowe zostały wyznaczone za pomocą chromatografii żelowej (SEC-MALLS). Natomiast zdolność do krystalizacji oraz morfologia otrzymanych materiałów została zbadana za pomocą różnych technik wśród których można wyróżnić mikroskopię sił atomowych (AFM), układ złożony z mikroskopu ze światłem spolaryzowanym wyposażony w stolik grzejny (PLM) oraz technikę wykorzystującą pomiar światła zdepolaryzowanego (PLD).

Przeprowadzone badania analizy struktury chemicznej wykazały, iż makrocząsteczki wszystkich otrzymanych materiałów zawierających od 10% do 90% części aromatycznej charakteryzują się prawie bezładnym rozmieszczeniem elementów aromatycznych i alifatycznych (Tab. 1). Okazało się również, że znaczna ich większość zachowała zdolność do krystalizacji. Badania wykazały, iż w przypadku kopoliestrów z zachowaną zdolnością do krystalizacji tylko bloki tereftalanu butylenu (**BT**) są zdolne do krystalizacji w postaci kryształów o trójskośnej strukturze krystalograficznej charakterystycznej dla aromatycznego homopolimeru - politereftalanu butylenu.

Tabela 1: Dystrybucja sekwencji wytworzonych kopoliestrów z różną zawartością części aromatycznej.

Próbka	f_{ArAr}	f_{ArAl}	f_{AlAr}	f_{AlAl}	P_{Ar}	P_{Al}	$\bar{L}_{Ar}$	$\bar{L}_{Al}$	R
PBASGT 10% ar	0.017	0.112	0.116	0.754	0.131	0.869	1.147	7.598	1.003
PBASGT 20% ar	0.055	0.176	0.192	0.576	0.240	0.760	1.301	4.127	1.011
PBASGT 30% ar	0.113	0.222	0.237	0.428	0.343	0.657	1.494	2.867	1.018
PBASGT 40% ar	0.192	0.246	0.256	0.306	0.443	0.557	1.766	2.218	1.017
PBASGT 50% ar	0.287	0.253	0.253	0.207	0.540	0.460	2.136	1.818	1.018
PBASGT 60% ar	0.397	0.234	0.234	0.135	0.631	0.369	2.695	1.576	1.005
PBASGT 70% ar	0.529	0.201	0.196	0.074	0.728	0272	3.667	1.373	1.001
PBASGT 80% ar	0.658	0.164	0.145	0.033	0.813	0.188	5.255	1.213	1.015
PBASGT 90% ar	0.813	0.098	0.081	0.008	0.902	0.098	10.091	1.091	1.016

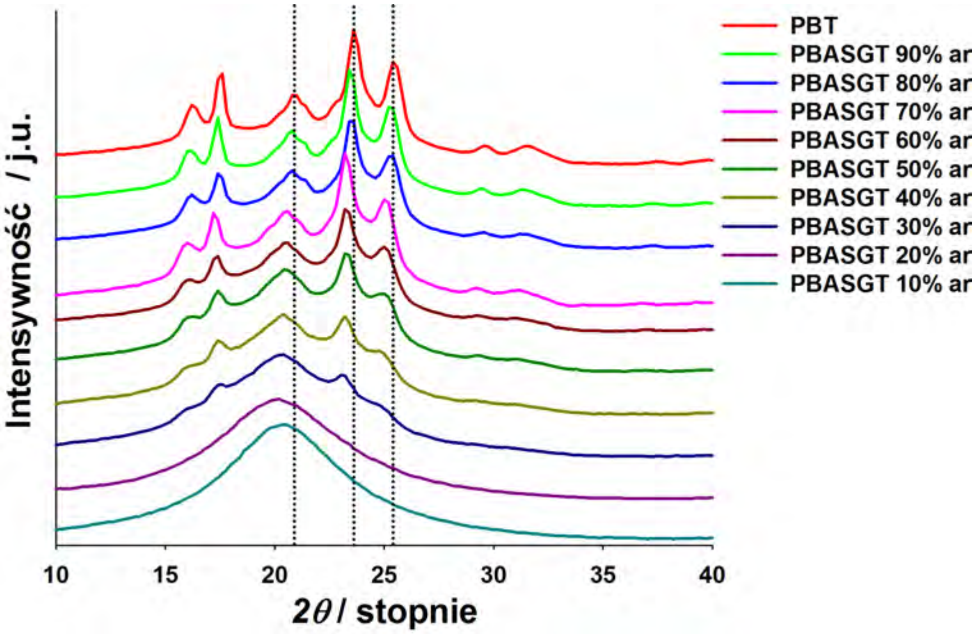

Rysunek 1: Rozkłady kątowe 2θ intensywności rozpraszania promieniowania rentgenowskiego pod dużymi kątami wytworzonych kopoliestrów z różną zawartością części aromatycznej oraz wytworzonego PBT. Krzywe kopoliestrów z zawartością części aromatycznej powyżej 20% oraz wytworzonego PBT zostały przesunięte w pionie dla lepszej przejrzystości wykresu.

Wzrost zawartości jednostek alifatycznych nie zmienił struktury krystalograficznej (Rys. 1) z trójskośnej na jednoskośną w przeciwieństwie do wyników uzyskanych przez Li i innych [7] dla podobnego materiału zawierającego jeden ester alifatyczny - bursztynian butylenu. Warto zauważyć, iż na otrzymanych dyfraktogramach występują nieznaczne przesunięcia niektórych refleksów od płaszczyzn krystalograficznych przy porównaniu dyfraktogramów otrzymanych kopoliestrów i aromatycznego homopolimeru. Przesunięcia takie mogą być wywołane defektami wynikającymi z wtrąceń w fazie krystalicznej lub ze względu na występujące naprężenia powierzchniowe spowodowane przez znaczną redukcję grubości kryształów. Termogramy różnicowej kalorymetrii skaningowej (DSC) wykazały zmiany temperatur przejść fazowych wraz ze wzrostem zawartości merów części aromatycznych. Zaobserwowano przesunięcie temperatury topnienia do niższych temperatur wraz ze zmniejszeniem zawartości bloków **BT**. Odnotowano również, iż obniżenie zawartości części tereftalanowej powoduje obniżenie maximum piku krystalizacji kopoliestrów, jak również poszerzanie się tego piku (Rys. 2).

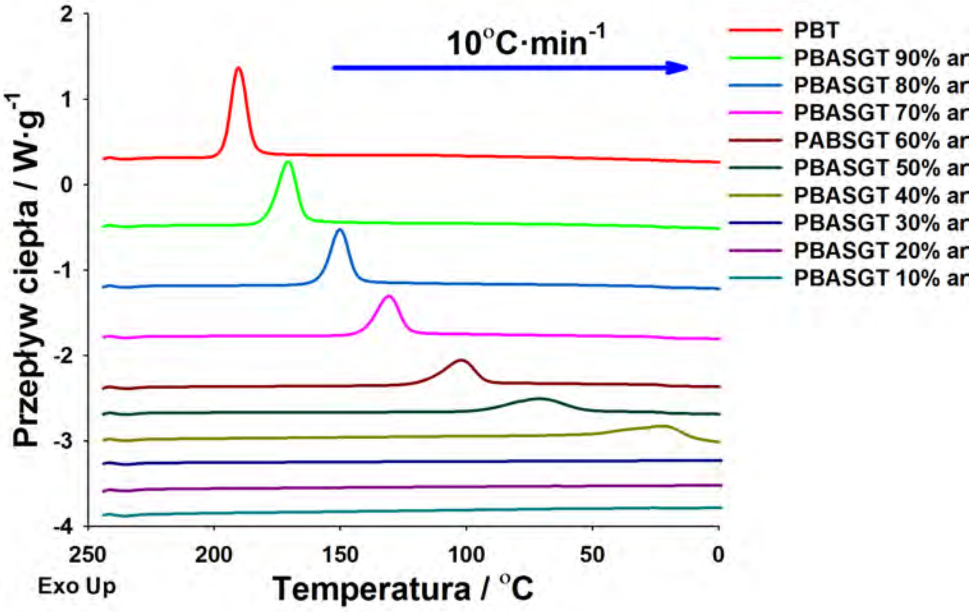

Rysunek 2: Termogramy chłodzenia z szybkością 10°C·min^{-1} homopolimeru PBT oraz kopoliestrów PBASGT z różną zawartością części aromatycznej. Krzywe kopoliestrów PBASGT zostały przesunięte w pionie dla lepszej przejrzystości wykresu.

Pomiary termograwimetryczne nie wykazały znaczącego wpływu obecności jednostek alifatycznych na stabilność termiczną otrzymanych materiałów w porównaniu z aromatycznym homopolimerem. Ze względu na zróżnicowane przedziały temperatur krystalizacji oraz związany z tym zróżnicowany stopień krystaliczności zbadano właściwości mechaniczne kopoliestrów w trakcie jednoosiowej deformacji. Materiały o zawartości części aromatycznej poniżej 60% ulegają jednorodnej deformacji w sposób charakterystyczny dla kauczuków. Przy wzroście zawartości części aromatycznej pojawiają się fluktuacje naprężenia w trakcie rozciągania. Dla kopoliestru zawierającego 80% jednostek

BT zaobserwowano oscylacyjny wzrost naprężenia spowodowany okresową zamianą mechanizmu deformacji z etapu powstawania szyjki do jej propagacji i na odwrót (Rys. 3). Zwiększanie zawartości części aromatycznej powoduje dalszą zmianę mechanizmu deformacji. W przypadku kopoliestrów zawierających 90% części aromatycznej deformacja zachodzi w sposób charakterystyczny dla termoplastów częściowo krystalicznych, na co składa się silnie zlokalizowana granica plastyczności oraz formowanie dobrze wykształconej szyjki. Alternatywnie próbki z zawartością 90% jednostek **BT** pękają w sposób kruchy przy dużych naprężeniach, który jest również charakterystyczny dla aromatycznych homopolimerów.

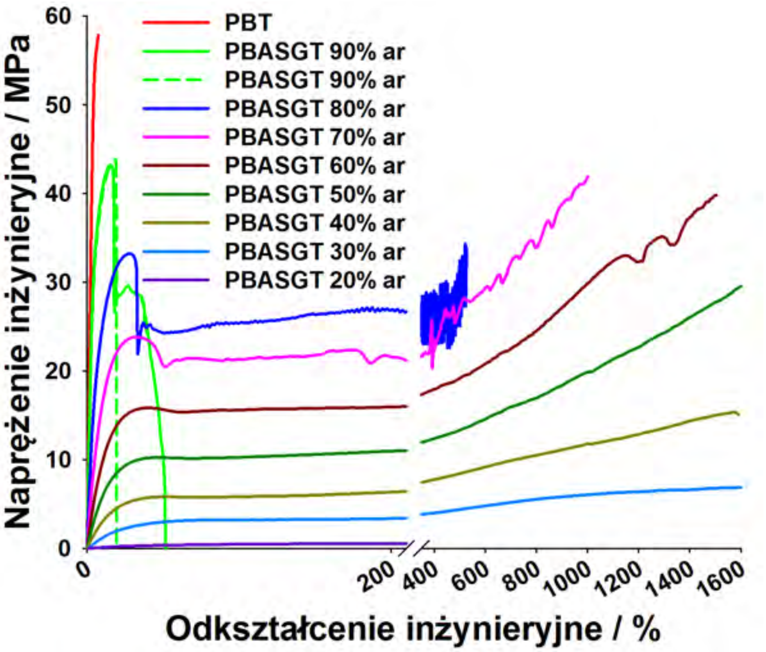

Rysunek 3: Krzywe zależności naprężenia-odkształcenia PBT oraz kopoliestrów PBASGT z różną zawartością części aromatycznej.

Do dalszych badań nad procesem krystalizacji wybrano, spośród serii kopoliestrów, materiał o kompozycji optymalnie łączącej zdolność do biodegradacji oraz dobre właściwości termiczne i mechaniczne. Badania biodegradacji tych kopoliestrów przeprowadzone w IBWCh wykazały, że kopoliester PBASGT zawierający 45% frakcji aromatycznej jest w pełni biodegradowalny i taki został wybrany do dalszych badań. Przeprowadzone obserwacje oraz analizy pokazały, że ten kopolimer PBASGT krystalizuje w postaci sferolitów wypełniających całą objętość materiału, o średnim promieniu wynoszącym powyżej 7 µm (Rys. 4). Sferolity te są uformowane przez kryształy o grubości kilku nanometrów, a stopień krystaliczności materiału osiąga wartość około 20%. Grubości kryształów okazały się główną przyczyną obniżenia temperatury topnienia kopolimerów PBASGT. Kopolimer ten wykazuje zdolność do samozarodkowania krystalizacji (Rys. 5). Badania samozarodkowania pokazały, iż samozarodki ulegają stopieniu

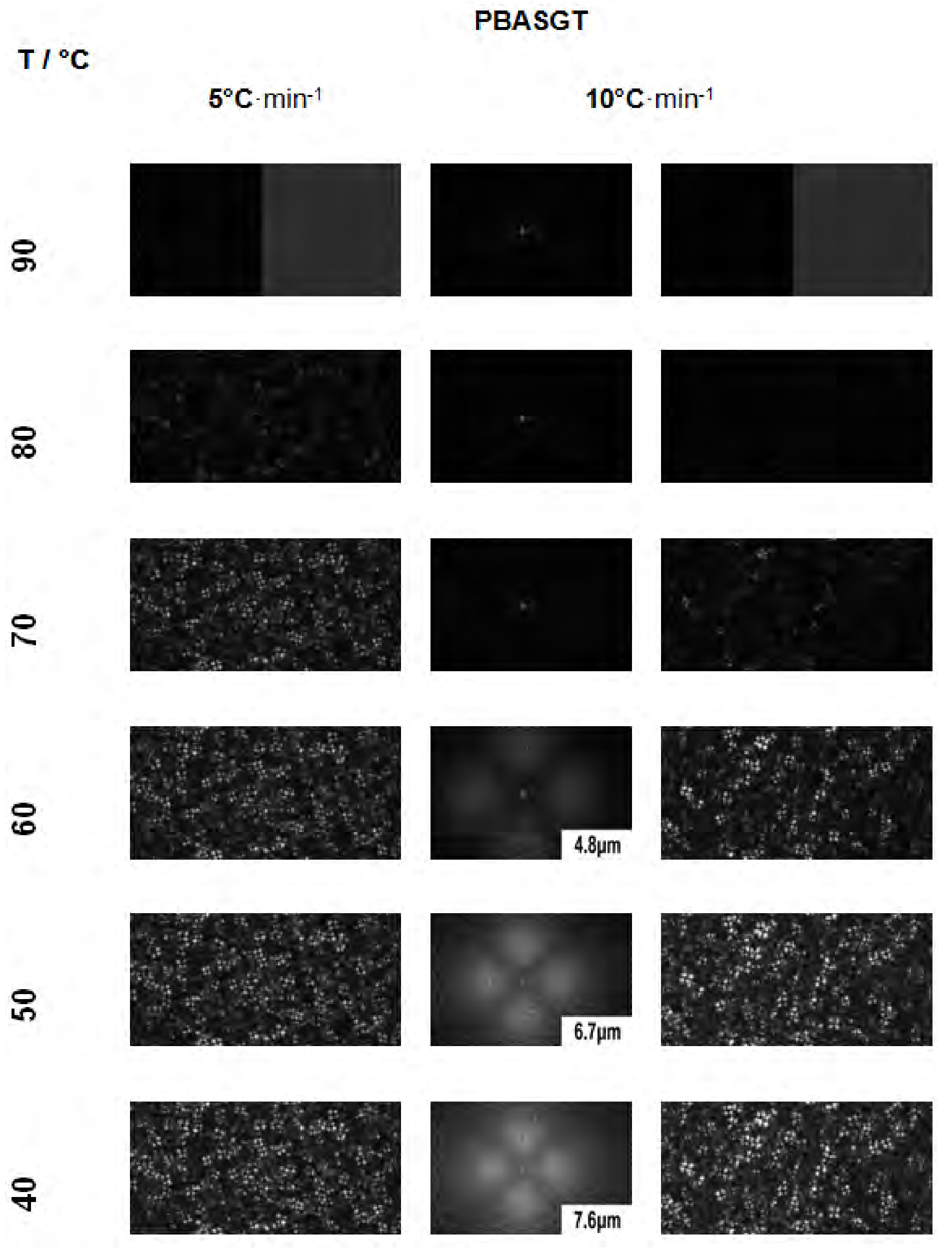

Rysunek 4: Przykładowe mikrofotografie PLM oraz SALS wzrostu sferolitów kopoliestru PBASGT otrzymanych w trakcie nieizotermicznej krystalizacji podczas chłodzenia z szybkością 5°C·min^{-1} i 10°C·min^{-1}. Mikrofotografie PLM zarejestrowane dla $T = 90$°C zostały w części rozjaśnione dla uwidocznienia pierwszych zarodków krystalizacji. Liczby umieszczone na mikrofotografiach SALS są wartościami średniego promienia piątego rzędu sferolitów wyznaczonego przy użyciu dystrybucji kątowej światła rozproszonego.

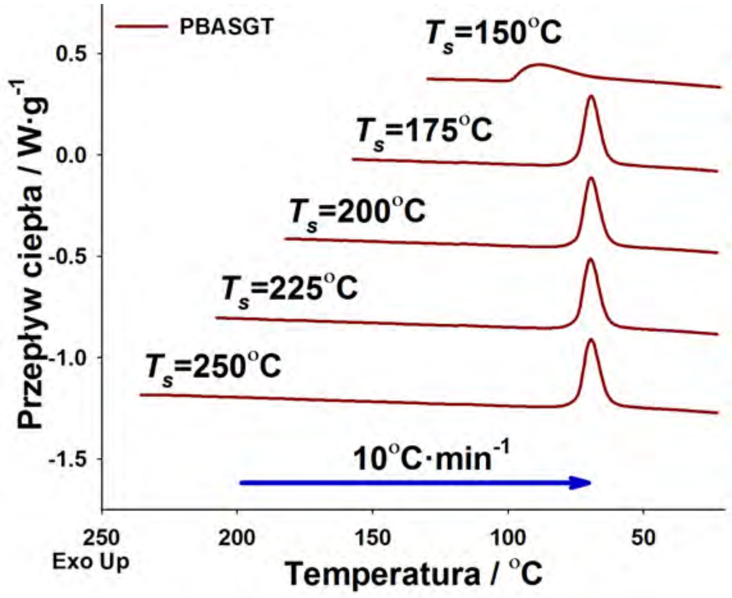

Rysunek 5: Termogramy nieizotermicznej krystalizacji podczas chłodzenia z szybkością 10°C·min^{-1} ze stopu w różnych temperaturach. Krzywe dla próbek pozbawionych samozarodków są przesunięte w pionie dla lepszej przejrzystości wykresu.

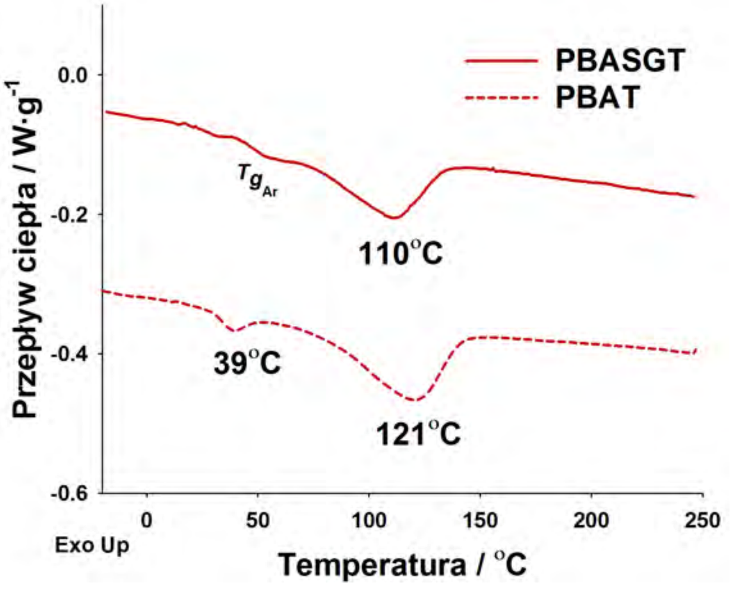

Rysunek 6: Termogram grzania z szybkością 10°C·min^{-1} próbek kopoliestru PBASGT oraz PBAT przechowywanych wcześniej w niskich temperaturach. Krzywa PBASGT została przesunięta pionowo dla lepszej przejrzystości wykresu.

powyżej 160°C. Analiza samozarodkowania wykazała, że istnieją trzy przedziały temperaturowe samozarodkowania, w której wybrany kopoliester PBASGT został stopiony, zdefiniowane za pomocą intensywności zjawiska.

Struktura chemiczna, morfologia oraz proces krystalizacji kopoliestru PBASGT o wybranej kompozycji zostały porównane z komercyjnie dostępnym kopoliestrem alifatyczno-aromatycznym zawierającym jeden komonomer aromatyczny (ester dimetylowego kwasu tereftalowego) oraz jeden komonomer alifatyczny (ester dimetylowego kwasu adypinowego) o komercyjnej nazwie Ecoflex® (PBAT). Przypuszczano, iż krystaliczne sekwencje **BA** w bezładnym kopoliestrze zawierającym również jednostki **BT** obniżą temperaturę krystalizacji oraz topnienia w porównaniu z analogicznymi homopolimerami. W celu sprawdzenia zdolności do krystalizacji komponentów alifatycznych próbki kopolimerów zostały schłodzone do temperatury 4°C i pozostawione w niej przez 24 h. Topnienie kryształów utworzonych z aromatycznych merów zostało zaobserwowane w 110°C oraz 121°C odpowiednio dla PBASGT oraz PBAT (Rys. 6). Dodatkowo na termogramie kopolimeru PBAT zaobserwowano endotermiczny pik w temperaturze 39°C, który zidentyfikowano jako topnienie kryształów zbudowanych z alifatycznych sekwencji. Nie odnotowano takiego piku dla próbek kopolimeru PBASGT poddanego takim samym warunkom. Okazało się więc, iż alifatyczna część kopolimeru PBASGT w przeciwieństwie do alifatycznej części kopolimeru PBAT, nie jest zdolna do krystalizacji pomimo przechowywania w obniżonej temperaturze.

Wiele istotnych informacji uzyskano z badań nisko-kątowego rozpraszania promieniowania rentgenowskiego, SAXS. Porównanie ewolucji funkcji korelacyjnych SAXS kopoliestrów PBASGT i PBAT wykazało, że krystaliczna struktura PBASGT formuje się w sposób stopniowy, a kryształy PBAT formują się w sposób raptowny (Rys. 7). Jednakże ostatecznie średnia grubość utworzonych kryształów **BT** w obu przypadkach jest zbliżona (3.5 nm).

Zaobserwowane wyraźne i silne zjawisko samozarodkowania zasugerowało, że krystalizacja PBASGT może zostać przyspieszona poprzez wprowadzenie środków zarodkujących. Udowodniono, iż środki zarodkujące, które są efektywne dla PBT są również efektywne dla PBASGT. Efektywnymi środkami okazały się być dwa rodzaje ftalocyjaniny oraz talk (Rys. 8).

Zarodkowanie zieloną ftalocyjaniną przesunęło pik nieizotermicznej krystalizacji z 70°C do 84°C podczas chłodzenia z szybkością 10°C·min^{-1} ze stopu o temperaturze 150°C zawierającego samozarodki. Zaobserwowano również tę samą temperaturę krystalizacji dla próbki z dodatkiem zielonej ftalocyjaniny krystalizowanej ze stopu z usuniętymi samozarodkami poprzez ogrzanie próbki do temperatury 250°C. Jednakże, aktywność i efektywność heterozarodków jest mniejsza niż samozarodków (Rys. 9).

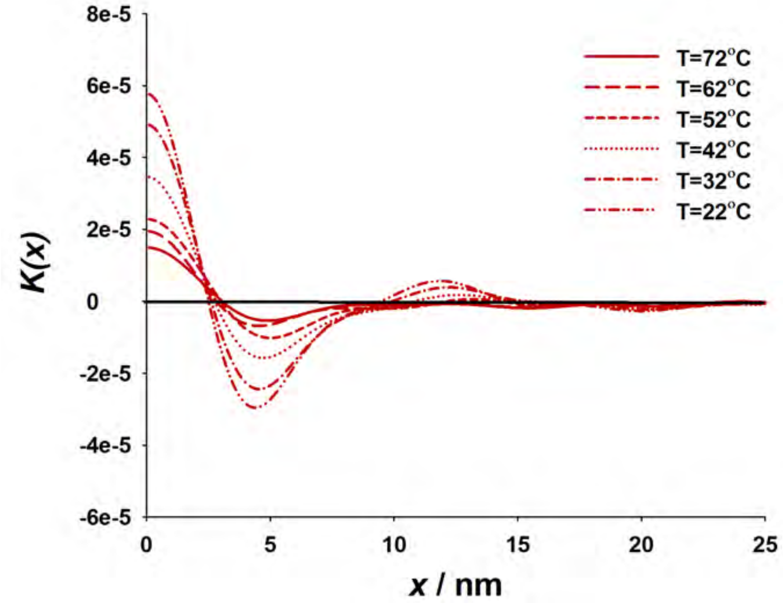

(a) PBASGT

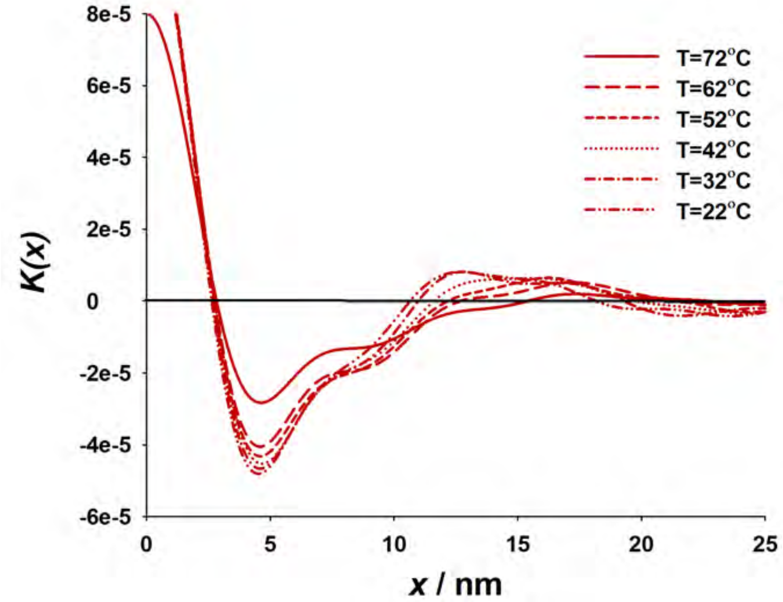

(b) PBAT

Rysunek 7: Ewolucja jednowymiarowej funkcji korelacyjnej kopoliestru (a) PBASGT oraz (b) PBAT w trakcie nieizotermicznej krystalizacji podczas chłodzenia z szybkością 10°C·min^{-1}.

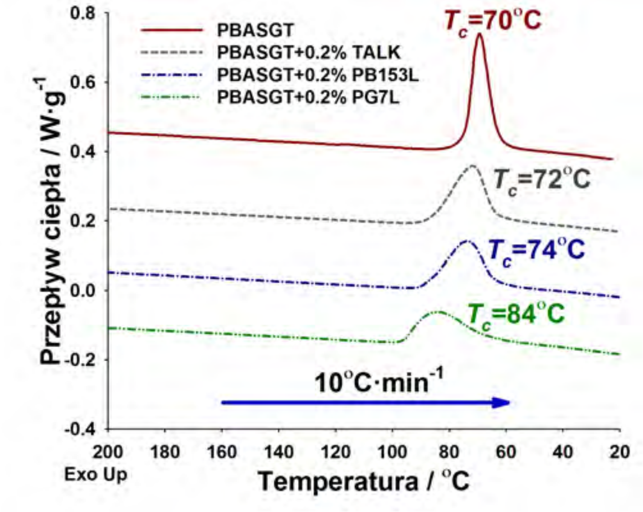

Rysunek 8: Porównanie termogramów krystalizacji czystego oraz nukleowanego kopoliestru PBASGT podczas chłodzenia z szybkością 10°C·min^{-1}. Samozarodki zostały usunięte poprzez ogrzanie próbek do temperatury 250°C. Krzywe nukleowanego kopoliestru są przesunięte w pionie dla lepszej przejrzystości wykresu.

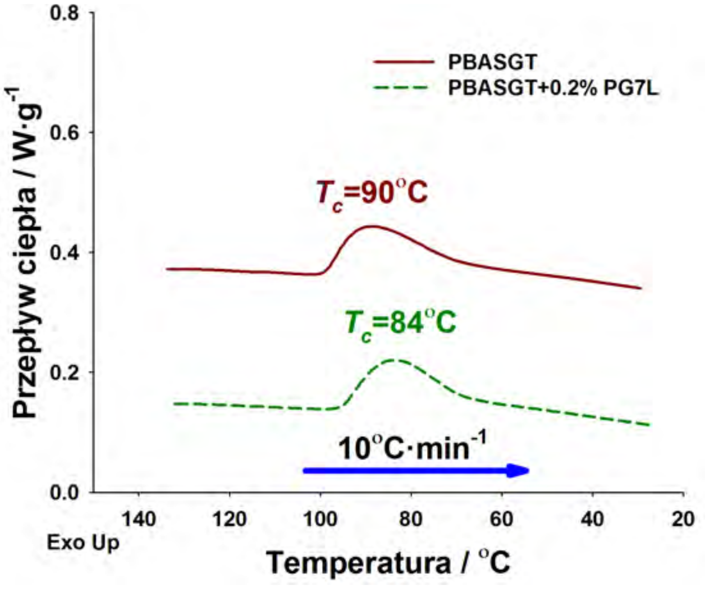

Rysunek 9: Porównanie termogramów krystalizacji czystego kopoliestru PBASGT z zachowanymi samozarodkami oraz nukleowanego kopoliestru PBASGT zieloną ftalocyjaniną PG7L podczas chłodzenia z szybkością 10°C·min^{-1} ze stopu odpowiednio w temperaturze 150°C i 250°C. Krzywa próbki z dodanymi heterozarodkami jest przesunięta w pionie dla lepszej przejrzystości wykresu.

Reasumując, przeprowadzone badania pozwoliły na pełne zrealizowanie celów rozprawy, w tym na:

- określenie rozkładu sekwencji merów aromatycznych i alifatycznych wzdłuż makrocząsteczek kopoliestrów aromatyczno-alifatycznych PBASGT i na skorelowanie tych parametrów ze zdolnością do ich krystalizacji
- scharakteryzowanie głównych aspektów krystalizacji kopoliestrów PBASGT takich jak zarodkowanie i wzrost sferolitów
- zebrana wiedza pozwoliła na wybór najbardziej obiecującego kopoliestru PBASGT, ze względu na zastosowania, o zawartości 45% frakcji aromatycznej, który łączy dobrą przetwarzalność, dobre właściwości mechaniczne i termiczne z biodegradowalnoscią
- scharakteryzowano strukturę nadcząsteczkową PBASGT oraz poznano najważniejsze parametry pozwalające kontrolować jej formowanie się i kinetykę tego procesu

Ta szczegółowa wiedza pozwoliła na wytypowanie i znalezienie efektywnych środków zarodkujących krystalizację PBASGT, co umożliwia lepszą kontrolę zestalania się PBASGT i poprawę właściwości przetwórczych.

Acknowledgements

I am heartily thankful to my supervisor, *prof. dr hab. Andrzej Gałęski* for helping me during preparation of this thesis.

I would like to thank to *dr Sławomir Dutkiewicz*, for copolyesters synthesis.

I am also grateful to *prof. dr hab. Ewa Piórkowska-Gałęska* and *dr hab. Andrzej Pawlak*, for all helpful discussions we have sheared.

I would like to thank a lot to *my parents and husband*, who supported me in any respect during the completion of this thesis.

The European Union European Regional Development Fund, Contract No. POIG.01.01.02-10-025/09 is also acknowledged for partial financial support.

Research grant N N209 230638 from Polish Ministry of Science and Higher Education is acknowledged for partial financial support.

Research project I-20110505 EC Small angle X-ray scattering studies of plastic deformation in semicrystalline homopolymers and DESY Hamburg is also acknowledged for giving the possibility to make *in situ* measurements.

Research Grant for Young Researchers Development from CMMS PAS 2014 is also acknowledged for partial financial support.

Contents

Introduction

Large consumption of polymers results from their superior mechanical properties, resistance to chemical and biological attacks, low costs and uncomplicated but complete processing, that brings ready-made articles with finished surfaces. The volume of yearly production of polymeric materials already exceeded that of steel. A vast fraction of polymer based products are single-use like packaging or used for short term. However, those favorable features of polymeric materials have led to an increasing disposal problem. Due to growing awareness about the global environment a range of new polymeric materials is being developed, especially biodegradable materials. Contrary to conventional polymers, biodegradable one can be converted into biomass or into carbon dioxide and water by microorganisms in their environment. Conversion of polymers into carbon dioxide and water seems to be environmentally friendly solution, however, in this way the energy stored in polymeric materials is lost. This is unlike in regular recycling of polymer waste, either the material is restored or the energy is recovered. Biodegradability is always connected with the loss of energy, however, in many instances such as supermarket bags, this is accepted. A major role with respect to the industrial relevance is played by various polyesters, especially the aliphatic ones due to their susceptibility to biodegradation. The well-known commercially available example is poly(lactic acid) (PLA). Even though it is not the only one available on the market, there are drawbacks which do not allow it to be used in many applications. To improve the physical properties without sacrificing the biodegradability, introduction of aromatic units into main chains of aliphatic polyesters has been explored and aliphatic-aromatic copolyesters (AAC) have been developed. The effort was made to obtain materials with varied composition by changing types of aliphatic and aromatic comonomers or even introducing several types of aliphatic comonomers into macromolecules. Most of aliphatic-aromatic copolyesters are biodegradable under rigorous condition of sufficiently short aromatic sequences. However, it can decrease the ability of AAC to crystallize if only the aromatic units are able to crystallize. Crystallization and its peak temperature during cooling is very important for polymer processing and applications involving hot drinks and food. Thus, the investigation of crystallization of such copolyesters is crucial for their use. Furthermore, the understanding of AAC behavior during nonisothermal crystallization is very important for optimization of the processing conditions and the end-properties of products.

Therefore, the first Chapter aims in summarizing the state of knowledge on crystallization of copolymers. Firstly, it concerns the known polyesters composed from monomers contributing to the synthesized copolyesters. The crystallization characterization is mainly presented to give an idea about conceivable properties of the synthesized copolyester. Moreover, it shows the obstacles, which can come across during industrial processing. Secondly, the known copolyesters are described to give the notion how the properties of homopolymers differ from copolymers characteristics.

Then, the basic concepts connected with the crystallization will be discussed. Starting from the crystallization models for homo and copolymers, which can help to predict how the crystallization can occur in a given case. Further, a description of polycrystalline aggregates growth and spherulitic structure, which affect the mechanical properties of a polymer, will be presented. The influence of chemical composition and nucleating agents on the peak crystallization temperature will be also discussed, because it has an impact on solidification and resulting spherulitic structure.

The objectives of the thesis are described in the second Chapter.

In the third Chapter a list of materials used for synthesis and commercially available copolyesters used for comparison are shown. The conditions of synthesis are described in details. The preparation of nucleated AAC is also presented.

In the fourth Chapter the experimental data are presented. They contain the description of all equipments used during the investigation together with the operating condition.

Results of the experiments and discussions concerning the aliphatic-aromatic copolyesters crystallization will be presented in the fifth Chapter. The fifth Chapter is divided into five Subsections. First of them is focused on the influence of chemical composition on copolyesters properties. Second relates to crystallization characterization of selected aliphatic-aromatic copolyester. Third subsection tells about the nucleating agents found to accelerate crystallization of AAC. The dissertation ends with general conclusions derived from the studies, the summary of the studies and with references cited in this thesis.

Chapter 1

State of knowledge

1.1 Polyesters

Polyesters is a general term encompassing all polymers in which the monomer units are linked together by the group -COO-. Their main polymer backbones are usually formed by polymerizing a polyhydric alcohol with a polybasic acid [8]. Polyesters are usually synthesized by polyesterification of a diol (or triol, etc) with a diacid, or with a derivative of diacid (especially a diester) by ester interchange via alcoholysis (Fig. 1.1). High temperatures are demanded for these methods, thus frequently they are performed as melt polymerizations [9].

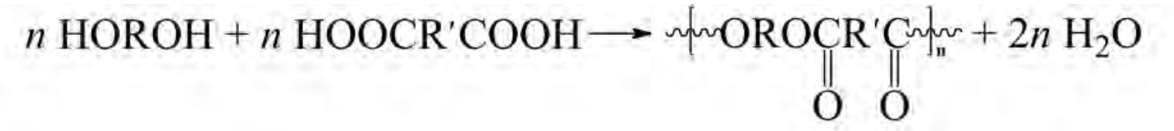

$$n\,\mathrm{HOROH} + n\,\mathrm{HOOCR'COOH} \longrightarrow \sim\!\!\left[\mathrm{ORO}\underset{\underset{\|}{\mathrm{O}}}{\mathrm{C}}\mathrm{R'}\underset{\underset{\|}{\mathrm{O}}}{\mathrm{C}}\right]_n\!\!\sim + 2n\,\mathrm{H_2O}$$

(a) diol with a diacid

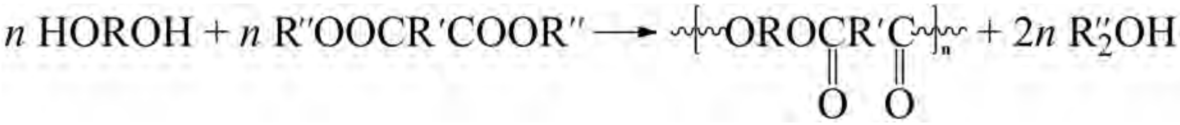

$$n\,\mathrm{HOROH} + n\,\mathrm{R''OOCR'COOR''} \longrightarrow \sim\!\!\left[\mathrm{ORO}\underset{\underset{\|}{\mathrm{O}}}{\mathrm{C}}\mathrm{R'}\underset{\underset{\|}{\mathrm{O}}}{\mathrm{C}}\right]_n\!\!\sim + 2n\,\mathrm{R''_2OH}$$

(b) diol with a diester

Figure 1.1: Schemes of polyesters polyesterification: a diol (or triol, etc) **(a)** with a diacid, **(b)** with a derivative of diacid (especially a diester).

A very wide range of different polyesters is known. Many of them are being used commercially in a various and important applications. For instance, aliphatic polyesters in low molecular weight form are useful as polyester plasticizers and as polyol prepolymers for polyurethanes. High molecular weight poly-(ε-caprolactone) has found a limited use as a biodegradable plastic. Most of aliphatic polyesters have low melting temperatures (T_m) and glass transition temperature (T_g) values, so the softening points are too low for film and fiber applications [9].

However, aliphatic polyesters are considered as the most easily biodegradable polymers. It is the consequence of aliphatic polyester chain flexibility. The polymer chain must be flexible enough to fit into the active site of the enzyme to be degradable by enzymes [10].

The aliphatic polyesters are also produced and stored during sugar fermentation by many types of microorganisms. Certain bacteria feeding on sugars enzymatically produce polyhydroxybutyrate (PHB), which is stored as 'bacterial fat' [10]. The most widely used polymer is extracted from Alicagenes eutrophus [11]. Afterwards it is dried, formed as powder or pellets [10].

PHB is a biodegradable and simultaneously biocompatible polymer [12]. Its crystals has orthorhombic [13] structure with T_m around 180°C and T_g around 0°C, however, it can be shifted to 30°C depending on the crystallinity degree [14]. Semicrystalline PHB has been found commercially useful in biodegradable packaging [15] and has undergone trials as a biomedical implant [16]. However, bacterial PHB is too brittle for many applications, due to its high crystallinity. Furthermore, DSC studies indicate that some secondary crystallization may occur over a timescale of days, therefore the progressive reduction of amorphous phase may cause further development of fragility [17]. Moreover, its melting point is just slightly lower than its degrading temperature (around 185°C), this makes its melt processing difficult. Nevertheless, PHB has several advantages such as moisture resistance, water insolubility and optical purity. Those properties differentiate PHB from other currently available biodegradable plastics, which are either water soluble or moisture sensitive [18].

Synthetic aliphatic polyesters are also available. The most popular examples are poly(lactide) (PLA) and poly(ε-caprolactone) (PCL). Another commercialized type of biodegradable aliphatic polyester is succinate-based [10]. Initial studies with succinate polyesters was successful only in producing polymers with molecular weight (M_w) less than 5,000. Unfortunately obtained polymers were weak and brittle. To change these properties, Takiyama and co-workers started developing high M_w aliphatic polyesters for pressure sensitive or thermosetting adhesives [19]. This research showed usefulness of high M_w succinate polyesters and in 1990 the means was discovered for making these polyesters with a number average M_w in the range 20,000-200,000. Preparation of high M_w polymers contains two steps. Firstly dehydration condensation of a dihydric alcohol, such as 1,4-butanediol, with succinic acid is performed in order to obtain a hydroxy-terminated aliphatic polyester prepolymer. Afterwards, the prepolymer is reacted with a diisocyanate chain extender to form a high M_w succinate polyester [20].

Poly(butylene succinate) (PBS, Fig. 1.2(a)) is an example of succinate-based biodegradable polyesters. PBS is a crystallizable polymer with flexible macromolecules, which equilibrium melting point (T_m^0) and T_g temperatures were found to be about 132°C and -38°C, respectively [21]. The exothermic crystallization peak was observed at 68°C by Miyata [21]. Qiu [22] observed the double melting behavior of nonisothermally crystallized PBS and showed that it fits to the melt-recrystallization model. The model assumes simultaneous melting of some crystals and perfectioning of others by annealing during heating. Yoo and Im [23] showed that isothermally crystallized samples exhibit multiple endotherm with main melting point at 113°C [24]. Wang [25] suggested the explanations for each melting point of isothermally crystallized PBS. The T_{m_1} was ascribed to the melting of crystallites formed through recrystallization. The T_{m_2} and T_{m_3} derived from two crystal populations with different thermal stability. The T_{m_4}, which is the annealing peak, represents the transition of the rigid amorphous fraction (RAF) from solid-like RAF into liquid-like amorphous fraction. Moreover, Yoo [23] showed that amount enthalpy under the melting peaks depends on the isothermal crystallization temperature, but only one crystal form exists regardless of crystallization temperature (T_c). Normally, PBS crystallize in α-form having monoclinic symmetry with unit cell parameters $a = 0.523$ nm, $b = 0.908$ nm, $c = 1.079$ nm and $\beta = 123.87°$. PBS chains in α-crystals have a $T_7GT\bar{G}$ conformation [26], where T, G and $\bar{G}$ denotes trans, gauche, and minus gauche, respectively. However, Ichikawa [27] reported that PBS crystals exhibit a reversible crystallographic transition. The transition occurred reversibly under application and removal of stress at stretched PBS fibers. For the β-form it contains the T_{10} helical chains. The transition was recognized as thermodynamically first order transition with the free energy difference ΔG =1.6 kJ·mol^{-1} of monomer units [27]. Ichikawa et al. [28] have determined the unit cell parameters for the β-form as follows $a = 0.584$ nm, $b = 0.832$ nm, $c = 1.186$ nm, and $\beta = 131.6°$. Crystalline PBS exhibits slow degradation rate and low mechanical flexibility [29].

Other example of a typical biodegradable and industrially available plastic is poly-(butylene adipate) (PBA, Fig. 1.2(b)). PBA has lower melting temperature (T_m around 60°C) and is more readily biodegraded than PBS (T_m around 117°C) [30]. Furthermore, its glass transition point is also lower T_g =-76°C [31] in comparison to PBS. PBA is similar to PBS in the sense that it exhibits also two crystal forms, but no other similarity. Generally, PBA chains are packed in a monoclinic unit cell with dimensions of $a = 0.673$ nm, $b = 0.794$ nm, $c = 1.42$ nm, and $\beta = 45.5°$ [32]. β-form, which chains are packed in an orthorhombic unit cell with dimensions of $a = 0.506$ nm, $b = 0.735$ nm, $c = 1.467$ nm [32], can be obtained under condition of strain and annealing. The β-form of quenched in liquid nitrogen and stretched film, after storage at room temperature or annealing at 52.8°C transforms back into α-form crystals. Due to these spontaneous transformation monoclinic α-form crystals are considered to be more stable. However, it was reported that transformation initiation can be caused also in another way. The PBA polymorphic crystals can be prepared simply by melt-crystallization at different temperatures. Gan [33, 34] showed that α-form crystals are formed during annealing above 29°C while β-crystals are formed below 31°C. However, both crystal forms are produced simultaneously at 30±1°. Moreover, both the α and β crystals of PBA show double melting behavior. Gan [34] suggested that annealing causes the molecular displacement of polymer chains in both amorphous and crystal phases. Therefore the β-to-α-crystal transformation is a solid-solid phase-transition process accompanied by the thickening of lamellar crystals. PBA polymorphism can be also controlled by nucleating agents [35]. It was revealed that nucleating agents preferably initiate the nucleation of the α-form crystal. However, these studies showed also that high cooling rate during nonisothermal crystallization assists to the formation of the β-form crystals.

Next example of crystalline aliphatic polyester is poly(butylene glutarate) (PBG,

Fig. 1.2(c)), however, there are not many reports about its physical properties in the literature. Generally it was used as admixture in blends preparation [36]. It is known that PBG has low melting temperature around 39°C [37]. Its advantage for processing is a lack of decomposition at a significant rate below 250°C. The glass transition is around -55°C and the solidification occurs at -5°C. Due to its low T_m value PBG is not useful for conventional thermoplastic applications.

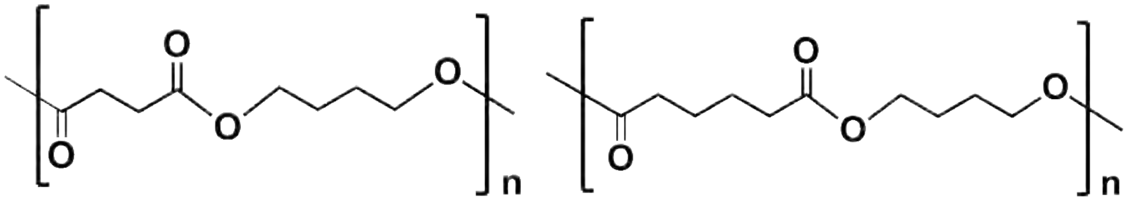

(a) PBS (b) PBA

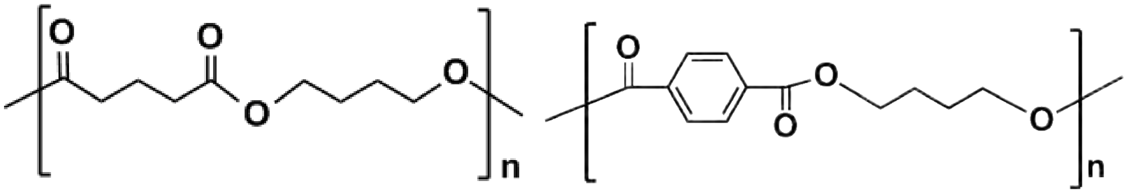

(c) PBG (d) PBT

Figure 1.2: Structure of polyesters: **(a)** PBS, **(b)** PBA, **(c)** PBG and **(d)** PBT.

On the other hand wholly aromatic polymers are high temperature resistant plastics but are very difficult to melt process. Aromatic polyesters are more rigid than aliphatic polyesters, thus they are considered as bioinert and not biodegradable [10]. The partially aromatic linear polymers are very important, especially polyethylene terephthalate (PET) and polybutylene terephthalate (PBT, Fig. 1.2(d)). PBT is also known as polytetramethylene terephthalate (PTMT) or 4GT [38]. Both are stiff and tough enough to be considered as engineering plastics [9].

Thermal history of the material influences the melting and crystallization behavior. In the case of PBT the melting temperature ranges from 222°C to 232°C, and the heat of melting is found to be 144.5 J·g^{-1} [39]. Unannealed samples usually reveal a single peak with a maximum at around 224°C. Multiple melting peak of PBT was also reported [40]. Thermal studies showed that PBT can exhibit up to three melting peaks. The complex fusion behavior of PBT is accepted to involve simultaneously melting and recrystallization [41].

PBT specimens recrystallize when heated above T_g from the amorphous state after quenching. The T_g value relies on the degree of crystallinity, annealing, amount and type of fillers, and measuring method. T_g of PBT is in the range from 30°C to 50°C [42]. Although it was determined that fully amorphous PBT has a glass transition point at 15°C [43].

In the solid state PBT is a mixture of regularly ordered spherulites and amorphous, uncrystallized regions. Two different types of spherulites can be distinguished. One showing the usual extinction pattern when viewed between crossed polarizers, with extinction parallel to the axes of the polarizers. Another type can be viewed with extinction pattern rotated at 45° [44].

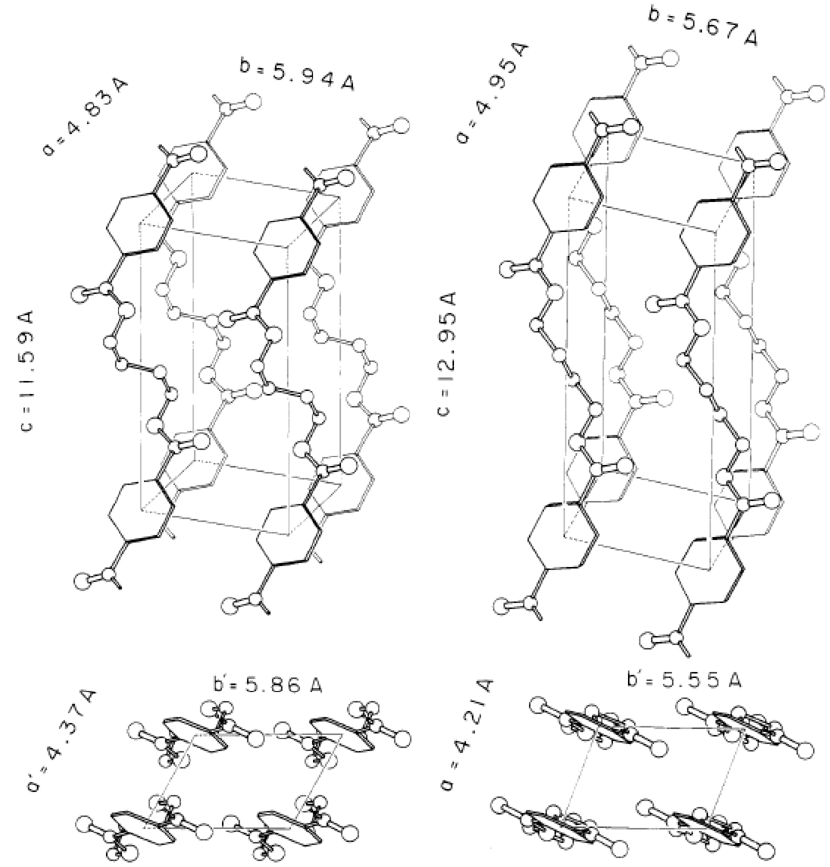

(a) α-form (b) β-form

Figure 1.3: Arrangement of molecules in crystal of the **(a)** α and **(b)** β form of poly(butylene terephthalate): above, projection normal to the 010 plane; below, projection along c axis [45].

PBT crystals have triclinic structure. However, they exhibit reversible α-form and β-form. The typical elementary cells are shown in Figure 1.3 The cell dimensions are as follows a = 0.483 nm, b = 0.594 nm, c = 1.159 nm, α=99.7°, β=115.2°, and γ=110.8° for the α-form; and a = 0.495 nm, b = 0.567 nm, c = 1.295 nm, α=101.7°, β=121.8°, and γ=99.9° for the β-form [45]. In the nonextended state, the α-form with gauche-trans-gauche conformation of butylenes moiety has got privilege. The β-form appears in tensile drawing with all trans conformation in concentration depending on the drawing condition.

PBT macromolecules form folded chain lamellae. Depending on the crystallization conditions, the lamellar thickness is between 8 and 15 nm. The long period was measured to be 9 to 16 nm [43].

PBT crystals are resistant to most of solvents at room temperature. Due to crystals PBT exhibit superior mechanical strength. The amorphous regions have a glass transition temperature of about 45°C and is responsible for excellent drawability [46]. The density of PBT is 1.31 g·cm^{-3} (ISO 1183) [42] while the density in the amorphous state was found in the range from 1.265 g·cm^{-3} to 1.268 g·cm^{-3} [43]. Generally the crystallinity degree is around 35% [47] and the transition from a melt to a solid results in a moderate shrinkage.

PBT is made of a more expensive raw material in comparison to PET (1,4-butanediol vs. ethylene glycol), thus it is manufactured on a smaller scale than PET. Furthermore, PBT has slightly poorer mechanical properties than PET. However, it offers benefits as compared to PET such as faster crystallization kinetics, lower processing temperature, which results in a smaller susceptibility to hydrolytic degradation [46].

Commercial production of PBT is based on a reaction of 1,4-butandiol (**BD**) with dimethyl terephthalate (DMT) or terephthalic acid in the presence of a transesterification catalyst. Generally polycondensation theory calls for careful stoichiometric balance, but industrial manufacture of PBT involves initial excess of **BD**, which is later removed and recycled in the polycondensation process [46].

The commercial success of PBT is ascribed to its fast crystallization. Ability to rapid crystallization allows injection-molding with fast cycle times and higher productivity for molders. Due to complete crystallization during molding better dimensional stability of the molded part is achieved, thus higher production yields is obtained and it outweighs PBT drawbacks in most injection-molding applications. For other methods of shaping plastics, which requires orientation during processing, the slower-crystallizing PET is preferred. Moreover, thin PBT films are less transparent than PET products [46].

Due to absorption of water, flawless processing of PBT requires drying, for instance before molding. Otherwise the presence of absorbed water during melting causes PBT hydrolysis and the loss of viscosity and a decrease of molecular weight. Chain cleavage has a detrimental effect on the mechanical properties of PBT. Loss of molecular weight during processing is the most common problem associated with PBT molding [46].

PBT is used in various applications. For instance it has been found useful in textile applications due to its drawing ability for improved sportswear, and in apparel, underwear and hosiery. Furthermore, it is also used for swim wear since it has high tenacity, stability and good resistance to chlorine. The combination of dimensional stability, tensile strength, increased flexibility and fast crystallization rate guaranties its application as engineering plastics. Moreover, PBT is used in drapery hardware, pen barrels, heavy duty zippers, hair dryers, pocket calculators, iron and toaster housings and food processor blades [38].

1.2 Copolyesters

Linear aliphatic polyesters have ability to crystallization. However, they have low melting temperature (from ambient to about 70°C) and low T_g values. The T_m and the T_g values are risen by introducing a benzene ring into the polymer chain [9]. Moreover, the mechanical properties are significantly improved. Thus, polymers which contain more than one type of repeat unit were introduced and known as copolyesters. In the most common case only two types of repeat unit are present (a binary copolymer). Copolymers with three (terpolymer) or more different units are synthesized more rarely. In the case of biodegradable copolyesters several various units are present [9].

Copolymers classification is done by the way in which the repeating units are arranged in the polymer molecular chains. The most common type of synthetic polymer is a random copolymer. The main feature of random copolyesters is that the different repeat units are arranged in a random manner. Polymer units are arranged exchangeably in an alternating copolymer. Units arrangement distinguishes also block copolymer, in which long sequences of repeating units are present.

The aim of developing aliphatic-aromatic copolyesters (AAC) is to combine good material properties with biodegradability. Synthetic copolymers preparation is based on copolymerization. Therefore, preparation of random copolymers involves simultaneous polymerization of a mixture of comonomers. The copolymer structure is controlled, during preparation, by the amounts and reactivity ratios of the comonomers used. The preparation of a type of copolymers other than random demands more specialized methods of preparation [9].

Aliphatic-aromatic copolyesters promotion for biodegradable applications has been started by major polyester producers. Ecoflex®, which is a copolyester of butanediol, adipic acid, and dimethyl terephthalate, is manufactured by BASF. However, it has its equivalent by Eastman called Eastar Bio Copolyester 14766 [10].

In the literature several aliphatic-aromatic copolyesters are described such as: random poly(butylene adipate-*co*-terephthalate) (PBAT) [1, 29, 34, 48, 49], random poly(butylene succinate-*co*-terephthalate) (PBST) [7], random poly(butylene adipate-*co*-succinate-*co*-tere- phthalate) (PBAST) [4, 6], and copolymer of random poly(butylene adipate-*co*-succinate-*co*-glutarate) - with blocks of poly(butylene terephthalate) (PBASG-**b**-PBT) [5].

The most well-known binary copolyesters are PBST and PBAT. Li [7] demonstrated that molecular weights of synthesized PBST become to fall down with the increase of **BT** comonomer content in the composition leading to a viscosity decrease. With the increase of **BT** units, the phase transition temperatures (T_g, T_m, T_c) and decomposition temperature (T_d) of PBST [50] and PBAT [29, 34] copolyesters tend to increase. This is due to the fact that aromatic repeating units of **BT** are more stable and more rigid than the aliphatic repeating units of **BA** or **BS**. The increase of **BT** comonomer fraction causes a gradual shift from monoclinic crystal structure (characteristic for PBS or PBA) to triclinic one (characteristic for PBT). The transition of PBST [7, 51] and PBAT [34] crystal lattice was observed for aromatic units content at around 30%. As to the tensile properties, the higher content of **BT** units, the higher initial modulus the PBST sample is displayed. The elongation to break decreases with the increase of **BT** *co*-units [52]. In the case of PBAT, Shi [49] presented that the triclinic α-form of **BT** crystals is able to transform into β-form for strain around 43%, whereas the β-form of PBT homopolymer was noticed when the strain reached 30%. With further increase of tensile deformation, the β-form dominated when tensile strain was above 63%. Moreover, the β-form reversed to α-form when a sample was relaxed.

The knowledge about the binary copolyester gave a possibility to develop ternary copolyester such as PBAST. Kang [4] conducted the studies about developing random PBAST synthesis. The higher the mixing time was applied the more random structure of the copolyester was obtained. However, PBT content caused fluctuation of randomness. It was also reported that the increase of PBT content in composition increases the average aromatic block length. The viscosities of prepolymers (PBAS and PBT) were higher than PBAST copolymer viscosity. It was also observed that the viscosity was influenced by the PBT content, mixing time and temperature. However, only increase of aromatic units content caused the density rise. For copolyesters without mixing Kang [4] observed multimelting, which disappeared with the increase of mixing time and PBT content. Obtaining rather a blend than a copolymer without mixing was also supported by the coexistence of two components in the X-ray pattern. Although it is worth to underline that copolyester composition affects the crystal structure. Copolymers with higher aliphatic unit content exhibit monoclinic crystal structure (characteristic for aliphatic homopolymers), whilst copolyesters with overweight of **BT** units possess triclinic crystal lattice. So, it was suggested that when a rich component crystallize, the poor component is excluded completely from the crystal formation. Only amorphous halo was found for copolyesters, which composition contained 40% of **BT** units. Generally the tear strength of PBAST was much lower as compared to pure PBAS. Shi [6] reported about random PBAST copolyester, which due to average block length of aromatic units below 3, was biodegradable also in the aromatic part. PBAST exhibited one broad melting peak with a maximum at around 115°C. Moreover, it was presented that WAXS pattern of PBAST is similar to PBT α-form pattern. Shi [6] studied the mechanical properties, which revealed rubber-like behavior of PBAST. The presence of aliphatic units caused a development of elastomeric properties and a decrease of modulus and tensile strength of PBAST as compared to PBT. Shi [6] did not observed the transition from α to β form of crystal up to 45% of strain, whereas the β-form of PBT homopolymer was noticed when strain reached 30%.

There are also known examples of copolyesters with more than three comonomers, for instance PBASGT. Park [5] prepared block copolyester PBASG-**b**-PBT by molten-state processing for various times. It was presented that mixing time and content of PBT in copolyester composition influence transestrefication degree. However, copolyester randomness depended on mixing time independently of the aromatic polyester content. Moreover, an increase of mixing time caused gradual decrease of melting temperature. The melting point is shifted to higher values together with increasing amount of aromatic units. Additionally the heat of fusion became higher. Furthermore, synthesized copolyesters with aromatic unit content above 40% exhibited 2θ wide angle X-ray scattering (WAXS) pattern characteristic for triclinic crystal system of PBT.

It is worth to underline that most of the above mentioned publications concern random copolymers. The most characteristic exception is the last one [5]. Owing to the presence of PBT blocks the PBASG-**b**-PBT copolymer exhibits strong crystallization ability but its susceptibility to biodegradation is strongly reduced [1]. It can be also noticed that all characterization showed gradual changes of properties together with the variation in composition independently of the amount of comonomers. Summarizing it is possible to obtain aliphatic-aromatic copolyesters with desired characteristics including biodegradability, required mechanical and thermal properties by manipulating the composition of monomers and assuring the randomness of their distribution along macromolecular chains.

1.3 Polymer crystallization

Just like in substances of low molecular weight the crystallization of polymers is controlled by nucleation. First a nucleus is created and then the crystal grow. Polymers crystallize usually in the form of lamellar crystals of transverse dimensions large in comparison to the thickness being of the order of 10-20 nm. Crystallization of polymers usually takes place with folding of macromolecular chain. Chains can participate in a single lamella or can be span over several adjacent crystals. Single crystals of polymers may be formed by crystallization from dilute solutions, while crystallization from the melt takes place generally in the form of polycrystalline aggregates-spherulites formed by radiating from a nucleus via non-crystallographic branching at small angles. Spherulite grows in all directions, until it impinges with the other spherulites. Within spherulite adjacent crystals are separated by amorphous phase containing fragments of chains linking adjacent crystals, chain loops, and chain ends. All additives are exuded into amorphous layers. In the amorphous phase there are also chain defects, branching of a chain, and those parts that do not build into the crystal as a result of a different chemical structure or configuration. The content of the crystalline phase of the polymer is usually characterized by a degree of crystallinity.

1.3.1 Nucleation of crystallization

As it was shown, the growth of crystals and finally crystalline aggregates starts on a surface of previously formed nucleus. Thus, in this Section the nucleation is considered.

Nuclei formation requires overcoming a barrier in the free energy. Density fluctuations in the undercooled phase can overcome this barrier and proceed to a stage of stable, ordered regions of a critical size. The formation process is called primary nucleation and the nuclei are described as primary. Hence, nucleation may be defined as the process by which a new phase is initiated within an existing phase [53]. The changes of enthalpy $\Delta\, G$ connected with nuclei formation are caused by changes related to the increase of ordering $\Delta\, G_c$ and changes connected with surface formation $\Sigma\sigma S$, which are related witch each other in the following way:

$$\Delta G = \Delta G_c + \Sigma\sigma S \tag{1.1}$$

where S is a surface and σ is a surface energy.

The $\Sigma\sigma S$ part depends on crystal surface properties and it is positive, whereas $\Delta\, G_c$ is tied with nuclei volume and it is negative below the melting temperature.

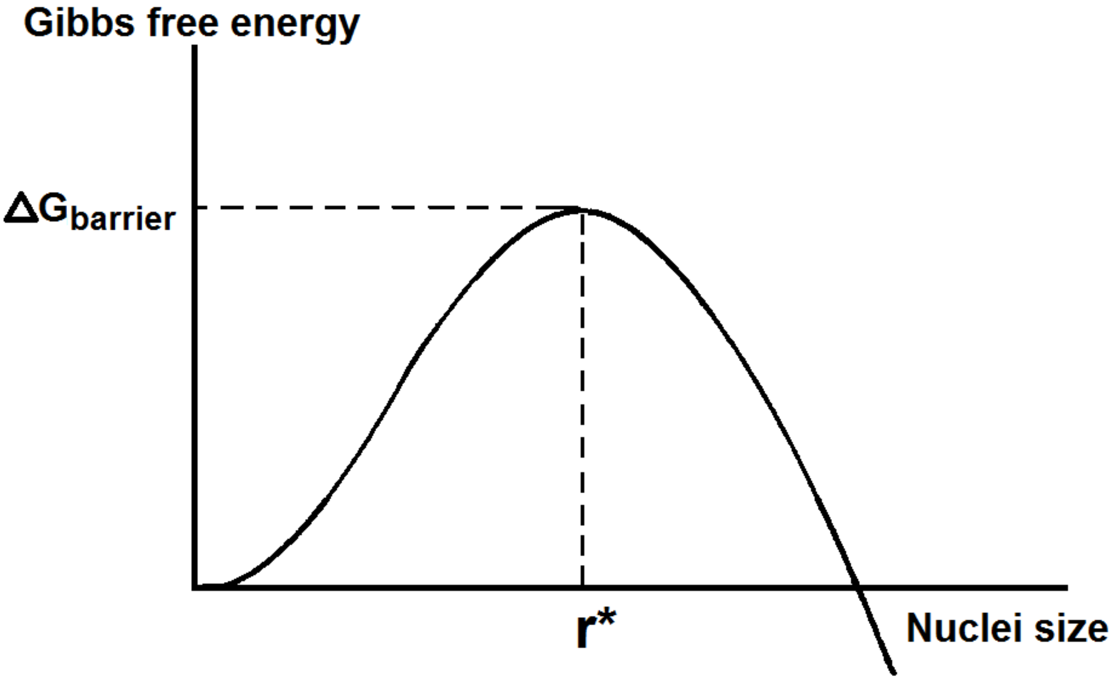

Figure 1.4: Illustration of ΔG changes versus nuclei sizes r.

As Figure 1.4 shows, at the beginning $\Delta\, G$ is positive and increases and subsequently it decreases. Nuclei, which size is equal to r^* are called critical nuclei. This size is related to the maximum value of the $\Delta\, G$. Nuclei smaller than r^* are unstable and they are named subcritical or embryonic nuclei. Nuclei which exceed this critical dimension are called supercritical when $\Delta\, G > 0$ and are stable nuclei because those nuclei can grow in size with $\Delta\, G < 0$. The maximum value of $\Delta\, G$ represents the free energy barrier, which must be overcome to develop the new stable phase [53]. Summarizing, nucleation is the process of nuclei formation, which possess critical dimension and is stable enough to initiate the growth of crystals. The height of this barrier is related to the mobility of the segments of the macromolecules and viscosity of the medium.

The likelihood of an embryo formation in temperature, T, is described by Boltzmann distribution. Turnbull and Fisher [54] proposed an Equation describing the rate of nucleation per unit volume in a supercooled melt in the form of:

$$I = I_o exp\left[\frac{(-\Delta\, G^* - \Delta\, G_\eta)}{kT}\right] \tag{1.2}$$

where: $\Delta\, G_\eta$ - activation energy for diffusion of crystallizing segments through phase boundary, $I_o = NKT/h$, N - number of not crystallized segments that may be involved in nucleation in a single step, k - Boltzmann's constant, h - Planck's constant.

In the case of polymer crystallization from the melt, it is assumed [55] that the temperature ΔG_η dependence can be approximated by the activation energy of viscous flow and the temperature of the polymer present in the form of WLF Equation named after the names of the authors: Williams, Landel and Ferry [55, 56]:

$$\frac{\Delta G_\eta}{kT} = \frac{U}{R(T - T_\infty)} \tag{1.3}$$

where: U - activation energy for molecular motion in the polymer melt, R - gas constant, T_∞ - temperature below which viscosity is infinite. At this temperature the required segmental motion becomes infinitesimally slow. It is understood that $T_\infty = T_g - 51.6$ K, where T_g is the transition temperature of the polymer into the glassy state.

At high temperatures ΔG_η is almost constant, but increases rapidly when the temperature is approaching the T_g.

Generally, there are others types of nucleation, which can be distinguished. The first one, called molecular nucleation, is the incorporation of a molecule into the crystal. It can occur in every phase of the nucleation. Secondary nucleation determine formation of new layer on a polymer crystal, whilst tertiary nucleation is addressed to the macromolecular segments attachment to growing crystal edges [57].

Although, other classifications of nucleation are also known. For instance, the time dependency of the nucleation process determines thermal and athermal nucleation. When formation of all crystals starts simultaneously then it is characterized as athermal nucleation, whereas in a contrary case it is thermal. The thermal or athermal character of the nucleation can be investigated by polarized light microscope. When the spherulites boundaries are bent the spherulites started the growth at different time, but when they are planar or straight they were formed simultaneously.

Nucleation of polymers is a complex phenomenon which depends on the temperature, time and thermal history of a polymer. The following types of primary nucleation can be distinguished based on the type of material involved: homogeneous - without the involvement of foreign surfaces, heterogeneous - on the surfaces of foreign bodies and self-seeding - connected with crystals or fragments thereof, chemically identical with crystallizing polymer that survived the previous dissolution or melting [57].

Nevertheless, all of those nucleation are a kind of primary nucleation.

Homogeneous nucleation

Homogeneous nucleation occurs when the nuclei are formed in a chemically homogeneous material containing no foreign surfaces. Usually, the homogeneous nuclei are generated at a large undercooling, due to a big free energy barrier to overcome, which is proportional to $1/(\Delta T)^2$. The homogeneous nucleation is characterized by the nucleation rate, thus it is always thermal [57]. In practice true homogeneous nucleation is rare because usually heterogeneous nuclei that are active at higher melt temperature are present and crystallization starts on them. The course of primary nucleation was first demonstrated by Burns and Turnbull [58] and by Koutsky, Walton and Baer [59] employing the droplet technique developed originally by Vonnegut for tin and water droplets [60]. The method relies on a dispersion of crystallizing material into plenty of small droplets embedded in another inert medium. The number of droplets must be larger than the number of heterogeneous nuclei so, a fraction of droplets would not contain heterogeneous nuclei and they can crystallize only by forming homogeneous nuclei. The lack of interphase influence on the nucleation process is also required.

Another way of approaching homogeneous nucleation is by fast quenching of a thin film. In this way heterogeneous nuclei would not have sufficient time to grow large and a fraction of a polymer may reach the temperature of strong activation of homogeneous nucleation without being crystallized [61].

The third possibility to observe homogeneous nucleation is in the case of block copolymers showing the microphase separation. The following conditions are important for observing homogeneous nucleation: high purity of the synthesis, small size of the microdomains, presence of the inert interphase [62].

In the case of the crystallization of polymers mostly cuboidal shaped embryos are assumed with a length l and a square base of side a. Assuming that the embryo surfaces lying in planes parallel to the axis of the upright portions of the macromolecules have a free surface energy σ, and those lying in planes perpendicular to the axis have the energy σ_e, free energy change associated with the formation of the embryo of l and a sizes may be expressed:

$$\Delta G = -a^2 l \Delta g_f + 4al\sigma + 2a^2\sigma_e \tag{1.4}$$

where: Δg_f - free enthalpy of fusion of the crystalline phase.

During the crystallization of the molten polymer, at about 50 K of supercooling the volume of a homogeneous nucleus is about 10 nm^3 while macromolecule having a weight of 60 to 6000 kg·mol^{-1} will occupy the volume of approx. 100 - 10000 nm^3 [63]. Therefore, only a portion of the macromolecule or small fragments of several macromolecules are sufficient to create a nucleus. In the first case the macromolecule has to fold, while in the second case, the formation of micelle-type embryo is preferred, as shown in Figure 1.5.

In the case of the folded chain embryo surface perpendicular to the axis of the chain is the plane containing the folds of macromolecules thus σ_e is associated with the folding of the single chain. For PE σ_e surface comprising folds is of order of 9·10^{-6} J·cm^{-2} [64], while the energy of the projecting surface of the micelles with unfolded chains was estimated to be 28·10^{-6} J·cm^{-2} [65]. Thus, the folding of the chain is energetically favorable.

From the Equation 1.4 the critical dimensions of the embryo can be derived as well as the change in free energy for creating the homogeneous nucleus of a critical size:

$$l^* = \frac{4\sigma_e}{\Delta g_f} \tag{1.5}$$

$$a^* = \frac{4\sigma}{\Delta g_f} \tag{1.6}$$

$$\Delta G^* = \frac{32\sigma^2\sigma_e}{(\Delta g_f)^2} \tag{1.7}$$

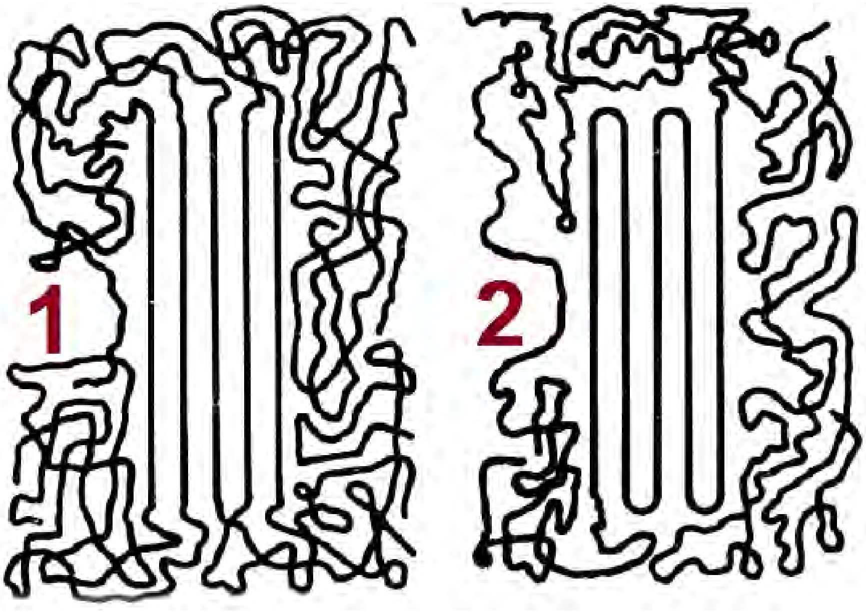

Figure 1.5: Schematic representation of the seed crystal **1** - micelle type, **2** - macromolecule formed by folding [63].

Free enthalpy, Δg_f, can be represented as:

$$\Delta g_f = \Delta h_f - T \Delta S_f \tag{1.8}$$

It can be assumed that at the temperatures much lower than the melting point the change of entropy, ΔS_f, is independent of the temperature and therefore equal to the change in entropy at the transformation occurring at the melting point [63]:

$$\Delta S_f = \frac{\Delta h_f}{T_m^0} \tag{1.9}$$

T_m^0 in the Expression 1.9 represents the equilibrium melting temperature of the polymer - i.e. a melting point of a perfect crystal structure possessing infinite dimensions. From the Equations 1.8 and 1.9 the Relationship follows:

$$\Delta g_f = \frac{\Delta h_f \Delta T}{T_m^0} \tag{1.10}$$

where: $\Delta T = T_m^0 - T$ is supercooling. The Equation 1.10 can only be used when considering small undercooling. Hoffman and Weeks [66] proposed the modification allowing the use Equation 1.10 also at the larger undercooling:

$$\Delta g_f = \left[\frac{\Delta h_f \Delta T}{T_m^0} \right] f \tag{1.11}$$

where the factor f equal to $2T/(T+T_m^0)$, results from the dependence of Δh_f on the temperature. Finally, the formation free enthalpy of the homogeneous cuboidal embryo with critical dimensions is described by the Relationship:

$$\Delta G^* = \frac{32\sigma^2\sigma_e(T_m^0)^2}{(\Delta h_f f \Delta T)^2} \tag{1.12}$$

Thus, the rate of homogeneous nucleation can be described by the Equation:

$$I = I_o exp\left[\frac{-U^*}{R(T-T_\infty)}\right] exp\left[\frac{-32\sigma^2\sigma_e(T_m^0)^2}{(\Delta h_f f \Delta T)^2}\right] \tag{1.13}$$

The frequency of homogeneous nucleation depends strongly on the crystallization temperature, primarily by ΔG^* proportional to $(1/\Delta T^2)$. The large energy barrier that meets homogeneous nucleation causes the homogeneous nucleation to become active only at high undercooling.

Heterogeneous nucleation

In the presence of foreign surfaces the nuclei critical size is decreased and the heterogeneous nucleation occurs [57]. The free energy barrier is proportional to $1/(\Delta T)$ as it will be later shown. Hence, heterogeneous nucleation can happen at smaller undercooling in contrary to homogeneous nucleation. In most cases heterogeneous nucleation is athermal, but it may be also thermal [57]. The foreign surface nucleating crystallization can be even the DSC pan.

Heterogeneous nucleation differs from the homogeneous nucleation in that the nuclei are formed in contact with foreign surfaces. Assuming a cuboidal shape of the embryo, which one wall contacts with a flat surface of a foreign surface the following Equations describing the size and the formation enthalpy of the heterogeneous critical embryo can be derived:

$$l^* = \frac{4\sigma_e}{\Delta g_f} \tag{1.14}$$

$$a^* = \frac{4\sigma}{\Delta g_f} \tag{1.15}$$

$$b^* = \frac{2\Delta\sigma}{\Delta g_f} \tag{1.16}$$

$$\Delta G^* = \frac{16\sigma\sigma_e\Delta\sigma}{(\Delta g_f)^2} = \frac{16\sigma\sigma_e\Delta\sigma(T_m^0)^2}{(\Delta h_f f \Delta T)^2} \tag{1.17}$$

where: $\Delta\sigma = \sigma + \sigma_{cs} - \sigma_{ms}$; σ_{cs} i σ_{ms} are surface energies of the contacting surface of the crystal - substrate and melted polymer-substrate. When $\sigma_{cs} - \sigma_{ms} < \sigma$ the lowering of the formation free enthalpy of the critical embryo, ΔG^* occurs and lowering of the critical size of the embryo [67, 68, 69]. Lowering the formation free enthalpy of the embryo, ΔG^*, makes the heterogeneous nucleation easier and it occurs at much lower undercooling than homogeneous nucleation. As a result the crystallization of most of polymers proceeds at low and moderate undercooling originated on heterogeneous germs.

At sufficiently large undercooling or small values of $\Delta\sigma$ the size of the embryo, b^*, approaches monolayer thickness, b_0. Equation 1.17 then takes the form:

$$\Delta G^* = \frac{4b_0\sigma\sigma_e T_m^0}{\Delta h_f f \Delta T - \frac{\Delta\sigma T_m^0}{b_0}} \tag{1.18}$$

From Equation 1.18 it follows that the height of the energy barrier is not proportional to the $1/(\Delta T)^2$ but to $1/\Delta T$.

If nucleation does not occur on a flat surface of a substrate, but near its irregularities, e.g. at a step, the free energy of formation of the embryo is:

$$\Delta G^* = \frac{8(\Delta\sigma)^2\sigma_e}{(\Delta g_f)^2} = \frac{8(\Delta\sigma)^2\sigma_e(T_m^0)^2}{(\Delta h_f f \Delta T)^2} \tag{1.19}$$

and critical dimensions are as follows:

$$l^* = \frac{4\sigma_e}{\Delta g_f} \tag{1.20}$$

$$a^* = b^* = \frac{2\Delta\sigma}{\Delta g_f} \tag{1.21}$$

Also in this case, for small values of $\Delta\sigma$ or sufficiently high undercooling the critical lateral dimensions of the embryo can reach values close to a_0 and b_0 and ΔG^* is practically independent of supercooling. This means that embryos may occur instantaneously, upon reaching the crystallization temperature of the system.

The crystallization of polymers from melt could be enhanced in the region of the temperature where heterogeneous nucleation is observed by adding some extra heterogeneous nuclei. The interest in such experiments was stimulated by industrial efforts to decrease the size of spherulites for improvement of optical and mechanical properties. By adding finely subdivided foreign material it was shown that solids, liquids, and even gas bubbles are able to nucleate spherulites. Generally nucleating agents are divided on reactive and non-reactive one. Chemical nucleation occurs by ionic end groups formation obtained by the reaction of the nucleating agent with the polymer chain. In the case of thermoplastic polyesters, alkali metal salts of organic acids (e.g. sodium benzoate) have been reported to be very effective [70]. Unfortunately, the molecular weight was also affected. Thus, the lack of degradation and efficient nucleation caused a wide application of non-reactive nucleating agents.

Heterogeneous nucleating agents include non-reactive, non-melting nucleants, such as mica or talc [71]. However, sometime the impurities added accidentally also lead to heterogeneous nucleation. Generally, incorporation of nucleating agents increases nonisothermal crystallization peak temperature, and therefore crystallinity degree. Simultaneously, the crystallization is accelerated and the spherulite sizes are reduced. The high crystallization temperature is advantageous for processing. Moreover, the larger crystallinity of a polymer is reflected in an increased elastic modulus and yield stress, whereas the decreased grain size is beneficial for toughness and ultimate mechanical properties.

The importance of epitaxy in the heterogeneous nucleation was also pointed out. In general, Royer [72] determined the rules that govern epitaxial crystallization. The main one states that there must be a dimensional match between the crystal lattice of the substrate and the deposit in the contact plane. The mismatch should be below 15% or even below 10%. Oriented crystal growth is characteristic for epitaxial crystallization. There are three types of epitaxial crystallization distinguished. Graphoepitaxy describes an oriented growth of crystal caused by the surface topography of the substrate. In this process no clear-cut lattice is required. Soft epitaxy is characterized by oriented growth on a substrate when no clear lattice matching is present. In contrary, hard epitaxy requires clear-cut lattice and dimensional match between substrate and deposit [73]. Establishing of the exact substrate/deposit relationship is not easy task. During epitaxial crystallization one specific crystal plane parallel to the polymer chain axis is selected as the contact plane. Hence, thin polymer film with single crystal orientation for e.g. optoelectronic application can be achieved.

Nucleating agents can be divided into inorganic and organic or particulate and soluble. Nucleation efficiency depends on the combination of epitaxy quality and dispersion quality. However, in practice also factors including toxicity, thermal stability, discoloration and price must be taken into account. Low prices caused that inorganic nucleating fillers become commonly used. Beside of the mechanical properties improvement minerals can leads to flame retardancy, shrinkage reduction or even to induce formation of another crystallographic forms, e.g. β-crystalline form in polypropylene [74]. Minerals nucleation efficiency depends on concentration, filler treatment, crystallographic plane exposed (different for ground material and precipitated), particle size, distribution and particle shape. Due to the particle shape the classification of fillers is made [75]. Fibers and needles are included to one-dimensional shapes, flakes and platelets are two-dimensional and particulate, spheres and beads are included to three-dimensional shapes. Moreover, the resulting properties of polymer treated with heterogeneous nuclei are not only the result of a combination between polymer and nucleating agent. They are affected also by processing method and processing conditions [76].

Self-nucleation

The nucleation of macromolecular melt or solution by polymer own crystals grown previously is defined as the self-nucleation (SN). The SN can be detected for instance by differential scanning calorimetry when a polymer is heated just above its melting point and is kept at a given temperature (denoted T_s) for a short time then the peak crystallization temperature shifts to higher temperatures during cooling down. The shift of peak crystallization temperature is caused by the preserved nuclei, which help to initiate the crystallization process at a higher temperature [77, 78]. The term melt memory characterizes a polymer sample, which is considered to be molten, when in fact retains somehow a partial memory of its former crystalline structure and it may be closely related to the existence of precursors [79].

Fillon et al. [80] divided the melt temperature (T_s) range into three domains based on nucleation activity. The temperature range where complete melting occurs, defined by Fillon et al. as Domain I, is usually much higher than the peak melting temperature (T_m) of a polymer. Domain II or SN domain is observed at lower T_s values. It is characterized by an exponential decrease in nucleation density with increasing T_s and by a corresponding shift of the peak crystallization temperature T_c to lower values upon cooling from higher T_s. According to Fillon et al., Domain II corresponds to T_s temperatures that are high enough to melt almost all crystals in the sample, but low enough to leave crystal self-nuclei or seeds that can nucleate the polymer upon subsequent cooling from T_s. It has been shown for a range of crystallizable diblock and triblock copolymers that if a particular phase is segregated into a large number of individual microdomains, Domain II usually disappears and a direct transition from D_I to D_{III} is being observed [62, 81, 82, 83]. Domain III is located at even lower T_s where partial melting occurs and annealing takes place.

In the case of copolymers the existence of D_{II} determine the crystallization process of given material. It has been shown in a wide range of crystallizable diblock and triblock copolymers that if a particular phase is isolated and crystallizes in a large number of individual microdomains (like spheres or cylinders for instance) Domain II usually disappears and a direct transition from D_I to D_{III} has been observed [62, 81, 82, 83]. However, it was shown by Lorenzo et al. [78] that D_{II} is a transient phenomenon for homopolymers, which can even disappear if enough time at T_s is allowed. The last range of temperature, called as Domain III, occurs at lower T_s temperatures where partial melting occurs and annealing takes place.

1.3.2 Secondary nucleation and polymer crystal growth

In the following Subsection, the well-known and applied theory about the polymeric crystals growth from the melt developed by Lauritzen and Hoffman (LH) [55], will be discussed. This theory predicts the growth rate and initial lamellar thickness and that the growth advances at significant undercoolings. The theory states that the surface nucleus starts by incorporation of a polymer segment or set of segments from solution or undercooled melt to the crystal surface, as it is shown in Figure 1.6.

Attaching the first stem on the already formed crystal is the most difficult due to a high free energy barrier accompanied to the process. In the new stem affiliation, two steps can be distinguished. Firstly, a random coiled chain molecule is forced to lose its configuration due to the mers presence on the flat surface. It must develop its structure, therefore the entropy is reduced. This nucleation stage determines the rate of the whole process. Subsequently, the short sections are rapidly attached to the surface to form afterwards a crystalline stem of l_g^* length. The adsorbed chain is surrounded on either side by a niche. Simultaneously the bulk heat and free energy of fusion is released [64]. The molecule then folds back on itself and starts to crystallize in a position adjoining the first stem. The adjacent position is the most probable site for reentry after folding.

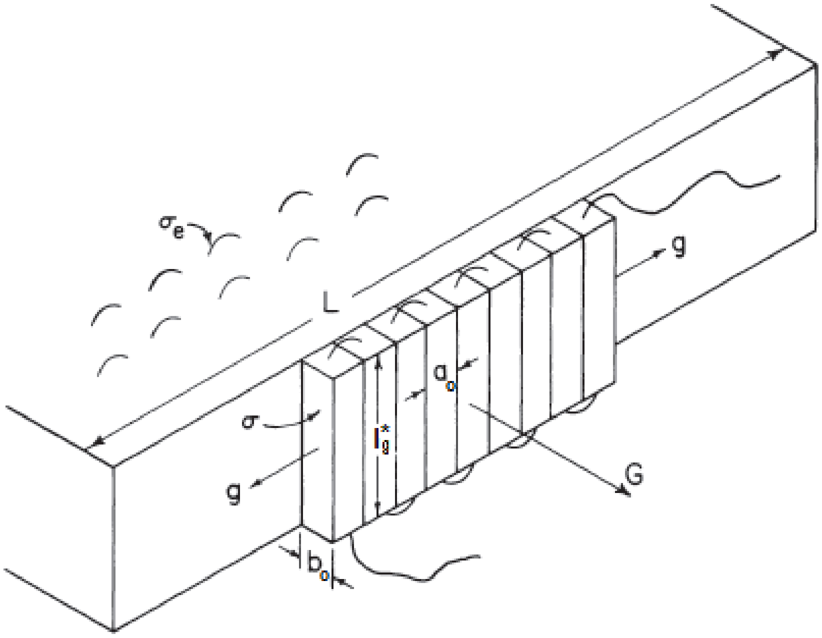

Figure 1.6: Schematic model for surface nucleation and growth [55]. Physical relationship showing substrate of length L, substrate completion rate g, fold surface free energy σ_e, lateral surface free energy σ, initial lamellar thickness l_g^*, a_o width of one molecular chain stem, b_o thickness of one molecular chain stem and growth rate G.

By repeating this act the nucleation surface spreads in the g direction with the rate g. Attachment of new stems is preferred at the niche, each new stem added decreases the free energy. When the free energy ΔG becomes negative the embryo on the surface of the crystal turns to a stable nucleus. Further process is a filling the layer on the surface of the crystal with the rate g. The attachment of new stems starts in the niche and continues until the completion of the layer [55]. The growth rate (G) is perpendicular to the layer filling rate g and in fact it is the number of layers filled in a time unit. Thus the G is reliant from the nucleation rate i and the substrate completion rate g. Depending on the undercooling the relation between i and g changes. It is caused by the fact the decrease of temperature leads to an increase of i whilst g is nearly independent of temperature.

Crystallization processes become more complicated at higher undercooling for which the nucleation rate and density significantly increases. It appeared that new nuclei can be formed on non-completed layers. The change is rather abrupt and it is reflected in the lower slope of growth rate G.

The original LH theory was based on the research on crystallization of polyethylene (PE) and only two regions were observed, denoted as Regime I in which a layer was completed before another nucleation attempt, and Regime II in which nucleation attempts were occurring before the layer was completed. However, a positive jump in the growth rate G slope versus temperature was noticed by Pelzbauer and Galeski [85] for poly(methylene oxide). Based on that observation, that was later confirmed for other polymers, a third region of crystallization was defined. Regime III of crystallization is characterized by very dense secondary nucleation in such a way that the layer build-up is by secondary nucleation only. Thus, the LH theory was extended and the number of regimes was increased. Nowadays the LH theory contain three regimes, which are schematically illustrated in Figure 1.7. Those regimes are distinguished by the relation of secondary nuclei rate i and surface spreading rate g. At high temperature, Regime I (Fig. 1.7) occurs. The i is much smaller than g. Subsequent nucleation event starts after fulfillment of the entire layer. The growth rate is then proportional to i, as follows:

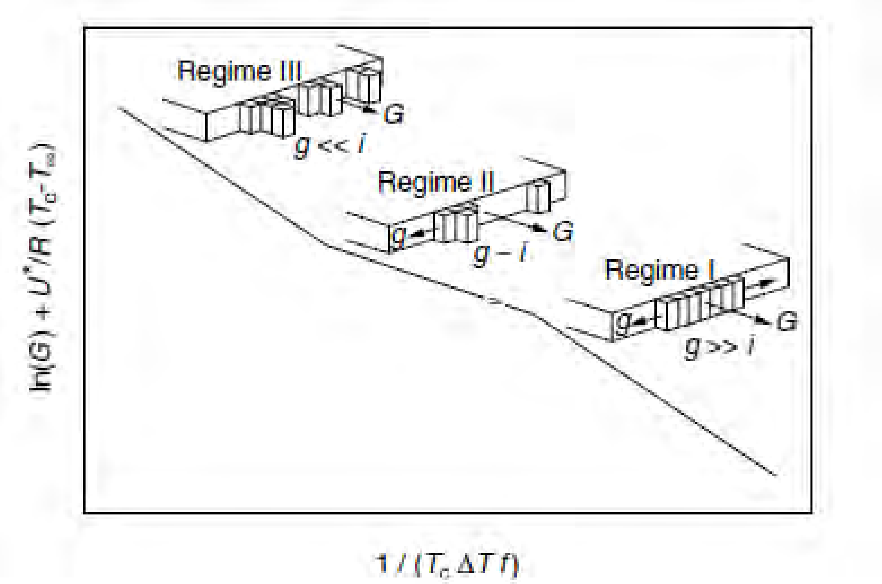

Figure 1.7: Scheme of regime analyses [86].

$$G_I = b_o i L \tag{1.22}$$

where L is the width of the base crystal and b_o is the thickness of one molecular chain stem. Crystals formed in Regime I are formed by many regular and tight foldings. Not many macromolecules linking neighboring crystals cause that the material is brittle and possess poor mechanical properties. With the decrease of crystallization temperature the i is increasing and it is almost equal to g. Thus new nuclei are appearing before completion of the whole layer. The G depends on both i and g in the following way:

$$G_{II} = b_o(2ig)^{1/2}. \tag{1.23}$$

Crystallization in Regime II (Fig. 1.7) leads to the formation less amount of folding, thus, more molecules join the neighboring crystals and the material becomes less brittle.

In the case of very large undercooling, many nuclei are formed on the surface leaving no time for regular spreading of a layer on the crystal surface, thus, the i is much higher than g. In such a case one macromolecule is often attached to various crystals. The growth rate is again proportional only to i:

$$G_{III} = b_o i L' \tag{1.24}$$

where L' is the niche average width in between neighboring stems on the crystal surface. Crystals formed in Regime III (Fig. 1.7) possess tangled chains and many macromolecules links neighboring lamellae. Furthermore, there are not many foldings on the crystals surfaces. It leads to good mechanical properties of the material. Hoffman also suggested that attaching of one macromolecule in many lamella is possible in the case of polymers with high molecular weight [64]. It leads to quasi Regime III formation even when the undercooling is relatively small.

Further considerations, taking into account the height of the energy barrier that meets the nucleation of a new layer and its completion, we obtain the crystal growth rate, G, on the temperature, T:

$$G = G_0 exp\left(\frac{-Q_D}{RT}\right) exp\left(\frac{-K_g}{T\Delta Tf}\right) \tag{1.25}$$

In Equation 1.25, the first exponential factor represents the probability to overcome the activation energy barrier of transport of crystallizing element; Q_D is the activation energy of curvy-linear movements - reptation. The second exponential factor is associated with overcoming the energy barrier resulting from the relationship between the energy gain from the creation of an ordered phase and energy expenditure to produce the interface. In contrast pre-exponential factor G_0 is associated with the transport chain segments and decreases with increasing molecular weight of the polymer. The f factor is often overlooked, especially for relatively small undercooling. When the energy of activation of reptation is unknown or in the case of crystallization at high undercooling Hoffman [64, 87] proposes to use the growth rate of spherulites in a slightly modified form:

$$G = G_0 exp\left(\frac{-U}{R(T - T_g + 30K)}\right) exp\left(\frac{-K_g}{T\Delta Tf}\right) \tag{1.26}$$

were the exponential, associated with overcoming the energy barrier for the transport chain segments is derived based on WLF Equation, although Hoffman uses the value of 30 K instead of usual 51.6 K.

For a given polymer G_0 and K_g depend on the regime of crystallization. K_g dependencies are described as follows:

$$K_{g_I} = \frac{4b_0\sigma\sigma_e T_m^0}{\Delta h_f k} \tag{1.27}$$

$$K_{g_I} = 2K_{g_{II}} = K_{g_{III}} \tag{1.28}$$

The occurrence of crystallization regimes provided by theory LH has been shown experimentally for many polymers, including for HDPE, POM and iPP [85, 87, 88]. Temperature transitions between regimes are evident in the plot, where the term $lnG + QD/RT$

(or $lnG + U/R(T - T_g + 30K)$) is plotted against $(T\Delta Tf)^{-1}$, which represents Figure 1.8 for iPP of different molecular weights [89]. Such dependencies allow to determine the constants G_0 and K_g in the respective regimes crystallization. Replacement of the expression QD/RT by $U/R(T - T_g + 30K)$ leads only to minor variations in the values of K_g [85]. Although LH theory is widely accepted and used, it has failed to show the transition between regimes for polymers such as isotactic polystyrene (iPS) and PES [90]. The LH theory does not include the important role of the width relationship of the crystal growth front a characteristic distance in the definition of regimes, as is demonstrated in a number of articles by Point [91, 92]. However, in order to consider this the crystallographic unit cell symmetry must be taken into account because the width of the crystal depends on the other direction of crystal growth.

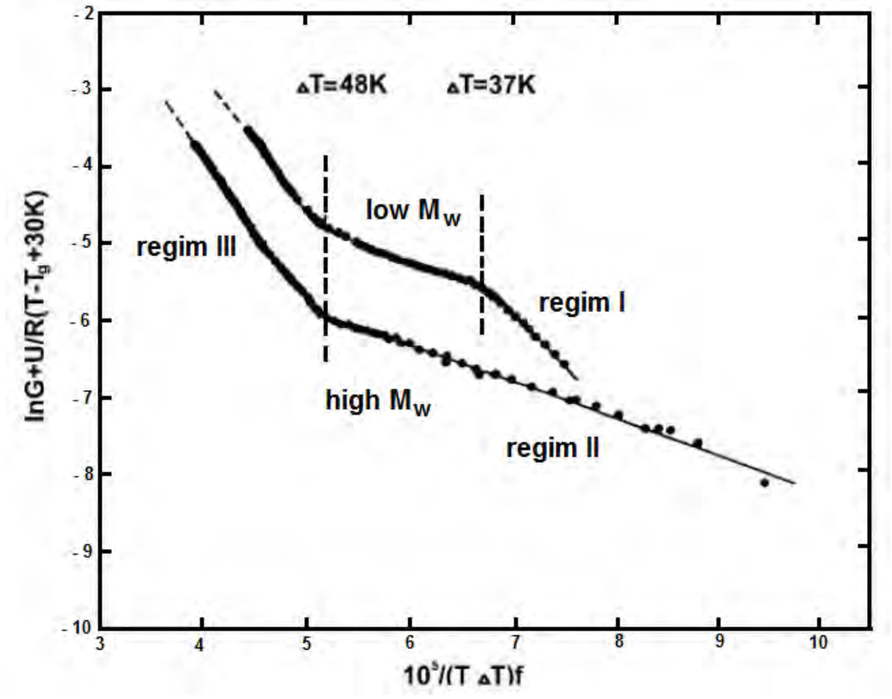

Figure 1.8: Dependence $lnG+U/R(T-T_g+30K)$ od $1/(T\Delta Tf)$ for isotactic polypropylenes with different molecular weights [89].

As far as the crystallization temperature lowering the growth rate of spherulites is increased, reaches a maximum and then decreases. Example of spherulite growth rate depending on the temperature is presented in Figure 1.9. While increasing the growth rate due to the lowering of the energy barrier crystal create a new layer, whereas the subsequent reduction of the rate is due to the restrictions on the movement of macromolecules. The maximum growth rate of spherulites can be observed only in certain polymers, for example iPS and PA [94], as rapidly crystallizing polymers cannot be achieved sufficiently large undercooling before the completion of crystallization. G passes through a maximum and then decreases for even lower crystallization temperature, as shown in

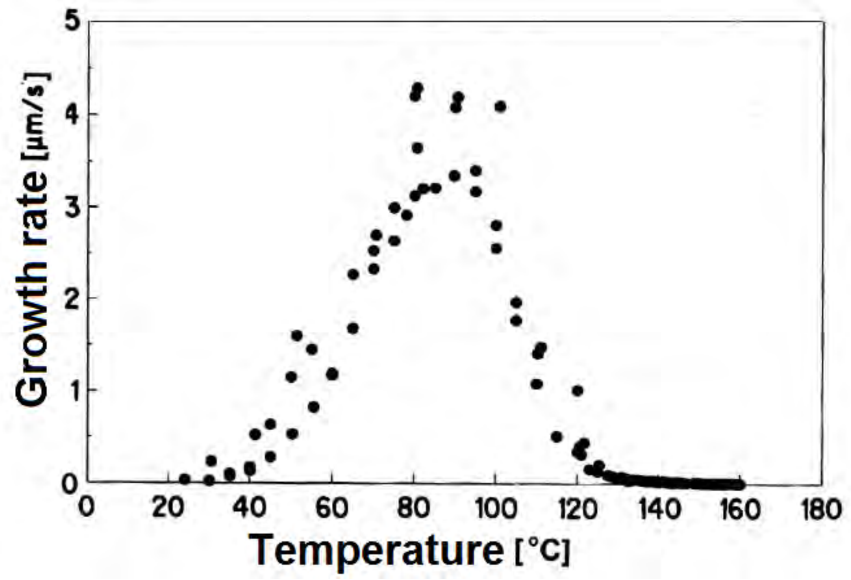

Figure 1.9: The dependence of the growth rate of spherulites of the temperature of poly(3-hydroxybutyric acid) [93].

Figure 1.9. This is due to the fact that the creation of a new layer of crystal requires overcoming a much smaller energy barrier than the creation of the original embryo, even heterogeneous. At lower temperature the transport of macromolecule fragments towards the crystallization front requires more time because of viscous obstacles.

It should be underlined that regime behavior varies from polymer to polymer [86]. Also the crystallization conditions affects the regimes. For instance high molecular weight polypropylene at atmospheric pressure exhibits Regime II and III, whereas the same material shows all regimes at 150 MPa [96]. Moreover, the reptation motion of entangled chains in the melt also control the growth rate, thus G is inversely proportional to the molecular weight. However, Hoffman presented that too high decrease of molecular weight can cause decrease of T_m^0 as well. Consequently the undercooling also decrease and the growth rate decrease too [64]. The dependence of the growth rate on crystallization temperature and molecular weight is shown in Figure 1.10.

In recent years, new theories of polymer crystallization were formulated, which postulate that a crystal growth is not a one-step process that occurs directly from the isotropic molten polymer by attaching subsequent segments of macromolecules. Based on the results of crystallization of iPP and syndiotactic polypropylene (SPP), Strobl [97] proposed multi-stage crystallization process through intermediate states, as shown Figure 1.11. In the molten polymer the intermediate mesomorphic form is formed that consists of a partially straightened chains having a density intermediate between the density of the polymer melt and the crystal density. Crystal growth starts from the attachment of a portion of the polymer chain to the layer. As time passes, the conformation of chains is further changed; getting longer fragments with ordered conformation and being arranged parallel to each other. In this way, the mesomorphic layer gradually

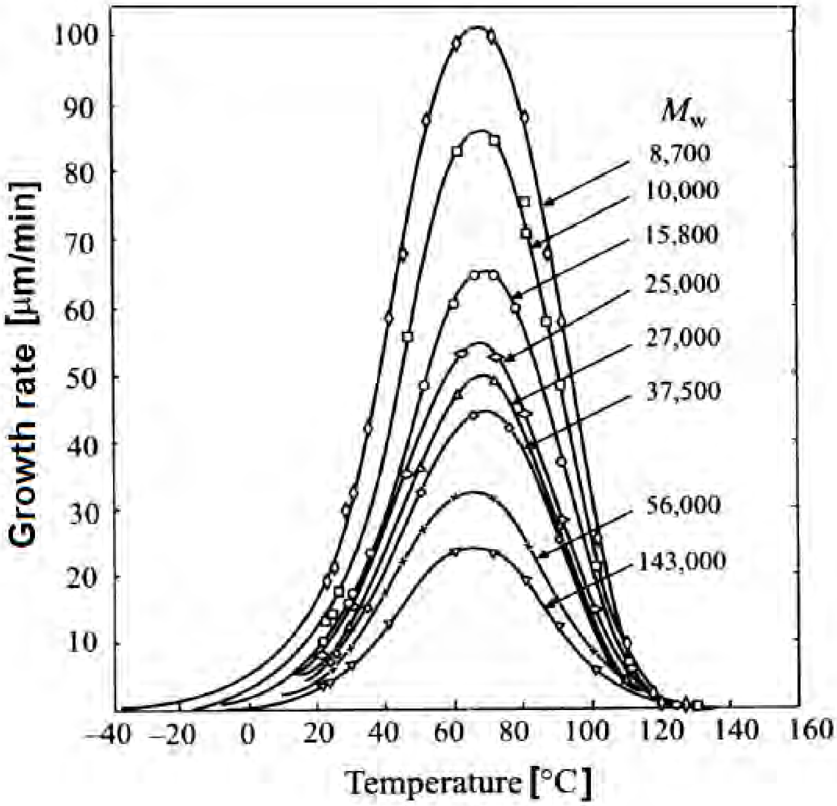

Figure 1.10: Spherulites growth rate of polysiloxane versus crystallization temperature and molecular weight [95].

increases in thickness, and the chains get closer to each other. Upon reaching a critical thickness a sudden increase in order happens and crystal is formed. Folding is then associated with a further reduction of the free enthalpy. In Figure 1.11 this step is shown

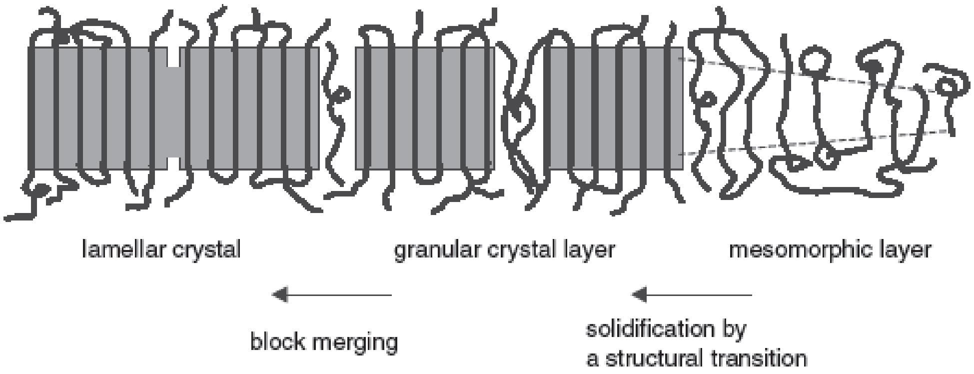

Figure 1.11: Scheme of polymer crystalline growth [98].

as combining the crystals in the larger lamellar crystal.

In a recent paper by Galeski et al. [99] it was suggested that the observation of blocky structure of lamellar polymer crystals by Strobl et al. [108] was a misinterpretaion of screw dislocations commonly present in all polymer crystals. The screw dislocations with large Burgers vectors were detected at a concentration estimated as 1-3·10^6 m^{-2}. Dislocations with low Burgers vectors most probably diffused outside the crystals due to annealing during long crystallization time. Screw dislocations are oriented with their Burgers vectors along the chain direction and protrude across the thickness of lamellae. When etched PE lamellae are examined in the edge-on position a segmented lamellae image appear, implying a "blocky architecture" of a polymer lamellae, observed earlier by Hugel, Strobl and Thomann [100]. However, when viewed flat-on the same lamellae appear as a continuous plates with occasional screw dislocations protruding the plate. The holes left after etching of the material around dislocations lead to the false impression of lamellae composed of separated blocks, when viewed edge-on.

Another theory, which states that polymeric crystal is formed in multi-step way, is proposed by Olmsted [101]. This theory is mainly based on spinodal decomposition (SD) from the assumed unstable state [102]. The unstable state is caused by orientation fluctuations of stiff polymer segments. Studies devoted to SD presents that its size changes from tens of nm to μm. Those variations are observed above a critical temperature near the T_g. Thus it is suggested that two kinds of SD phase exist. The theory states that firstly a nematic-like structure of liquid-liquid phase separation droplets is formed, which grow in size with time. These droplets are considered to obtain tens μm in size. Afterwards droplets exhibits separation of the nematic structure into smectic and amorphous structures.

Those two theories: by Strobl and by Olmsted, however, raised a number of controversies caused by the fact that the exact methods of X-ray crystallization studies using synchrotron radiation [103, 104] confirms the classic image of crystallization by nucleation and growth, with no intermediate states.

1.3.3 Growth of polycrystalline aggregates

Generally the crystallization from the melt consists from primary and secondary crystallization. The primary is called a crystallization by nucleation and growth of spherulites.

As their name suggests, spherulites are spherical aggregates of crystals in other words consist principally of chain-folded lamellae as shown in Figure 1.12 [55].

Nucleation mostly starts on the surface of low molar mass additives such as impurities, which come into the sample rather uncontrolled. However, in some cases the additives are incorporated deliberately as nucleating agents to change the crystallization temperature. Presence of the additives reduce the interfacial free energy, thus the required supercooling is greatly diminished. Afterwards the spherulite growth proceeds in the radial direction from the nuclei [105]. According to Keith [106] spherulites development goes through several stages (Fig. 1.13). Firstly, a chain-folded precursor forms, which is the basic for sheaf-like structure growth. The intermediate stages of the spherulite formation is hedrite or axialite. Axialites formation was observed for the

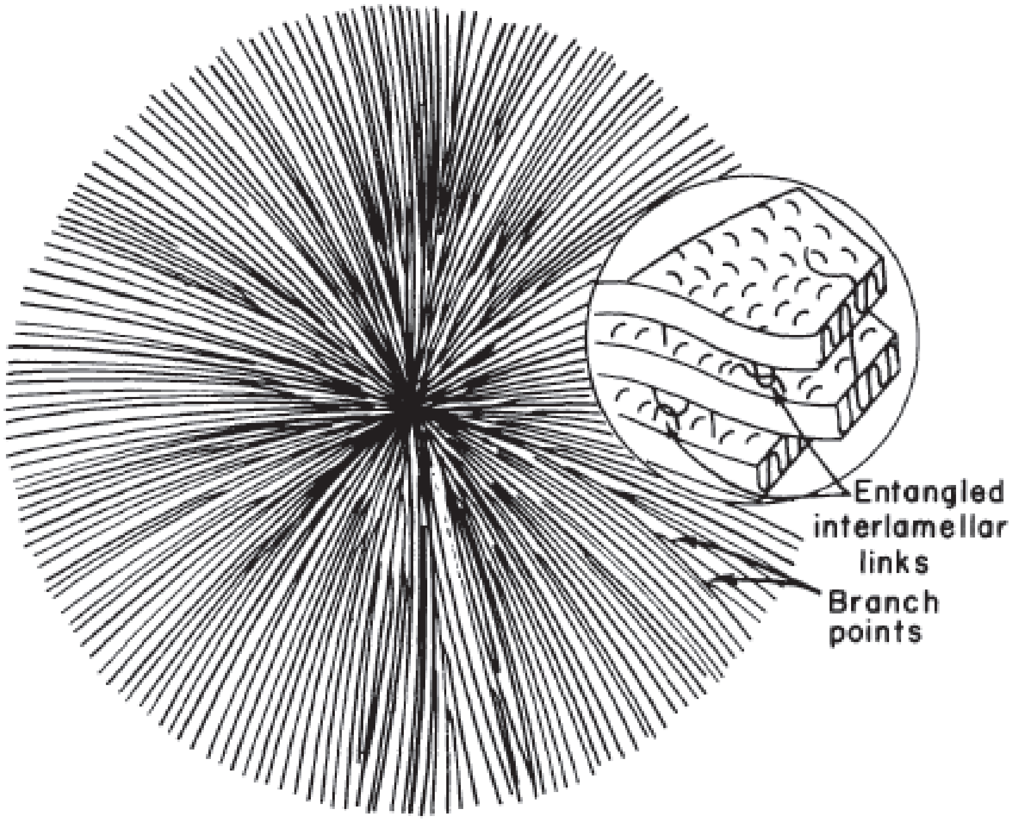

Figure 1.12: Scheme of polymer spherulite with chain-folded lamellae [55].

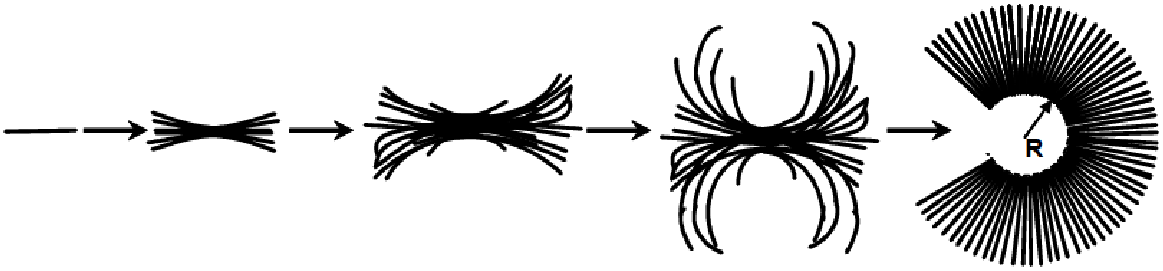

Figure 1.13: Scheme of spherulite development stages [84].

same materials, for which spherulites were revealed, but for instance in different temperatures of isothermal crystallization. They are known as symmetric structures, which are formed at small undercooling and in high temperatures. Afterwards, the spherulite appears, however the crystallization is not finished. The crystallinity still increases but does it very slowly. Further cooling of the sample cause the formation of additional crystallites in-between the primary stacks (Fig. 1.14(a)). Obviously crystals formed in higher temperature are thicker than those formed in lower temperatures. It was shown that the longest macromolecules has tendency to form the thickest lamellae, whilst the shorter one forms the thinner crystals [107]. However, Strobl [108] noticed also that crystallites are often slightly tilted with respect to each other. Thus, a growing lamellae in-between two tilted crystallites at e.g. T_0 stops at certain point. Subsequently at temperature T_1 it continuous its growth. Consequently the thickness of the crystallite decreases step by step (Fig. 1.14(b)). The isothermal thickening of the lamellae is also classified as the secondary crystallization effect.

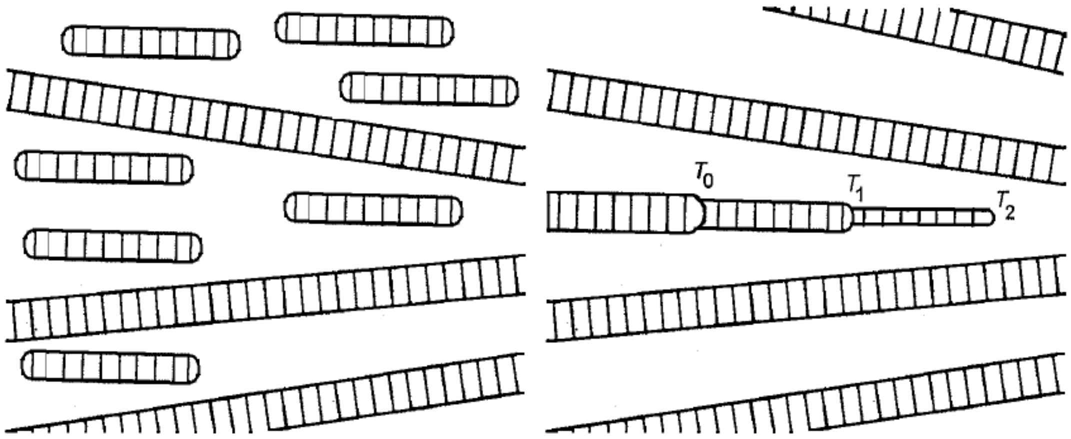

(a) in-between

(b) titlted

Figure 1.14: Mechanism of the structure development ($T_0 > T_1 > T_2$) [108].

Spherulites are observed in a polarized light microscope (PLM) as a spherical objects. In the PLM view-field crystallization starts from a small nuclei appearance, which subsequently grow in size. More careful investigations showed that the spherulites grow with a constant radial rate up to the point when they impinge with neighbors. The contact area is plannar if two spherulites were nucleated simultaneously, but if not then it is bent. At the end of crystallization the whole volume is fulfill with impinged bound spherulites. Nucleation density influence the spherulites sizes, which can vary from several μm up to some cm [108].

Spherulites possess birefringent nature, thus in many cases a 'Maltese cross' is observed between crossed polarizers. Optical indicatrices arrangement indicates the appearance of Maltese cross. The birefringence originates from the optical anisotropy of the stretched polymer chains in the crystallites, which are oriented perpendicular to the spherulite radius [108]. Although spherulites are optically anisotropic, they are not 100% crystals, they do contain considerable concentrations of amorphous regions [57]. The birefringent nature of spherulites gives possibility to investigate the kinetic growth by measurement of light transmitted through the sample during crystallization. Generally the obtained curves have similar sigmoidal shapes. The crystallization rate increases together with the temperature decrease. Firstly, an induction period is observed, which is required for nuclei formation. Afterwards accelerated crystallization occurs whilst the spherulites growth in radius. Subsequently, crystallization rate slows down when the spherulites begin to touch each other. Finally, the spherulitic crystallization completes when the spherulites fill the entire volume of the sample [108].

In PLM radial growth in concentric light-dark rings was also observed. Those spherulites are called ringed or banded spherulites. Figure 1.15 presents such a case. The optical micrographs shows in addition to the Malteses cross, light extinctions along radius in a periodic manner. It indicates a regular rotation of the chain direction and the layer normal to the radius vector. The crystallites are twisted periodically [108].

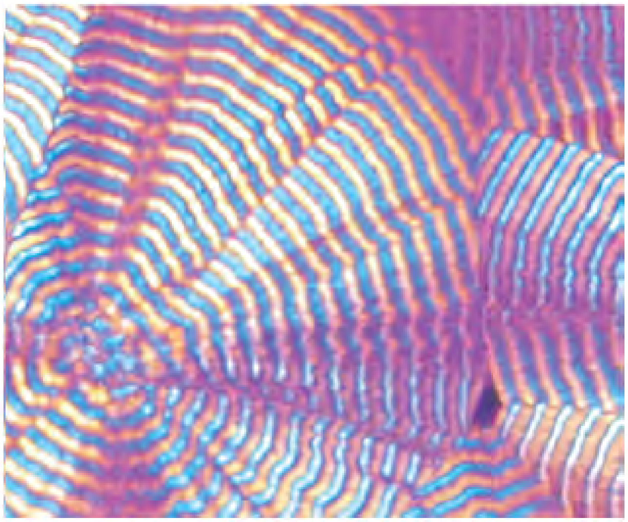

Figure 1.15: Banded spherulite of poly(ethylene adipate) [109].

Except PLM, small-angle light scattering (SALS) is also used to obtain certain information about spherulites. On the basis of SALS pattern, for instance, the fifth-order average spherulite radius $\langle R_5 \rangle$ can be calculated using the following formula [110, 111]:

$$\langle R_5 \rangle = \frac{4.09\lambda}{4\pi \cdot sin\left(\frac{\theta_{max}}{2}\right)} \tag{1.29}$$

where λ is the wavelength of used light and θ_{max} is the angular position of scattering intensity maximum.

1.3.4 Influence of chemical structure on crystallization

Polymers are made from repeating units at the molecular level. Thus the chemical nature of them determines the material properties. For instance, the chemical bonds type in the chain defines if the molecule is flexible or stiff. For flexible molecules it is characteristic that rotation around the chemical bonds in the backbone of the molecule is possible with activation energies of not more than a few kT. Whereas for rigid molecules such bond rotations are always impossible or the molecules are below their glass transition temperature, so the activation energies for bond rotation are prohibited [112].

Generally flexible molecules supply flexible materials like polyethylene and consequently stiff molecules provide stiff materials like Kevlar or polystyrene [112]. Polymers such as polyethene, polymethanal and polytetrafluoroethene possess low barriers to rotate around the bonds in the chain. They tend to have high crystallinity degree, high melting points and low glass transition temperatures [113]. Nevertheless, even in the case of flexible polymers a distinction can be made. For example, a comparison of two aliphatic polyesters such as poly(tetramethylene adipate) (PTMA) and poly(hexamethylene adipate) (PHMA) showed differences in crystallization. This subtle difference in the chain leads to the conclusion that PHMA crystallizes more rapidly than PTMA. It was suggested that it is due to lower concentration of O-C(=O)-groups in PHMA, which groups are stiffer than -CH_2-CH_2- [114]. In contrary, polymers such as polychloroethene (polyvinyl chloride), polyfluoroethene (polyvinyl fluoride), and polyethenylbenzene (polystyrene) are much less crystalline and have high T_g. It suggests that the chains attracts each other weaker than e.g. polyethene. The low crystallinity degree of those polymers is caused by a low degree of regularity of the stereochemical configuration of the chiral carbons in the chain. For instance, three various polypropenes were synthesized of propene with Ziegler catalysts. Two of them have high crystallization degree, whereas one is amorphous and elastic. Respectively, two former are isotactic (Fig. 1.16(a)) and syndiotactic (Fig. 1.16(b)), whilst the last is called atactic (Fig. 1.16(c)). As we can see on Figure 1.16(a) isotactic form has a regular structure with the methyl groups all on the same side of the chain. Whereas methylene groups are distributed randomly in atactic polypropene. The syndiotactic form is an intermediate form due to alternating distribution of methyl groups. Those differences of structures lead of course to the variation of properties. Isotactic polypropene is high crystalline and hard polymer, which melts around 175°C, while the atactic one is soft and elastic [113].

Many different types of structural irregularities can be introduced into the chain. For instance, region defects, geometric or stereo isomers can be incorporated depending upon the chemical nature of the major chemical unit. Diene polymer contains in a chain the units, which are chemically identical and isomeric to each other. Thus, their crystallization behavior is similar to copolymers. For instance, for poly(butadiene) three structures, presented in Figure 1.17, are known. Hence, polymers containing similar units can exhibit the trans-1,4 or cis-1,4 configuration and as pendant vinyl groups existing in D or L configuration [116]. Other types of structural irregularities are represented by branch points and cross-links [53].

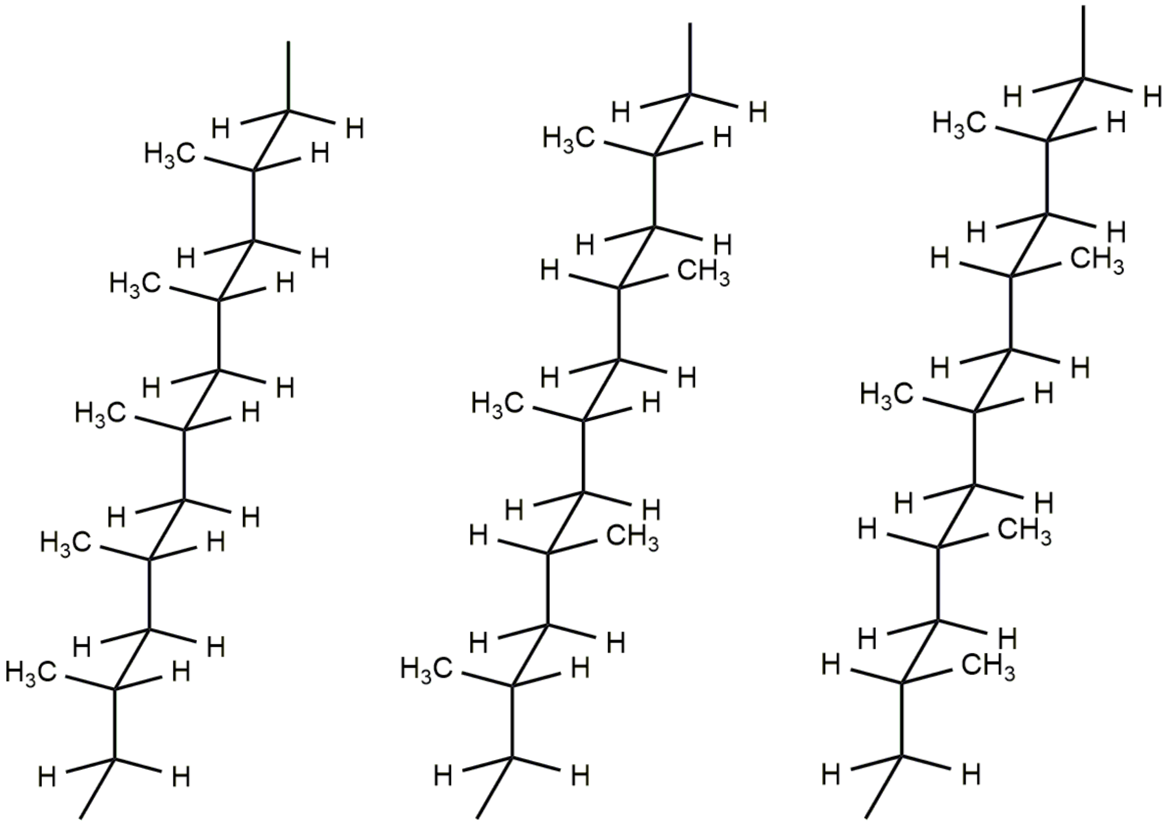

(a) isotactic (b) syndiotactic (c) atactic

Figure 1.16: Configuration of (a) isotactic, (b) syndiotactic and (c) atactic (random) polypropene [113].

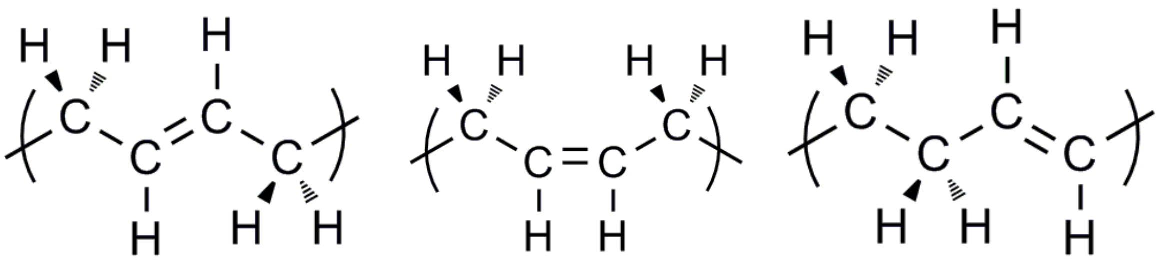

(a) 1,4 trans (b) 1,4 cis (c) 1,2 vinyl

Figure 1.17: Existing structures of poly(butadiene) [53].

Nevertheless, there are many more subtle ways in which the structure can affect the material properties. For example, the crystallization behavior may be significantly influenced by the chemical composition of the chain. It is possible that the material will be unable to crystallize if the chain contain several different monomers arranged at random manner [112]. Therefore, concentration of the *co*-units is important in copolymers, but the sequences, their length and distribution require more attention. Whilst, in low molecular weight binary mixtures emphasis is given to the molecules [53]. With respect to the dispersion of *co*-units the two existing possibilities are described in detail in Section 1.4. Briefly speaking, in one case the crystalline phase contain only one crystallizing *co*-unit and the other are excluded. In the second case all *co*-units are allowed to enter the lattice. Example of copolymers, which possess crystals containing one *co*-unit, are ethylene copolymers. The particular copolymer was prepared by Richardson [115] by the copolymerization of mixtures of diazomethane and the corresponding higher diazoalkane. In the agreements with the theory a signoidal melting curve was observed. The melting peak was broad as compared to homopolymers and becomes broader as the concentration of noncrystallizable units was increased. As it was expected, small amount of crystallinity persisted just above the T_m. Similar observation were reported for other random ethylene copolymer [117] prepared in different way and for copolyamides of caprolactam with capryllactam [118].

However, it is worth to underline that attachment, for instance, of flexible chains to the rigid backbone is made on purpose to increase the solubility and to decrease the melting points of materials. This attempts has been successfully applied to many polymers with stiff backbones such as aromatic polyamides and polyesters, polyimides, polyphthalocyaninatosiloxanes, poly-p-phenylenes and polydiacetylenes [96]. Gilbert [119] reported comparison of five aromatic polyesters with various length of the aliphatic component inside the chain (poly(ethylene terephalate) - notation 2**T**, poly(tetramethylene terephthalate) - 4**T**, poly(pentamethylene terephthalate) - 5**T**, poly(hexamethylene terephthalate) - 6**T**, poly(tetramethylene isopthalate) - 4**I**). It was shown that for 2**T**, 4**T** and 6**T** of average molecular weight, the melting time and temperature influence the crystallization rate less than the length of aliphatic section. The conclusion was that polymers with more flexible chains crystallize more willingly. Although, the 4**T** and 6**T** sample had more similar crystallization degree than 2**T**. It turned out also that 5**T** polyester requires greater undercooling than polyesters with even number of carbon atoms in the diol component. The same demand of great undercooling was notices for 4**I** polyester.

Summarizing: properties are affected by the chemical nature of the molecules, the distribution of monomers along the chain, the strength and flexibility of the chemical bonds between monomers, and any interactions between monomers in chain [112].

1.4 Copolymers crystallization

In Section 1.3 recent state of knowledge on polymer crystallization was briefly described. However, the notion was given of crystallization in general. In the case of copolymers the crystallization process is more sophisticated due to the presence of at least two kinds of mers. Therefore in this Section the well-known models of copolymers crystallization are presented.

In the literature, there are two basic theoretical approaches, which correlate the thermal and crystallization behavior with comonomer composition. Usually, the notation **A** and **B**, as used by Flory [120], describe the crystallizable and noncrystallizable *co*-units, respectively. Flory [120] suggested also that if **A** monomer of a random copolymer crystallizes, then **B** monomer will remain in the amorphous phase. The crystallization abilities are determined by the **A** units sequences length and on the crystallization temperature. Flory defines a limiting crystallites size, which separates ranges of sizes at which crystallites may or may not exist at equilibrium. At temperatures slightly below T_m only very long sequences may convert into crystallites due to the very large critical size. As the crystallization temperature decreases the critical size decreases as well and the shorter sequences are able to convert into crystals. Thus the broad melting peak with ill-defined maximum of copolymers results from the lengths variations of sequences. However, more stable crystals formed by the longest sequences melt at the highest temperatures [121]. According to Flory, the melting temperature of a copolymer, T_m, is defined by the following relation:

$$\frac{1}{T_m} - \frac{1}{T_m^o} = -\frac{R}{\Delta H_u} lnp \tag{1.30}$$

where T_m^o is the melting point of the pure homopolymer containing **A** units, R is a gas constant, $\Delta\, H_u$ is the heat of fusion per repeating unit and p is a probability that unit **A** is followed by other unit **A** along the chain. In a truly random copolymer p is the mole fraction of **A** units.

Equation 1.30 presents the independence of copolymer melting temperature of the chemical nature of unit **B**. The Flory treatment of the problem does not include the effect of crystal thickness on melting temperature which is significant even for homopolymers with relatively large crystals.

The model of Eby [122] assumes that both monomers may crystallize. Therefore two extreme crystalline states are possible. First is very similar to the Flory's model due to the assumption of complete exclusion of **B** units from the crystal lattice (see Fig. 1.4). However, Eby does not disqualify the opportunity of **B** units incorporating into crystals (Fig. 1.4). Eby's model states that the copolymer crystalline morphology is determined by kinetics of crystallization. Moreover, it shows that when the concentration of the **B** *co*-units increases an increase of crystal thickness for isothermal crystallization is observed but a decrease for quenching or nonisothermal crystallization [123]. The depression of the melting point is predicted for both the inclusion and exclusion models. In the case of the exclusion model, the entropy of fusion raises because of preferential ordering of the copolymer chains required for crystallization, as follows:

$$T_m = T_m^0 \left(1 - \frac{\varepsilon R}{\Delta\, H_u^o} X\right) \tag{1.31}$$

where ε is the excess free energy of a defect (due to the presence of a **B** *co*-unit) in the crystal lattice, $\Delta\, H_u^o$ is the heat of fusion of the homopolymer, T_m^0 is the equilibrium

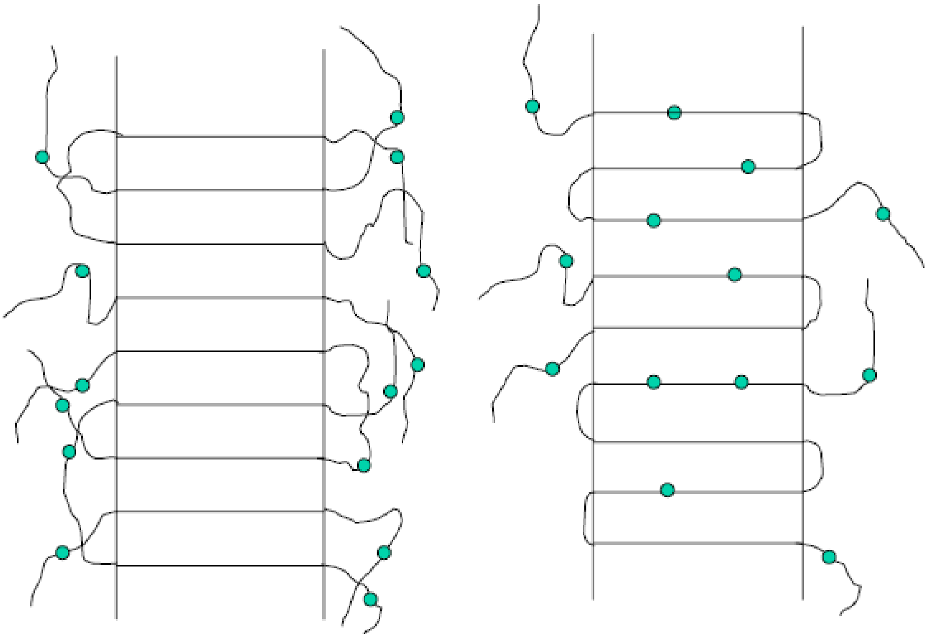
(a) complete exclusion (b) uniform inclusion

Figure 1.18: Schematic drawing showing (a) the complete exclusion and (b) uniform inclusion of the comonomer units in the crystal. [122]

melting temperature of the homopolymer and X is the overall composition of *co*-units in the copolymer.

In contrast, in the inclusion model the melting point depression is due to a defective heat of fusion that accompanies the crystallization, as follows:

$$\frac{1}{T_m} = \frac{1}{T_m^0} + \frac{R}{\Delta H_u^o} ln\left(\frac{1}{1-X}\right) \tag{1.32}$$

Thus, the melting temperature depression in the case of *co*-unit inclusion is principally an enthalpic effect whereas the rejection model describes the entropic case. Furthermore, the exclusion model from this theory is consistent with the model proposed by Flory [120, 121].

Theory of copolymer crystallization was also developed by Helfand and Lauritzen [124]. Their theory is based on the kinetic theory for polymer crystallization due to Lauritzen, DiMarzio and Passaglia. It also accounts for both the incorporation of **B** units into **A** crystals and their exclusion. However, it reveals the free energy costs connected with including the comonomer unit in the crystal lattice. For instance, addition of an **A** unit leads to crystal free energy decrease, but a **B** unit insertion to its increase. It is suggested that the incorporation not only modifies the thermodynamic properties, but also affects the kinetic barriers to crystal growth. Moreover, the theory states that the depression of melting temperature predicted by the equilibrium theory is larger due to higher B co-units concentration in the crystal lattice. A decrease in temperature leads to a decrease in the crystal free energy and a subsequent increase in the non-equilibrium inclusion of **B** units. Furthermore, it is said that the copolymer lamellae are thinner than crystals of pure homopolymer formed at the same temperature. The increased thickness compensates the free energy costs resulted from the *co*-units incorporation into crystal. The model does not clearly refers to the chemical nature of **B** *co*-units. Summarizing, this theory not only deliberates the kinetic factors of copolymer crystallization, but also takes into account the effects of the different states of a growing substrate on the growth rate of the crystals.

Nevertheless, the theory is in agreement with models proposed Eby [122, 123] for the crystallization of copolymers.

Chapter 2

Objective of the thesis

Aliphatic-aromatic copolyesters are products that are based on components from petrochemical origin. Most of them are biodegradable under rigorous condition of sufficiently short aromatic sequences. In the literature several aliphatic-aromatic copolyesters are described as it was presented in Section 1.2. It is worth to remind that all mentioned previously publications concern random copolymers except the last one [5]. Owing to the presence of PBT blocks the PBASG-**b**-PBT copolymer exhibits strong crystallization ability but its susceptibility to biodegradation is strongly reduced [1]. It can be also noticed that in most of the compositions adipate units are present. Thus, the knowledge about copolyesters with adipate units led to the development of commercial PBAT-Ecoflex® (BASF AG). The exploitation of those materials depends on their solidification mode either by vitrification or by crystallization. Often two glass transition temperatures can be noticed: one for aliphatic component at -40°C to -30°C and the second for aromatic component at +50°C to +65°C. Solidification can also occur by crystallization. The distribution of comonomer units plays a crucial role in crystallization. It is rather obvious that shortening of sequences that are able to crystallize decreases the ability of AAC to crystallize. The amorphous AACs with the main glass transition temperature much below room temperature become useless for many applications. On the other hand too long crystallizing sequences may create problems with biodegradability of AACs.

In the literature there are no reports on a synthesis of a random copolyester consisting of all four butylene units: adipate, succinate, glutarate and terephthalate. This thesis focuses on such a novel copolyester of poly(butylene adipate-*co*-succinate-*co*-glutarate-*co*-terephthalate) (PBASGT), with a random distribution of comonomers, synthesized for the purpose of this thesis. The synthesis was essentially based on a two-step melt polycondensation method that was described and used originally for the synthesis of poly(tetramethylene succinate) with terephthalic acid [125] and for the synthesis of a block copolymer of poly(butylene terephthalate) with poly(butylene cyclohexenedicarboxylate)-**b**-poly(ethylene glycol) [126]. We intended to synthesize a copolymer that will be able to crystallize yet biodegradable. For this purpose a range of copolyesters were synthesized varying in the ratio of aliphatic to aromatic components. Further, we planned to characterize the crystallization and the development of supermolecular structures of the copolyester.

The particular aims of this study are:

- to determine the distribution of comonomer units along macromolecular chains of PBASGTs and correlate sequence distribution with their crystallization ability
- to characterize habits of PBASGTs to form crystals, such as habits of nucleation of crystallization
- selecting a composition of copolyester, which optimally joins good processability, good mechanical and thermal properties with ability to biodegradability
- to characterize supermolecular structures of PBASGTs

The structure and some of the properties of the synthesized PBASGT were compared to the structure and properties of a commercial aliphatic-aromatic copolyester PBAT produced by BASF AG.

It has to be emphasized that for applications such as melt-blowing of nonwovens, fiber spinning, film extrusion, film blowing or injection molding fast solidification is required to maintain high yield of melt processing. Thus, other objective of this thesis is to find a means of shortening the solidification cycle and increase crystallization peak temperature during cooling.

Chapter 3

Materials

3.1 Raw materials used for synthesis

Dimethyl terephthalate (DMT) was purchased from Mogilev (Belarus); 1,4-butanediol (BD) was obtained from PPH Standard Co., Ltd. (Poland); and Uniestrol was delivered by Pilot Plant "Organika" Co., Ltd. (Poland). The Uniestrol is a mixture of dicarboxylic acid dimethyl esters, which contain 31% of dimethyl adipate (DMA), 14% of dimethyl succinate (DMS), and 55% of dimethyl glutarate (DMG). Tetrabutyl orthotitanate ($Ti(OBu)_4$) was supplied by Sigma Aldrich®Co. All chemicals were used without purification.

3.2 Aliphatic-aromatic copolyesters of various compositions

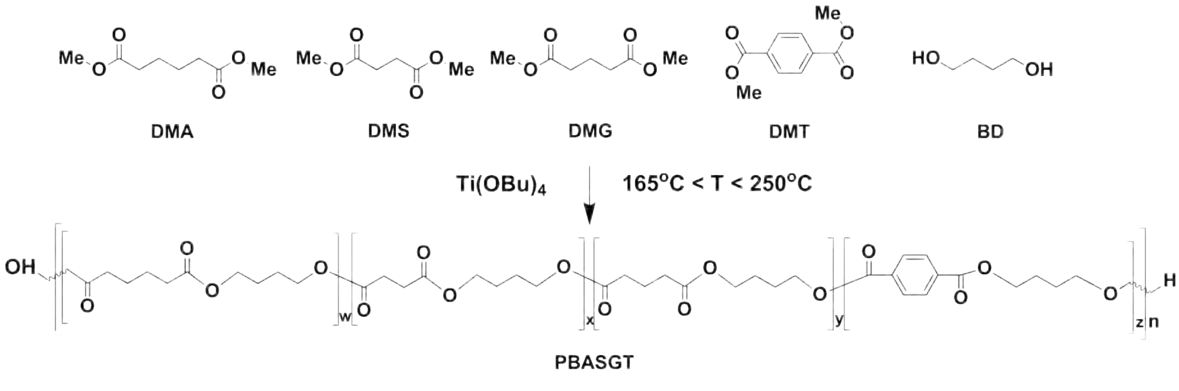

Figure 3.1: Preparation and chemical structure of poly(butylene adipate-*co*-succinate-*co*-glutarate-*co*-terephtalate) copolyesters.

The scheme of reactions leading to copolyesters is presented in Figure 3.1. Copolymers were prepared by a two-step melt polycondensation method. Exemplary recipe for PBASGT copolyester with 10% of aromatic comonomer molar content is as follows: into 9 dm^3 acid proof clave warmed to 140°C with nitrogen atmosphere were introduced 23 g of DMT, 150 g of BD, 173 g of Uniestrol and 0.05 g of $Ti(OBu)_4$ as a catalyst. The clave was then warmed up to the temperature in the range from 165°C to 225°C under atmospheric pressure. Simultaneously methanol was distilled out the clave.

Subsequently, 0.15 g $Ti(OBu)_4$ was added, the pressure was slowly decreased to 0.53 hPa and the reaction temperature was raised to 250°C. Excess of 1,4-butanediol was distilled in this period.

The molten polymer was extruded in the form of 2-3 mm thick strings after 80 min and pelletized.

Substrates weights for PBASGT copolyesters with aromatic comonomer molar content from 10% to 90% and for the homopolymer PBT are collected in Table 3.1. The synthesis procedure was the same as described above.

Table 3.1: Substrates weights for PBASGT copolyesters with aromatic comonomer molar content from 10% to 90% and for the homopolymer PBT.

Sample	**DMT**	**BD**	**Uniestrol**
		weight / g	
PBASGT 10% ar	23	150	173
PBASGT 20% ar	46.7	150	153.6
PBASGT 30% ar	69.6	150	135
PBASGT 40% ar	97	150	120
PBASGT 50% ar	116	180	96
PBASGT 60% ar	139	160	77
PBASGT 70% ar	163	160	58
PBASGT 80% ar	186	160	39
PBASGT 90% ar	192	160	18
PBT	213	160	0

3.3 Selected copolyester

PBASGT was homogenized using a Brabender batch kneader equipped with cam blades for 10 min at 60 rpm at 160°C. The mixer chamber was kept closed during homogenization and compounding to limit the access of air. Semicrystalline PBASGT copolyester films around 0.5 mm (for WAXS investigation) or 250 µm (for SAXS investigation) thick were prepared by melting at 160°C for 2.5 min between two Teflon films with a spacer followed by compression molding under the pressure of 100 atm for a 0.5 min. The molded polymer films were taken out from the press and left to crystallize in air for the WAXS investigation, but for the SAXS characterization were cooled between hollow metal blocks filled with liquid nitrogen to accelerate the solidification of the material which, anyway, was melted and melt annealed before *in situ* SAXS measurements. Powdered substances that were selected as potential nucleating agents for PBASGT were incorporated in concentration of 0.2 wt.% in a similar way and conditions.

3.4 Commercial materials

For comparison, copolyester of butylene adipate and butylene terephthalate esters, Ecoflex®, supplied by BASF AG and poly(butylene terephthalate) (PBT) supplied by Goodfellow in the form of pellets were used.

Chapter 4

Apparatus and experimental techniques

Results presented further in the thesis were obtained on the basis of a number of research methods and techniques. Measuring equipments used to characterize materials which are the objects of the thesis include a nuclear magnetic resonance spectrometer (NMR), size exclusion chromatography (SEC-MALLS), thermogravimetric analyzer (TGA), differential scanning calorimeter (DSC), dynamic mechanical thermal analyzer (DMTA), polarized light microscope (PLM), small-angle light scattering setup (SALS), small- (SAXS) and wide-angle (WAXS) X-ray diffractometer, synchrotron facilities SAXS and WAXS at DESY, Hamburg for *in situ* measurements,tensile testing machine and thermovision camera.

4.1 ^{1}H Nuclear Magnetic Resonance (^{1}H NMR)

To investigate the composition of synthesized copolyesters and the sequence distribution of comonomers, ^{1}H NMR measurements were conducted under ambient temperature using a Bruker Avance DRX500 spectrometer operated at a resonance frequency of 500 MHz. Copolyester pellets were dissolved in deuterated chloroform ($CDCl_3$).

Copolyester molar composition of comonomers was obtained from the corresponding methylene proton resonance integrals.

Resonance peaks were assigned according to Park and Kang [5]. The sequence distribution of comonomers was further quantitatively determined.

4.2 Size exclusion chromatography (SEC-MALLS)

Determination of molecular weights of studied copolyesters were carried out at room temperature using a SEC-MALLS instrument equipped with two detectors: a MALLS DAWN EOS photometer (Wyatt Technology Corporation, Santa Barbara, CA) and a Optilab Rex differential refractometer. The apparatus consisted of an Agilent 1100 isocratic pump, an autosampler, a degasser and a thermostatic box for columns. Two

PLGel 5-micron MIXD-C columns were applied with methylene chloride as the eluent at the flowing rate of 0.8 mL·min^{-1}. The calibration of the DAWN EOS was performed using analytical purity grade toluene. The normalization was performed using a polystyrene standard (M_n =30,000 g·mol^{-1}). The volume of the injection loop was 100 μL. The samples were injected as a solution in methylene chloride. The ASTRA 4.90.07 software package (Wyatt Technology Corporation) was used for data collection and processing. The molecular weights (M_n, M_w) and polydispersity index (M_w/M_n) were evaluated for the range of synthesized copolyesters.

4.3 Thermogravimetric Analysis (TGA)

The thermal stability of copolyesters was evaluated using TA Instruments Thermograwimetric Analyzer TGA 2950 both in air and under a nitrogen atmosphere at the flow rate of 60 mL·min^{-1}. The samples around 13 mg in weight were heated to 600°C at the rate 10°C·min^{-1}.

4.4 Differential Scanning Calorimetry (DSC)

The thermal properties were analyzed using a differential scanning calorimeter (DSC 2920 TA Instruments) equipped with a refrigerated cooling system, operated under a dry nitrogen flow, at the rate of 50 mL·min^{-1}. About 10 mg of copolyester sample was encapsulated in aluminum DSC pan and then thermally treated in the DSC apparatus.

Melting and crystallization temperatures were taken at peak rates of melting and crystallization, respectively.

The DSC measurements of copolyesters' pellets obtained after the synthesis were carried out from -50°C to 250°C at a heating rate of 10°C·min^{-1}. The sample was kept at 250°C for 1 min and then cooled down to 0°C at a rate of 10°C·min^{-1}.

The measurements were repeated for films prepared for tensile testing and X-ray characterization. The procedure was carried out from 0°C to 250°C at the heating rate of 10°C·min^{-1}. Then the sample was kept at 250°C for 1 min and then cooled down to 0°C at the rate of 10°C·min^{-1} and kept at that temperature for 1 min. Then the samples were heated above their melting temperature in order to obtain heat of second melting.

The DSC measurements for selected copolyesters were carried out from room temperature to 250°C at the heating rate of 10°C·min^{-1}. The sample was kept at 250°C for 1 min and then cooled down to 0°C at the rate of 10°C·min^{-1}. The DSC measurement of PBAT and PBT were also carried out for comparison. The glass transition temperature (T_g) was measured during heating with the rate 10°C·min^{-1} from -50°C which was selected as the temperature corresponding to the glass transition temperature of aliphatic homopolymers.

To maintain the same conditions as during the crystallization inside the hot-stage in the synchrotron SAXS experiments, a pellet of the material was sandwiched between two Kapton films and the DSC measurements were carried out from room temperature to 250°C at the heating rate of 5°C·min^{-1}. After keeping for 1 min at 250°C the sample was cooled down at a rate of 5°C·min^{-1} to 0°C. The experiment was also repeated without Kapton films, because we suspected some crystallization nucleation activity of Kapton film, and also to have opportunity to examine the changes of crystallization temperature for different cooling rates.

The crystallization onset temperature was recorded by rapid heating the sample to 250°C, and then cooling down at the rate of 2°C·min^{-1}.

In addition the DSC measurements of PBASGT and PBASGT with additives (more precisely the films prepared for WAXS characterization) were carried out from 0°C to 250°C at various heating rates (of 2.5°C·min^{-1}, 5°C·min^{-1}, 7.5°C·min^{-1}, 10°C·min^{-1}). The sample was kept at 250°C for 1 min and then cooled down to 0°C at similar rates. From the thermograms the melting peak temperature, enthalpy of melting and crystallization peak temperature were determined. Melting temperatures were taken at the minima of the melting endotherms while crystallization temperature at the maxima of crystallization exotherms.

4.5 Dynamic Mechanical Thermal Analysis (DMTA)

Dynamical mechanical properties of all samples were measured with a MkII DMAT apparatus (Rheometric Scientific, Epson, UK) in a dual-cantiliver bending mode (deformation amplitude 32 µm, peak to peak). Samples in the form of strips $30 \times 10 \times 1$ mm^3 were investigated. The dynamic storage and loss moduli, E' and E'', respectively, were determined at the constance frequency of 1 Hz and the heating rate of 2°C·min^{-1} in the temperature range from -100°C up to the temperature near melting of crystals.

4.6 Polarized Light Microscopy (PLM)

The morphology development and nonisothermal crystallization of investigated copolyesters were observed using a polarized optical microscope, equipped with Linkam CSS450 Optical Rheology System hot stage and recorded with digital camera Nikon DS Fi1. A piece of the film was sandwiched between two quartz glasses inside the hot stage. During the heating, above the melting point, the film was pressed to its final thickness of 20 µm. The sample was heated up to 250°C, kept at this temperature for 1 min to erase any thermal and mechanical history and cooled down to 0°C at the rate of 5°C·min^{-1} or 10°C·min^{-1}.

4.7 Small-angle Light Scattering (SALS)

Samples crystallized nonisothermally at the rate 10°C·min^{-1} were investigated by SALS technique in order to determine the average spherulite radius from the H_v scattering patterns. A He-Ne laser (λ=632.8 nm) was used for the purpose. The 2D H_v patterns (obtained with crossed polars) were recorded using a high sensitivity full frame Canon

Eos 5D camera. From H_v patterns the scattering light intensity distribution as a function of a scattering angle θ was measured at a fixed angle $\mu = 90°$ using the Image Quant software (Molecular Dynamics). From the angular position of scattering intensity maximum, θ_{max}, the fifth-order average spherulite radius $\langle R_5 \rangle$ was calculated using the Formula 1.29.

4.8 Small-angle X-ray Scattering (SAXS)

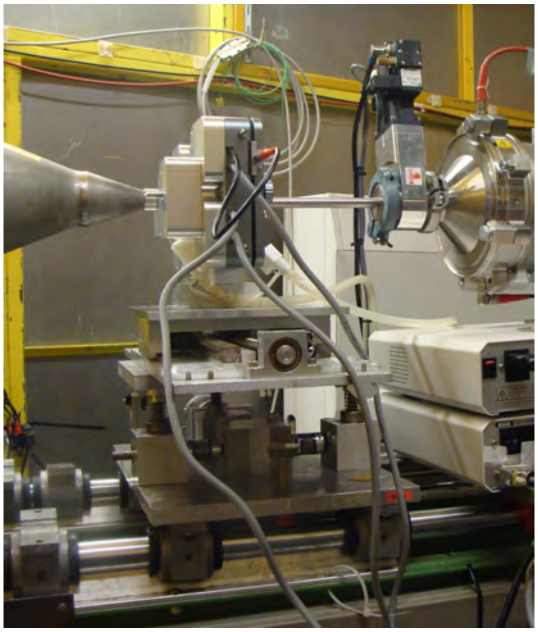

Figure 4.1: Hot-stage Linkam CSS450 Optical Rheology System fitted to the synchrotron beamline A2.

Samples in the form of 250 μm thick film prepared as described in Chapter 3 were used for SAXS studies. SAXS measurements for copolyesters with various composition and selected PBASGT copolyester were performed in a synchrotron beamline P03 and A2, respectively, at Hasylab (Desy) in Hamburg with the aim to study nonisothermal crystallization process *in situ*. X-ray wavelength from synchrotron source in beamline P03 was 0.0957 nm and the distance from a sample to a detector was 2.6 m. In the case of beamline A2 X-ray wavelength was 0.15 nm and the distance from the sample to a detector was 2.6 m. The crystallization was carried out in a hot-stage Linkam CSS450 Optical Rheology System fitted to the beamline (Figure 4.1). To reduce unwanted scattering, the original material of cell windows was replaced with Kapton film glued to stainless steel lid and base shearing plates. Polymer disc with radius of around 25 mm, was cut from 250 μm thick film and inserted between the Kapton films at room temperature. Then the sample was slightly pressed during closing of the heating-stage. The copolymer film was heated up to 250°C at the rate of $5°C{\cdot}min^{-1}$ or $10°C{\cdot}min^{-1}$

and pressed to its final thickness of 200 μm. Then, the sample was melt annealed for 1 min in order to erase the memory of previous thermal history. Afterwards, the sample was cooled down to 0°C at the rate 5°C·min^{-1} or 10°C·min^{-1}. SAXS patterns were recorded every 5°C or 10°C depending on the cooling rate, starting from 250°C for copolyesters with various composition and 100°C for selected PBASGT copolyester. The patterns were used for the determination of crystal thickness using a correlation function method [127, 128].

4.9 Wide-angle X-ray Scattering (WAXS)

Semicrystalline copolyesters films around 0.5 mm or 1 mm thick, for WAXS investigation, were prepared by melting polymer in the way as described in the Chapter 3.

Wide-angle X-ray scattering (WAXS) analysis of the materials were performed at room temperature with $2\theta - \theta$ goniometer coupled to a source of Ni filtered CuK$_\alpha$ radiation (ceramic sealed-tube with line focus powered by Philips PW3830 generator operating at 30 kV and 50 mA). The scans were performed on 1 mm thick films within the range of 2θ=10-60° with a scanning step of 0.05°, in the reflection mode.

4.10 Atomic Force Microscopy (AFM)

Materials were crystallized by cooling from the melt at 250°C on a glass support with free surface. Subsequently, the exposed surface was investigated using a Nanoscope IIIa atomic force microscope (Digital Instruments/Veeco) operating in the tapping mode. Rectangular silicon cantilevers model RTESP (Nanosensors, Wetzlar-Blankenfeld, Germany) were used throughout the study.

The free surface of nucleated copolyester was also investigated at temperatures of 25°C, 50°C and 70°C. AFM was focused on the same sample area.

4.11 Tensile mechanical properties

Semicrystalline PBASGT copolyester films around 0.5 mm thick were prepared in the same way as for the WAXS characterization. The tensile samples were cut out from the films using the template according to ISO 527-2 1BA. Mechanical tensile properties of PBASGT copolyesters were studied at room temperature using Instron 5582 mechanical testing machine. In order to characterize tensile properties of materials, two tests with different cross-head speeds were performed. For determination of the modulus of elasticity, E, an extensometer with a gauge length of 25 mm and an accuracy of the 1% was utilized. A cross-head speed of 1 mm·min^{-1} which corresponds to strain rate of 4%·min^{-1} was applied. The tensile properties were measured at the rate equal to 50%·min^{-1} until break. The modulus of elasticity and selected tensile parameters of studied materials were determined on the basis of recorded stress-strain curves.

To detect precisely the behavior of crystals during deformation the SAXS and WAXS studies were performed in a synchrotron beamline P03 in Hasylab in Hamburg (λ=0.0957 nm), the same on which the nonisothermal crystallization was investigated. Two-dimensional scattering patterns with the use of Pilatus detector (Dectris, Switzerland) were registered. *In situ* observations of tensile deformation process were possible thanks to a custom-made tensile testing machine fitted to the beamline. Signals from the load cell and from the transducer measuring elongation were recorded simultaneously during the experiment. It was possible to observe the sample and the position of the X-ray beam by TV-camera and to record the consecutive video frames. The X-ray beam was positioned in the middle of the sample. The deformation was performed at the rate 100%$\cdot$min^{-1}. The deformation was limited to the engineering strain 100%, much below the strain to break. However, the scattering patterns for samples that were broken were also recorded for the area adjacent to the location of fracture.

4.12 Infrared thermography

Thermo Vision A320 camera from Flir Systems AB, of resolution 320 × 240 pixels and thermal sensitivity of 0.08°C with autofocus, in compliance with its own software, was used to record the temperature changes of the samples during tensile deformation. The software enabled constant monitoring of the temperature distribution in the selected regions of the deformed samples.

Chapter 5

Results and Discution

5.1 Influence of chemical structure and composition on copolyesters' properties

5.1.1 Composition and comonomer sequence distribution analysis

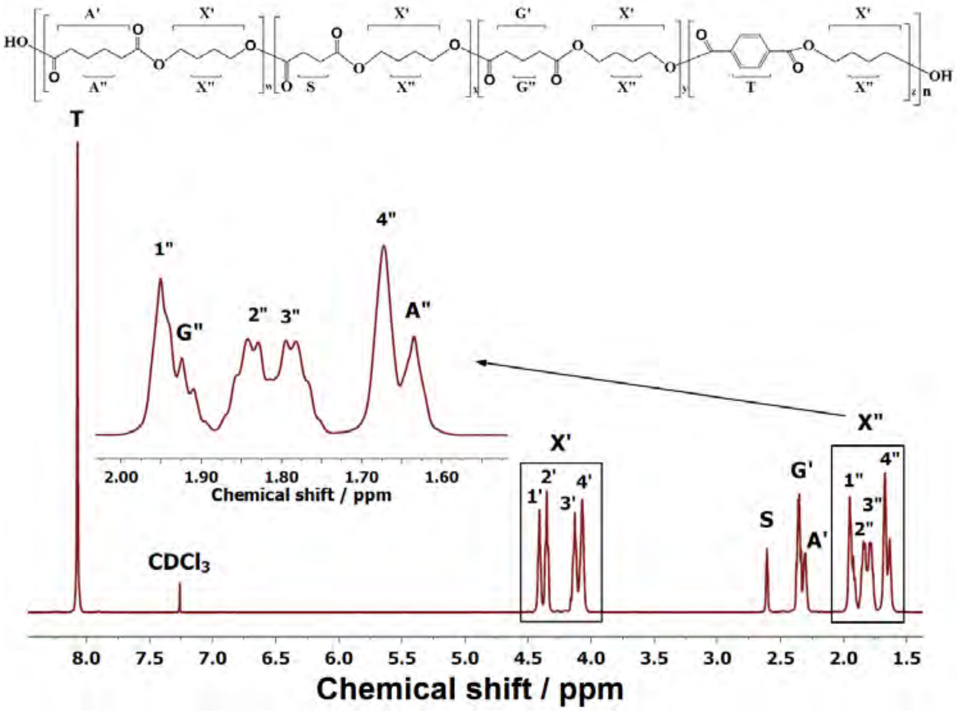

Figure 5.1: Exemplary ^{1}H NMR spectrum of the PBASGT copolyester with peaks assigned according to Ref. [5]. **S**, **G**, **A** and **T** peaks are from protons in succinate, glutarate, adipate and terephthalate units, respectively, while peaks in **X'** and **X"** bands are from protons in respective butylene units.

So far, it has been recognized that properties of aliphatic-aromatic copolyesters, such as biodegradability and crystallization behavior, are inherently influenced by their macromolecular chain architecture. Thus, to interpret the properties of aliphatic-aromatic copolyesters and occurring phenomena it was necessary to determine the composition and sequence distribution of comonomers.

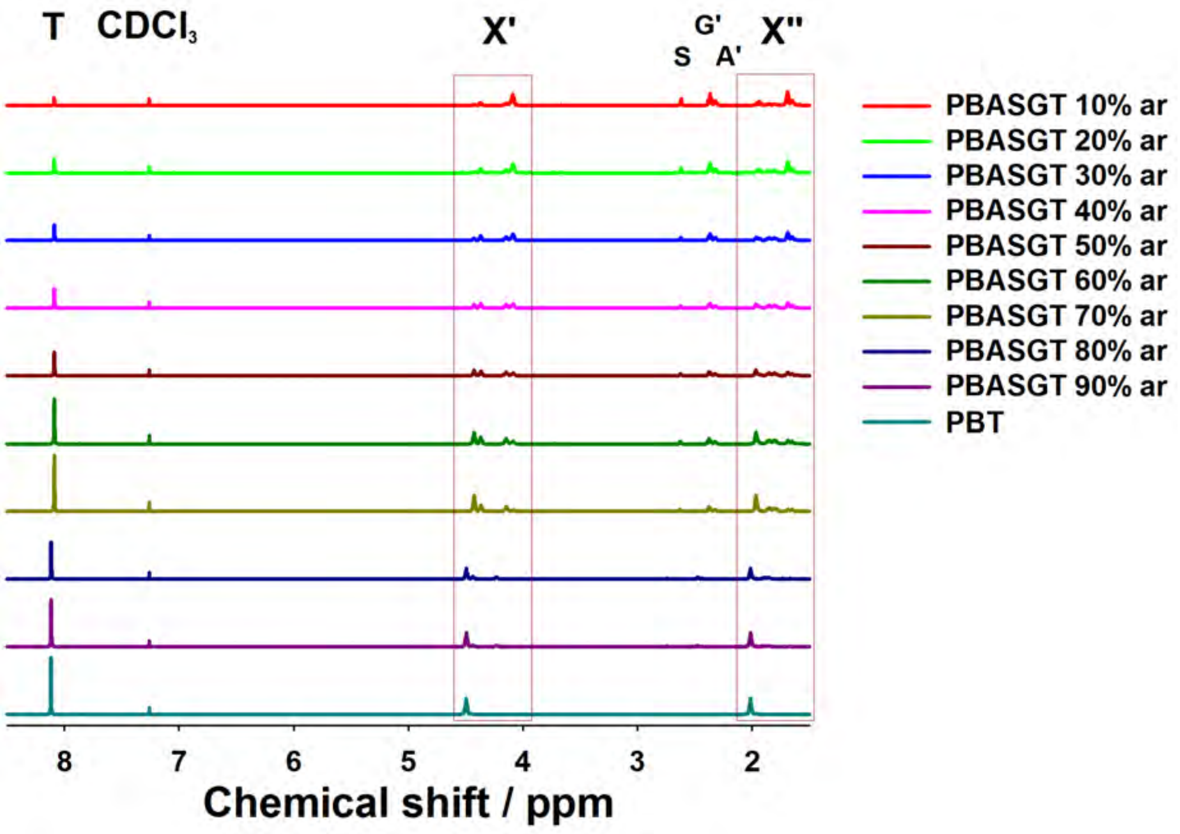

Figure 5.2: ^{1}H NMR spectra of aliphatic-aromatic copolyesters. Description of peaks as in Figure 5.1.

Figure 5.1 shows the exemplary ^{1}H NMR spectrum of PBASGT and highlights the methylene proton peaks related to butylene units of adipate, succinate, glutarate and terephthalate comonomers. The assignment was made according to Park and Kang [5] who studied a block copolyester of butylene terephthalate and aliphatic comonomers.

In Figure 5.2 the ^{1}H NMR spectra of PBASGT copolyesters with various compositions are shown. As expected the peak corresponding to aromatic ring increased smoothly with increasing aromatic units content. Simultaneously, the decrease of signals related to aliphatic units occurs. Comonomer molar composition of the copolyester was obtained from the corresponding proton resonance integrals as shown in Figure 5.3. The sequence distribution of comonomers was further quantitatively determined. The integrated proton resonance intensities for the signals at 2.30 ppm (adipate unit, **A**), 2.35 ppm (glutarate unit, **G**), 2.61 ppm (succinate unit, **S**) and 8.07 ppm (terephthalate

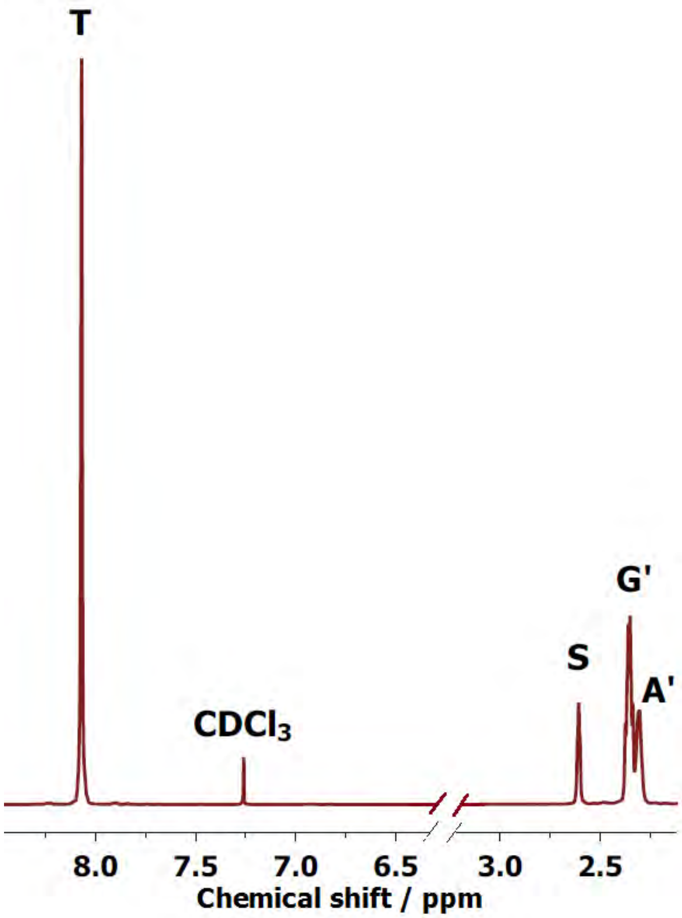

Figure 5.3: Part of exemplary ^{1}H NMR spectrum of aliphatic-aromatic copolyester with peaks used for determination of comonomer composition. Description of peaks as in Figure 5.1.

unit, **T**) were employed to quantitatively determine the contents of butylene adipate (f_{BA}), butylene succinate (f_{BS}), butylene glutarate (f_{BG}), butylene terephthalate (f_{BT}) according to dependencies presented in Ref. [7]:

$$f_{BA} = \frac{A_{A'}}{A_{A'} + A_{G'} + A_S + A_T} \tag{5.1}$$

$$f_{BG} = \frac{A_{G'}}{A_{A'} + A_{G'} + A_S + A_T} \tag{5.2}$$

$$f_{BS} = \frac{A_S}{A_{A'} + A_{G'} + A_S + A_T} \tag{5.3}$$

$$f_{BT} = \frac{A_T}{A_{A'} + A_{G'} + A_S + A_T} \tag{5.4}$$

The obtained data are collected in Table 5.1.

Table 5.1: Comonomer composition of copolyesters with various content of aromatic units.

Sample	f_{BA}	f_{BG}	f_{BS}	f_{BT}
PBASGT 10% ar	0.236	0.494	0.145	0.126
PBASGT 20% ar	0.215	0.432	0.128	0.226
PBASGT 30% ar	0.186	0.374	0.111	0.329
PBASGT 40% ar	0.157	0.318	0.091	0.434
PBASGT 50% ar	0.131	0.259	0.076	0.534
PBASGT 60% ar	0.104	0.209	0.060	0.627
PBASGT 70% ar	0.075	0.156	0.043	0.726
PBASGT 80% ar	0.040	0.114	0.027	0.819
PBASGT 90% ar	0.025	0.050	0.017	0.908

Figure 5.4 shows NMR spectra of aliphatic homopolymers PBA, PBS, PBG and aromatic homopolymer PBT. Those spectra depicts the single signals related to butylene and respectively aliphatic or aromatic units. Comparison of homopolymers (see Fig. 5.4) and copolymers (Fig. 5.2) spectra show differences of signals related to buty-

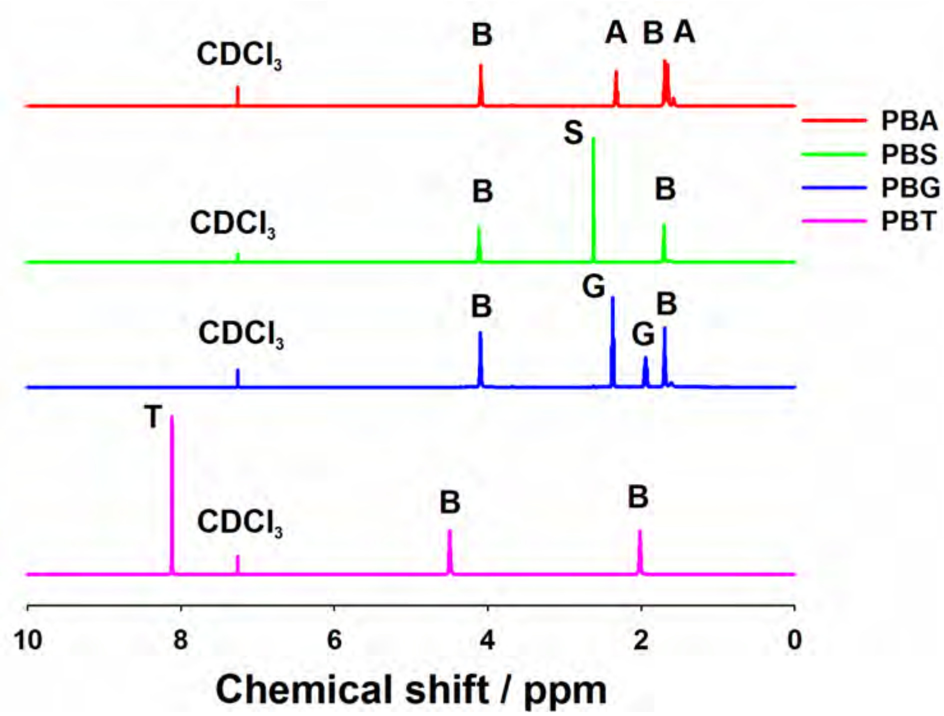

Figure 5.4: ^{1}H NMR spectra of aliphatic (PBA, PBS, PBG) and aromatic (PBT) homopolyesters. **A**, **S**, **G**, **T** and **B** are peaks originating from adipate, succinate, glutarate and terephthalate units while **B** are signals from protons of associated butylene groups.

lene units. The same observation was done by Park and Kang [5] in the case of block copolyester.

Generally, there are sixteen kinds of butylene units (**X**) distributed in copolyester macromolecules, in which we can distinguish ten homolinkages (**AXA**, **AXS**, **AXG**, **SXA**, **SXS**, **SXG**, **GXA**, **GXS**, **GXG**, **TXT**) and six heterolinkages (**AXT**, **SXT**, **GXT**, **TXA**, **TXS**, **TXG**). We should also underline that nine of the homolinkages are formed by aliphatic units (**A**, **S**, **G**) adjacent to butylene unit and one formed by two aromatic units (**T**). Thus, the observed multiplets arise from splitting up butylene proton signals that stand for four potential environments for butylene units, which integrals are changing with respective amount of aliphatic/aromatic units in the chain of copolyester.

Since the **BT** is asymmetric, the heterolinkages with **T** are not commutative, i.e. **SXT** is not the same as **TXS**. It concerns also other heterolinkages: **AXT** and **GXT**. Hence, the chemical shifts for methylene proton of butylenes units of **SXT** and **TXS** are different which is evident from Table 5.2. Following Park and Kang [5], we considered four types of sequences as presented in Table 5.2. There are two groups of ^{1}H NMR signals, the first in the narrow range of 4.5-4.0 ppm (**X'**) and the second in the narrow range of 2.0-1.5 ppm (**X"**) (Figure 5.5). Thus, a precise sequence analysis requires a high signal resolution. One can distinguish two ways of analysis: by choosing both groups of signals [6] or by taking into consideration only signals in the **X'** range [5, 7, 29]. We have used the butylene protons related peaks, in the **X'** range, because they are better resolved. In this way the precision of sequence determination should be higher.

Table 5.2: Possible diester environment (AlAl is an aliphatic-aliphatic, AlAr is an aliphatic-aromatic, ArAl is an aromatic-aliphatic, ArAr is an aromatic-aromatic) and chemical shift of PBASGT copolyesters.

Type of Dyads		**AlAl**	**AlAr**	**ArAl**	**ArAr**
Symbols		AXA, AXS, AXG, SXA, SXS, SXG, GXA, GXS, GXG	AXT, SXT, GXT	TXA, TXS, TXG	TXT
Chemical shift / ppm	**X'**	4.07	4.13	4.35	4.41
	X"	1.67	1.79	1.84	1.95

The integrated intensities of chosen sequences were taken into account in order to determine the copolymer composition and comonomer sequences. The fractions of AlAl, AlAr, ArAl and ArAr sequences as shown in Figure 5.5 were defined by Equations 5.5-5.8 according to Kang and Park [4].

$$A_{AlAl} = A_{AXA} + A_{AXS} + A_{AXG} + A_{SXA} + A_{SXS} + A_{SXG} + A_{GXA} + A_{GXS} + A_{GXG} \quad (5.5)$$

$$A_{AlAr} = A_{AXT} + A_{SXT} + A_{GXT} \quad (5.6)$$

$$A_{ArAl} = A_{TXA} + A_{TXS} + A_{TXG} \quad (5.7)$$

$$A_{ArAr} = A_{TXT} \quad (5.8)$$

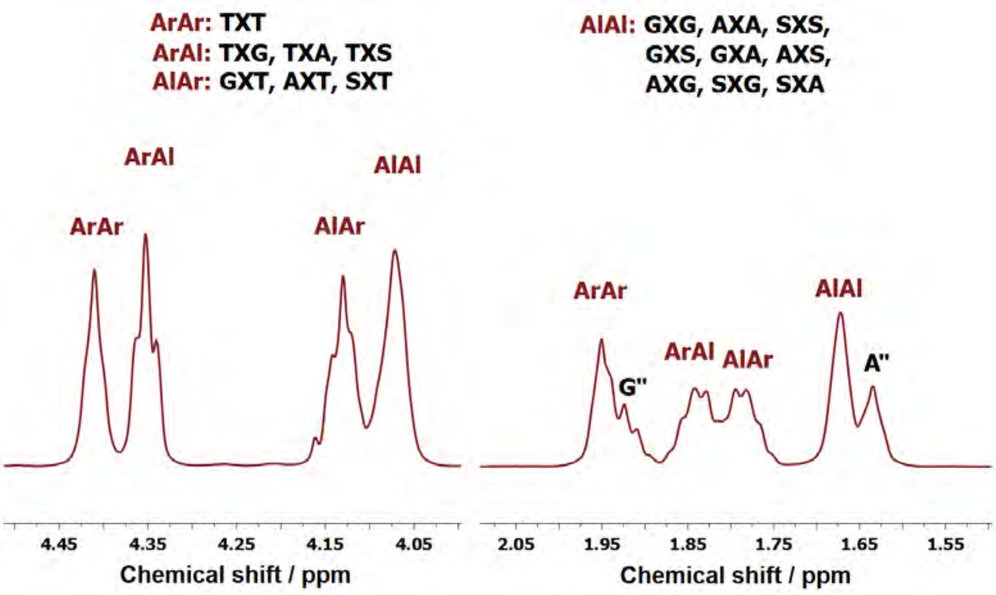

Figure 5.5: Two groups of ^{1}H NMR signals. Assignment according to Table 5.2 and Figure 5.1.

Using the integrated proton resonance intensities for **X'** signals, each fraction of dyads (f_{AlAl}, f_{AlAr}, f_{ArAl}, f_{ArAr}) can be determined from the above Equations:

$$f_{AlAl} = \frac{A_{AlAl}}{A_{AlAl} + A_{AlAr} + A_{ArAl} + A_{ArAr}} \tag{5.9}$$

$$f_{AlAr} = \frac{A_{AlAr}}{A_{AlAl} + A_{AlAr} + A_{ArAl} + A_{ArAr}} \tag{5.10}$$

$$f_{ArAl} = \frac{A_{ArAl}}{A_{AlAl} + A_{AlAr} + A_{ArAl} + A_{ArAr}} \tag{5.11}$$

$$f_{ArAr} = \frac{A_{ArAr}}{A_{AlAl} + A_{AlAr} + A_{ArAl} + A_{ArAr}} \tag{5.12}$$

According to Yamadera and Murano [130], the molar fraction, (P), of aromatic and aliphatic components can be calculated on the basis of molar fractions of diesters.

$$P_{Al} = \frac{(f_{AlAr} + f_{ArAl})}{2} + f_{AlAl} \tag{5.13}$$

$$P_{Ar} = \frac{(f_{AlAr} + f_{ArAl})}{2} + f_{ArAr} \tag{5.14}$$

The average block length $\bar{L}_n$, and the degree of randomness, R, can be obtained by the following Equations:

$$\bar{L}_{nAl} = \frac{2P_{Al}}{(f_{AlAr} + f_{ArAl})} \tag{5.15}$$

$$\bar{L}_{nAr} = \frac{2P_{Ar}}{(f_{AlAr} + f_{ArAl})} \tag{5.16}$$

$$R = \frac{1}{\bar{L}_{nAl}} + \frac{1}{\bar{L}_{nAr}} \tag{5.17}$$

The randomness index, R, assumes characteristic values depending on the molecular architecture: for a mixture of homopolymers $R = 0$, the values between 0 and 1 are obtained for a sequential structure, R is 1 for fully random copolyester, and it becomes 2 for strictly alternating distribution (see Fig. 5.6). The fractions of aliphatic/aromatic sequences, their average lengths and randomness index are presented in Table 5.3. Tables 5.1 and 5.3 show that the P_{Ar} is close to f_{BT} and P_{Al} to $f_{BA} + f_{BG} + f_{BS}$, so the analysis methods supports and complements each other.

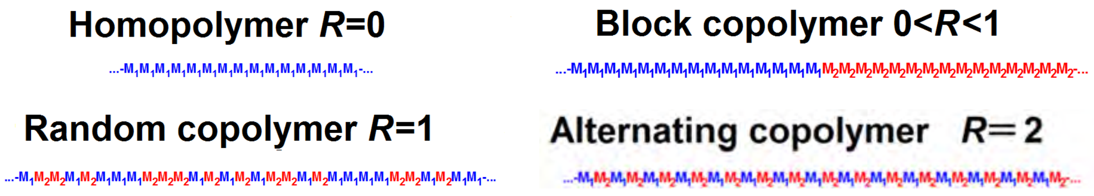

Figure 5.6: Scheme of copolymers' chains distribution.

Table 5.3: Sequence distribution of the synthesized copolymers with various content of aromatic units.

Sample	f_{ArAr}	f_{ArAl}	f_{AlAr}	f_{AlAl}	P_{Ar}	P_{Al}	$\bar{L}_{Ar}$	$\bar{L}_{Al}$	R
PBASGT 10% ar	0.017	0.112	0.116	0.754	0.131	0.869	1.147	7.598	1.003
PBASGT 20% ar	0.055	0.176	0.192	0.576	0.240	0.760	1.301	4.127	1.011
PBASGT 30% ar	0.113	0.222	0.237	0.428	0.343	0.657	1.494	2.867	1.018
PBASGT 40% ar	0.192	0.246	0.256	0.306	0.443	0.557	1.766	2.218	1.017
PBASGT 50% ar	0.287	0.253	0.253	0.207	0.540	0.460	2.136	1.818	1.018
PBASGT 60% ar	0.397	0.234	0.234	0.135	0.631	0.369	2.695	1.576	1.005
PBASGT 70% ar	0.529	0.201	0.196	0.074	0.728	0.272	3.667	1.373	1.001
PBASGT 80% ar	0.658	0.164	0.145	0.033	0.813	0.188	5.255	1.213	1.015
PBASGT 90% ar	0.813	0.098	0.081	0.008	0.902	0.098	10.091	1.091	1.016

As it can be seen from Table 5.3, all of synthesized PBASGT copolyesters are nearly random, as it can be judged from the values of R all close to 1. Table 5.3 presents also that there is a decrease of aliphatic units molar fraction in the final product in comparison to the initial molar fraction. The variation is from 1% to 3% depending on the composition. It is connected with the formation of volatile aliphatic components during the synthesis, which may escape during pressure decreasing in the second stage of polycondensation. Moreover, a continuous increase of average length of sequences of aromatic units is noticeable together with the increase of aromatic molar fraction. Also a continuous increase of average length of sequences of aliphatic units is noticeable together with the increase of aliphatic molar fraction. It is worth to note that the average block length of aromatic units (**BT**) is below 3 units for copolyesters with aromatic content below 70%. Such short average aromatic sequences are degradable by microbes as it was found by others [1, 131]. Hence, those copolymers should be biodegradable, not only in its aliphatic part. Other important parameter is the molar fraction of aromatic units, which should be between 35 mol% and 55 mol% [131, 132] to ensure a good compromise between biodegradability and physical properties. In our case the most promising materials are those, which have 30%, 40% or 50% of initial aromatic molar fraction.

Table 5.4: Molecular weights as measured by SEC-MALLS of the synthesized copolymers with various content of aromatic units. Molecular weights of copolyesters with aromatic units content above 60% were not measured due to the lack of solubility in methylene chloride.

Sample	**Molecular weights**				
	$M_w(\times 10^{-4})$ $/\,g \cdot mol^{-1}$	$M_n(\times 10^{-4})$ $/\,g \cdot mol^{-1}$	$M_z(\times 10^{-5})$ $/\,g \cdot mol^{-1}$	M_w/M_n	M_z/M_n
PBASGT 10% ar	6.782	2.273	2.377	2.984	10.457
PBASGT 20% ar	6.653	2.711	1.908	2.454	7.039
PBASGT 30% ar	6.150	2.913	1.419	2.111	4.874
PBASGT 40% ar	5.490	2.820	1.044	1.946	3.703
PBASGT 50% ar	5.723	3.002	1.203	1.907	4.007
PBASGT 60% ar	5.370	2.767	1.886	1.941	6.817

As it was described in Subsection 1.3.3 the crystallization can be influenced by the molecular weight. Thus, the average molecular weights and other molecular weight parameters of synthesized copolyesters were determined and the results are collected in Table 5.4. One can notice that the M_n is slightly increasing together with the increase of aromatic units content, whilst the M_w is slightly decreasing. However, the differences between molecular weights of copolyesters with various aromatic unit content are not exceeding 1500 g·mol^{-1}. So, the variation of molecular weight should not affect the crystallization of copolyesters of different compositions. Moreover, it can be observed that the M_z reaches the highest values for copolyesters with the highest content of aliphatic units, also M_z increases with the increase of aromatic fraction. Hence, the longest chains are present in copolyesters with the highest content either of aliphatic or aromatic units. When the composition is around 50% of aliphatic units and 50% of aromatic units then the M_z is the lowest. It must be mentioned that larger amount of long chains can increase the nucleation density and rate of crystallization [133, 134].

5.1.2 Crystal structure of copolyesters

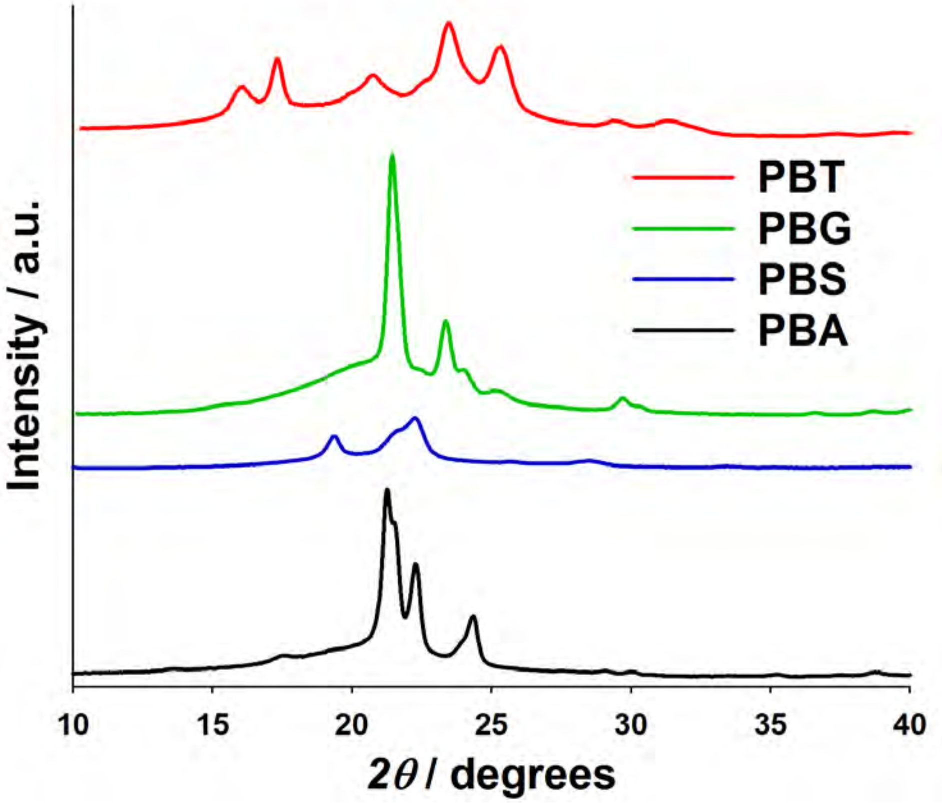

Figure 5.7: WAXS 2θ scans of homopolymers PBT, PBG, PBS and PBA. Curves for aliphatic homopolymers are shifted vertically for clarity.

Figure 5.7 shows the WAXS 2θ scans of synthesized homopolymers (PBT, PBG, PBS and PBA), which mers are included in the composition of PBASGT copolyesters, while, Figure 5.8 shows the WAXS 2θ scans of synthesized copolyesters with various amount of aromatic units and synthesized PBT homopolymer. Although, all of the synthesized copolyesters were found to be nearly random, sharp peaks are observed in the WAXS pattern of copolyester with initial aromatic unit content above 20%. Furthermore, it is worth to underline that there are small differences between the diffraction angle 2θ positions of respective diffraction peaks of synthesized copolyesters and synthesized homopolymer PBT.

Based on the obtained results for the synthesized copolyesters, there is a suggestion that the aliphatic units might be partially included in **BT** crystal lattice or at least

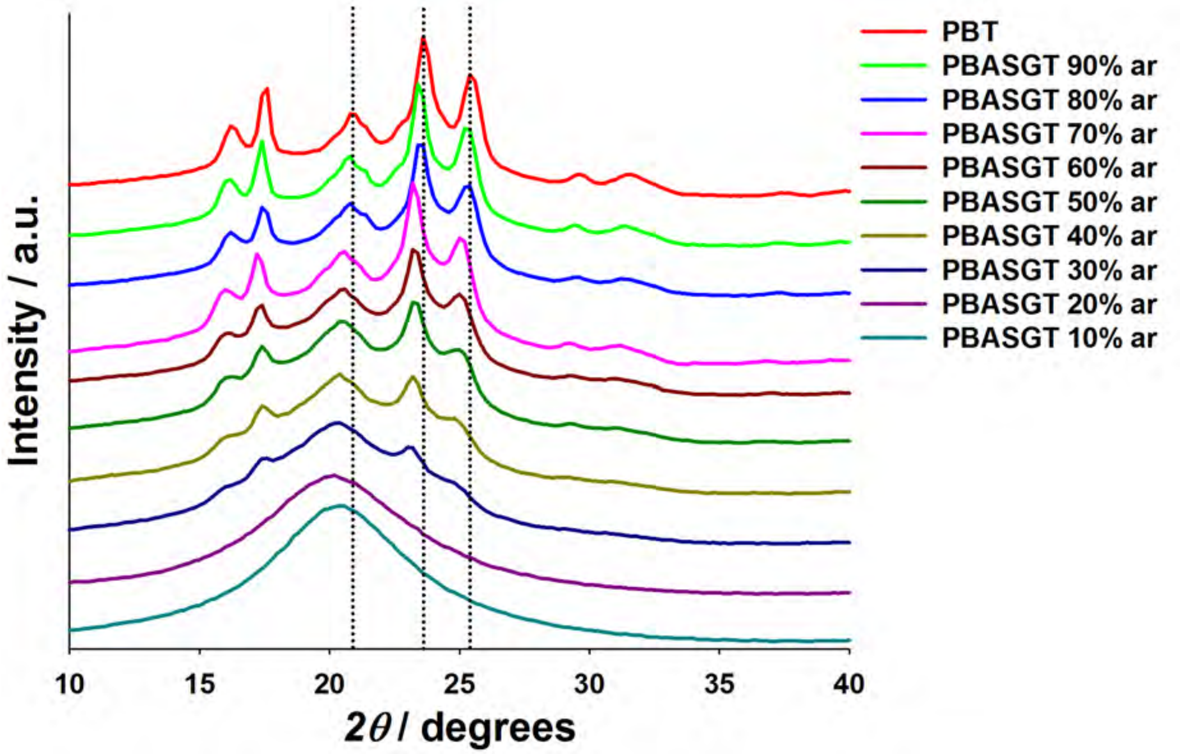

Figure 5.8: WAXS 2θ scans of synthesized copolyesters with various amount of aromatic units and synthesized PBT. Curves for copolyesters with aromatic units above 20% and synthesized PBT are shifted vertically for clarity.

distort the crystal lattice. Increasing shifts of the diffraction peak together with the increase of aliphatic unit content suggests that both aliphatic and aromatic units can be introduced into crystal lattice. Such crystallization behavior is defined as mixed-crystallization [135, 136]. It is known that mixed-crystallization in a binary random copolymer demands two preconditions [49]. First one is a similar main-chain conformation between two comonomer segments in the crystal lattice, which occurs in avoiding geometrical hindrance during mixed-crystal formation. The second precondition determines that two comonomers should have comparable cohesive energy. If not, the comonomer with larger cohesive energy will migrate to form a rich domain and will crystallize. In the case of PBASGT copolyesters there are three aliphatic units and one aromatic, but the chains of the aliphatic units differs only with the amount of CH_2, so we would consider the copolymer as binary copolymer build from aliphatic and aromatic units. It was suggested already that chain conformation of **BA** unit can be consider to be similar to that of **BT** unit [137]. If we widen the assumption to the other aliphatic units, then the first precondition is fulfilled. The second precondition concerns the cohesive energies of aliphatic units and aromatic units. These were calculated using group contribution method [138]. Table 5.5 lists the cohesive energy values of each functional group contained in the synthesized copolyester, and corresponding number

Table 5.5: Cohesive energy of function group and the number of corresponding functional group in PBASGT copolyesters.

Function group	Cohesive energy of function group / kJ·mol^{-1}	Number of function group			
		BA	BS	BG	BT
-CH$_2$-	4.19	8	6	7	4
-COO-	13.41	2	2	2	2
Aromatic ring	31.00	-	-	-	1

of functional group for each unit. Using the above data and by taking into account the molar fraction of aliphatic and aromatic units (see Tab. 5.1), the cohesive energies of aliphatic and aromatic units for all copolyesters are collected in Table 5.6. The values in Table 5.6 suggests that the mixed-crystallization could be most possible in the case of PBASGT copolyester with 40% of initial aromatic units.

Table 5.6: Cohesive energy of aliphatic and aromatic units in PBASGT copolyesters with various compositions.

Sample	Cohesive energy of	
	aliphatic units	aromatic units
PBASGT 10% ar	49.51	9.40
PBASGT 20% ar	43.88	16.86
PBASGT 30% ar	37.99	24.54
PBASGT 40% ar	32.06	32.37
PBASGT 50% ar	26.40	39.83
PBASGT 60% ar	21.13	46.76
PBASGT 70% ar	15.52	54.15
PBASGT 80% ar	10.22	61.08
PBASGT 90% ar	5.20	67.72

However, it is found that the WAXS pattern obtained for copolyesters is similar to that of PBT and no other peaks of aliphatic homopolymers are observed (compare with Fig. 5.7). Such observation was already reported for other copolyesters [5, 6, 49]. Moreover, one can notice that the crystallinity increases together with the increase of aromatic unit content. Surprisingly, the crystallization structure is not changing with the change of composition in contrary as it was observed by Li et al. [7] for binary random copolyester PBST. Thus, the aliphatic part of PBASGT coplyesters seems not to have the ability to crystallize. Following Alter and Bonart [139] and Li et al. [7], we suggest that the crystals of the PBASGT copolyesters are built of triclinic unit cells of PBT (see Figure 5.9) that are slightly distorted by the close vicinity of aliphatic units.

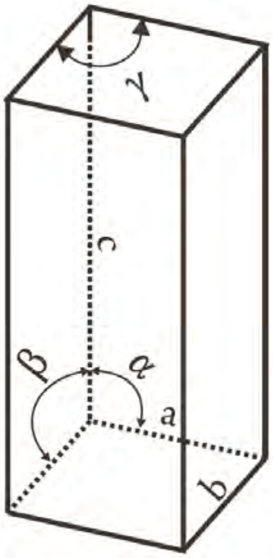

Figure 5.9: Scheme of triclinic crystal system, where $a \neq b \neq c$, $\alpha \neq \beta \neq \gamma \neq 90°$.

5.1.3 Thermal stability and properties of copolyesters

Figures 5.10 and 5.11 illustrate the TGA and corresponding dTGA curves recorded under nitrogen atmosphere of aliphatic homopolymers (PBA, PBS, PBG) and PBASGT copolymers, respectively. It was observed that all samples of PBASGT copolyesters show TGA traces with only one weight-loss stage, regardless of their quite different comonomer molar compositions. It can be noticed, that the thermal degradation profiles of the copolyesters in nitrogen atmosphere are found to differ much from PBA and PBS polyesters, and both of them exhibit lower degradation temperature under nitrogen atmosphere than PBASGT. The exception is PBG copolyester exhibiting higher degradation temperature than PBASGT. It supports the well-known statement that for a random structural copolymer, step-wise thermal degradation of the individual building blocks merge into one-step habit of thermal degradation. Moreover, the temperature at the maximum thermal degradation rate is mediated between two individual temperatures of maximum degradation rates attributable to corresponding homopolymers [140]. Comparison of the 2% weight loss temperature (T_{id}) (see Tab. 5.7) presents that the degradation initiation of PBASGT copolymers shifts to higher temperatures together with the increase of the aromatic units content. However, simultaneously the temperature of maximum weight loss rate (T_{max}, see Table 5.7) decreases due to the diminishing content of more stable **BG** units.

The studies in thermal degradation under air atmosphere were also conducted. Figures 5.12 and 5.13 present the TGA and dTGA profiles of aliphatic homopolymers (PBA, PBS, PBG) and the PBASGT copolyesters under air atmosphere, respectively. The TGA curve in air atmosphere depicted two step-wise degradation. The first stage is similar to the degradation in nitrogen. It is concluded then that the character of this

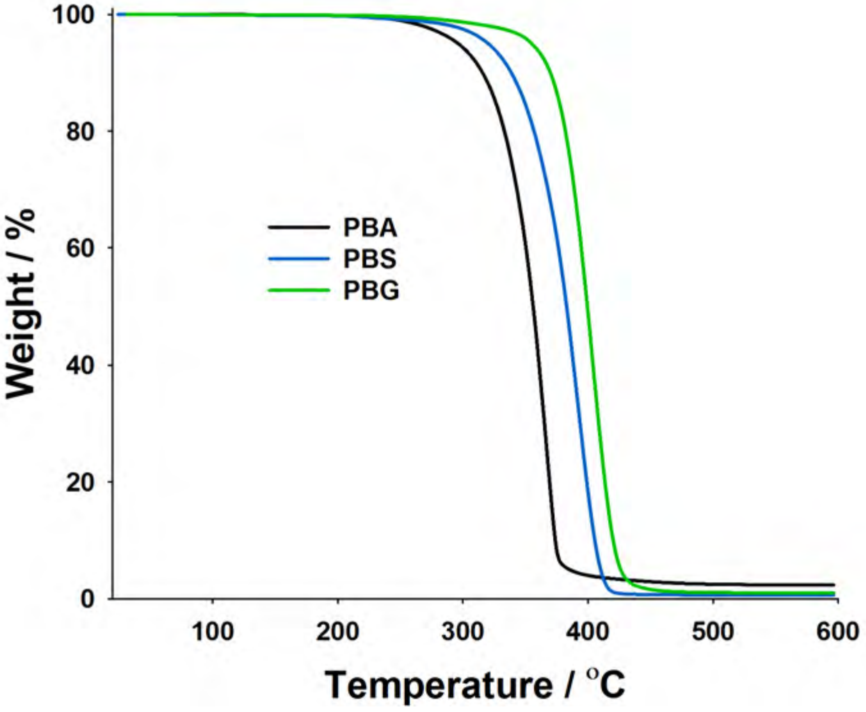

(a) TGA under nitrogent

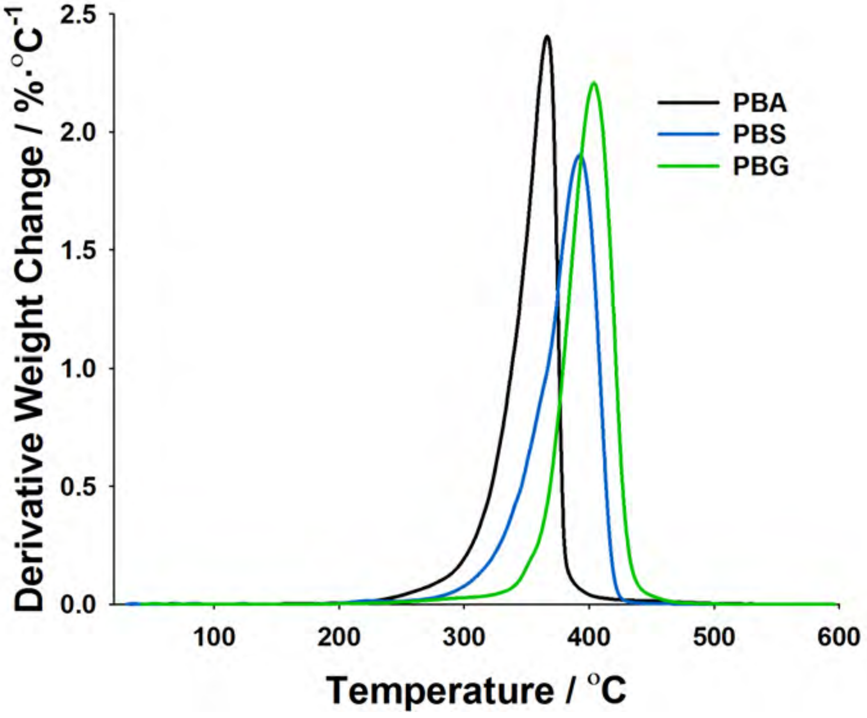

(b) dTGA under nitrogent

Figure 5.10: Homopolymers (a) TGA and (b) dTGA curves under nitrogen atmosphere.

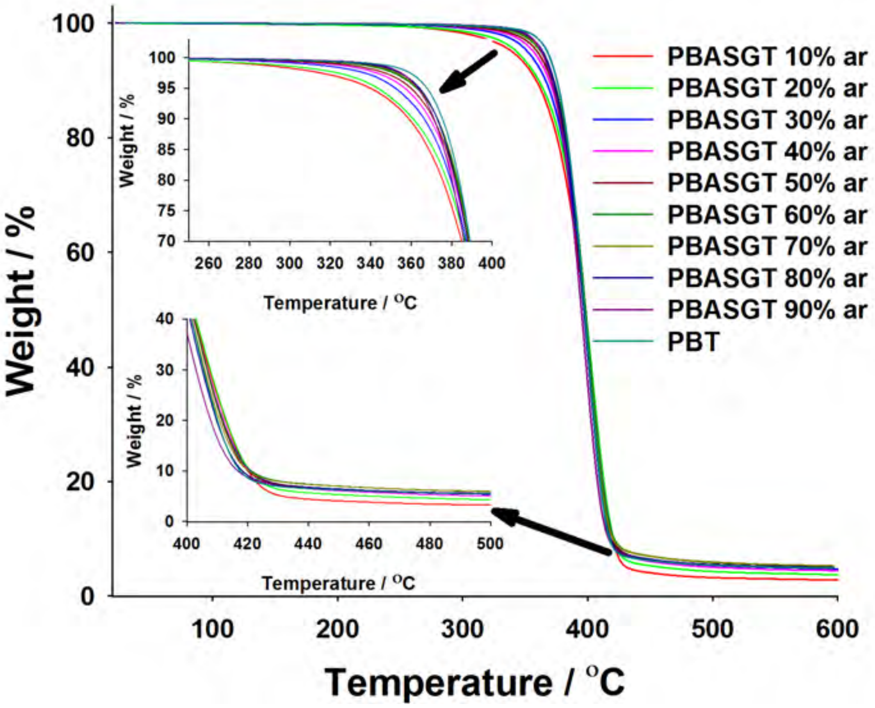

(a) TGA under nitrogent

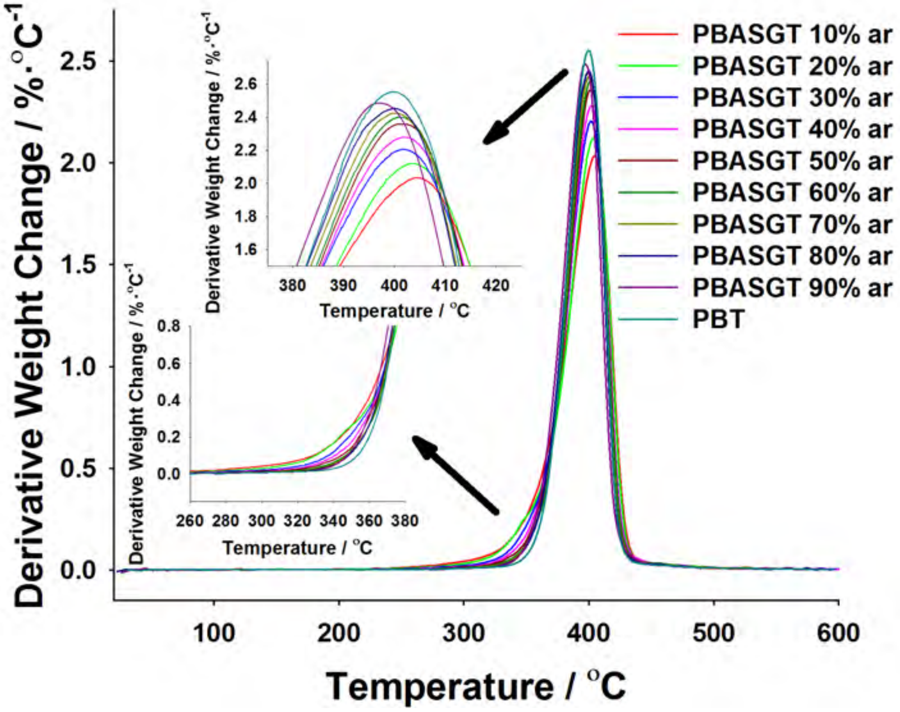

(b) dTGA under nitrogent

Figure 5.11: PBASGT copolymers (a) TGA and (b) dTGA curves under nitrogen atmosphere.

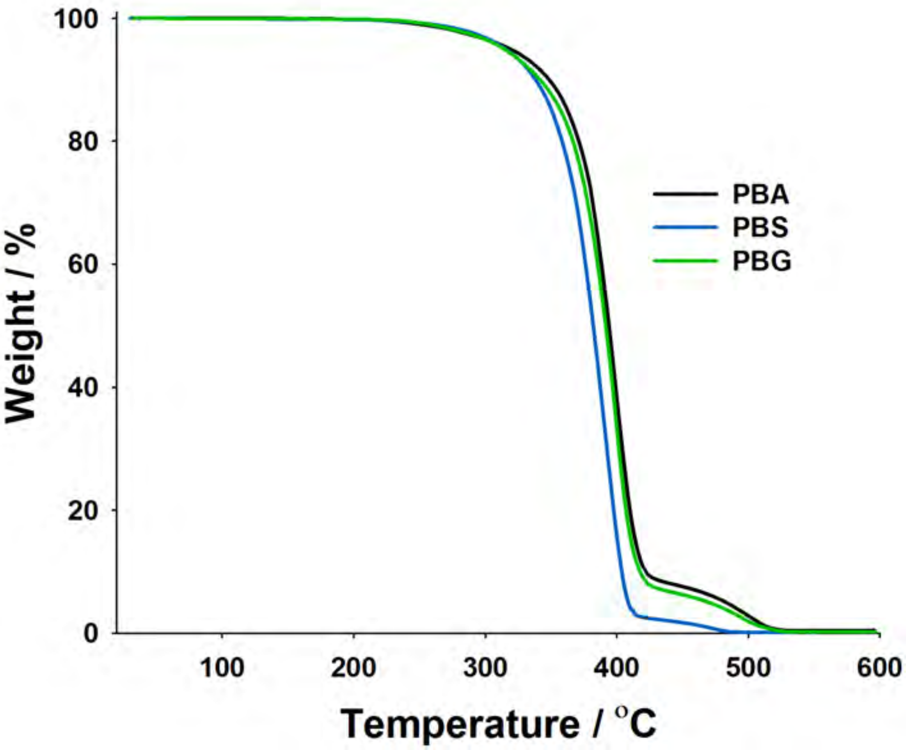

(a) TGA under air

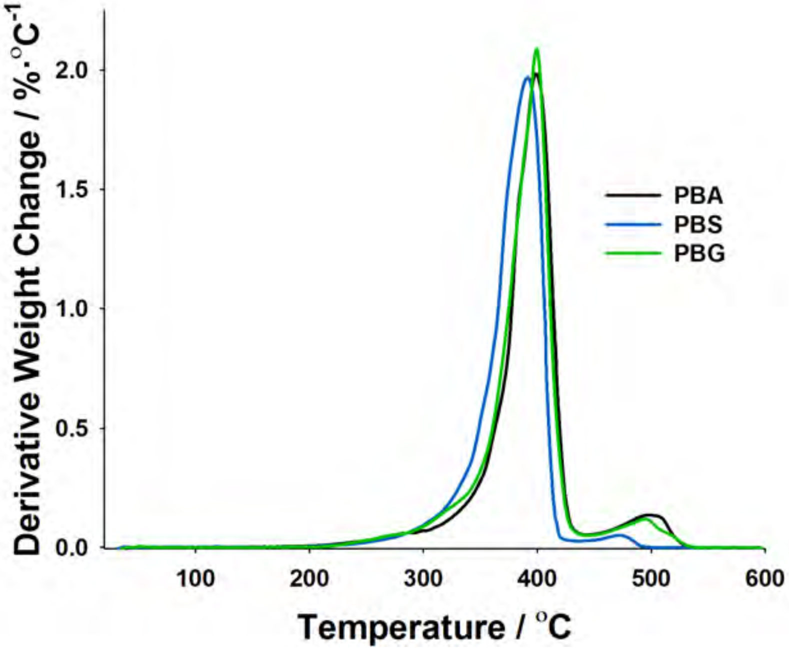

(b) dTGA under air

Figure 5.12: Homopolymers (a) TGA and (b) dTga curves under air atmosphere.

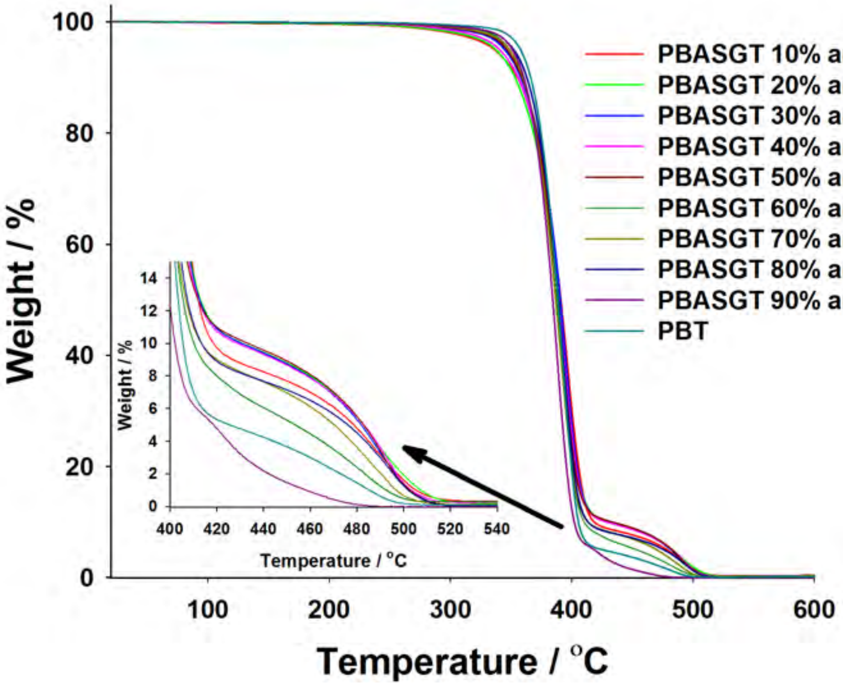

(a) TGA under air

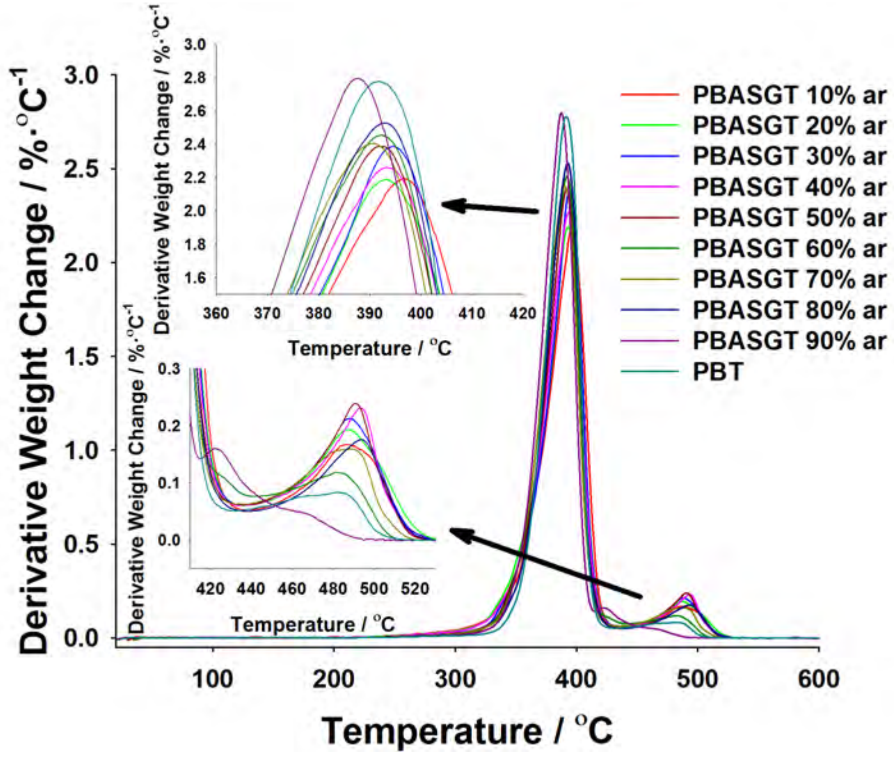

(b) dTGA under air

Figure 5.13: PBASGT copolymers (a) TGA and (b) dTGA curves under air atmosphere.

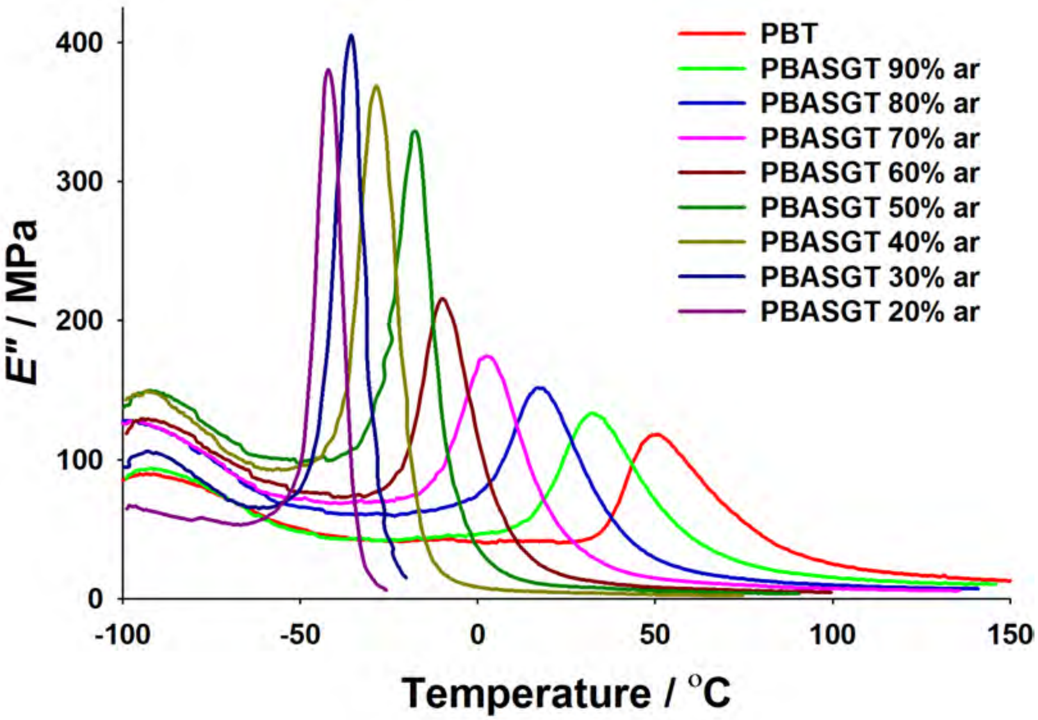

(a) E''

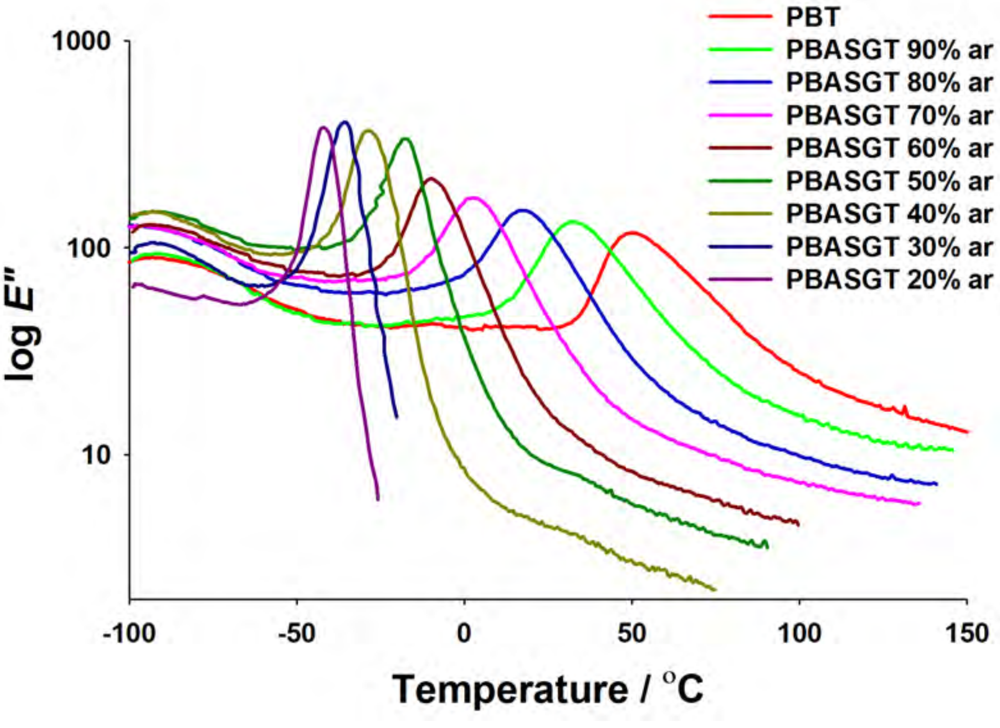

(b) $\log E''$

Figure 5.14: Dynamic mechanical relaxation behavior of PBT and PBASGT copolymers presented as (a) E'' and (b) $\log E''$.

step of degradation is purely thermal. Li et al. [140] described it as the thermal degradation of copolyesters from high molecular weight macromolecules into smaller chain fragments via an initial scissoring of the chain end. The second stage of degradation is observed in oxygen atmosphere and it is related to an oxidative degradation process, reported in the literature for aromatic copolyesters [142] and aliphatic-aromatic ones [140].

Table 5.7 summarizes the determined thermal degradation parameters of the 2% weight loss temperature (T_{id}), the temperature of maximum weight loss rate (T_{max}) under both atmospheres and oxidation temperature (T_{ox}) under air atmosphere. It can be noticed that all samples of PBASGT shows slightly lower temperatures of degradation initiation and temperatures of maximum weight loss rate in the air atmosphere in comparison to the nitrogen atmosphere. However, no such tendency can be noticed in the case of oxidation process. There are some fluctuations of the peak oxidation temperature that can be caused by less stable chain structures of aliphatic-aromatic copolyesters with random comonomer sequential distribution and/or by obtaining various small molecular weight polymer fragment during the thermal degradation, which

Table 5.7: Thermal analysis results of homopolymers: PBA, PBS, PBG and random copolymers PBASGT of various composition. T_g values taken from the dependence of loss modulus vs. temperature shown in Fig. 5.14(a). The crystallinity (χ) was calculated for the aromatic fraction of the copolyester, as shown in Subsection 5.1.2, based on the heat of fusion of 100% crystalline PBT, ΔH_m^0, of 144.5 J·g^{-1} [141] and by taking into account weight fraction of aromatic component from Tab. 5.3 and heat of second melting. (nr - not related)

Sample	T_{id}		T_{max}		T_{ox}	T_g	T_m	T_c	χ
	nitrogen	**air**	**nitrogen**	**air**	**air**				
			/°C						/wt.%$_{BT}$
PBA	268	277	366	398	498	nd	59	30	nr
PBS	292	285	393	392	472	nd	115	68	nr
PBG	321	279	404	400	495	nd	46	-21	nr
PBASGT 10% ar	306	300	404	397	486	-	-	-	-
PBASGT 20% ar	315	305	404	393	487	-42	46	-	-
PBASGT 30% ar	331	322	402	395	488	-36	74	-	7
PBASGT 40% ar	338	313	402	393	493	-28	108	22	19
PBASGT 50% ar	342	325	402	392	491	-18	136	71	22
PBASGT 60% ar	347	332	401	392	481	-10	158	102	23
PBASGT 70% ar	349	328	400	391	488	3	180	131	28
PBASGT 80% ar	351	335	400	393	494	17	196	150	32
PBASGT 90% ar	352	336	397	388	470	32	211	171	34
PBT	356	345	400	392	483	51	225	190	40

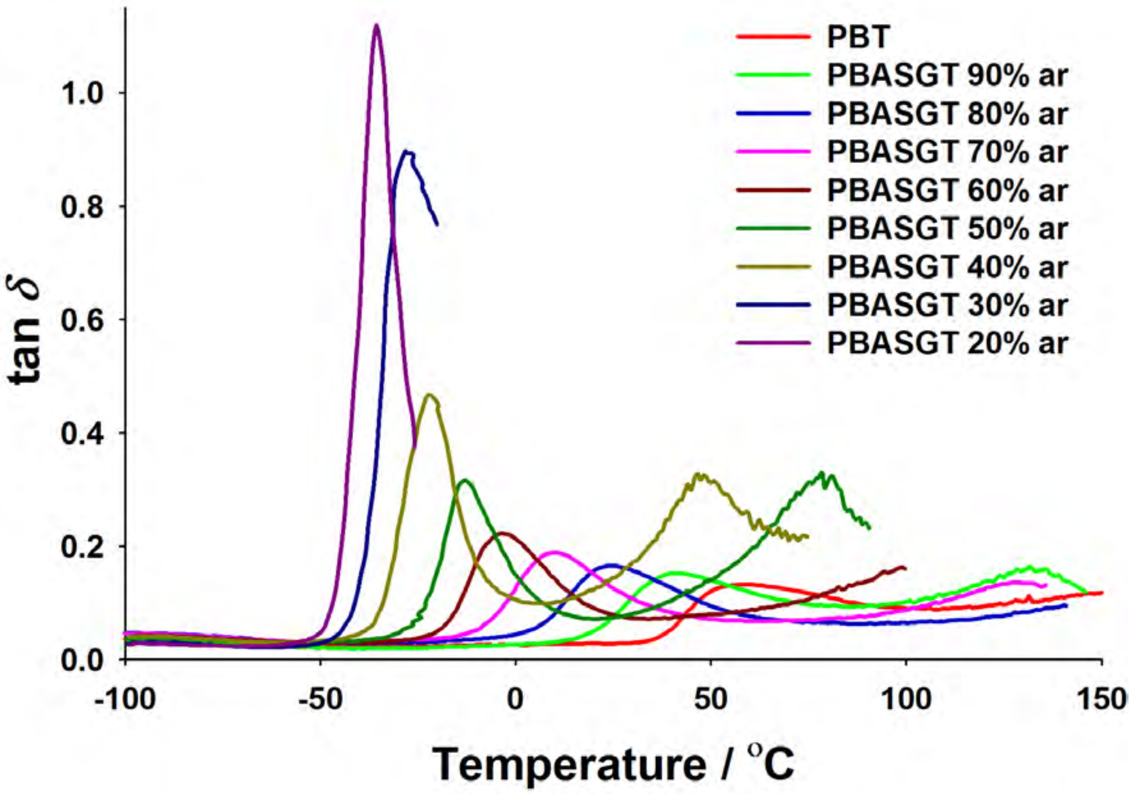

Figure 5.15: Dynamic mechanical relaxation behavior of PBT and PBASGT copolymers presented as tanδ.

are further thermally-oxidized into volatile small-molecular products [140].

The dependence of loss modulus vs. temperature presents one relaxation peak (Fig. 5.14(a)). The relaxation at -42°C corresponds to the glass transition of aliphatic part of PBASGT. The high intensity of the peak resulted from the low crystallinity of copolyesters with low content of aromatic units. With increasing terephthalate content, the peak decreased in intensity and gradually shifted to higher temperatures. However, log$E$" (see Fig. 5.14(b)) showed that there is small second relaxation peak for copolyesters for initial composition of 40% and 50% of aromatic units. Those peaks are better visible in Figure 5.1.3 where the dynamic mechanical relaxation behavior is presented as the temperature dependence of tanδ. Those peaks corresponds to the glass transition of aromatic component. Thus, regarding the T_g, three groups of copolyesters can be determined. Copolyesters with initial aromatic content below 40% exhibits one relaxation peak characteristic for aliphatic components. Second group contains copolyesters with 40% and 50% of initial aromatic content, which possess aliphatic and aromatic glass transition. The third group is composed of copolyesters with aromatic content above 50% of initial aromatic content. Those copolyesters possess one relaxation peak, corresponding to the glass transition in the aliphatic/aromatic-rich amorphous phase.

The changes of other transition temperatures together with the increase of aromatic

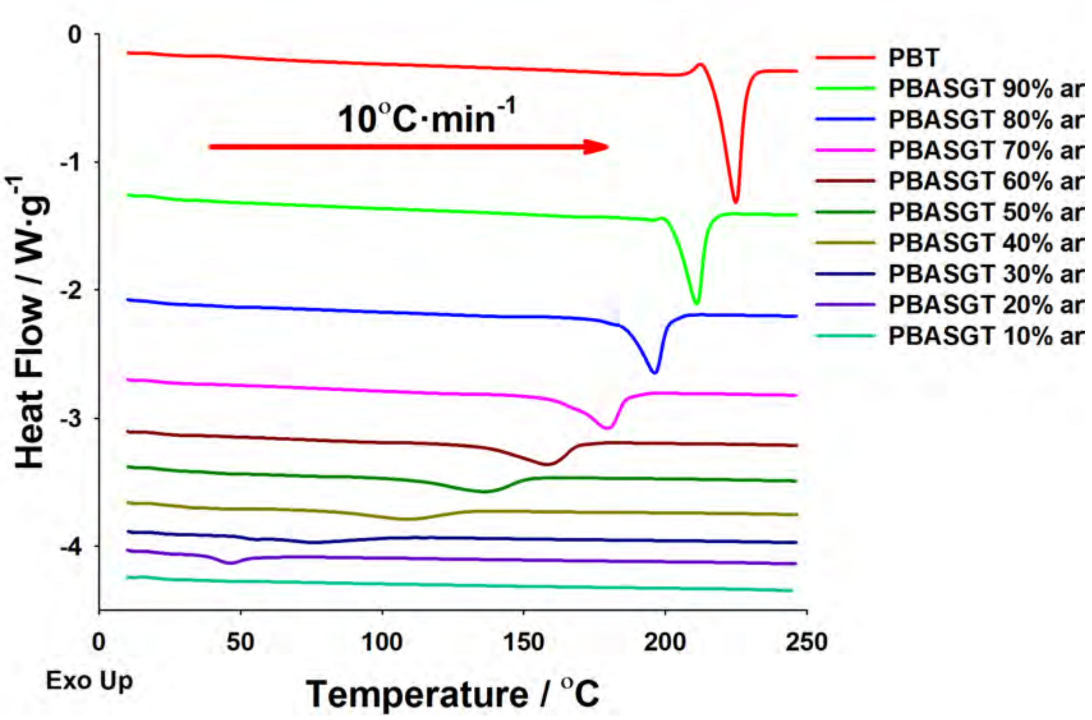

(a) heating

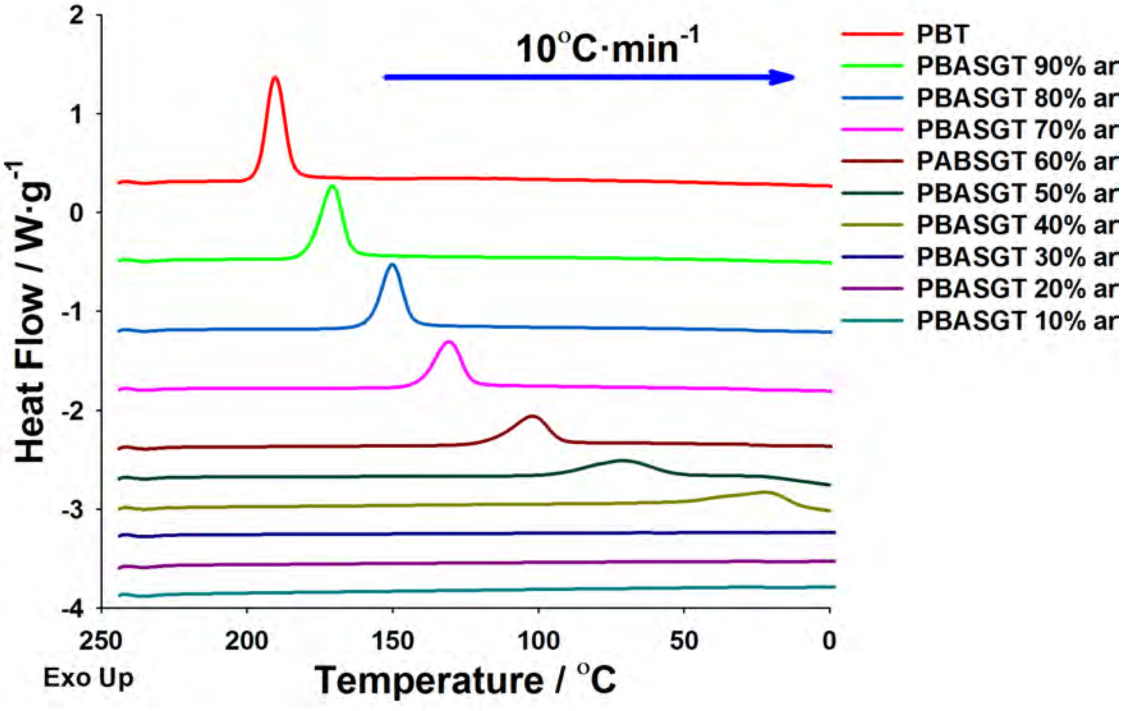

(b) cooling

Figure 5.16: (a) Heating and (b) cooling thermograms at the rate 10°C·min^{-1} of PBT and PBASGT copolyesters. PBASGT copolymers curves are shifted vertically for better visualization.

units content was also observed in calorimetry. DSC thermograms are presented in Figure 5.16. PBASGTs exhibit clear and distinct melting. For PBASGT with aromatic content more than 60% there is a clear and narrow melting peak. On the DSC heating traces for copolyesters with aromatic content between 20% and 60% of aromatic content the peak is broad and flat. The melting peak of the PBASGT copolyester with aromatic content equal to 10% is invisible. The increase of aromatic units content causes narrowing of the melting peak and shift of melting peak temperature to higher values (see Fig. 5.16(a)). Similar observations are made for the crystallization peak (see Fig. 5.16(b)). However, the crystallization process is pronounced for samples containing more than 30% of aromatic component in the range of temperatures between 250°C to 0°C. PBASGT copolyesters containing less than 40% of initial **BT** content do not show crystallization peak at the cooling rate 10°C·min^{-1}. Nevertheless a small melting peak is observed in heating runs of these sample. It suggests that copolyesters with less than 40% of initial aromatic content needs a lot more time to crystallize. Thermal data of PBASGT are summarized in Table 5.7.

5.1.4 Crystal growth

Increase of the peak crystallization temperature together with the increase of aromatic unit content is also visible in the SAXS patterns obtained *in situ* during the non-isothermal crystallization with the rate of 10°C·min^{-1}. Moreover, Figures 5.17 and 5.18 demonstrate that first crystals are detected in the SAXS patterns at the temperature around 10°C higher than the crystallization peak determined by DSC (see Tab. 5.7). It is also visible that together with the increase of aromatic units content the development of scattering peaks in SAXS patterns in Figures 5.17 and 5.18 is more rapid, especially if we consider patterns collected in the vicinity of peak crystallization temperature. Moreover, Figures 5.17 and 5.18 show that together with the temperature decrease a formation of peak is visible, which intensity is decreasing afterwards and the peak is flatten.

Figure 5.19 shows SAXS pattern profiles obtained for copolyesters with various compositions during the nonisothermal crystallization, SAXS patterns recorded at 20°C. Peaks are observed in the scattering vector (q) range of -0.10 nm^{-1} to -0.06 nm^{-1}. The increase of the **BT** unit in compositions causes the increase of peak intensity and the shift to lower q values. The intensity increase is connected with the increase of crystallinity degree of the copolyester while the q peak value shift is connected with the lamellae thickness. Determination of the lamellae thickness supports this observation. Calculation showed that there is 0.2 nm differences between the final crystals thickness for PBASGT copolyester possessing 70% and 90% of initial aromatic content. Apparently the increases of intensity and crystal thickness are connected with the increase of aromatic sequence length as it is shown in Table 5.3.

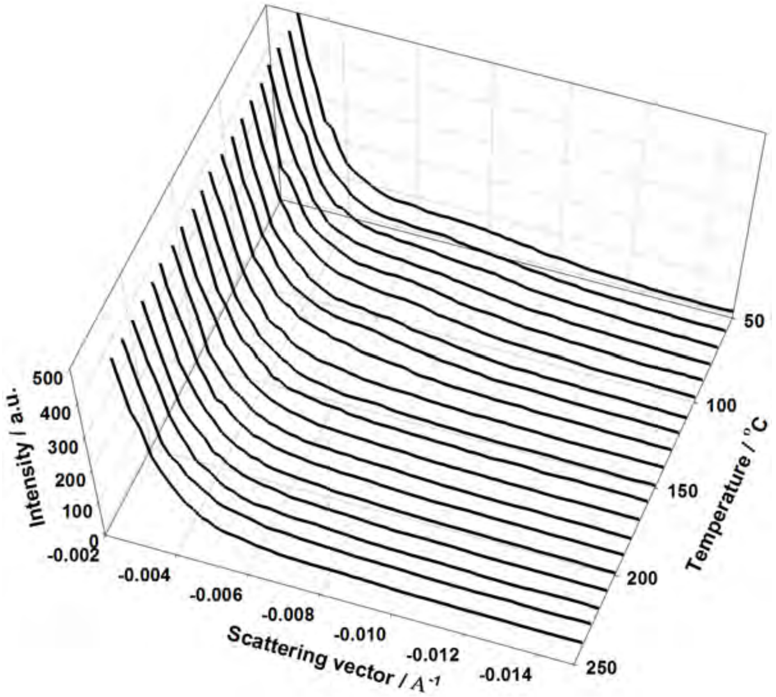

(a) heating

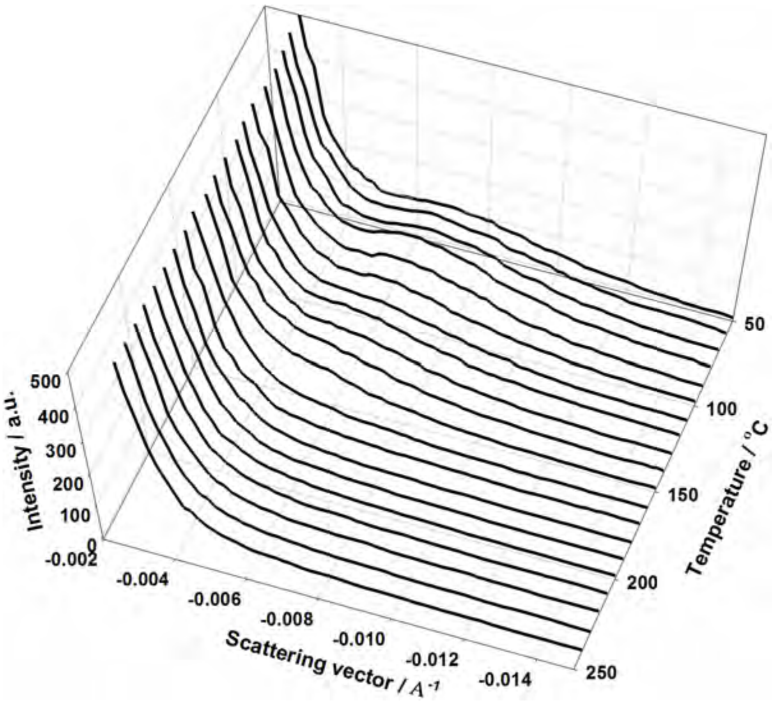

(b) cooling

Figure 5.17: SAXS profile development during the nonisothermal crystallization during cooling with the rate at 10°C·min^{-1} of PBASGT copolyester with feed aromatic content equal to (a) 70% and (b) 80%.

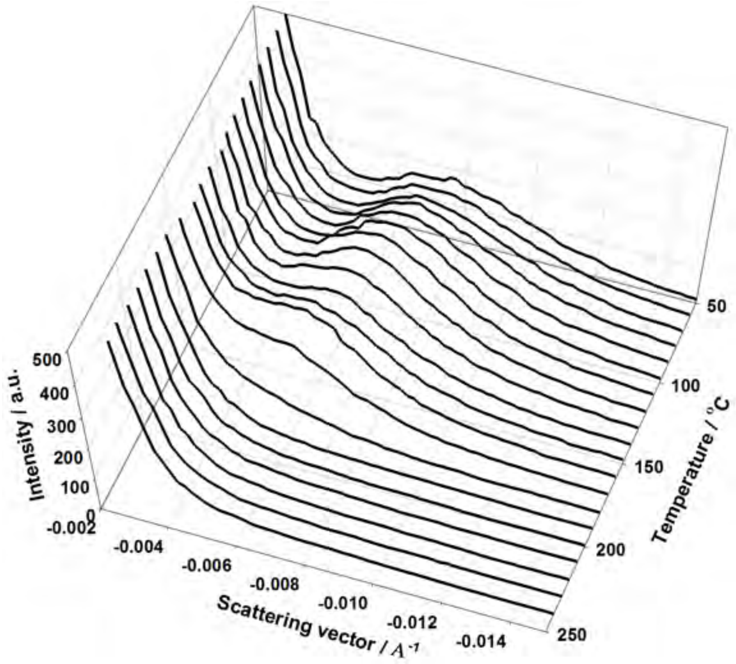

Figure 5.18: SAXS profile development during the nonisothermal crystallization during cooling with the rate at 10°C·min^{-1} of PBASGT copolyester with feed aromatic content equal to 90%.

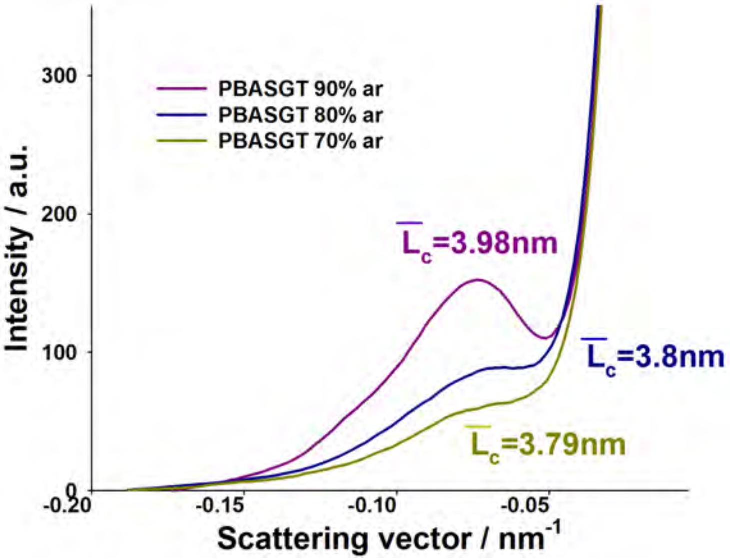

Figure 5.19: Comparison of SAXS profiles, recorded after nonisothermal crystallization at 20°C, of copolyesters with various composition.

5.1.5 Stress-Strain Behavior

Figure 5.20 presents the stress-strain behavior of PBASGT copolyesters with various compositions.

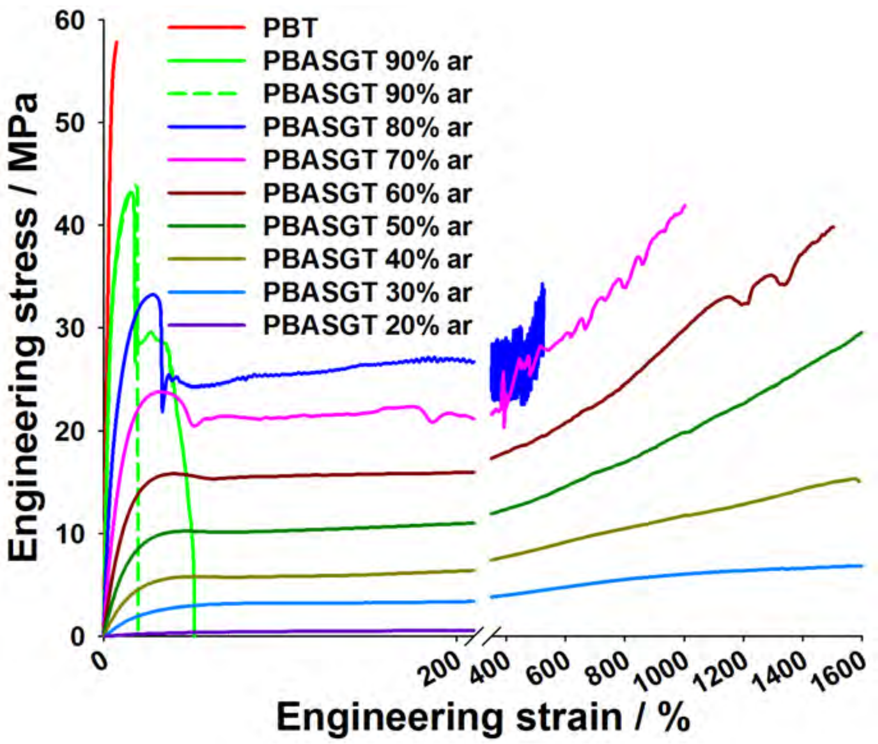

Figure 5.20: Tensile stress-strain curves of PBT and PBASGT copolyesters.

These polymeric materials exhibit the internal structure at all levels from the molecular to the macroscopic scales. At the molecular level polymers are made up from repeating units, and the chemical nature of these units clearly must have a large effect on the material as a whole. For example, depending on the type of chemical bonds in the chain the molecules may be stiff or flexible. Flexible molecules are those in which rotation around the chemical bonds in the backbone of the molecules is possible with activation energies of not more than a few kT. Rigid molecules include both the rigid rod molecules in which such bond rotations are always impossible and also molecules which are below their glass transition temperatures where the activation energies for bond rotation are prohibitive. In general flexible molecules provide flexible materials while stiff molecules provide stiff materials [112]. One of the main factors influencing mechanical properties of polymeric materials is their ability to crystallize and their crystallinity.

In the case of PBASGT copolyesters the transformation from flexible to stiffer materials is also observed together with the increase of **BT** units. The PBASGT copolyester with 10% of initial aromatic units content is so flexible that it was not possible to form a film from it, also because it does not show any sign of crystallinity. In the case of

PBASGT copolyester with 20% of initial **BT** unit content it was necessary to leave the film for few days for slow crystallization to be able to cut from it a sample for measurements.

Copolyesters with aromatic unit content below 60% deformed in an uniform manner characteristic for rubbers (see Fig. 5.20). With increasing aromatic units content the yield stress point becomes well-defined and the deformation manner changes. For copolyester with 80% of aromatic content a rubber deformation manner changes to stress-oscillating (or self-oscillating) due to jumping from uniform stable necking to neck propagation form of deformation and reverse. Thus stress oscillation means that the stress developing during drawing is not constant anymore, but exhibit periodic fluctuations as a function of time. Such a behavior was already reported in the literature for copolyesters by Karger-Kocsis [143]. This phenomenon cause the formation of a pattern (see Fig. 5.21) containing alternating opaque-white and transparent regions in the sample.

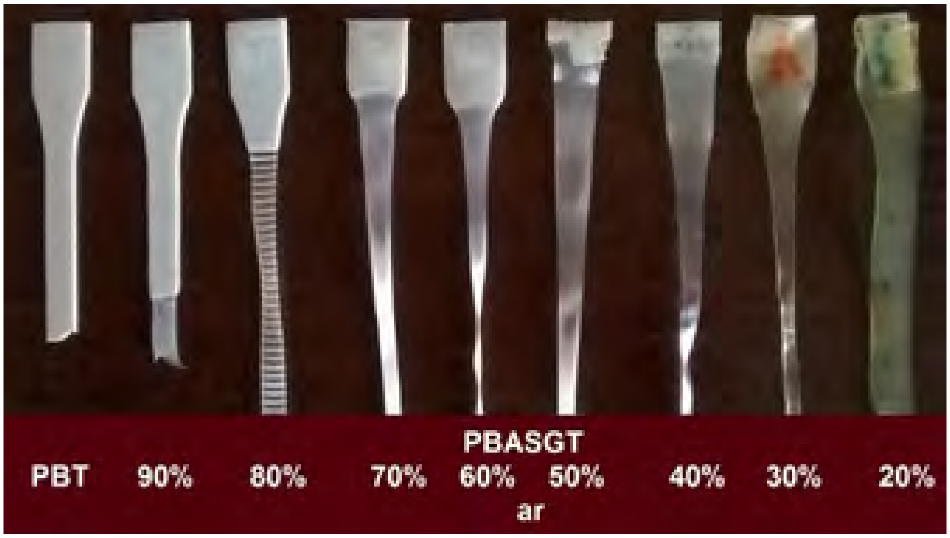

Figure 5.21: Photo of PBASGT samples with various composition after the uniaxial deformation.

Moreover, Figures 5.22 and 5.23 show the temperature of the sample surface as recorded with thermovision camera, with synchronous recording of stress-strain behavior during uniaxial stretching. It is seen that the increased temperature at point A indicate the termination of neck formation and the beginning of its propagation through the sample as it was reported by Pawlak et al. [144]. While the simultaneous decrease of temperature and stress, as it is shown in Figure 5.22 for other systems, can be connected with the change of localization of neck propagation from point C to D or from E to F. Furthermore, in Figures 5.22 and 5.23 it is noticed that higher stress build-up values causes higher heating of the sample. The stress oscillation cause formation of a pattern (see Fig. 5.21) containing alternating opaque and transparent areas on the sample surface. The SAXS observations showed that the reason for visible stress whitening

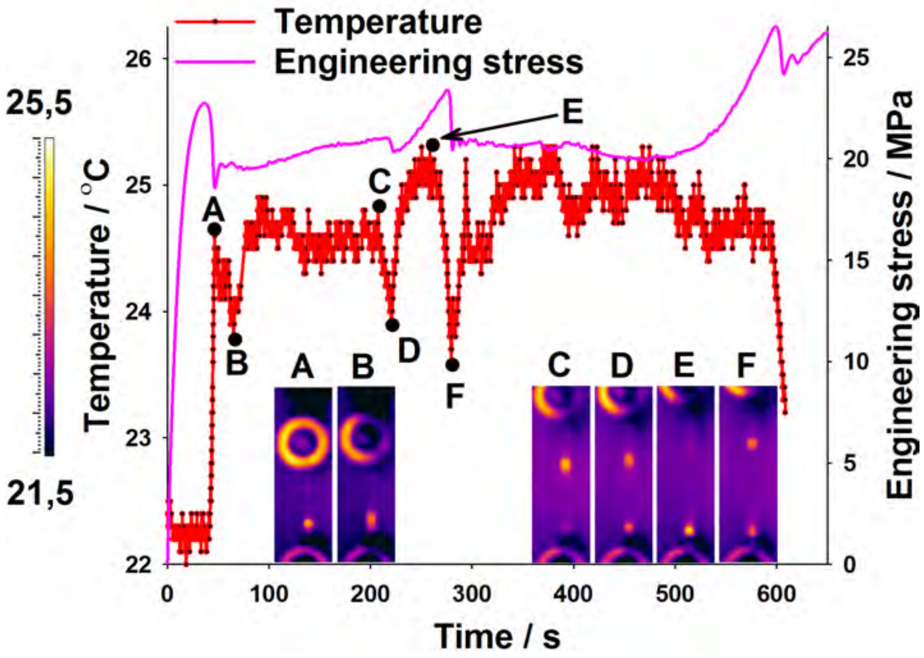

Figure 5.22: Deformation of PBASGT 70% of initial aromatic units content: pink curve presents behavior of engineering stress and red one shows maximal surface temperature of the sample. All curves plotted as a function of time of drawing. Thermovision photographs of drawn samples are taken at moments of time as indicated by letter A, B, C, etc. on the temperature-time curves. The yellow circles visible on thermovision photographs are tensile machine holders.

in PBASGT 80% was the formation of voids (Fig. 5.24).

The reasons of this oscillation were discussed in the literature. The following explanations are proposed: local heating induced by orienting elongation [145], oscillation of local deformation rates in the critical stress range during necking [146] or crystallization during orientation caused by adiabatic heating [147]. In the case of PBASGT thermovision camera has shown that, within the oscillation cycle, simultaneously with the increase of the stress the temperature of the deformation zone increased, but when the stress decreased (during neck propagation) the temperature decreased (see Fig. 5.23).

The shape of scattering pattern for PBASGT with 80% aromatic fraction indicates that the voids were elongated in the direction of stretching which was horizontal. Moreover, the cavitation is a potential reason of the intensive heat generation and an increase of the sample temperature during stress oscillation (Fig. 5.23). However, the generation of voids itself is not very energetic process, it is rather the intensification of deformation processes around cavities as chain slips and/or lamella fragmentation. The SAXS patterns that are recorded from the areas as shown in Figure 5.24 indicate also that the voids located further from the breaking point are smaller than those located closer.

With further increase of aromatic content to 90% (see Fig. 5.20) the deformation

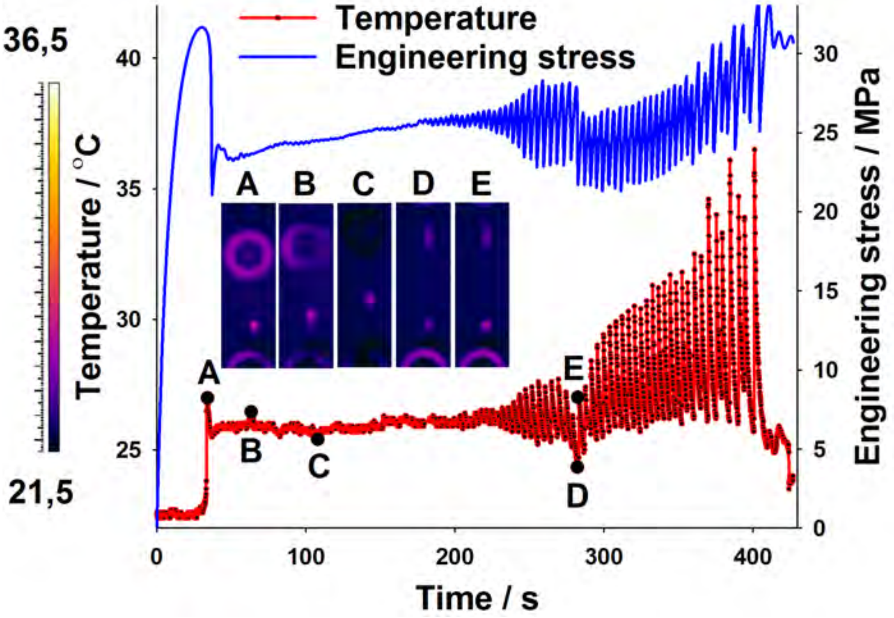

(a) PBASGT 80% ar

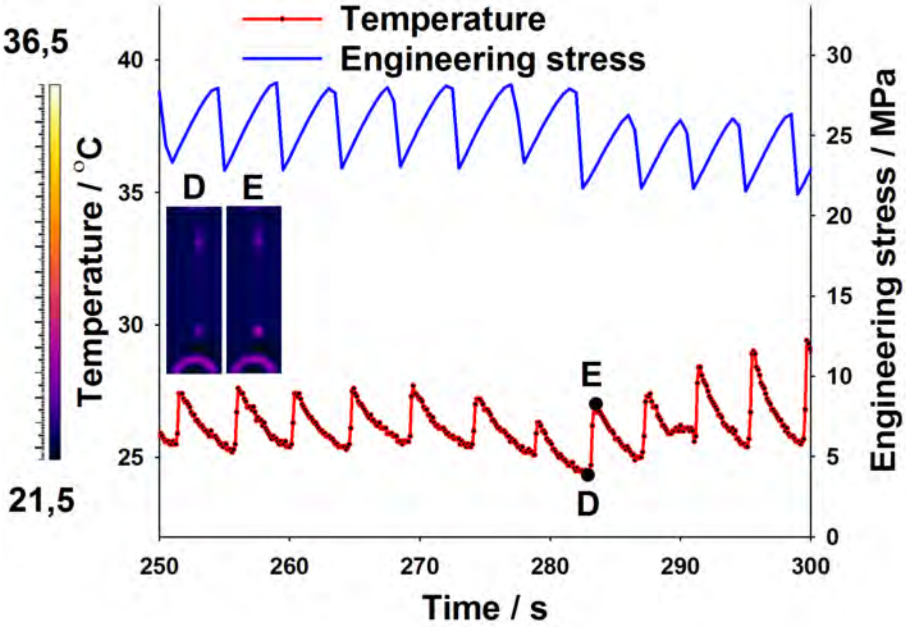

(b) magnification of oscillations

Figure 5.23: Deformation of PBASGT 80% of initial aromatic units content: blue curve presents oscillations of engineering stress and red one shows maximal surface temperature of the sample. All curves plotted as a function of time of drawing. Thermovision photographs of drawn samples are taken at moments of time as indicated by letter A, B, C, etc. on the temperature-time curves. The blue circles visible on thermovision photographs are tensile machine holders.

proceeds in a manner characteristic for semicrystalline thermoplastics with highly localized yielding and formation of a well-defined neck or by breaking shortly before reaching the yield point, which is characteristic for aromatic homopolymer. The effects of uniaxial deformation of PBASGT copolyesters, shown in Figure 5.21, presents clearly the transformation from flexible to brittle material while increasing the aromatic fraction of copolyester composition. The characteristics of mechanical properties are collected in Table 5.8. It shows that together with the increase of aromatic units the stress at break is increasing also, but simultaneously the elongation at break is decreasing.

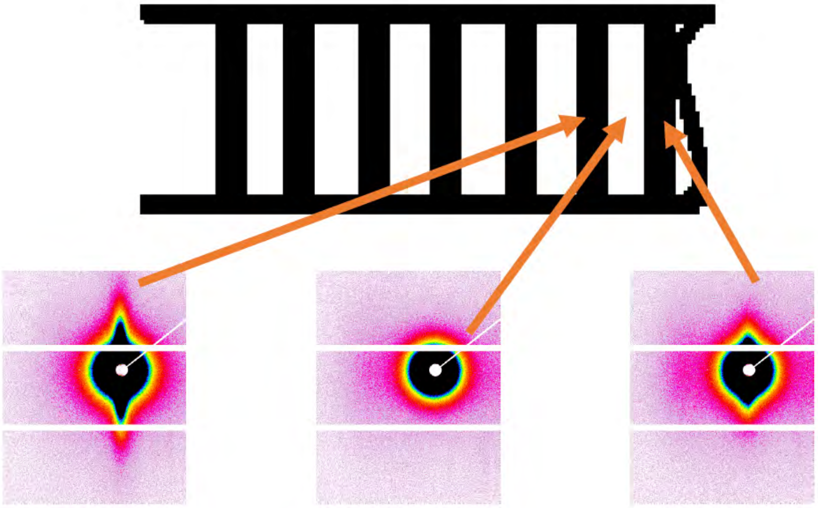

Figure 5.24: SAXS pattern from the neck regions of PBASGT with feed aromatic content equal to 80%. The patterns were recorded for the broken sample. Stretching direction was horizontal. The black areas in the sample scheme correspond to the whitening sample areas and the white one to the transparent one.

Figure 5.25 shows the SAXS and 2D WAXS patterns recorded *in situ* at different engineering strains. It is clear that the samples become gradually oriented with increasing strain. From the inspection of SAXS pattern (Fig. 5.25), a broad circular maximum is observed, demonstrating that PBASGT copolyesters samples are unoriented before drawing. Upon an increase in strain, the broad rings start deforming. For copolyesters with the lowest amount of aromatic units the circle is deformed into an ellipsoid. For similar engineering strain of 25% the ellipsoid becomes less pronounced for PBASGT with increasing aromatic unit content. However, simultaneously an increase of two maxima in the equator are noticeable. Together with the increase of strain, depending on the composition, two-lobe patterns develop.

In the case of PBASGT 60% ar and PBASGT 70% ar the two lobe patterns are less pronounced. This effect is apparently caused by the formation of the neck, i.e. the enginnering strain of 100% includes a neck zone with 500% or 450% for samples with 60% and 70% of aromatic units, respectively. Moreover, for all the samples no cavitation

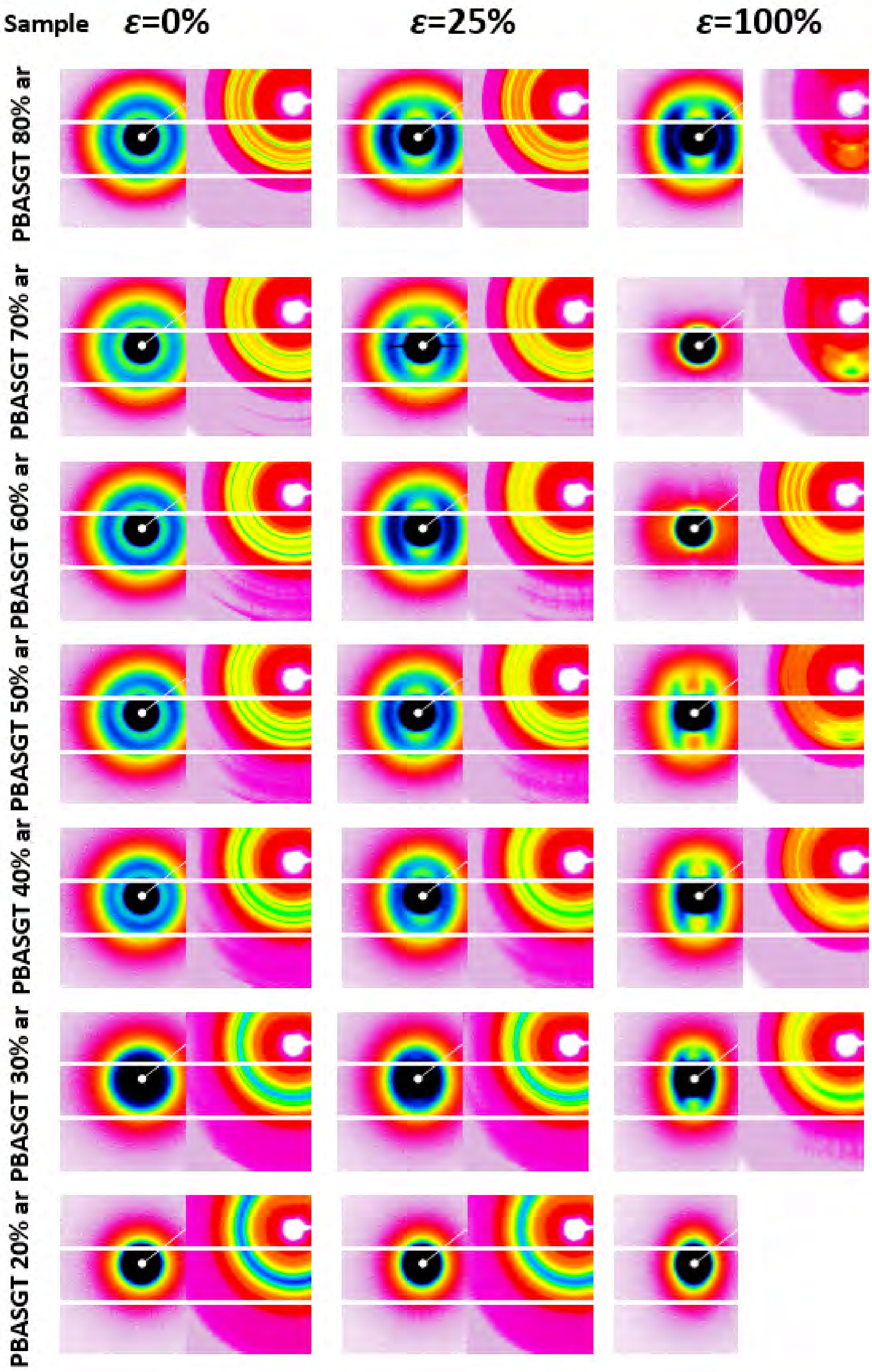

Figure 5.25: SAXS and WAXS patterns for PBASGT copolyesters stretched at various engineering strains with the stretching rate 100%·min^{-1}. The stretching direction is horizontal.

Table 5.8: Selected tensile parameters for copolyesters with various compositions. (nd - not determined)

Sample	**Engineering Stress at break**	**Engineering Elongation at break**	**Modulus of elasticity**
	$\bar{\sigma}_b$/MPa	$\bar{\epsilon}_b$/%	E/MPa
PBASGT 20% ar	0.5	260	nd
PBASGT 30% ar	6.8	1775	nd
PBASGT 40% ar	15.3	1600	65
PBASGT 50% ar	28.6	1550	111
PBASGT 60% ar	34.2	1250	201
PBASGT 70% ar	40.6	1000	360
PBASGT 80% ar	35.3	560	690
PBASGT 90% ar	33.9	30	1730
PBT	54.2	10	2650

was observed until engineering strain equal to 100%. However, the SAXS patterns for broken PBASGT samples present, that in the case of copolyesters containing between 80% and 50% of the initial **BT** content, the presence of voids. Thus, the cavitation is ensued for engineering strain higher than 100%.

Before drawing, the WAXS 2D patterns (see Fig. 5.25) consist of circular reflections corresponding to the reflection of PBT crystals α-form. Together with the engineering strain increase an arcing of the Bragg reflections are produced, which finally leads to a spot diagram. In the most composition the spot possess two maxima, but in the case of PBASGT 80% of aromatic units there is only one maximum. Depending on the copolyesters composition and local strain the spot pattern coexist with the ring pattern. Further analysis showed that, maxima of the peaks are not located exactly in the same position as the initial rings, but there exists a small displacement [148]. It can be caused by a reversible solid-state transition between the α and the β form of PBT-like crystals induced by extension and relaxation of the extension. However, the reflections from β-form crystals are at the noise level on those WAXS patterns. Moreover, due to the presence of soft segments, the percentage of stretching necessary to initiate this transition is higher, since some of the applied deformation is absorbed by the soft segments.

Furthermore, the aliphatic segments affects also the WAXS pattern of PBASGT copolyesters after the stretching (see Fig. 5.26). Generally, it was reported that there were observed two reflections for the PBT stretched films [149, 150]. In the case of PBASGT copolyesters it is observed that together with the increase of aliphatic part content the maxima of those two reflection become more intensive and the third one is becoming visible.

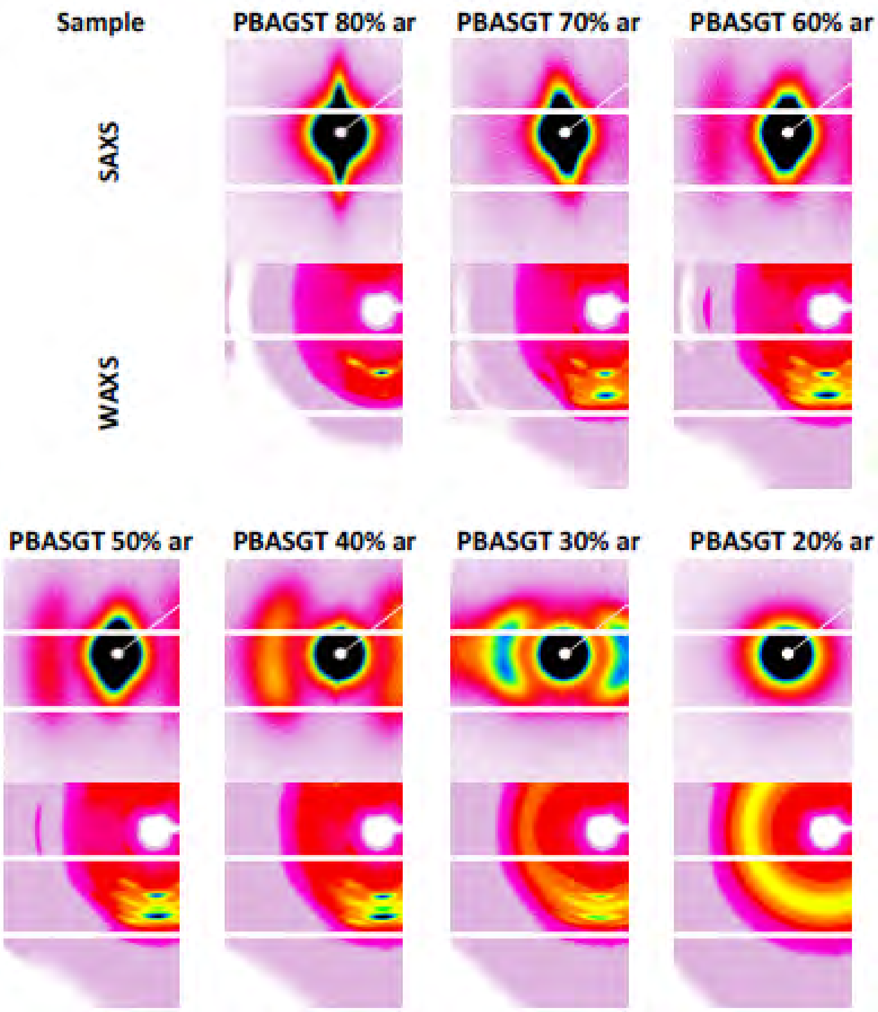

Figure 5.26: SAXS and 2D WAXS patterns for broken unloaded PBASGT copolyesters after stretching with the rate 50%·min^{-1}. The stretching direction is horizontal.

5.2 Crystallization characterization of selected copolyester

Most of aliphatic-aromatic copolyesters are biodegradable under rigorous condition of sufficiently short aromatic sequences. However, it can decrease the ability of aliphatic-aromatic copolyesters to crystallize and limit possible applications. The NMR analysis of the length of aromatic sequences in a series aliphatic-aromatic copolyesters, presented in Subsection 5.1.1, together with the crystallinity data from DSC, indicated that the composition with initial aromatic component content of 40% should be a compromise between proper fast solidification during processing (and hence, good mechanical properties) and biodegradability. Biodegradability of AAC containing initially 40% of aromatic comonomer was studied by accredited Laboratory of Biodegradation at the Institute of Biopolymers and Chemical Fibers, Lodz, Poland. I got the permission to use their data to support the selection of the 40% aromatic AAC for further detailed studies. The main facts concerning its biodegradability are presented in Appendix.

5.2.1 Composition and comonomer sequence distribution analysis

For the purpose of further detailed studies of chemical structure, morphology, crystallization habits and other physical properties a batch of 30 dm^3 of aliphatic-aromatic was synthesized according to the same polycondensation procedure. A 30 dm^3 acid proof clave was used for the reaction. All physical parameters was kept identical as for 9 dm^3 clave only the amounts of reagents were increased by 30/9 ratio. The same NMR analysis, as in Subsection 5.1.1, was repeated for the copolyester synthesized in 30 dm^3 reactor. The fractions of aliphatic/aromatic sequences, fractions of aromatic and aliphatic components and their average lengths are presented in Table 5.9. In addition, for comparison, similar measurements were conducted for commercial aliphatic-aromatic copolyester PBAT by BASF and the respective data are also collected in Table 5.9. As it can be seen from Table 5.9, PBASGT copolyester is nearly random, because R is nearly 1. It is worth to note that the average block length of aromatic units (**BT**) is only 1.791. Such short average aromatic sequences are degradable by microbes as it was found by others [1, 131] and confirmed for this material by accredited laboratory (see Appendix). Hence PBASGT is fully biodegradable, not only its aliphatic units. Other important value is the molar fraction of aromatic units, which is 0.452 for PBASGT. This value ensures a good compromise between biodegradability and physical properties when it is kept on the optimal level between 35-55mol% [131, 132].

Table 5.9: Comparison of sequence distribution of the synthesized PBASGT copolymer and commercial PBAT by BASF.

Sample	f_{AlAl}	f_{AlAr}	f_{ArAl}	f_{ArAr}	P_{Al}	P_{Ar}	$\bar{L}_{nAl}$	$\bar{L}_{nAr}$	R
PBASGT	0.295	0.253	0.251	0.200	0.548	0.452	2.170	1.791	1.019
PBAT	0.264	0.249	0.249	0.238	0.513	0.487	2.057	1.952	0.998

Table 5.9 shows also that the commercial aliphatic-aromatic copolyester PBAT exhibits similar molecular characteristics as PBASGT: with similar aliphatic to aromatic component ratio, PBASGT and PBAT exhibit similar average length of aliphatic and aromatic sequences and similar randomness index. However, it must be realized that aliphatic components in PBASGT are three different aliphatic esters while PBAT aliphatic part contains only dimethyl adipate ester (see Table 5.9). It should be mentioned that the molecular weight of synthesized PBASGT is lower than that of commercial PBAT copolymer as shown in Table 5.10. Such difference is the result of addition of "chain extenders", CESA, in the production of PBAT (Ecoflex$^{®}$) [151].

Table 5.10: Molecular weights as measured by SEC-MALLS of PBASGT and commercial PBAT.

Sample	**Molecular weight**		
	$M_w(\times 10^{-4})$ / $g \cdot mol^{-1}$	$M_n(\times 10^{-4})$ / $g \cdot mol^{-1}$	M_w/M_n
PBASGT	4.94	3.14	1.56
PBAT	7.62	4.02	1.89

In order to describe the sequence distribution of aromatic units the Bernoulli statistics can be used, as suggested by Bovey and Tiers in other cases [152]. Since the aromatic sequence distribution is nearly random, we can use the Poisson distribution (Equation 5.18) to estimate the fraction of longer aromatic sequences.

$$P(k) = \frac{exp(-\lambda)\lambda^k}{k!} \tag{5.18}$$

where $P(k)$ is the probability, λ is the average block length of aromatic units, and k is the number of aromatic units next to each other.

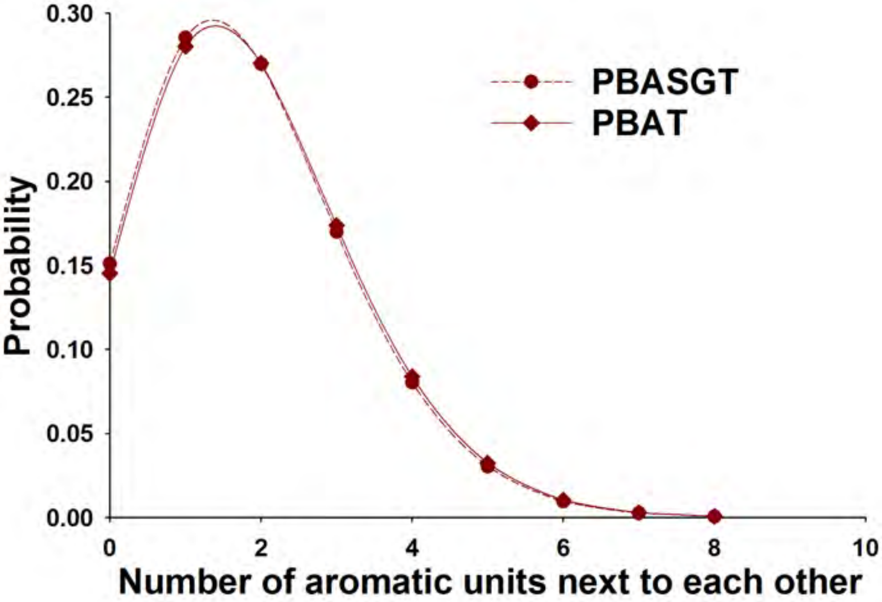

Figure 5.27: The Poisson distribution of the aromatic units for the average number of adjacent aromatic units as it follows from NMR analysis for PBASGT and PBAT (see Table 5.9).

The probability of finding one, two or more sequences of aromatic unit next to each other is plotted in Figure 5.27. It shows, that the most probable is to find in the

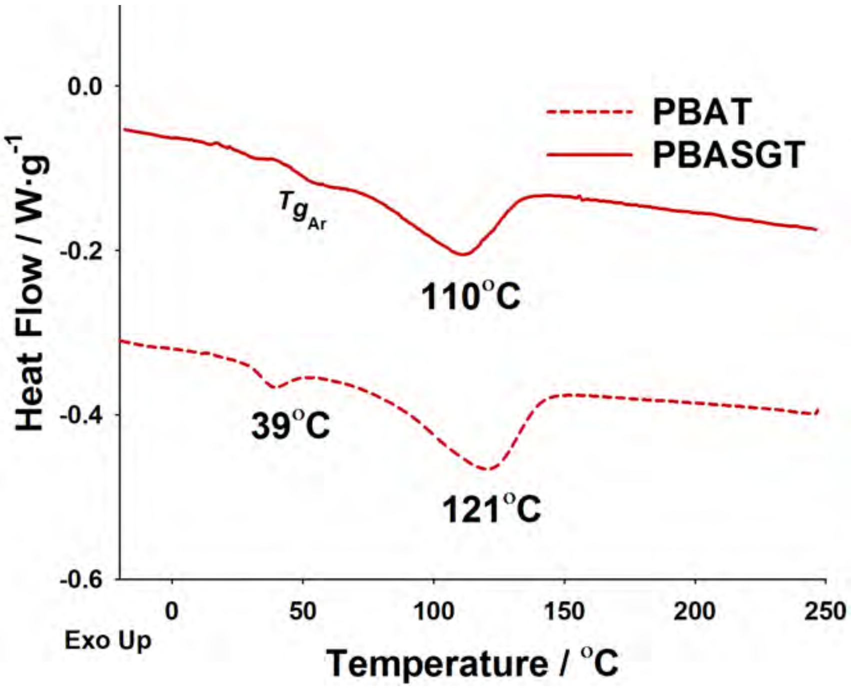

Figure 5.28: Heating thermogram at the rate 10°C·min^{-1} of PBASGT and PBAT subjected to low temperature annealing. PBASGT curve is shifted vertically for clarity.

chain a single aromatic unit or two next to each other. It is also worth to underline that three, four or five consecutive aromatic units appear in the chain with the probability of approximately 17%, 8% and 3%, respectively. Such structure makes the crystallization of PBASGT probable, hence, it is feasible that 3, 4 or 5 unit aromatic sequences can form small crystals. Similar consideration applies to the aliphatic part of copolyesters with the exception for that aliphatic part of PBASGT is composed of three different aliphatic units and its *co*-crystallization is rather unlikely. In contrast to PBASGT it is probable that aliphatic part of PBAT can crystallize because it comprises only one type of aliphatic units - adipate comonomer. Homopolymer of butylene adipate crystallizes having melting temperature of 56°C. It is expected that butylene adipate crystalline sequences in a random copolymer with butylene terephthalate would show much lower crystallization and melting temperatures than those of homopolymer. In order to check the possibility of crystallization of aliphatic component, samples of the copolymers were cooled down to +4°C and kept at this temperature for 24 hrs. Figure 5.28 presents melting endotherm of PBASGT and PBAT samples subjected to such low temperature annealing.

On PBASGT curve T_g of the aromatic component can be distinguished at around 47-50°C. In order to confirm the interpretation of T_g of aromatic component we have performed partial heating up to 60°C in a DSC apparatus of the same PBASGT film sample as in Figure 5.28. Then the sample was cooled down to 0°C and heated to 250°C with the rate of 10°C·min^{-1}. Before this experiment the film was kept at room

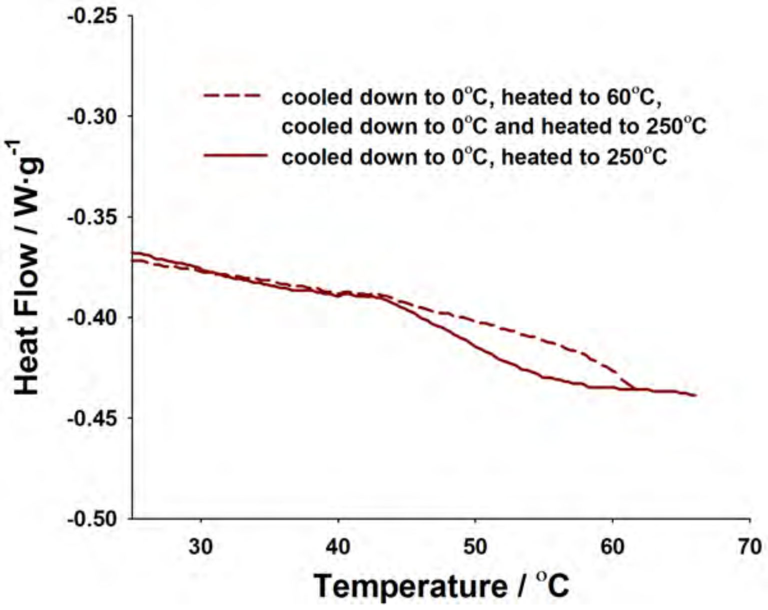

Figure 5.29: DSC traces of PBASGT film during heating to 60°C (solid line) then cooled down to 0°C and heated again (broken line). Heating and cooling 10°C·min^{-1}.

temperature for more than one year, so the sample was aged sufficiently long to show enthalpy relaxation upon heating. It appeared that by partial heating we relaxed the enthalpy connected with T_g of aromatic component which is clearly visible from the Figure 5.29.

The glass transition of aromatic component is supported by a clear peak of tanδ of dynamic mechanical relaxation spectrum around 50°C (see Sec. 5.1.3, Fig. 5.1.3). On Figure 5.28 in addition a small endothermic peak at 39°C is seen on the thermogram of PBAT that is identified as melting of crystals of aliphatic sequences. No such peak can be detected for similarly treated PBASGT sample. Melting of crystals of aromatic components is observed at 110°C and 121°C for PBASGT and PBAT, respectively.

5.2.2 Crystal structure of selected copolyester

In Subsection 5.1.2 it was already shown that only few units next to each other in macromolecules are sufficient to form crystals although most of the synthesized copolyesters were found to be nearly random. It was also underlined that there are differences in the diffraction angle positions between respective diffraction peaks of synthesized copolyesters and synthesized PBT. Figure 5.30 shows the WAXS 2θ scans of the PBASGT and commercially available PBAT copolymer as well as PBT homopolymer. The differences in the diffraction angle positions between respective diffraction peaks of copolyesters and homopolymer PBT are presented. Table 5.11 compares the obtained experimentally (d_{exp}) lattice spacing of PBT and PBASGT. Miller indices are ascribed to reflections according to Alter and Bonart [139] and Hsiao et al. [153], however, it should be men-

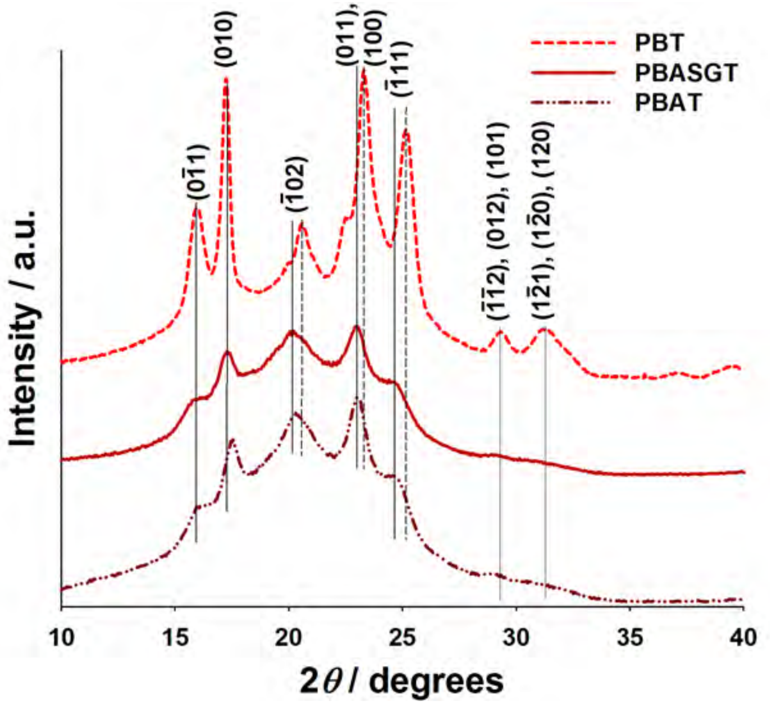

Figure 5.30: WAXS pattern of PBASGT, PBAT and PBT. Curves for PBAT and PBT are shifted vertically for clarity.

tioned that there are split opinions about the Miller indices ascribed to the diffraction peaks at 2θ of 20° and 23° [4, 5, 154]. It has been demonstrated repeatedly that in statistical copolymers the unit cell expands with increasing *co*-unit concentration [155, 156].

Table 5.11: Comparison of the lattice spacing of synthesized PBASGT and commercially available PBAT and PBT.

hkl[139, 153]	**PBT**	**PBASGT** d_{exp} /Å	**PBAT**
$0\bar{1}1$	5.60	5.60	5.60
010	5.13	5.12	5.05
$\bar{1}02$	4.31	4.42	4.37
$011, 100$	3.81	3.86	3.86
$1\bar{1}1$	3.53	3.62	3.62

Howard and Crist [155] studied the unit cell dimensions of a series of hydrogenated polybutadienes containing 0-73 ethyl branches per 1000 C atoms using X-ray diffraction. Both the **a** and **b** axes of the unit cell lengthen with increasing *co*-unit content but begin to level off above 20 ethyl branches per 1000 C atoms, while the **c** axis shows a very slight contraction, resulting in a net expansion of the unit cell volume with increasing *co*-unit concentration. Such phenomenon was observed in many other random copolymers and we also found it in PBASGT copolymer.

The two most widely accepted mechanisms for this phenomenon are: defects inclusion in the crystalline phase and surface stresses related to reduced lamellar thickness [117, 155, 156]. In the second mechanism defects are mostly rejected from the crystals, but preferentially reside in the interfacial layer, thereby exerting stress on the crystal surface [155, 157, 158]. As the *co*-unit concentration increases, the lamellar crystal becomes thinner. This leads to an increase in the crystal's surface-to-volume ratio, which in turn amplifies the magnitude of this stress-induced unit cell deformation. The current state of knowledge concerning crystallization of copolymer was recently summarized and critically reviewed by Li and Register [159]. In Figure 5.31 the deconvolution of WAXS pattern is presented. As it was noticed above, the WAXS pattern consists of the sharp diffraction peaks originated from the **BT** crystalline phase, but it also contains two amorphous peaks which are known for materials with aromatic rings inside the chain [160]. WAXS derived crystallinity of the PBASGT, calculated as the ratio of the total area under the crystalline peaks to the total area under the diffraction curve,

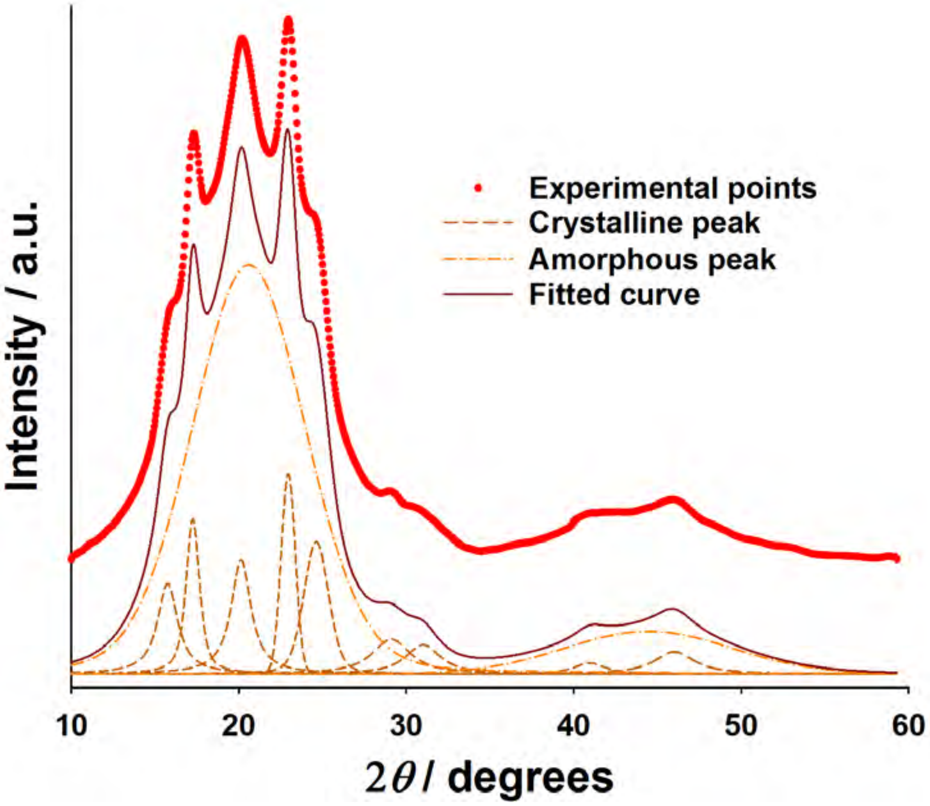

Figure 5.31: The deconvolution of PBASGT WAXS profile into diffraction components by a free available program WAXSFIT created by M. Rabiej and S. Rabiej from University of Bielsko-Biala. The curves are shifted vertically for clarity.

amounts ca. 27%. The deconvoluted peaks are characterized by width and height (see Tab. 5.12). The most narrow peaks are for (010) and (011) reflections which indicate the largest undisturbed dimension of crystals in the directions normal to those planes. It must be noted that the angle between (010) and (011) directions is low (21°) because the fiber axis of the crystals is large (1.295 nm) as compared to the **a** and **b** axes which are only 0.495 nm and 0.567 nm, respectively [45].

Table 5.12: Half-width of deconvoluted peaks of PBASGT copolyester.

hkl[139, 153]	**PBASGT peaks' half-width** /°
$0\bar{1}1$	1.45
010	0.95
$\bar{1}02$	1.43
011, 100	1.00
$1\bar{1}1$	1.75

The SAXS measurements during nonisothermal crystallization of PBASGT provided the information on the development of crystalline structure. The most complete information is unraveled when presenting the data in the form of SAXS density correlation function. The SAXS density correlation functions for PBASGT plotted in

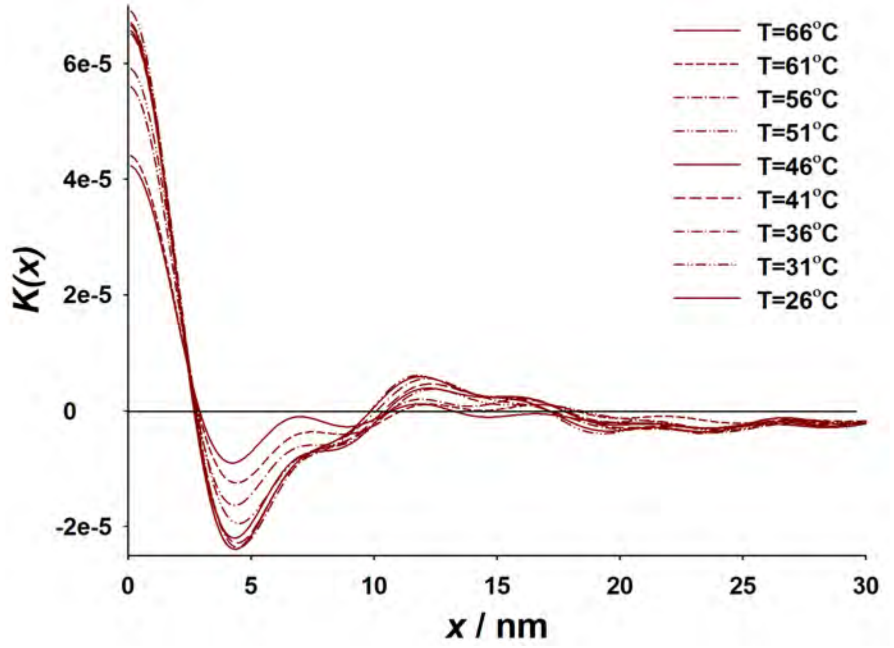

Figure 5.32: The evolution of one-dimensional correlation function of PBASGT structure at the cooling rate 5°C·min^{-1}.

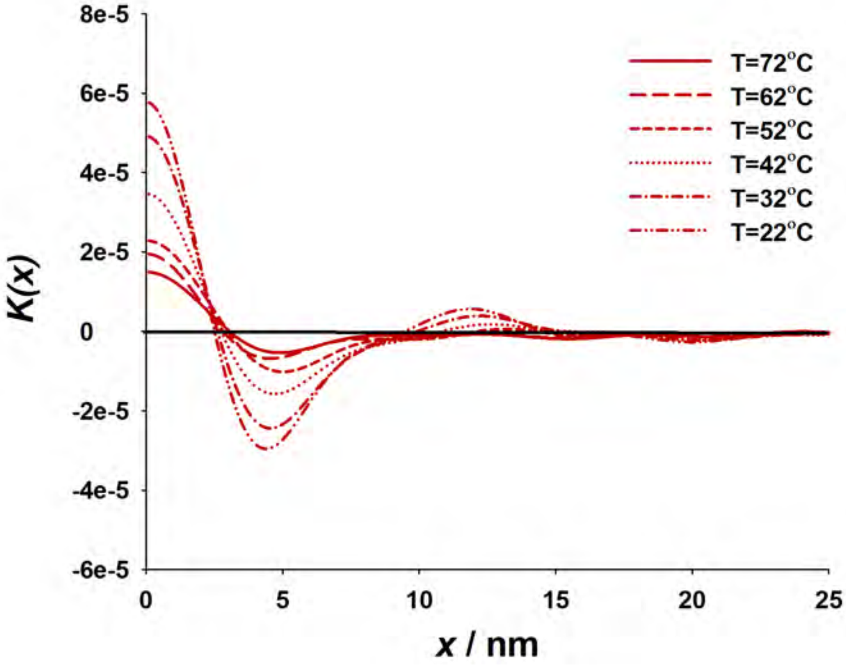

(a) PBASGT

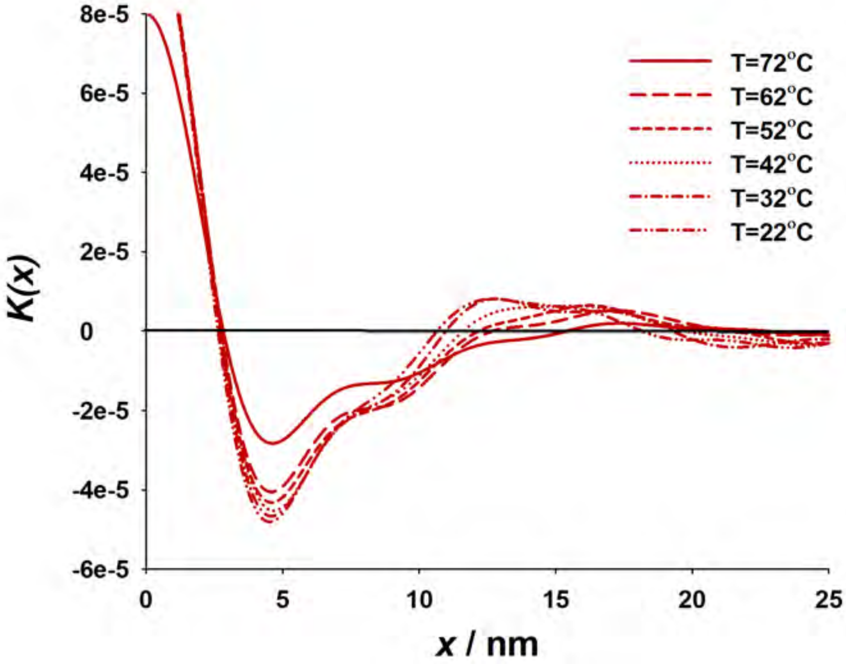

(b) PBAT

Figure 5.33: The evolution of one-dimensional correlation function of (a) PBASGT and (b) PBAT during nonisothermal crystallization at the cooling rate 10°C·min^{-1}.

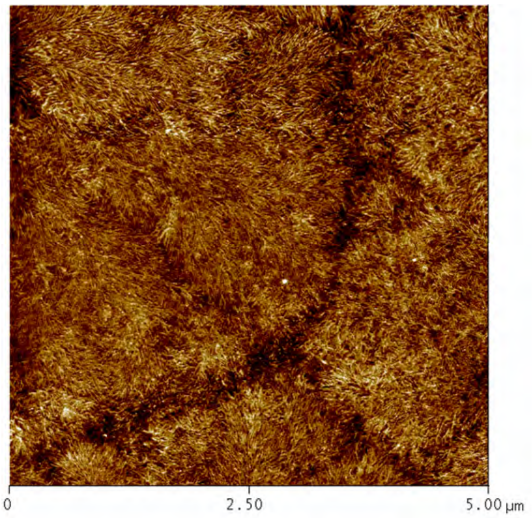

Figure 5.34: AFM images of PBASGT solidified by cooling with the rate of 10°C·min^{-1} from 250°C.

Figures 5.32 and 5.33(a) indicate a step-wise build-up of crystal structure during non-isothermal crystallization starting with the temperature at around 90°C for 5°C·min^{-1} and 80°C for 10°C·min^{-1}. The density correlation extends at the beginning of crystallization over a short distance and then quickly stabilizes at a final crystal thickness of about 3.6 nm. As the temperature decreases the correlation becomes stronger, however, without extending over farther distances. The crystal thickness (see Tab. 5.13) during the crystallization is most probably affected by secondary crystallization like thickening of crystals and forming of new crystals in-between the primary crystallites (see. Fig. 1.14), as described by Strobl [108]. However, it has to be emphasized that the thickness of PBASGT crystals is strongly limited by the length of aromatic sequences. Another important feature of the structure, as it follows from Figures 5.32 and 5.33(a), is that there is no long period formed. Usually the formation of a long period, i.e. parallel padding of adjacent crystals into packets, is enforced by lamellar shape of crystals. The crystal growth in PBASGT is strongly confined by the scarcity of neighboring aromatic elements and their short sequences. In such a case the growth of crystals is limited to one directional irregular growth resulting in fibrillar defective crystals (see Fig. 5.34). Such conclusion is supported by the narrow WAXS reflections from (010) and (011) planes indicating larger dimension of crystals in (010) and (011) directions and much smaller in all other directions (see Tab. 5.13). The other maximum of the correlation function emerges at the distance of approximately 12 nm which represents a slightly higher probability of finding another crystal in such a distance. Similar studies for PBAT copolyester point out (Fig. 5.33(b)) that the crystalline structure of aromatic component forms very quickly, not in a step-wise manner as the structure of PBASGT. However, the final average thickness of crystals of PBASGT and PBAT is nearly identical (3.5 nm). The measured average crystal thickness closely corresponds

Table 5.13: Microstructure evolution in PBASGT and PBAT during nonisothermal crystallization rate 10°C·min^{-1} based on SAXS density correlation function.

Temperature / °C	$\bar{L}_c$ / nm **PBASGT**	 **PBAT**
72	1.06	3.60
62	3.57	3.57
52	4.04	3.57
42	3.71	3.64
32	3.61	3.58
22	3.50	3.54

to the length of 3 butylene terephthalate repeat units (3.48 nm) in the PBT crystal structure. Two, three or four aromatic units in a row are the most probable in a macromolecule of PBAGST as it can be judged from Figure 5.27 The thickness of crystals is then connected with most probable length of sequences of aromatic units.

5.2.3 Thermal properties of selected copolyester

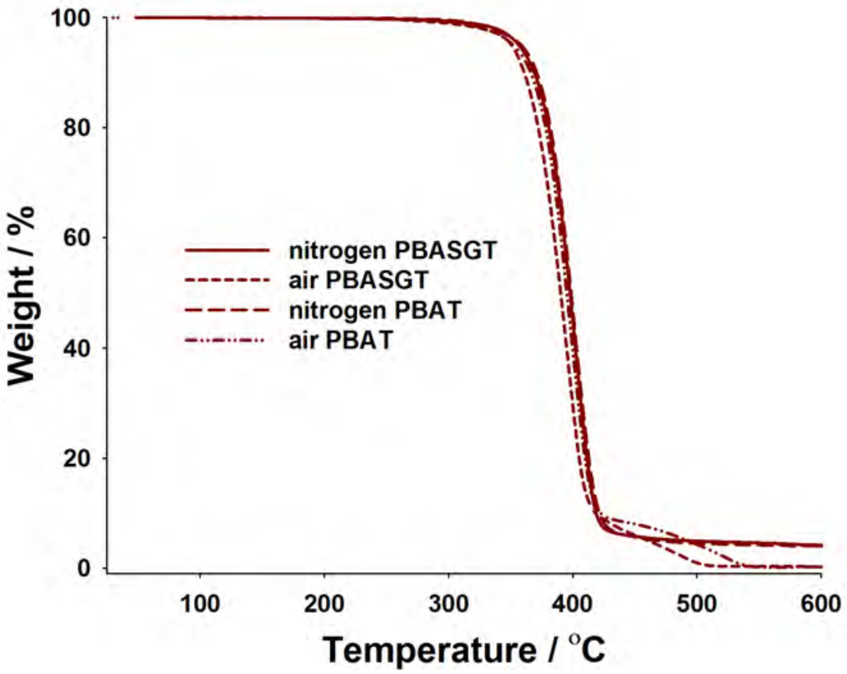

Figure 5.35: PBASGT and PBAT copolymers TGA curves under nitrogen and air atmosphere.

The TGA curve in air atmosphere depicts two step-wise degradation for both copolyesters. It was mentioned in Subsection 5.1.3 that the first stage is purely thermal and the second stage is related to an oxidative degradation process [140, 142]. However, TGA analysis showed that PBAT is slightly less susceptible to oxidation than PBASGT. Nevertheless, the peak of oxidation temperature for PBAT copolyester exhibits in higher temperatures. It can be connected with the presence of stabilizers which are added to commercially available materials. However, for both atmospheres the maximum degradation rate is around 400°C. The 2% weight loss (T_{id}), the temperature of maximum weight loss rate (T_{max}) and oxidation temperature (T_{ox}) were are collected in Table 5.14.

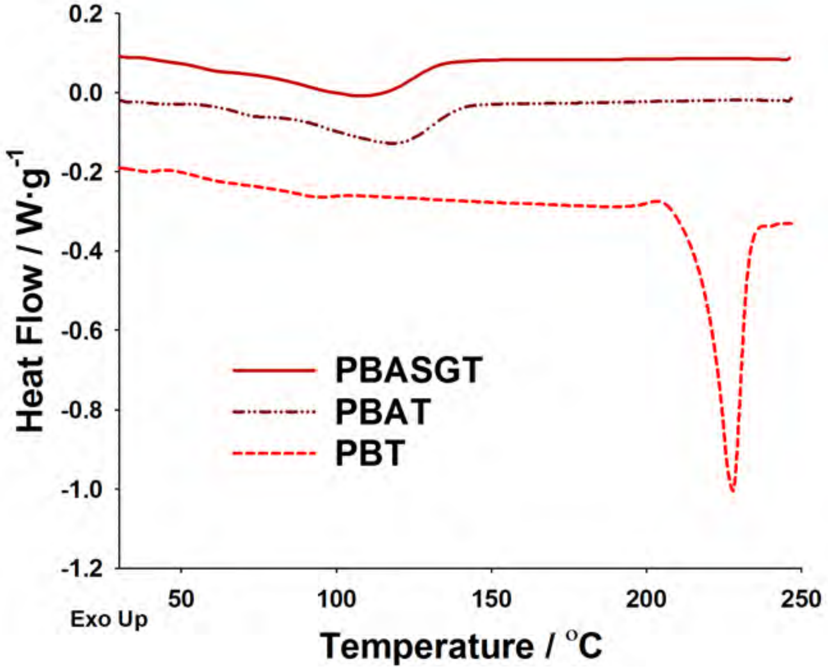

Figure 5.36: PBASGT and PBAT copolymers TGA curves under nitrogen and air atmosphere.

DSC thermograms are presented in Figure 5.36 whereas calorimetric data are summarized in Table 5.14.

From the DSC scans, recorded during heating from -50°C, T_g was determined at around -30°C which can be attributed to aliphatic component. Glass transition of aromatic component was observed at around 40°C. On the DSC curve (Figure 5.36) one can see a broad melting peak at around 108°C. No peaks corresponding to the melting of aliphatic homopolymers (PBA ca. 56°C [49], PBS ca. 114°C [31], PBG ca. 46°C, see Tab. 5.7) and aromatic homopolymer (PBT ca. 225°C, Tab. 5.7) were detected. It supports the suggestion that there is only one kind of the crystal lattice, for which the depression of melting temperature in comparison to PBT homopolymer is more than 100°C. It is caused by the randomness of the chain structure, which results in thin and

Table 5.14: Thermal properties of the PBASGT, PBAT and PBT. The crystallinity χ was calculated for the aromatic fraction of the copolyester, as shown in Subsection 5.2.2, based on the heat of fusion of 100% crystalline PBT, ΔH_m^0, of 144.5 J·g^{-1} [141] and by taking into account weight fraction of aromatic component, 0.47 and 0.51 wt.% for PBASGT and PBAT, respectively, determined based on the data from Tab. 5.9.

Sample	T_m /°	ΔH_m /J·g^{-1}	χ / wt.%$_{\mathrm{BT}}$	T_{id}/°C **nitrogen**	**air**	T_{max}/°C **nitrogen**	**air**	T_{ox}/°C **air**
PBASGT	108	15	22	337	326	402	396	485
PBAT	118	17	23	334	328	402	396	524
PBT	228	44	30	353	348	398	393	460

defective crystals. However, the T_gs of components may have values characteristic of homopolymers [138].

As it was described in Section 1.4, there are two basic theoretical approaches, which correlate the thermal and crystallization behavior with comonomer composition. Usually, the notation **A** and **B**, suggested by Flory, describe the crystallizable and non-crystallizable *co*-units, respectively. Flory [120] suggested also that if **A** monomer of a random copolymer crystallizes, then **B** monomer will remain in the amorphous phase. The model of Eby et al. [122] assumes that both monomers *co*-crystallize. Unfortunately, the uncertainty of surface energy of such *co*-crystals allows to calculate the depressed melting temperature only using the Flory model (Eq. 1.30).

The difference in the melting temperature of PBT and PBASGT crystallized during cooling at the same rate, 120°C, was obtained to be much larger than the value based on the Flory model, 86°C.

The important factor that can also lower the melting temperature of a crystal is significant thinning. The T_m depression is described by a well-known Thomson-Gibbs Equation:

$$T_m^0 - T_m = \frac{2\sigma_e T_m^0}{\Delta H_m^0 \cdot l} \tag{5.19}$$

where σ_e is the surface energy of the basal crystal plane, T_m^0 is the equilibrium melting temperature of the crystals and l is the crystal thickness. Assuming σ_e=75·10^{-7}J·cm^{-2} [161] and T_m^0=244°C [161] for PBT crystals and l =3.5 nm for PBASGT crystals we have $T_m^0 - T_m$ =117°C. The above result indicates that the main source of melting temperature depression is a decrease in crystal thickness. However, there is a difference between melting temperatures of PBASGT and PBAT, 108°C vs. 118°C, in spite of nearly identical crystal thickness (see Tab. 5.13). This inconsistency is probably caused by the difference in surface energy of crystals embedded in different aliphatic components: adipate for PBAT and a mixture of three various aliphatic units for PBASGT. It also affects the crystallization process, as evidenced in the following Subsection 5.2.4.

5.2.4 Crystal growth and morphology

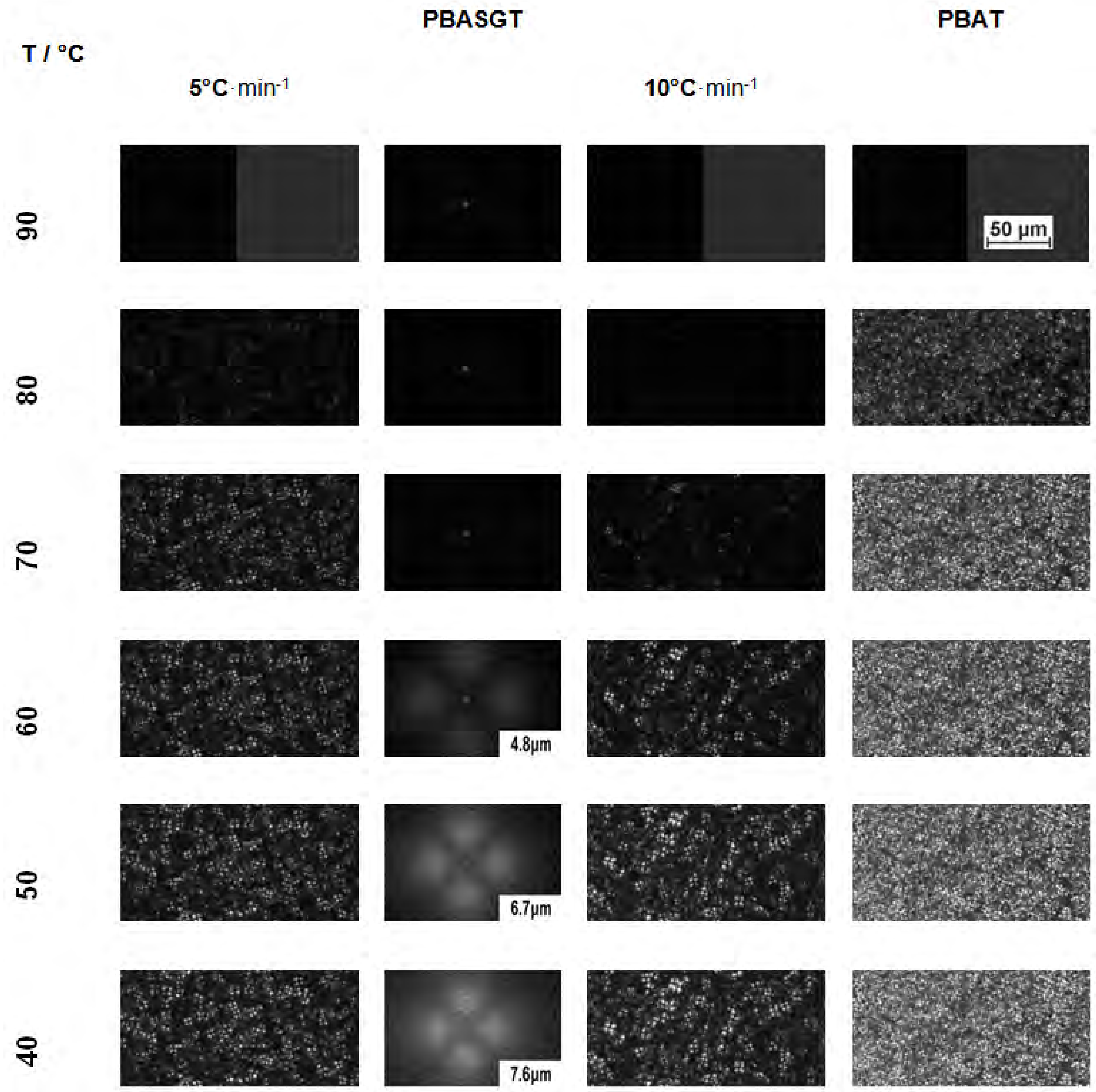

Figure 5.37: Representative PLM and SALS micrographs of PBASGT spherulites non-isothermally grown from the melt at the cooling rates of 5°C·min^{-1} and 10°C·min^{-1}. The micrographs of PBAT crystallized at the cooling rate 10°C·min^{-1} are also presented for comparison. PLM microphotographs taken at $T = 90$°C have been brighten to show first nuclei. Numbers on SALS patterns denote the average fifth order radius of spherulites calculated from scattered light angular distribution.

Figure 5.37 shows a series of PLM micrographs for PBASGT cooled at the rates 5°C·min^{-1} and 10°C·min^{-1}. The micrographs suggests that the main crystalline structures grown during cooling are spherulites. The micrographs indicate that the first spherulites are nucleated at around 90°C or 80°C, depending on the cooling rate. The nucleation density is very high: decrease of temperature favors the growth of many small spherulites, which fully fill the whole volume of the sample. In order to determine the average radius of spherulites the H_v SALS patterns of samples crystallized nonisothermally were examined (Fig. 5.37). The average radius calculated from Equation 1.29 reaches 7 μm which confirms that there is high nucleation density (see also Fig. 5.34). The left column of micrographs in Figure 5.37 shows nonisothermal crystallization of PBAT cooled down at the rate 10°C·min^{-1}. The first nuclei of spherulites appear at 90°C. At 80°C many spherulites are already formed while at 60°C most of spherulites impinge upon each other filling fully the sample. The appearance of the first nuclei and complete filling the space with spherulites occur for PBAT approximately at the temperature higher by 10°C than for PBASGT during cooling at the rate 10°C·min^{-1}.

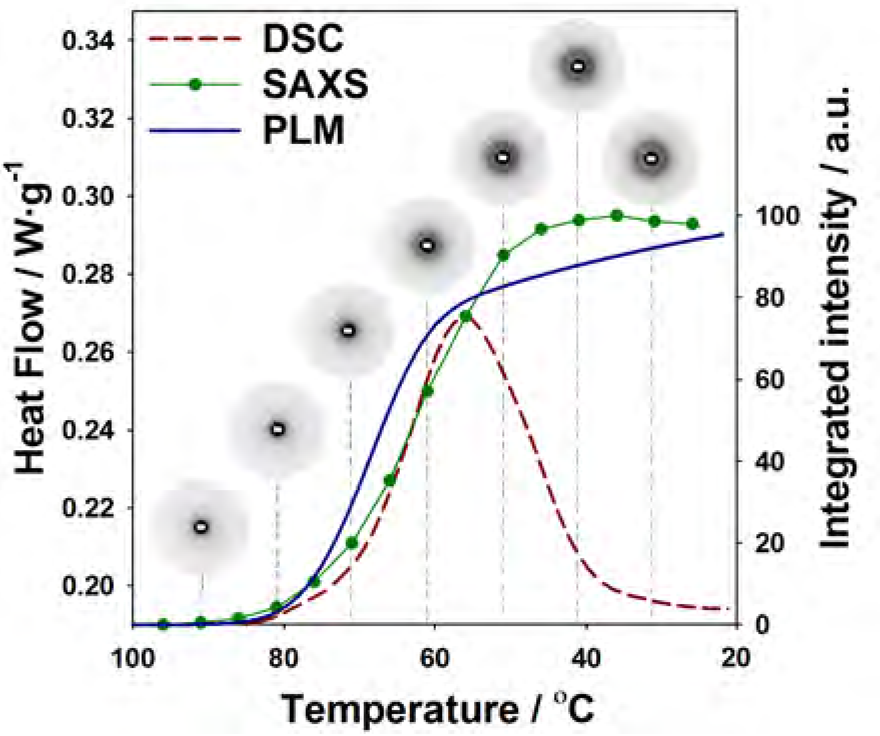

Figure 5.38: Collection of data obtained from various techniques on crystallization of PBASGT during cooling at the rate of 5°C·min^{-1}: DSC thermogram, SAXS total integrated intensity obtained at DESY, Hamburg synchrotron facilities and depolarized light integrated intensity (PLM). SAXS scattering patterns illustrate the formation of supermolecular structure during cooling.

The onset of crystallization process at around 90°C was also determined by recording the integrated intensity of the depolarized light during nonisothermal crystallization at the rate of 5°C·min^{-1}. The most intensive increase of polarized light intensity is observed between 80°C and 60°C (Figure 5.38).

Polarized light micrographs obtained during cooling and presented in Figure 5.37 demonstrate that the crystallization proceeds from nuclei. The aggregates fill the entire sample when the temperature reaches around 35-40°C. This observation is in agreement with DSC data in Figure 5.38. The DSC crystallization peak has characteristic bell-like, nearly symmetric-shape, with the onset of crystallization at around 90°C. It reaches its maximum at around 55°C and then decreases to 35-40°C; at that temperature crystalline aggregates filled the entire volume of the material. The integrated SAXS intensity (see Fig. 5.38) increases with decreasing temperature during cooling, indicating a continuous increase of the crystallinity degree, and saturates at around 35°C. Also the integrated depolarized light intensity (see Fig. 5.38) increases continuously as it has two components originating from depolarized transmitted light and light scattered at small angles. The first component is proportional, to a first approximation, to crystallinity degree while the second component is proportional to the second power of volume of growing crystalline aggregates. The integrated depolarized light intensity curve changes abruptly its slope when the growing aggregates come in contact and become truncated. The values of average crystal thickness were determined from SAXS one-dimensional electron density correlation function [127] and are collected in Table 5.13. It seems that the average crystal thickness in PBASGT slightly decreases below 50°C.

5.3 Nucleation of copolyester

Since the nucleation kinetics can have significant impact upon the bulk properties and processability of polymer materials, the methods that control nucleation are of great industrial relevance. Therefore the following Section 5.3 presents possibilities of copolyester nucleation control.

5.3.1 Self-nucleation

Self-nucleation (SN) can be detected by differential scanning calorimetry when a polymer is heated to the temperature T_s, above the melting point, and is kept at this temperature for a period of time. The SN is present when the peak crystallization temperature during subsequent cooling depends on the Ts and also on the time of annealing at T_s. For homopolymers T_s must be higher than T_m^0 in order to erase the melt memory. No such observations were yet made for random aliphatic-aromatic copolymers. Figure 5.39 presents the SN behavior of the PBAGST copolyester. It shows that the peak crystallization temperature is at 90°C when cooling down from melt at 150°C. When the melt is heated up to higher temperature than 150°C the peak crystallization temperature during subsequent cooling decreases to 70°C and remains constant for all higher melting temperatures. It means that the melt memory is erased for the melt temperature above 150°C. The samples retained no memory of prior crystallization and the crystallization during cooling takes place always at the same temperature. Such behavior suggests a

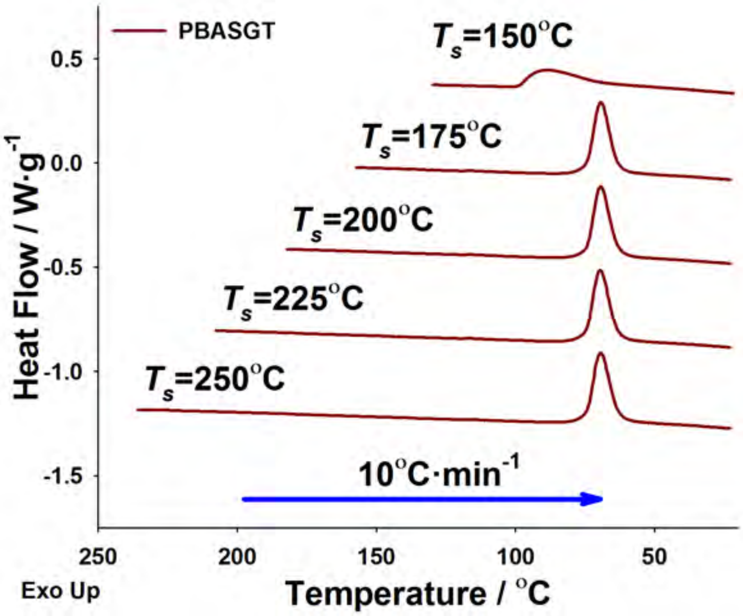

Figure 5.39: DSC thermograms during nonisothermal crystallization of PBASGT with the cooling rate 10°C·min^{-1} from the melt at various temperatures.

constant nucleation activity and density and existence of SN. The classification of SN domains determined by Fillon et al. was described in the Subsection 1.3.1.

In order to determine the temperature ranges of all SN domains for PBAGST copolyester the samples were heated to various temperatures above the melting range, held for 1 min, and then cooled to 20°C with the constant cooling rate of 10°C·min^{-1}. The peak temperature of the crystallization exotherm was used to characterize the effect. The data obtained from thermograms are presented in Figure 5.40. As it is seen from Figure 5.40 the peak temperature of the exotherm is at high level of 94°C for melt temperature of 145°C, while for higher melt temperatures decreases to 70°C and remains at 70°C for all melt temperatures higher than 160°C. Thus Figure 5.40 shows that after heating above 160°C complete melting is achieved. All three domains, as suggested for homopolymers by Fillon et al. [80], can be distinguished, including the transition Domain II which ranges from 145°C to 160°C of the melt temperature (Fig. 5.40). Moreover, the presence of clear DII domain suggests that homogeneous nucleation is not the main source of crystallization seeds above 70°C. In fact homogeneous nucleation was observed in the past in block copolymers only for large undercooling [62, 81, 82, 83].

Furthermore, the peak for self-nucleated crystallization is followed by a long tail which implies prolonged solidification over a larger temperature range: the onset of crystallization is slightly above 110°C while the completion of crystallization is around 40°C (see Fig. 5.39, crystallization thermogram of a PBAGST molten at 150°C). In the Figure 5.39 it is also evident that the conversion from the melt to crystals occurs in a narrow range of temperature for the sample crystallized from the melt at 175°C or higher

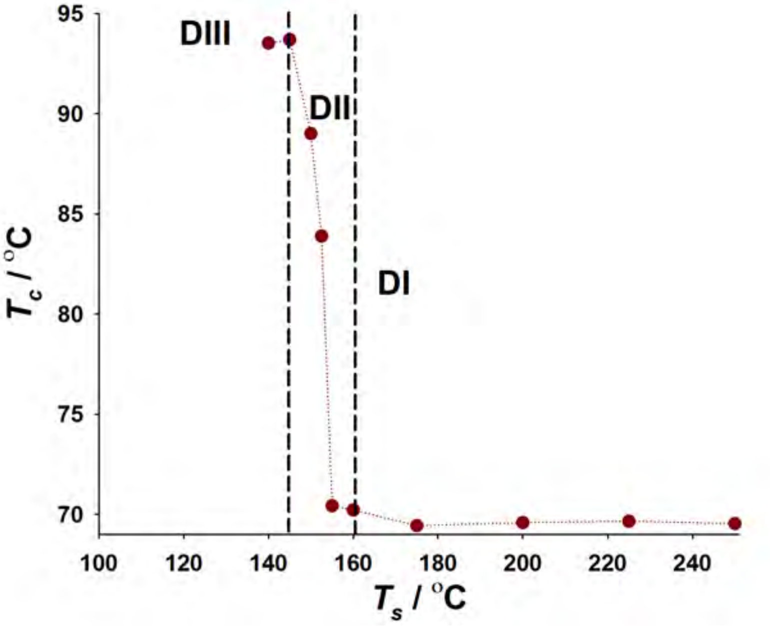

Figure 5.40: The influence of melt temperature T_s on the peak crystallization temperature T_c during cooling with the rate of 10°C·min^{-1}.

and the efficiency of rapid conversion is the best after exceeding the Domain I/Domain II transition temperature of the self-nucleation in comparison to samples crystallized from the melt below 175°C. In the PBASGT case complete melting occurred above 160°C, since no change was detected in the peak crystallization temperature, T_c.

The X-ray scattering in the small angle range were employed to detect *in situ* the formation of crystals. The recorded SAXS patterns were used for the determination of crystals thickness using a correlation function method [127, 128]. There is very little evolution of one dimensional correlation function during nonisothermal crystallization from the melt at 150°C (Figure 5.41(a)). Figure 5.41(b) shows that the average crystals thickness is at the very beginning of crystallization at the level of 3.5-4 nm and fluctuates very little. With further cooling below 60°C a minor decrease of average crystal thickness is noticed which indicates that new slightly thinner crystals are appearing in temperatures below the nonisothermal crystallization peak temperature.

Due to the fact that cooling of the sample from the melt at 250°C at the rate 10°C·min^{-1} takes 10 min longer than that from the melt at 150°C the influence of annealing during cooling was investigated. Figure 5.42 presents comparison of crystallization from the melt at 250°C at the cooling rate 10°C·min^{-1} and the sequence of cooling rates as follow: 30°C·min^{-1} to 150°C and then 10°C·min^{-1}. Obtained thermograms show that even though the cooling time is shorter the crystallization peak is similar as for the sample which was cooled at 10°C·min^{-1}. Thus, the prolonged melt annealing during cooling is not influencing the crystallization provided that the melt temperature was in Domain I.

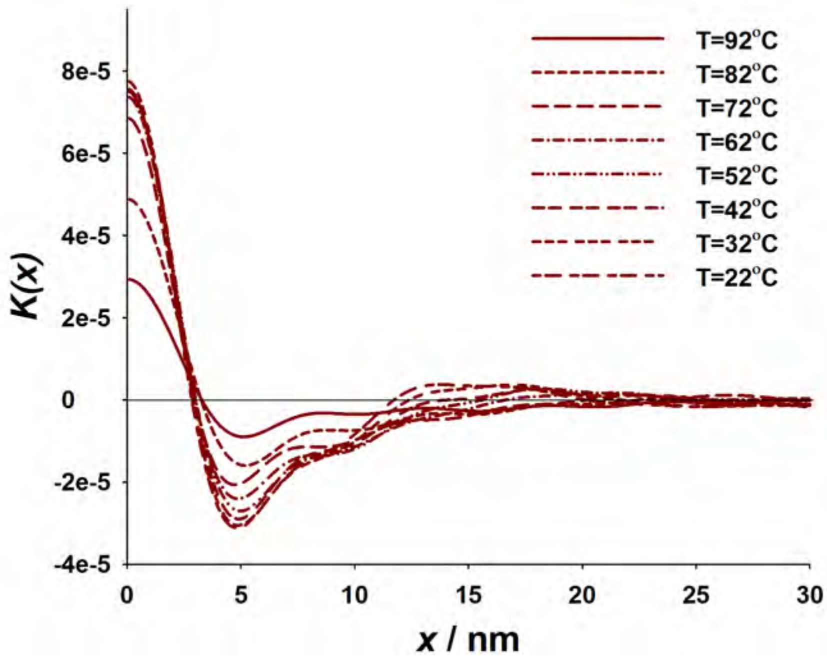

(a) correlation function

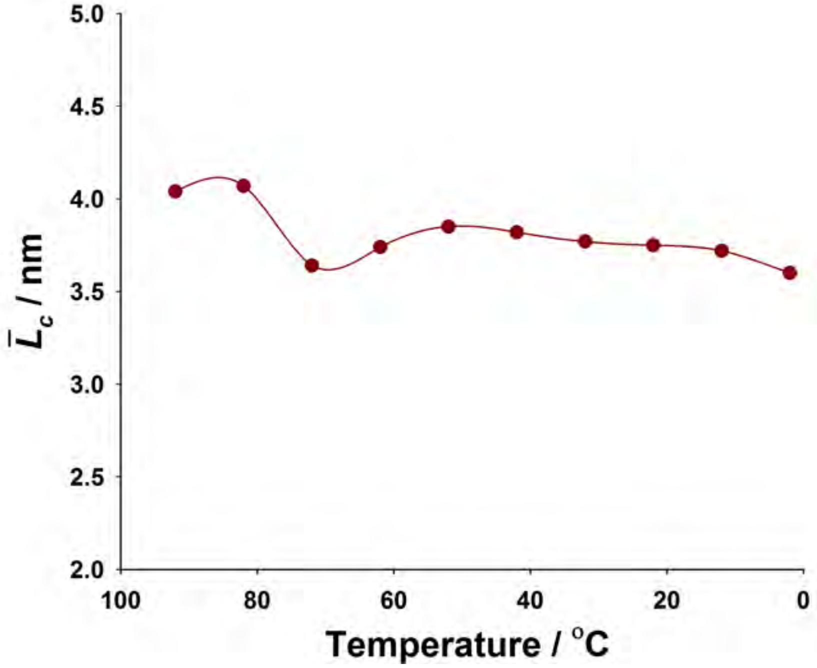

(b) average thickness of fibrillar crystals

Figure 5.41: The evolution of (a) one-dimensional correlation function and (b) average thickness of fibrillar crystals of neat PBASGT during nonisothermal crystallization at the cooling rate 10°C·min^{-1} from the melt at 150°C.

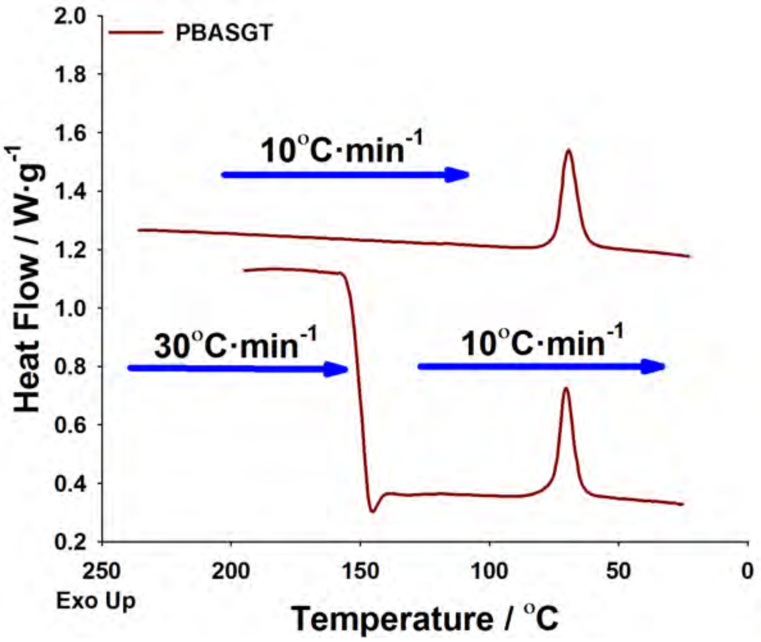

Figure 5.42: Comparison of crystallization from the melt at 250°C at the cooling rate 10°C·min^{-1} and the sequence of cooling rates as follow: 30°C·min^{-1} to 150°C and then 10°C·min^{-1}. The thermogram with only one cooling rate is shifted vertically for better visualization.

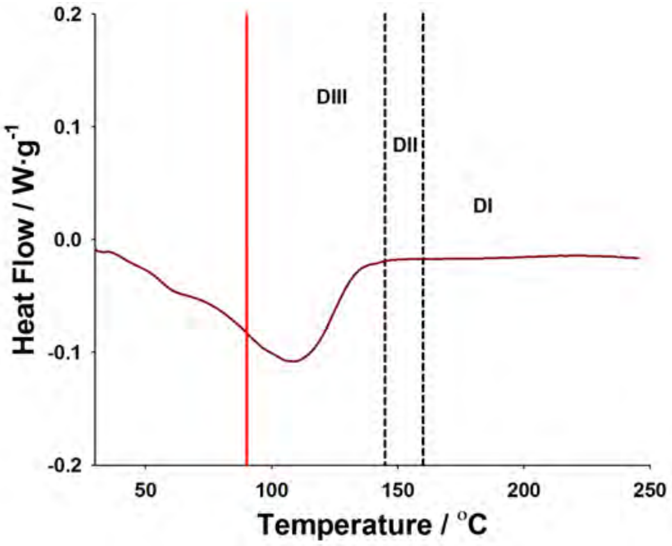

Figure 5.43: Location of the self-nucleation domains on the melting thermogram for PBASGT copolyester. Vertical red line indicates the self-nucleated non-isothermal crystallization peak temperature from the melt at 150°C.

The locations of the self-nucleation, the melting thermogram and the nonisothermal crystallization peak on the temperature axis are shown in Figure 5.43. It can be seen that the location of self-nucleation domains is different from that described in the literature until now. Domain II is usually located between the temperature on the descending slope of melting peak and the temperature on the DSC base line after melting [81, 82, 83]. The beginning of Domain II was found in the paper [73] just at the end of descending slop of the melting peak. In the PBASGT case this Domain is located entirely at the baseline beyond the melting endotherm (see Fig. 5.43). Strong and distinct self-nucleation suggests that nucleating agents for crystallization of PBASGT can be found.

5.3.2 Hetero-nucleation

Several rules that govern nucleation of crystallization were established in the past by Royer et al. [73]. The basic rule says that there must be a dimensional match around 90% between the crystal lattice of the substrate and the deposit in the contact plane of a nuclei [73]. The dimensional mismatching is partly compensated by the lattice elasticity and/or generation of local crystallographic defects (point dislocations).

Epitaxial crystallization leads to oriented growth of the depositing material. Several kinds of epitaxy can be distinguished due to the interaction between deposit and substrate. Graphoepitaxy defines an orientation induced by the surface topography of the substrate, for example, the existence of ditches or strations in the substrate induced, for instance, by rubbing. No clear-cut lattice match is necessary or involved in this process. Soft epitaxy is a more general or even generic term frequently used to characterize oriented growth on a substrate when no clear lattice matching can be defined or envisaged. By contrast, hard epitaxy defines a substrate/deposit relationship that involves clear-cut structural and dimensional match between substrate and deposit. Several analyses of polymer/nucleating agent interaction have been performed over the years and it appears that most epitaxial interactions belong to the class of hard epitaxy [73].

Designing a new nucleating agent is not easy, due to the fact that it must fulfill several requirements often contradictory. The epitaxy analysis does not consider such issues as: compatibility with a molten polymer, proper dispersion, shape of particles, thermal stability of the agent within polymer processing window, exposition to a polymer of the proper crystallographic plane, etc. [73]. Polymer epitaxial crystallization possesses significant original features in which the following is worth mentioning: epitaxial crystallization takes place usually at large undercooling. It suggests that the epitaxial nucleation of crystallization can be active in the case of PBASGT, because as it has been shown in Subsection 5.2.3 the undercooling reaches more than 100°C.

Since crystals of PBASGT exhibit crystallographic form characteristic for crystals of PBT it can be anticipated that known nucleating agents for PBT can nucleated crystallization of PBASGT. There are several such nucleating agents for crystallization of PBT. Among them there are several types of phthalocyanines and talk. The increase of crystallization temperature caused by application of those nucleating agents was reported for homopolyester PBT [162], which is the crystallizing comonomer in the synthesized copolyester (Subsections 5.1.2 and 5.2.2). Hence, for further studies we have chosen green (PG7L), particle size 0.03-0.07 μm and blue (PB153L), particle size 0.05-0.08 μm, phthalocyanine pigments supplied by Chemical Industry Organika - Wola PLC (Wola Krzysztoporska, Poland), which formulas are presented in Figure 5.44. Talc, Steamic Talc 00S, provided by Talc de Luzenac having a tapped bulk density of 0.33 g·cm^{-3} and a loose bulk density 0.17 g·cm^{-3} was also used as a nucleating agent for PBASGT. Talc particle size distribution by sedigraph: median diameter: D50: 2.0 μm, D95: 5.7 μm, by laser master-sizer: D50: 4.9 μm, D95: 10.4 μm. The nucleating agents were added to PBASGT in the amount of 0.2 wt.% by melt blending using Brabender batch mixer at 160°C for 10 min at 60 rpm. The DSC thermograms for the cooling rate of 10°C·min^{-1} are presented in Figure 5.45. Figure 5.45 shows that crystallization peak temperature is shifter towards higher temperature with its simultaneous widening. The largest shift and widening can be observed for PG7L. A long tail after the peak crystallization is noticed for all nucleated and pristine PBASGTs. For each nucleating agent, PBASGT nonisothermal peak crystallization temperature has been measured at various cooling rates (2.5°C·min^{-1}, 5°C·min^{-1}, 7.5°C·min^{-1}, 10°C·min^{-1}). The collected data are presented in Figure 5.46. All three nucleating agents induce an important increase of PBASGT nonisothermal crystallization peak temperature. PG7L, a green phthalocyanine pigment, exhibits the strongest influence on PBASGT crystallization for all cooling rates. PB153L and talc have a smaller influence on PBASGT crystallization as compared to PG7L, although all agents increase the peak crystallization temperature for wide range of cooling rates. The strong broadening of the DSC crystallization peaks can be observed for all nucleated samples for all cooling rates. It gives nonisothermal crystallization temperature from 2°C to 14°C higher than the T_c of virgin PBASGT at the cooling rates of 10°C·min^{-1}. Due to the fact that PG7L appears to be the most

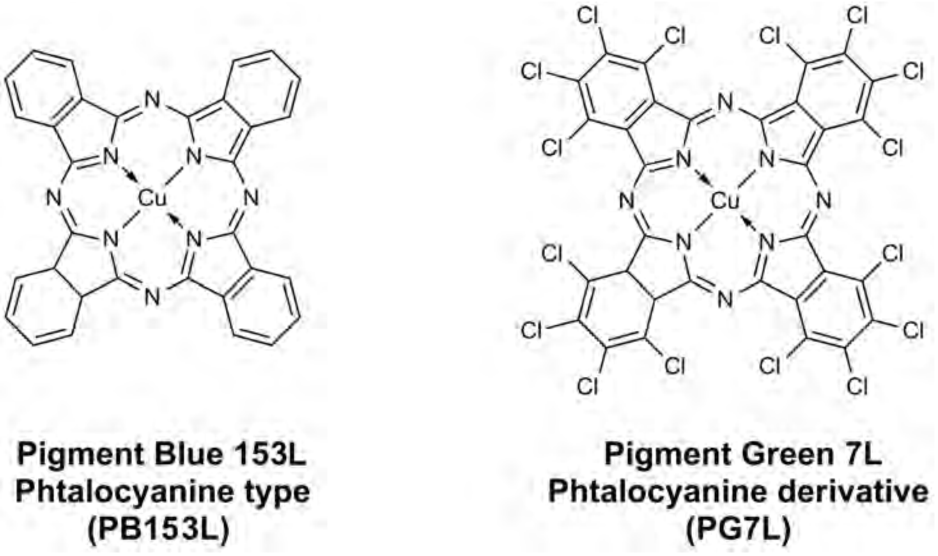

Figure 5.44: Formula of used nucleating pigments.

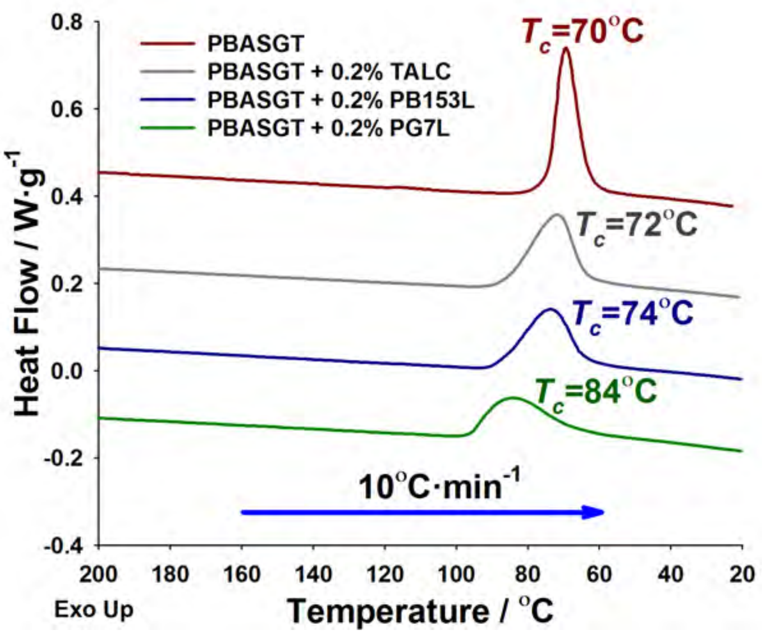

Figure 5.45: Comparison of DSC thermograms of neat and nucleated PBASGT for the cooling rates of 10°C·min^{-1} in which all self-seeded nuclei were removed by melting at 250°C. The nucleated materials' curves are shifted vertically for better visualization.

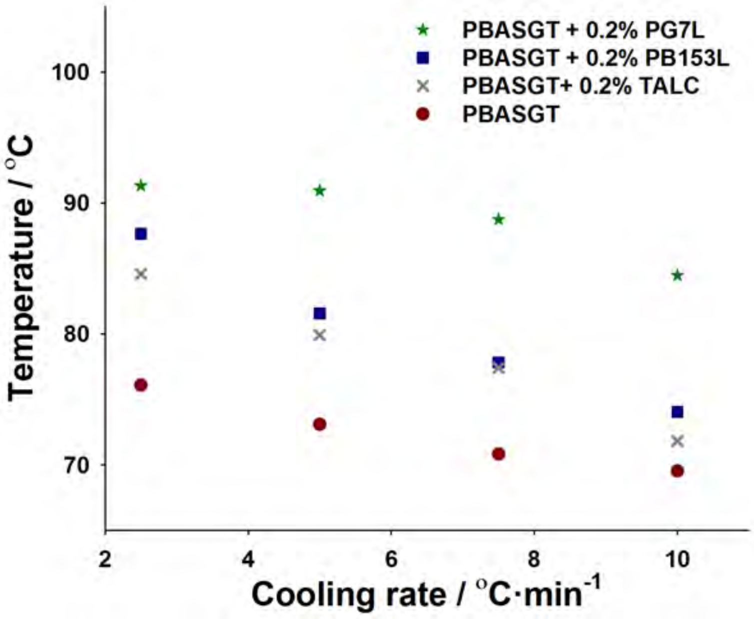

Figure 5.46: Peak crystallization temperatures in the nonisothermal crystallization of PBASGT for various cooling rates and for PBASGT with different nucleating agents.

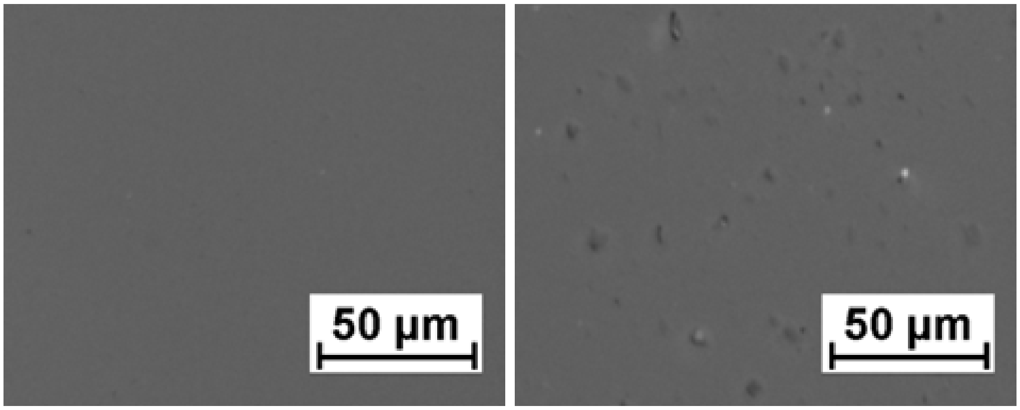

(a) neat PBSGT (b) PBASGT with talc

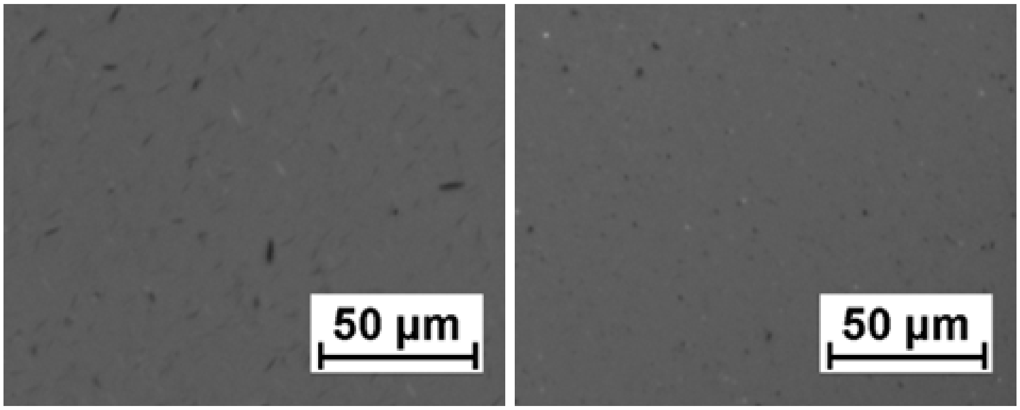

(c) PBASGT with PB153L (d) PBASGT with PG7L

Figure 5.47: PLM microphotographs of molten at 250°C (a) neat PBASGT and nucleated with (b) talc, (c) blue phthalocyanine and (d) green phthalocyanine.

efficient nucleating agent similarly as it occurred for PBT, it can be supposed that as it was reported by Pillin [162] for PBT the 0.02% of PG7L is sufficient to increase significantly PBASGT nonisothermal crystallization temperature.

The observed nucleating effect induced by the presence of dyes in PBASGT suggests that it can be correlated to the chemical structures of pigments. Espinoza-Martinez [163] proposed that aromatic structure of carbon nanotubes can act as templates by means of $\pi - \pi$ interactions for the nucleation of semicrystalline polymers containing aromatic ring in their backbone such as poly(butylene terephthalate) (PBT). In both cases of PBASGT and PG7L or PBASGT and PB153L the aromatic rings are present, so the structure can be important. PLM microphotographs recorded at 250°C (see Fig. 5.47) show that the added nucleants do not dissolve in the molten polymer, but their distribution in PBASGT differ. The green phthalocyanine is better dispersed and it can be the main reason for its better nucleating efficiency. However, both phtalocyanines form aggregates much larger that the declared particle sizes (PG7L - 0.03-0.07 µm, PB153L

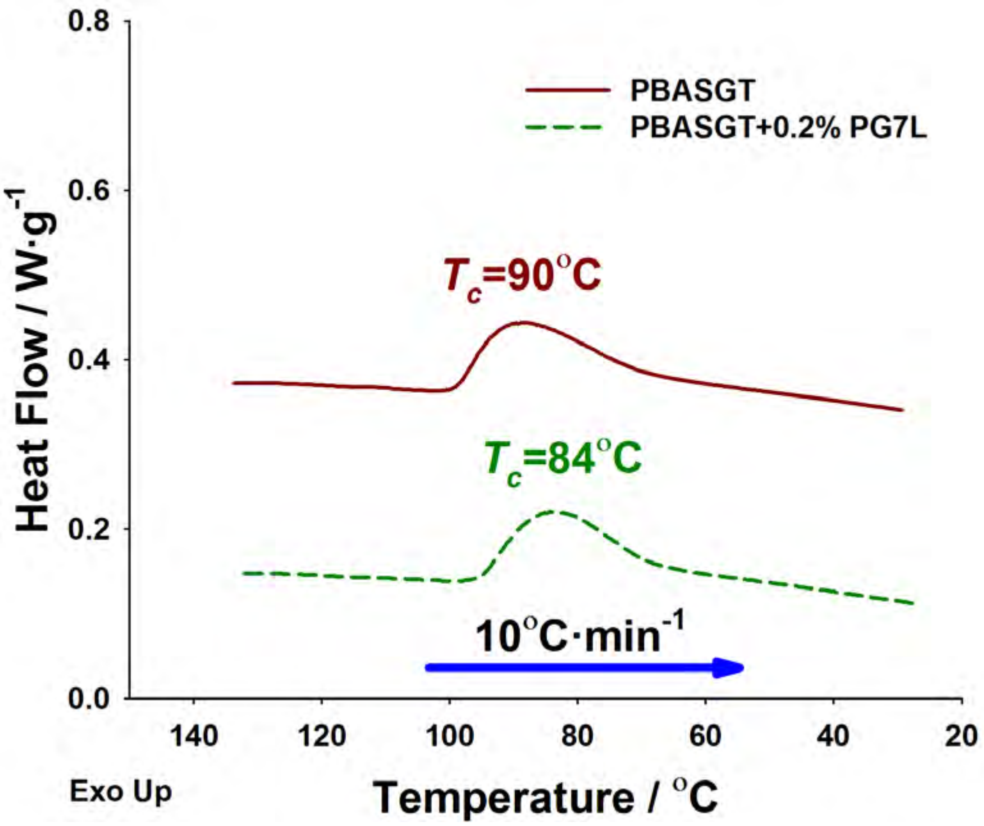

Figure 5.48: Comparison of DSC cooling thermograms for neat PBASGT with self-nuclei active (melting at 150°C) and nucleated PBASGT with PG7L with self-nuclei removed (melting at 250°C). The cooling rate 10°C·min^{-1}. The nucleated PBASGT curve is shifted vertically for better visualization.

- 0.04-0.08 μm).

In Figure 5.48 the thermograms of nonisothermal crystallization from the melt of neat and nucleated by PG7L PBASGT are compared. As it was established above for the neat PBASGT crystallized from melt at 150°C the self-nuclei were active and the non-isothermal peak crystallization temperature is at 90°C. However, for nucleated PBASGT in which all self-nuclei were killed by melting at 250°C the non-isothermal peak crystallization temperature is only 84°C. This comparison demonstrates that the self-nuclei are the most effective for initiation of crystallization of PBASGT. The obtained result arise from the fact that the self-seeded nuclei of a polymer are crystallographically ideal for nucleating its crystallization [77, 164, 165].

As described in Subsection 5.2.1, although the selected copolyester was shown to be nearly random, sharp peaks were observed in WAXS pattern of PBASGT, confirming that only a few units next to each other in macromolecules are sufficient to form crystals. Furthermore, it is found that the obtained WAXS pattern for PBASGT is similar to WAXS pattern of PBT.

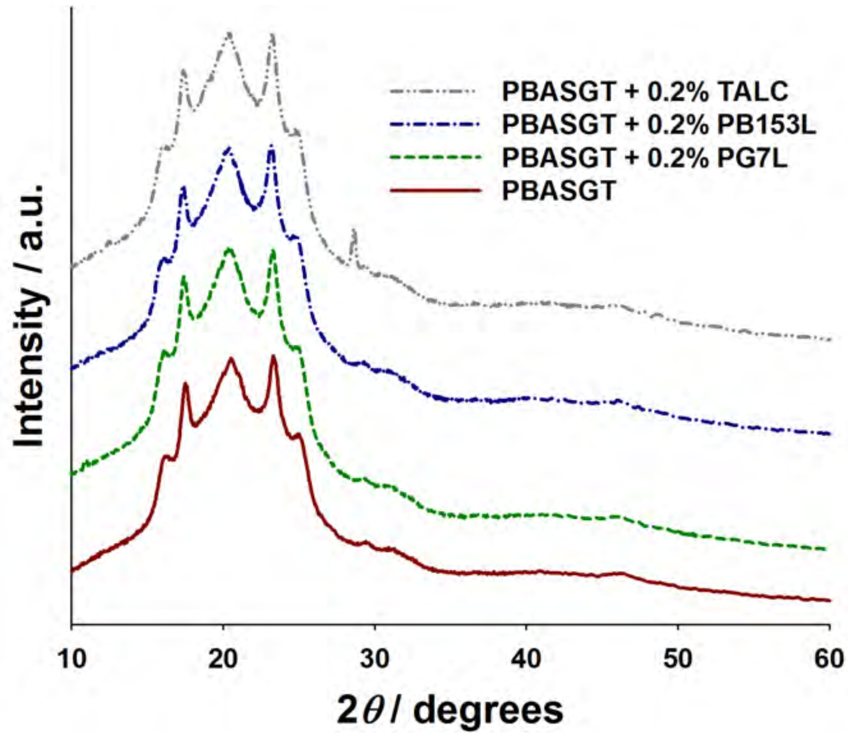

Figure 5.49: WAXS pattern of PBASGT and its blends with nucleating agents.

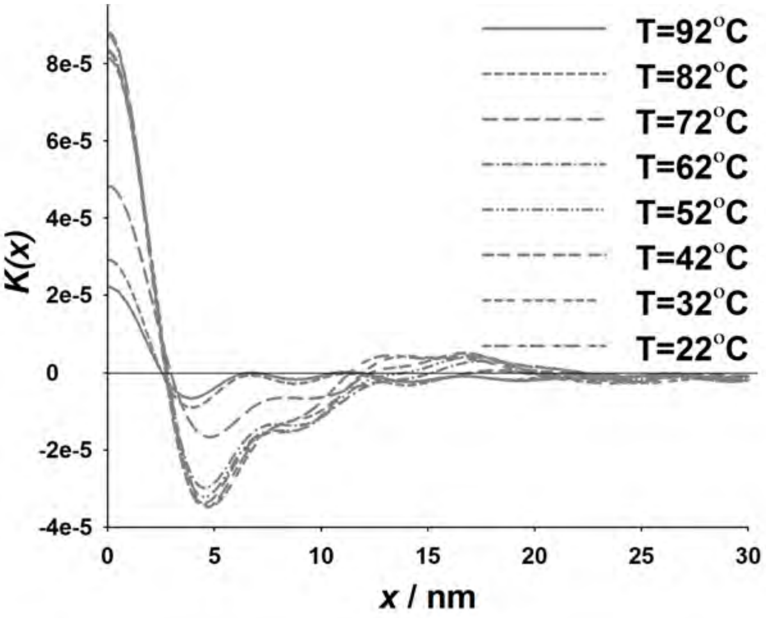

Figure 5.50: The evolution of one-dimensional correlation function of nucleated PBASGT with talc during nonisothermal crystallization at the cooling rate 10°C·min^{-1}.

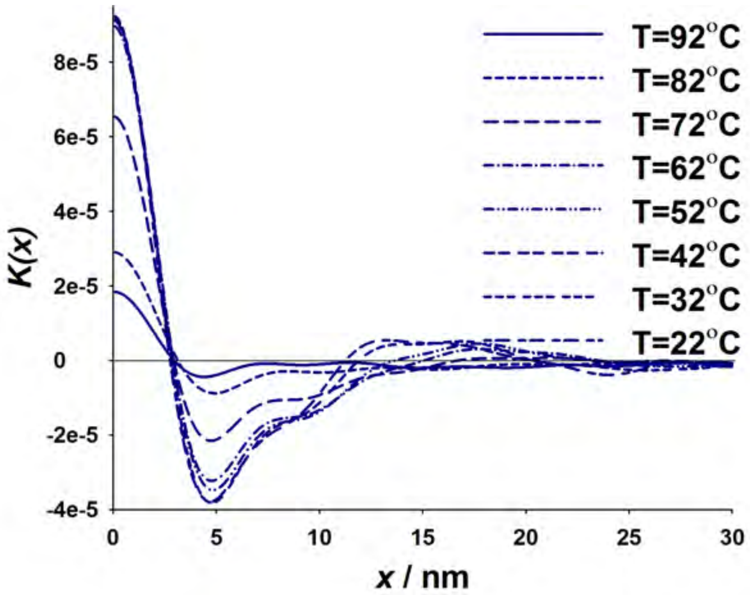

Figure 5.51: The evolution of one-dimensional correlation function of nucleated PBASGT with PB153L during nonisothermal crystallization at the cooling rate 10°C·min^{-1}.

Figure 5.49 shows the WAXS 2θ scans of PBASGT and PBASGT with nucleating agents. The similarity of the WAXS diffraction patterns as seen in Figure 5.49 indicates that the nucleating agents do not perturb the crystallographic form of the PBASGT crystals. The narrow but weak reflection at 28.65° for the 0.2 wt.% talc sample, confirms the presence of talc particles [166].

The *in situ* SAXS measurements during nonisothermal crystallization of PBASGT with nucleating agents provide the information on the development of crystals. Most complete information is unraveled when presenting the data in the form of SAXS density correlation function (see Figures 5.50, 5.51 and 5.52). At the beginning of cooling, at 92°C, the correlation functions show some clustering within the range of 3 nm, similar for all three nucleated PBASGTs. With further cooling the clustering range reaches 3.5-4.0 nm and intensifies similarly for all nucleated samples. No significant differences are seen although on the DSC cooling thermograms there are differences in crystallization peak temperatures at the level of more than 10°C (84°C for PBASGT with green phthalocyanine and 72°C for PBASGT with talk, see Figure 5.45). The clustering at the level of 3.5-4.0 nm is preserved until the completion of crystallization. However, there are differences between nucleated PBASGTs: PBASGT with green phthalocyanine produced the dense clustering earlier than PBASGTs with talc and with blue phthalocyanine. It must be noticed that no long range ordering is being developed, such as long period, until the end of solidification.

The SAXS density correlation functions for nucleated PBASGT plotted in Figures 5.50, 5.51 and 5.52 indicate a step-wise build-up of crystal structure during non-

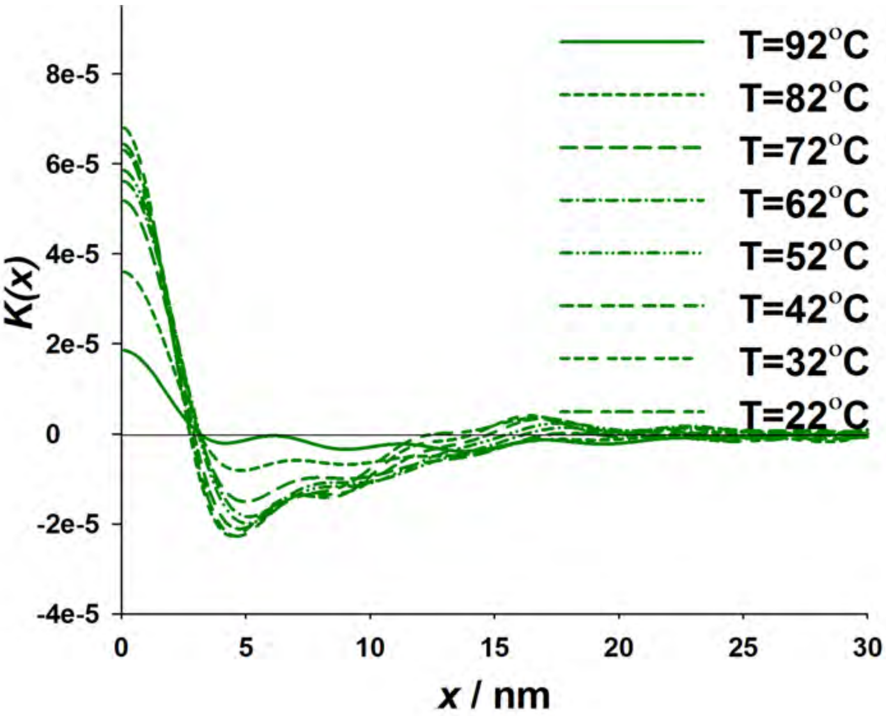

Figure 5.52: The evolution of one-dimensional correlation function of nucleated PBASGT with PG7L during nonisothermal crystallization at the cooling rate 10°C·min^{-1}.

isothermal crystallization starting with the temperature at around 80°C for 10°C·min^{-1}. The evolution of density correlation stabilizes at a final crystal thickness of slightly above 3.5 nm, as it was observed for neat PBASGT (Sec. 5.2.2).

Figure 5.53 shows that the crystals thickness is in the range of 3-4 nm during the nonisothermal crystallization. It presents also that the biggest differences in the thickness are obtained with the PG7L nucleant and the smallest one for the PB153L one.

Optical polarized micrographs, PLM, illustrating the spherulite morphologies of nucleated PBASGTs formed during nonisothermal crystallization are presented in Figures 5.54. Smaller spherulites are observed for the nucleated systems in comparison to pure PBASGT. The PLM micrographs show the increase of nucleation density and a decrease of spherulite size. As it was shown in Subsection 5.2.4, the average fifth order radius $\langle R_5 \rangle$ of pure PBASGT crystallized with removed self-nuclei was 7.9 μm at room temperature. An attempt to measure the spherulite sizes in nucleated PBASGTs with small angle light scattering (SALS) was made. Unfortunately, the sizes of the spherulites are so small that they are beyond the resolution of the SALS technique utilizing He-Ne laser (λ= 632.8 nm). Similarly spherulites in PBASGT sample with self-nucleation are too small to be resolved in PLM and in SALS. The introduction of nucleating agents to PBASGT increased both the nucleation density and shifted activity of nuclei to higher

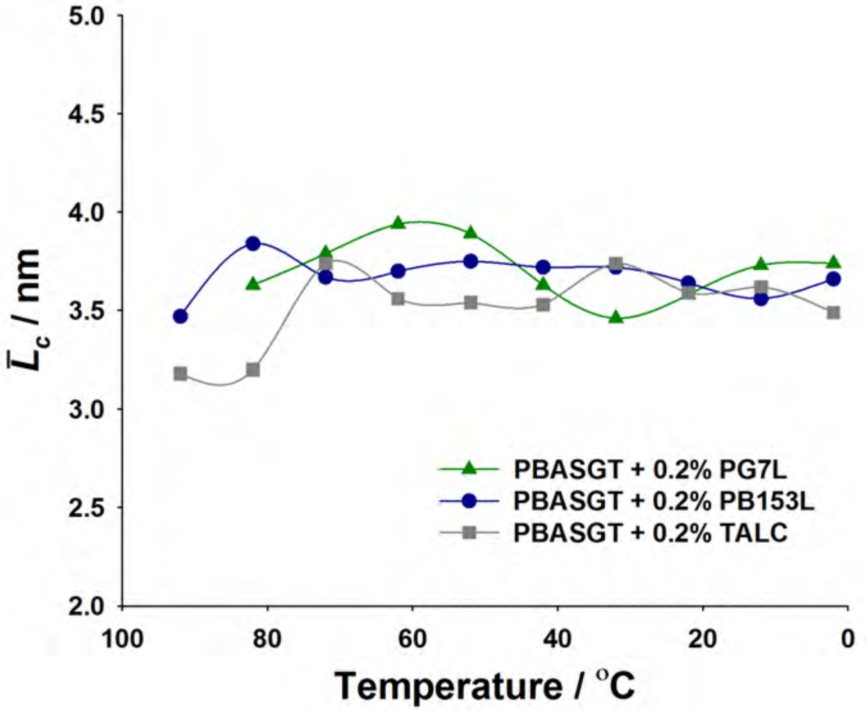

Figure 5.53: The evolution of average crystals thickness of nucleated PBASGT during nonisothermal crystallization at the cooling rate of 10°C·min^{-1}.

temperature.

Figure 5.55 presents the AFM phase images of neat PBASGT and nucleated PBASGT with green phthalocyanine. For neat PBASGT (Fig. 5.55(a)) the spherulites can be resolved. They impinged upon each other. The spherulites are built from short (less than 0.5 μm) and thin fibrous crystals. It is also seen that fibrous crystals spread radially and branch forming from 3 to 4 arm small fans. Such architecture is typical for spherulites of many other polymers except that here fibrous and not lamellar crystals are the basic elements of architecture. The AFM image of nucleated PBASGT in Figure 5.55(b) is very different as it contains of two fractions of fibrous crystals: the first one consisting of long thin fibrils and not forming spherulites is not present in nonnucleated PBASGT. The second fraction contains short fibrils, similar in character as those present in non-nucleated PBASGT, however, in lesser amount. The comparison of the two AFM images suggests the following scenario: artificial nuclei initiate crystallization at 15°C higher temperature and hence, those crystals have 1.5 min more time for the growth (at the cooling rate of 10°C·min^{-1}) and in addition the growth of those crystals undergoes in a warmer and less viscous medium than in non-nucleated PBASGT. When the temperature is decreased to a level for activation of the growth of short thin fibrils the material is already partially immobilized by long fibrils. The result is very surprising: nucleated PBASGT contain lower amount of crystals than non-nucleated. This conclusion is confirmed by the crystallinity degree calculated from the enthalpy of melting as measured

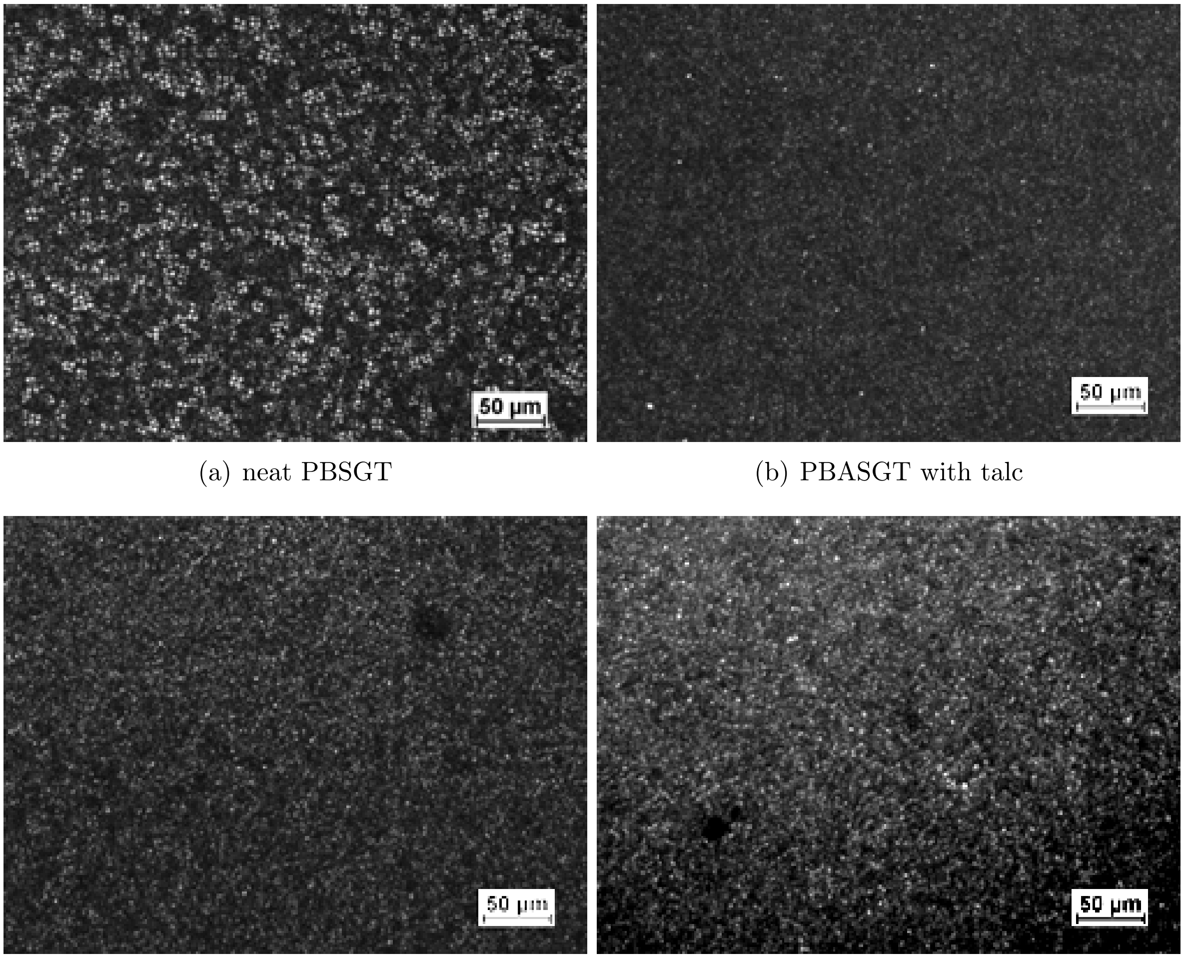

(a) neat PBSGT (b) PBASGT with talc

(c) PBASGT with PB153L (d) PBASGT with PG7L

Figure 5.54: Spherulitic morphologies of the (a) PBASGT with (b) talc, (c) PB153L and (d) PG7L, after non-isothermal crystallization at the cooling rate 10°C·min^{-1} from the melt at 250°C.

by DSC (see, Tab. 5.15).

The AFM images in Figures 5.55(c) and 5.55(d) show the same region of the sample as in Figure 5.55(b), however, they were recorded at increased temperature at 50°C and 70°C, respectively. While fibrils at 50°C are essentially the same as at room temperature though at 70°C they undergo drastic changes. Thinner long fibrils disappeared, thicker underwent thickening and capillary instability leading to their decomposition and recrystallization. The overall impression from the image in Figure 5.55(d) is that the degree of crystallinity nucleated PBASGT increased significantly at 70°C. This observation confirms the proposed scenario of partial immobilization of the material by the growth of long fibrils at higher temperature and inhibiting the growth of the population of short fibers. At 70°C when the long fibrils decompose, the constrains are released allowing the unrestricted growth of short fibrils. It must be remember that at higher

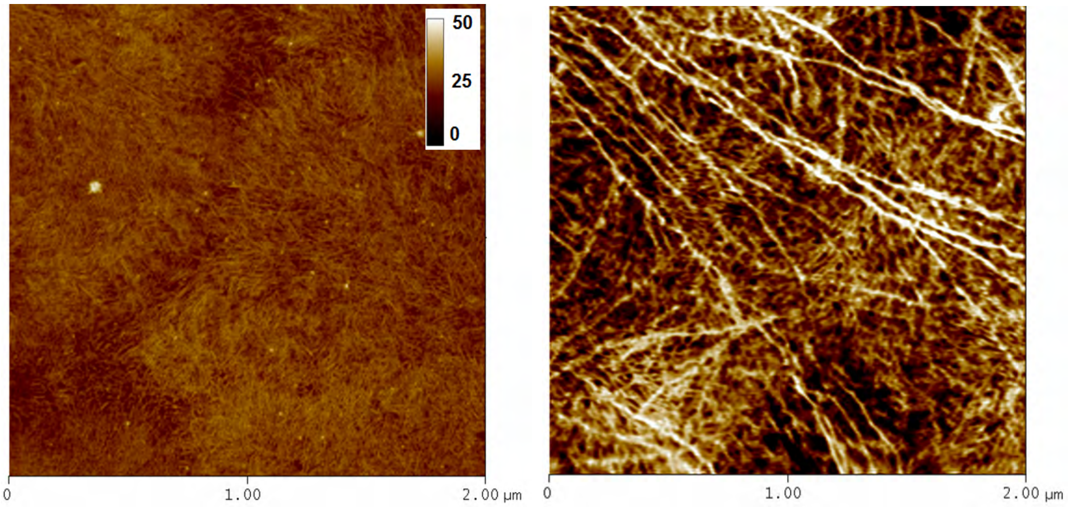

(a) neat PBSGT (b) PBASGT with PG7L at 25°C

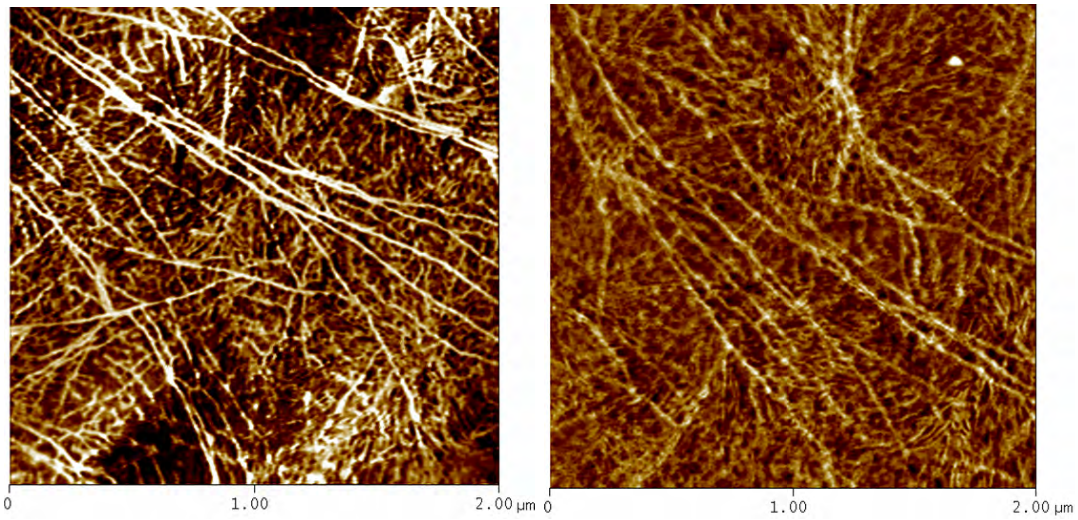

(c) PBASGT with PG7L at 50°C (d) PBASGT with PG7L at 70°C

Figure 5.55: AFM images of PBASGT solidified by cooling with the rate of 10°C·min^{-1} from 250°C (a) neat and (b) nucleated with PG7L at 25°C, (c) nucleated PBASGT with PG7L at 50°C and (d) nucleated PBASGT with PG7L at 70°C. The images (b), (c) and (d) are presenting the same region of the sample and to all the same phase scale is applied.

temperature (70°C) the crystal growth rate is faster because the viscosity is lower. The AFM image of PBASGT crystallized from self-nuclei is shown in Figure 5.56. Plenty of fine fibrils are seen but no clear spherulitic structure can be resolved. Apparently so large number of fibrilar crystals were nucleated from self-nuclei that they could not develop into long fibrils as in hetero-nucleated PBASGT. The other impression is that filling of the sample volume with fibrous crystals is more dense than for non-nucleated

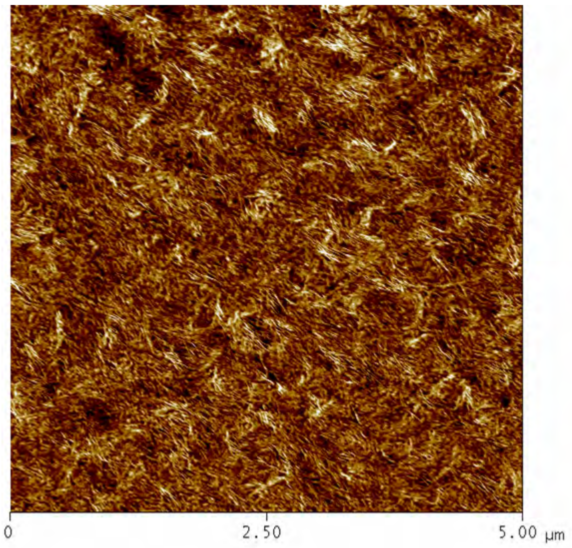

Figure 5.56: AFM images of self-nucleated PBASGT solidified by cooling with the rate of 10°C·min^{-1} from 150°C.

and hetero-nucleated PBASGT (compare Fig. 5.55(a) and 5.55(b) with Fig. 5.56).

In Table 5.15 the thermal and thermogravimetric data for PBASGT compositions are also collected. It shows that the introduced nucleating agents have almost unnoticeable influence on the copolyester stabilization.

Table 5.15: Thermal properties of the nucleated PBASGT at the heating rate 10°C·min^{-1}. The crystallinity (χ) was calculated for the aromatic fraction of the copolyester based on the heat of fusion of 100% crystalline PBT, ΔH_m^0, of 144.5 J·g^{-1} [141] and by taking into account the weight fraction of aromatic component, 0.47 wt.% for PBASGT, determined based on the data from Tab. 5.9. T_{id}, T_{max} and T_{ox} are the temperatures of: the onset of decomposition, maximum rate of decomposition, oxidation completion.

Sample	T_m /°	ΔH_m /J· g^{-1}	χ / wt.%$_{\mathrm{BT}}$	T_{id}/°C **nitrogen**	**air**	T_{max}/°C **nitrogen**	**air**	T_{ox}/°C **air**
PBASGT+ 0.2wt.% Talc	113	13.85	20	340	333	402	397	491
PBASGT+ 0.2wt.% PB153L	114	11.02	16	340	335	402	397	482
PBASGT+ 0.2wt.% PG7L	115	10.25	15	339	339	401	397	481

5.4 Conclusions

It has been recognized that properties of aliphatic-aromatic copolyesters, such as biodegradability and crystallization behavior, are inherently influenced by their macromolecular chain architecture.

This thesis focuses on novel copolyesters of poly(butylene adipate-*co*-succinate-*co*-glutarate-*co*-terephthalate) (PBASGT), with a random distribution of comonomers. A range of copolyesters were synthesized for the purpose of this thesis varying in the ratio of aliphatic to aromatic components. The synthesis was essentially based on a two-step melt polycondensation method. Molecular architecture of these copolyesters was investigated by ^{1}H NMR which allowed the determination of distribution of sequences of aliphatic and aromatic comonomers. It appeared that the lengths of sequences have nearly perfect random character independent of the aromatic unit concentration, though the average aromatic sequence length varied from ∼1 to ∼10. It appeared that all of synthesized copolyesters can crystallize independent of aromatic unit content, however, the crystallinity degree varied greatly and also the peak temperature of nonisothermal crystallization (from nearly 190°C to 45°C) and melting (from 240°C to nearly 40°C) varied. Although all obtained compositions of PBASGT copolymers exhibits nearly random sequence distribution, almost all of them are able to crystallize. It was shown that even very short sequences can provide the ability to crystallization. The crystallinity of all crystallizable copolyesters was sufficiently high to retain their shape and form at room temperature. All of them were able to deform plastically. The solidification of these new nearly random PBASGT copolymers and its influence on thermal, morphological and mechanical properties were studied to select material, which would incorporate simultaneously the ability to biodegradation and crystallization.

The structure analysis showed the increase of average length of aromatic units sequences together with its content. The crystallinity of PBASGT copolyesters increases smoothly with increasing butylene terephthalate (**BT**) unit content. It turned out also that in all the crystallizable copolyesters only **BT** blocks are able to crystallize in the crystallographic form characteristic of poly(butylene terephthalate). No other reflection peaks were observed and the *co*-crystallization process was disqualified. Furthermore, the increase of aliphatic untis' contents did not change the crystallographic structure, in contrary to the results obtained by Li et al. [7], due to the lack of significantly exceeding component in the composition. Nevertheless, several diffraction peak positions (not all) of the synthesized copolyesters and aromatic homopolymer PBT are slightly different. The two most widely accepted mechanisms for this phenomenon are: defects inclusion in the crystalline phase and surface stresses related to reduced lamellar thickness. In the case of PBASGT copolymers it was revealed that difference of 20% in aromatic content can cause 0.2 nm difference in crystals thickness. Moreover the small thickness of crystals was found as the main source of melting depression in comparison to PBT. Crystallization' of PBASGT copolyesters are initiated by nuclei, which give rise to radially growing crystalline aggregates. In the course of crystallization the aggregates grow, come into contact and truncate. The crystalline aggregates fill the entire volume of the material. The nonisothermal crystallization peak temperature depends strongly on the cooling rate.

It was also showed that crystallization process connected with the structure affects other properties. All of the transition temperature like glass transition, melting and crystallization peak temperatures increase with increasing aromatic unit content. Dynamic thermal-mechanical analysis showed however that the composition of copolyester can influence if the copolyester possess one reached glass transition or two separated. Thermagravimetry revealed that incorporation of aliphatic units between the aromatic does not have to affect significantly the stability of the material what widens its area of application and increase its potential to replace homo aromatic materials, which do not possess the ability to biodegradation.

Composition of PBASGT copolyesters also affects strongly their mechanical properties. Copolyesters with aliphatic units content up to 60% deformed in an uniform manner characteristic for rubbers. The increase of aromatic units content cause the deformation manner changes. With the aliphatic units decrease the yield stress point becomes well-defined and formation of neck is observed. However, the neck propagation is fluctuated by rapid increase or decrease of stress to strain ratio. For composition containing 80% of aromatic units content those fluctuation are becoming a regular oscillations, which are caused by interchangeable local heating and cooling of the sample.

Based on the literature data on susceptibility of aromatic sequences to biodegradation and the data from independent biodegradation experiments of our copolyesters, the copolyester with 45% of aromatic units content was chosen for further more detailed studies. Selected composition of PBASGT copolyester was compared with commercially available copolyester PBAT containing only one aliphatic unit - adipate. Thus, not only the influence of aromatic unit content was investigated, but also the influence of aliphatic units amount. Structure analysis of both copolyesters showed that they possess the ability for biodegradation even in the aromatic part of the materials. The results from NMR analysis were supported by compost studies conducted in Institute of Biopolymers and Chemical Fibers.

As it followed from the SAXS analysis the crystalline structure of PBASGT and PBAT copolyesters does not show a long period characteristic of other crystalline polymers. It is shown that aliphatic part of PBASGT does not crystallize in contrast to PBAT if kept below room temperature for longer time. Furthermore, the differences were observed in the correlation function development during nonisothermal crystallization. In the case of PBAT a quick stabilization of the correlation function was observed while in the case of PBASGT a step-wise build-up of crystal structure was indicated.

Further crystallization investigation revealed that PBASGT exhibits a strong self-nucleation (SN). Self-nuclei are stable below 160°C. If PBASGT is melted at higher temperature self-nucleation disappear and during subsequent cooling the peak crystallization temperature decreases. Self-nucleation studies evidenced the existence of three self-nucleating domains depending on the self-nucleation temperature. It was observed that the location of self-nucleation domains is different from that described in the literature until now. In the PBASGT case SN Domains II is located entirely at the baseline beyond the melting endotherm.

The activity of self-nuclei was suggestive to find artificial nucleating agents. Green phthalocyanine, blue phthalocyanine (pigments) and talc were found to be effective nucleating agents for PBASGT in absence of self-nuclei, increasing both the peak crystallization temperature and the density of nucleation. According to the results, the green phthalocyanine PG7L acts the best as nucleating agent. The lack of crystals polymorphism connected with nucleating agents introduction was observed. The unintentional effect was to obtain materials, which are green or blue depending from the applied pigment. The comparison of self-nucleated PBASGT and nucleated with best nucleating agent showed that the most effective in increasing the peak crystallization temperature is self-nucleation, although very difficult or even impossible to be exploited during industrial processing.

The average radius of spherulites is few μm in absence of self-nuclei. Spherulites in nucleated PBASGT are much smaller. SAXS analysis and AFM imaging showed that crystals of PBASGT are not aligned in stack of lamellae with characteristic "long period", instead crystals of PBASGT are formed as fibrils radiating from spherulite centers. Crystallization of nucleated PBASGT proceeds during cooling in a very peculiar way: first long fibrils are formed that partially immobilize the rest of material. During further cooling partially immobilized melt crystallized in the form of short fibrils, however, in significantly smaller fraction. Paradoxically the crystallinity degree of nucleated PBASGT is lower than non-nucleated being the strangest outcome of artificial nucleation. At 70°C long fibrils decompose by partial melting and capillary instability freeing the material from constraints. It is expected that other aliphatic-aromatic copolyesters for example such as Ecoflex® (PBAT) may exhibit similar features.

Summarizing, the studies led to reaching the main goals of the thesis:

- to determine the distribution of comonomer units along macromolecular chains of PBASGTs and correlate sequence distribution with their crystallization ability
- to characterize habits of PBASGTs to form crystals such as nucleation of crystallization
- selecting a composition of copolyester, which optimally joins good processability, good mechanical and thermal properties with ability to biodegradability
- to characterize supermolecular structures of PBASGTs

The detailed knowledge about crystallization of the complex aliphatic-aromatic copolyesters containing three aliphatic units and one aromatic was acquired. The influence of chemical composition concerning changes of crystallizable unit content and amount of *co*-units was elucidated. Furthermore, a composition containing 45% of aromatic units was found to optimally integrate the properties and ability to biodegradation. Moreover, efficient nucleating agents for crystallization of PBASGT were found.

Appendix

Biodegradability of PBASGT

A vast fraction of polymer based products are single-use like packaging or used for short term. However, those favorable features of polymeric materials have led to an increasing disposal problem. Contrary to conventional polymers, biodegradable ones can be converted into biomass or into carbon dioxide and water by microorganisms in their environment. Materials that after their final use would undergo in a short time a complete decomposition into harmless decomposition products are searched. A major role with respect to the industrial relevance and biodegradability is played by various polyesters, especially the aliphatic ones. However, there are drawbacks which do not allow them to be used in many applications. To improve their physical properties, the introduction of aromatic units into main chains of aliphatic polyesters has been explored and aliphatic-aromatic copolyesters (AAC) have been developed.The effort was made to obtain materials with varied composition by changing types of aliphatic and aromatic comonomers or even introducing several types of aliphatic comonomers into macromolecules. Most of aliphatic-aromatic copolyesters are biodegradable under rigorous condition of sufficiently short aromatic sequences. It was found that the fraction of aromatic component could be as high as 45-50% for a random sequences of comonomers.

Poly(butylene succinate-*co*-adipate-*co*-glutarate-*co*-terephthalate) (PBASGT) was developed by the Institute of Biopolymers and Chemical Fibers (IBWCh). It would find application in manufacturing of such materials as blown film, monofilaments, flat yarn, sheets and blow-molding. PBASGT may also be used in the production of nonwovens by spun-bonding and melt-blowing. The processing of PBASGT could be performed on standard polyolefin processing equipment with only minor modification. PBASGT with 45% of aromatic component which was chosen for more detailed studies of its solidification is characterized (by ^{1}H NMR) by rather short average sequences of aromatic units nearly 2. Such low average length of aromatic sequences indicated susceptibility to biodegradation. To support this statement a composting trials were performed for PBASGT in the dedicated Laboratory of Biodegradation at the Institute of Biopolymers and Chemical Fibers in Lodz, Poland [167]. The system of the Biodegradation Laboratory is under the auspices of the Polish Accreditation Centre (PCA) - Certificate of accreditation No. AB 388.

Method

The main goal of the studies was to assess the degradation efficiency of PBASGT. The degree of biodegradation of the PBSAGT polymer was estimated by measuring the mass loss. A testing procedure was prepared for this purpose which enables to estimate the degree of biodegradation of plastics in a compost medium on a lab scale conditions simulating an intensive aerobic compost. The procedure is based on the following standards: PN-EN ISO 14 045: 2005 [168], PN-EN ISO 20 200: 2007 [169] and PN-EN ISO 14 806: 2010 [170].

The amount of decayed material was taken as the mass loss used to calculate the decomposition degree. Reactors with the tested material were placed in a thermal chamber at constant temperature of 58±2°C. The compost applied in the biodegradation tests was taken from the Miejski Zaklad Uslug Komunalnych of Lodz Department of Municipal Services in Lodz. The compost used in the testing of biodegradation degree ought to show an adequate microbiological activity of not lower than 10^6cfu·g^{-1} (cfu - colony forming unit). The compost had pH equal to 7 and humidity equal to 42%. Before the test, photos of samples were taken and the weight of samples was recorded. The samples were inserted into a marked polyester net resistant to biodegradation. The biodegradation was performed in 3 repetitions. The reactor in which the incubation was made, was filled withthe compost. The reactors were weighed and placed in the thermal chamber. Humidity of the compost was intermittently measured by weighing the reactors, and water deficiency was eliminated by filling with water to the original weight of the reactors. During the incubation the samples were weighed at the time intervals of 1, 4, 8, 12, 16, 20, 24 weeks from the beginning of the test. After a given time the samples were dried to a constant weight in a vacuum dryer. The test biodegradability is positive if a 100% mass loss occurs in a time shorter than 24 weeks.

Examination of the biodegradation degree of the PBASGT polymer

Biodegradation of the PBASGT polymer was investigated during the incubation in the compost. The mass loss of the PBASGT polymer in the compost is shown in Figure 5.57. After a 24-weeks (that time is fixed in the method) of incubation time, the loss amounted to 98%. The advancing of biodegradation of PBASGT polymer in the compost is also illustrated by the photos in Figure 5.58 demonstrating the composting process.

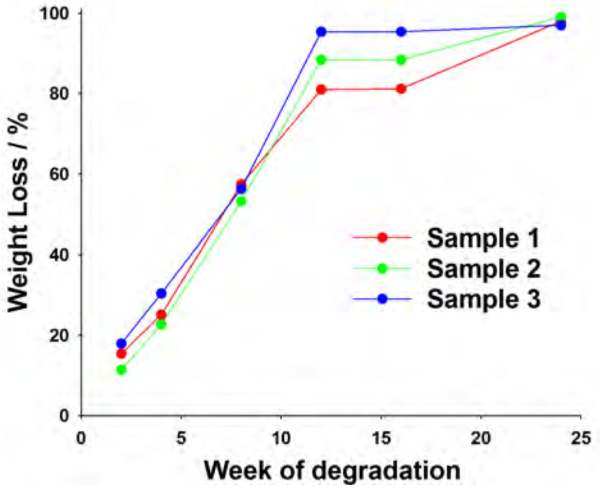

Figure 5.57: Dependence of the weight loss of PBASGT polymer on the biodegradation time in the compost at 58±2°C.

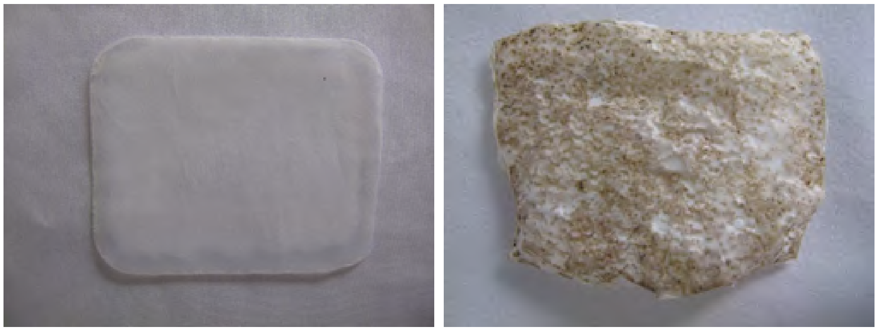

(a) 0 week of biodegradation (b) 2^{nd} week of biodegradation

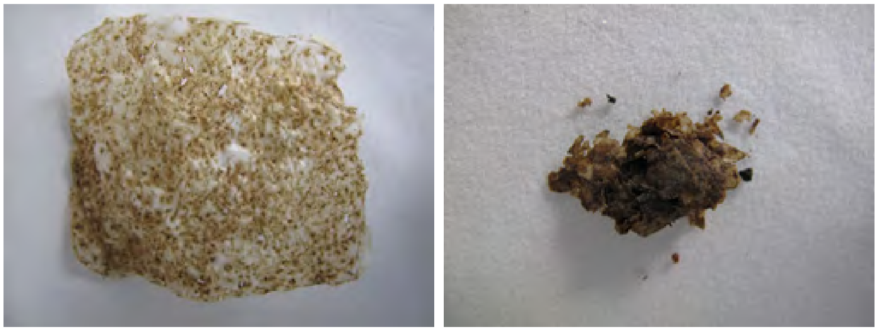

(c) 4^{th} week of biodegradation (d) 8^{th} week of biodegradation

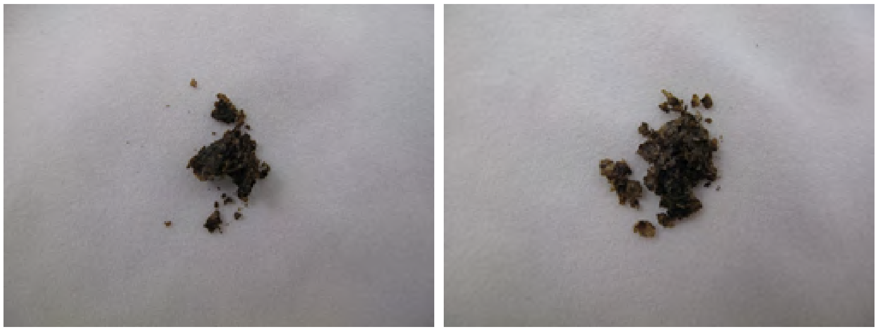

(e) 12^{th} week of biodegradation (f) 16^{th} week of biodegradation

(g) 24^{th} week of biodegradation

Figure 5.58: Photos of illustrating the biodegradation of PBASGT film as the dependence on the residence time in the compost.

INSTITUTE OF BIOPOLYMERS AND CHEMICAL FIBRES

LABORATORY OF ENVIRONMENTAL PROTECTION

The Laboratory works and specializes in three fundamental fields:

- **R& D activities**:
  - research works on new technology and techniques, particularly environmental protection
  - evaluation and improvement of technology used in domestic mills
  - development of new research and analytical methods
- **research services** (measurements and analytical tests) in the field of environmental protection, especially monitoring the emission of pollutants
- **seminar and training activity** concerning methods of instrumental analysis, especially the analysis of water and wastewater, chemicals used in paper production, and environmental protection in the papermaking industry

Since 2004 Laboratory has had the accreditation of the Polish Centre for Accreditation No. AB 551, confirming that the Laboratory meets the requirements of Standard PN-EN ISO/IEC 17025:2005

Investigations in the field of environmental protection technology:

- Research and development of waste water treatment technology, the treatment technology and abatement of gaseous emissions, and the utilization and reuse of solid waste
- Monitoring the technological progress of environmentally friendly technology in paper-making and the best available techniques (BAT)
- Working out and adapting analytical methods for testing the content of pollutants and trace concentrations of toxic compounds in waste water, gaseous emissions, solid waste and products of the paper-making industry

- Monitoring ecological legislation at a domestic and world level, particularly in the European Union.

A list of the analyses most frequently carried out:

- Global water & waste water pollution factors: COD, BOD, TOC, suspended solid (TSS), tot-N, tot-P
- Halogenoorganic compounds (AOX, TOX, TX, EOX, POX)
- Organic sulphur compounds (AOS, TS)
- Resin and chlororesin acids
- Saturated and unsaturated fatty acids
- Phenol and phenolic compounds (guaiacols, catechols, vanillin, veratrols)
- Tetrachlorophenol, Pentachlorophenol (PCP)
- Hexachlorocyclohexane (lindane)
- Aromatic and polyaromatic hydrocarbons
- Benzene, Hexachlorobenzene
- Phthalates
- Carbohydrates
- Glycols
- Polychloro-Biphenyls (PCB)
- Glyoxal
- Tin organic compounds

Contact:

INSTITUTE OF BIOPOLYMERS AND CHEMICAL FIBRES
ul. M. Skłodowskiej-Curie 19/27, 90-570 Łódź, Poland
Małgorzata Michniewicz Ph. D.,
tel. (+48 42) 638 03 31, e-mail: michniewicz@ibwch.lodz.pl

Bibliography

[1] U. Witt, R. J. Müller, W. D. Deckwer, *J. Environ. Polym. Degrad.* **1996**, 4, 9

[2] U. Witt, M. Yamamoto, U. Seeliger, R. J. Müller, V. Warzelhan *Angew. Chem. Int. Ed.* **1999**, 38, 1438

[3] S. Dutkiewicz, J. Wesołowski, D. Chojnacki, D. Ciechańska, *Fibres Text. East. Europe* **2012**, 20, 84

[4] H. J. Kang, S. S. Park, *J. Appl. Polym. Sci.* **1999**, 72, 593

[5] S. S. Park, H. J. Kang, *Polym. J.* **1999**, 31, 238

[6] X. Q. Shi, K. Aimi, H. Ito, S. Ando, T. Kikutani, *Polymer* **2005**, 46, 751

[7] F. Li, X. Xu, Q. Hao, Q. Li, J. Yu, A. Cao, *J. Polym. Sci. Pol. Phys.* **2006**, 44, 1635

[8] J. W. Gooch, Ed., *Encyclopedic Dictonary of Polymers, Springer-Verlag* **2011**, p. 746

[9] M. S. M. Alger, *Polymer Science Dictionary, Elsevier Applied Science, London and New York* **1989**, p. 407

[10] C. Bastioli, Ed., *Aliphatic-Aromatic Polyesters in: Handbook of Biodegradable Polymers, Rapra Technology Limited, Shawbury, Shrewsbury, Shropshire, SY4 4NR, United Kingdom* **2005**, Chapt. 10

[11] B. L. Hurrell, R. E. Cameron, *J. Mater. Sci.* **1998**,33, 1709

[12] R. W. Lenz, R. H. Marchessault, *Biomacromolecules* **2005**, 6, 1

[13] R. J. Pazur, P. J. Hocking, S. Raymond, R. H. Marchessault, *Macromolecules* **1998**, 31, 6585

[14] P. A. Holmes, *Biologically Produced (R)-3-Hydroxyalkanoate Polymers and Copolymers in: Developments in Crystalline Polymers-2*, D. C. Bassett, Ed., *Elsevier Applied Science, London, New York* **1988**, Chapt. 1

[15] I. Chodak, *Polyhydroxyalkanoates: Properties and Modification for High Volume Applications in: Degradable Polymers: Principles and Applications, Springer-Science+Business Media, B.V.*, G. Scott, Ed., *Dordrecht* **2002**, Chapt. 9

[16] N. D. Miller, D. F. Williams, *Biomaterials* **1987**, 8, 129

[17] F. Biddlestone, A. Harris, J. N. Hay, T. Hammond, *Polym. Int.* **1996**, 39, 221

[18] T. V. Ojumu, J. Yu, B. O. Solomon, *Afr. J. Biotechnol.* **2004**, 3, 18

[19] T. Fujimaki, *Polym. Degrad. Stabil.* **1998**, 59, 209

[20] E. Takiyama, T. Fujimaki, S. Seki, T. Hokari, Y. Hatano, inventors, Showa Highpolymer, assigne, US 5,310,782 **1994**

[21] T. Miyata, T. Masuko, *Polymer* **1998**, 39, 1399

[22] Z. Qiu, M. Komura, T. Ikehara, T. Nishi, *Polymer* **2003**, 44, 7781

[23] E. S. Yoo, S. S. Im, *J. Polym. Sci. Pol. Phys.* **1999**, 37, 1357

[24] Z. Gan, H. Abe, H. Kurokawa, Y. Doi, *Biomacromolecules* **2001**, 2, 605

[25] X. Wang, J. Zhou, L. Li, *Eur. Polym. J.* **2007**, 43, 3163

[26] K. J. Ihn, E. S. Yoo, S. S. Im, *Macromolecules* **1995**, 28, 2460

[27] Y. Ichikawa, J. Washiyama, Y. Moteki, K. Noguchi, K. Okuyama, *Polym. J.* **1995**, 27, 1230

[28] Y. Ichikawa, H. Kondo, Y. Igarashi, K. Noguchi, K. Okuyama, J. Washiyama, *Polymer* **2000**, 41, 4719

[29] X. Chen, W. Chen, G. Zhu, F. Huang, J. Zhang, *J. Appl. Polym Sci.* **2007**, 104, 2643

[30] Y. Doi, H. Abe, *Macromol. Symp.* **1997**, 118, 725

[31] M. S. Nikolic, J. Djonlagic, *Polym. Degrad. Stabil.* **2001**, 74, 263

[32] R. Minke, J. Blackwell, *J. Macromol. Sci. Phys.* **1979**, 16, 407

[33] Z. Gan, H. Abe, Y. Doi, *Macromol. Chem. Physic.* **2002**, 203, 2369

[34] Z. Gan, K. Kuwabara, H. Abe, T. Iwata, Y. Doi, *Biomacromolecules* **2004**, 5, 37

[35] W. Kai, B. Zhu, Y. He, Y. Inoue, *J. Polym. Sci. Pol. Phys.* **2005**, 43, 2340

[36] C. M. Buchanan, C. N. Boggs,D. D. Dorschel, R. M. Gardner, R. J. Komarek, I. Thelma, L. Watterson, A. W. White, *J. Environ. Polym. Degr.* **1995**, 3, 1

[37] C. M. Buchanan, S. C. Gedon, A. W. White, M. D. Wood, *Macromolecules* **1993**, 26, 2963

[38] P. Santhana Gopala Krishnan, S. T. Kulkarni *Polyester resins in: Polyesters and polyamides*, B. L. Deopura, R. Alagirusamy, M. Joshi and B. Gupta, Ed. *Woodhead Publishing Limited* **2008**, Chapt. 1

[39] A. Conix, R. Van Kerpel, *J. Polym. Sci.* **1959**, 40, 521

[40] M. C. Righetti, M. L. Di Lorenzo, *J. Polym. Sci. Pol. Phys.* **2004**, 42, 2191

[41] M. Yasuniva, S. Tsubakihara, K. Ohoshita, S. Tokudome, *J. Polym. Sci. Pol. Phys.* **2001**, 39, 2005

[42] H.-J. Radusch, *Poly(Butylene Terephthalate) in: Handbook of Thermoplastic Polyesters Homopolymers, Copolymers, Blends, and Composites*, S. Fakirov, Ed., *Wiley-VCH* **2002**, Chapt. 8

[43] K. H. Illers, *Colloid Polym. Sci.* **1980**, 258, 117

[44] R. S. Stein, A. Misra, *J. Polym. Sci. Pol. Phys.* **1980**, 18, 327

[45] M. Yokouchi, Y. Sakakibara, Y. Chatani, H. Tadokoro, T. Tanaka, K. Yoda, *Macromolecules* **1976**, 9, 266

[46] R. R. Gallucci, B. R. Patel, *Poly(Butylene Terephthalate) in: Modern Polyesters: Chemistry and Technology of Polyesters and Copolyesters, John Wiley & Sons, Ltd*, J. Scheirs, T. E. Long, Ed., *The Atrium, Southern Gate, Chichester, West Sussex, England* **2003**, Chapt. 8

[47] S. Z. D. Cheng, R. Pan, B. Wunderlich, *Macromol. Chem.* **1988**, 189, 2443

[48] K. Kuwabara, Z. Gan, T. Nakamura, H. Abe, Y. Doi, *Biomacromolecules* **2002**, 3, 390

[49] X. Q. Shi, H. Ito, T. Kikutani, *Polymer* **2005**, 46, 11442

[50] N. Honda, I. Taniguchi, M. Miyamoto, Y. Kimura, *Macromol. Biosci.* **2003**, 3, 189

[51] S. H. Lee, S. W. Lim, K. H. Lee, *Polym. Int.* **1999**, 48, 861

[52] S. Luo, F. Li, J. Yu, *J. Polym. Res.* **2011**, 18, 393

[53] L. Mandelkern, *Crystallization of Polymers, United States of America, Cambridge University Press, New York* **2002**

[54] D. Turnbull, J. C. Fisher, *J. Chem. Phys.* **1949**, 17, 71

[55] J. D. Hoffman, G. T. Davis, J. I. Lauritzen, *The Rate of Crystallization of Linear Polymers with Chain Folding in: Treatise on Solid State Chemistry*, N. B. Hannay, Ed., Vol. 3, *Plenum Press, New York, London* **1976**, Chapt. 7

[56] J. D. Ferry, *Viscoelastic Properties of Polymers, J. Willey and Sons, New York* **1970**

[57] J. D. Menczel, L. Judovits, R. B. Prime, H. E. Bair, M. Reading, S. Swier, *Differential Scanning Calorimetry (DSC) in: Thermal analysis of polymers*, J. D. Menczel, R. B. Prime, Ed., *John Wiley & Sons, Inc., Hoboken, New Jersey* **2009**, Chapt. 2

[58] J. R. Burns, D. Turnbull, *J. Appl. Phys.* **1966**, 37, 4021

[59] J. A. Koutsky, A. G. Walton, E. Baer, *J. Appl. Phys.* **1967**, 38, 1832

[60] B. Vonnegut, *J. Colloid Sci.* **1948**, 3, 563

[61] K. N. Okada, M. Hikosaka, *Polymer Nucleation in Handbook of Polymer Crystallization* E. Piorkowska, G. C. Rutledge, Ed., *John Wiley & Sons, Inc, Hoboken, New Jersey, Canada* **2013**, Chapt. 4

[62] A. J. Müller, V. Balsamo, M. L. Arnal, T. Jakob, H. Schmalz, V. Abetz, *Macromolecules* **2002**, 35, 3048

[63] B. Wunderlich, *Macromolecular Physics. Crystal Nucleation, Growth, Annealing,* Vol.2., *Academic Press, New York* **1976**

[64] J. D. Hoffman, R. L. Miller, *Polymer* **1997**, 38, 3151

[65] H. G. Zachman, Z. Kolloid-Z., *Polymer* **1967**, 180, 216

[66] J. D. Hoffman, J. J. Weeks, *J. Chem. Phys.* **1962**, 37, 1723

[67] D. M. Sadler, G. H. Gilmer, *Polymer* **1984**, 25, 1446

[68] D. M. Sadler, *J. Polym. Sci. Pol. Phys.* **1985**, 23, 1533

[69] A. C. Zettlemoyer, *Nucleation, Marcel Dekker, New York* **1969**

[70] F. Pilati, M. Toselli, M. Messori, C. Manzoni, A. E. Turturro, E. G. Gattiglia, *Polymer* **1997**, 38, 4469

[71] A. E. Brink, *Thermoplastic Polyester Composites in: Modern Polyesters: Chemistry and Technology of Polyesters and Copolyesters, John Wiley & Sons, Ltd*, J. Scheirs, T. E. Long, Ed., *The Atrium, Southern Gate, Chichester, West Sussex, England* **2003**, Chapt. 15

[72] L. Royer, *Bull Society for Mineral Crystallography* **1928**, 51, 7

[73] A. Thierry, B. A. Lotz, *Epitaxial Crystallization of Polymers: Means and Issues in Handbook of Polymer Crystallization* E. Piorkowska, G. C. Rutledge, Ed., *John Wiley & Sons, Inc, Hoboken, New Jersey, Canada* **2013**, Chapt. 8

[74] M. Gahleitner, C. Grein, S. Kheirandish, J. Wolfschwenger, *Int. Polym. Proc.* **2011**, 26, 2

[75] F. W. Maine, P. D. Shepherd, *Composites* **1974**, 5, 193

[76] R. Philips, G. Herbert, J. News, M. Wolkowicz, *Polym. Eng. Sci.* **1994**, 34, 1731

[77] D. J. Blundell, A. Keller, A. J. Kovacs, *J. Polym. Sci. Pol. Lett.* **1966**, 4, 481

[78] A. T. Lorenzo, M. L. Arnal, J. J. Sanchez, A. J. Müller, *J. Polym. Sci. Pol. Phys.* **2006**, 44, 1738

[79] J. U. Sommer, G. Reiter, *Polymer Crystallization: Observations, Concepts and Interpretations, Springer-Verlag, Berlin* **2003**

[80] B. Fillon, J. C. Wittman, B. Lotz, A. Thierry, *J. Polym. Sci. Pol. Phys.* **1993**, 31, 1383

[81] V. Balsamo, Y. Paolini, G. Ronca, A. J. Müller, *Macromol. Chem. Physic.* **2000**, 201, 2711

[82] H. Schmalz, A. J. Müller, V. Abetz, *Macromol. Chem. Physic.* **2003**, 204, 111

[83] M. L. Arnal, F. López-Carrasquero, E. Laredo, A. J. Müller, *Eur. Polym. J.* **2004**, 40, 1461

[84] F. Khoury, E. Passaglia *The Morphology of Crystalline Synthetic Polymers in: Treatise on Solid State Chemistry*, N. B. Hannay, Ed., Vol. 3, *Plenum Press, New York, London* **1976**, Chapt. 6

[85] Z. Pelzbauer, A. Galeski, *J. Polym. Sci. Pol. Latt.* **1972**, 38, 23

[86] R. Patki, K. Mezghaniy, P. J. Phillips, *Crystallization Kinetics of Polymers in: Physical Properties of Polymers Handbook*, J. E. Mark, Ed., *Springer Science+Business Media, LLC* **2007**, Chapt. 39

[87] E. J. Clark, J. D. Hoffman, *Macromolecules* **1984**, 17, 878,

[88] J. D. Hoffman, *Polymer* **1983**, 24, 3

[89] S. Z. D. Cheng, J. J. Janimak, A. Zhang, J. Chen, *Macromolecules* **1990**, 23, 298

[90] N. Okui, S. Umemoto, R. Kawano, A. Mamun, *Temperature and Molecular Weight Dependencies of Polymer Crystallization in: Understanding of Polymer Crystallization*, G. Reiter, G. Strobl, *Springer-Verlag, Berlin*, **2007**, p. 407.

[91] J. J. Point, M. Dossier, *Macromolecules* **1989**, 22, 3501

[92] J. J. Point, J. J. Janimak, *J. Cryst. Growth* **1993**, 131, 501

[93] P. J. Barham, *Crystallization and Morphology of Semicrystalline Polymers in: Materials Science and Technology*, Vol. 12, E. L. Thomas, Ed., *VCH Verlagsgesellschaft mbH, Weinheim, New York* **1993**, p. 153

[94] G. Strobl, *The Physics of Polymers, Springer, Berlin, Heidelberg, New York* **1996**, Chapt. 4

[95] J. H. Magill, *J. Appl. Phys.* **1964**, 25, 3249

[96] M. Dosière, *Crystallization of Polymers, Kluwer, The Netherlands* **1993**

[97] G. Strobl, *A Multiphase Model Describing Polymer Crystallization and Melting in: Progress in Understanding of Polymer Crystallization*, G. Reiter, G. Strobl, Eds., *Springer, Berlin* **2007**, Chapt. 23

[98] G. Strobl, *Eur. Phys. J.* **2000**, E3, 165

[99] A. Galeski, Z. Bartczak, T. Kazmierczak, M. Slouf, *Polymer* **2010**, 51, 5780

[100] T. Hugel, G. Strobl, R. Thomann, *Acta Polym.* **1999**, 50, 214

[101] P. D. Olmsted, W. C. K. Poon, T. C. B. McLeish, N. J. Terrill, A. J. Ryan, *Phys. Rev. Lett.* **1998**, 81, 373

[102] K. Kaji, K. Nishida, T. Kanaya, G. Matsuba, T. Konishi, M. Imai, *Adv. Polym. Sci.* **2005**, 191, 187

[103] Z. G. Wang, B. S. Hsiao, E. B. Sirota, S. Srinivas, *Polymer* **2000**, 41, 8825

[104] S. Z. D. Cheng, C. Y. Li, L. Zhu, *Eur. Phys. J.* **2000**, E3, 195

[105] G. Strobl, *Metastable Partially Crystalline States in: The physics of Polymers, Springer-Verlag Berlin Heidelberg* **1996**, Chapt. 4

[106] H. D. Keith, *J. Polym. Sci. Pol. Chem.* **1964**, 2, 4339

[107] C. Booth, C. Price, *Comprehensive Polymer Science, Pergamon Press, Oxford* **1989**

[108] G. Strobl, *The Semicrystalline State in The physics of Polymers, Springer, Berlin, Heidelberg, New York* **2007**, Chapt. 5, p. 167, 212

[109] K. Tashiro, *Growth of Polymer Crystals in Handbook of Polymer Crystallization* E. Piorkowska, G. C. Rutledge, Eds., *John Wiley & Sons, Inc, Hoboken, New Jersey, Canada* **2013**, Chapt. 5, p. 170

[110] R. S. Stein, M. B. Rhodes, *J. Appl. Phys.* **1960**, 31, 1873

[111] Z. Bartczak, A. Gałęski, *Polymer* **1990**, 31, 2027

[112] R. W. Cahn, P. Haasen, E. J. Kramer, *Materials Science and Technology, A comprehensive Treatment, Structure and Properties of Polymers; VCH Verlagsgesellschaft mbH, D-69451 Weinheim Federal Republic of Germany* **1993**, 12

[113] J. D. Roberts, M. C. Caserio, *Polymers in: Basic Principles of Organic Chemistry, W.A. Banjamin, Inc., United States of America, Canada* **1977**, Chapt. 29

[114] M. Gilbert, F. J. Hybart, *Polymer* **1974**, 15, 407

[115] M. J. Richardson, P. J. Flory, J. B. Jackson, *Polymer* **1963**, 4, 21

[116] H. R. R. Garrett, C. A. Hargreaves, I. I. Robinson, D. N. Robinson, *J. Macromol. Sci.* **1970**, A4, 1679

[117] R. G. Alamo, L. Mandelkern, *Thermochim. Acta* **1994**, 238, 155

[118] H. Kubota, J. B. Newell, *J. Appl. Polym. Sci.* **1975**, 19, 1521

[119] M. Gilbert, F. J. Hybart, *Polymer* **1972**, 13, 327

[120] P. J. Flory, *Transactions of the Faraday Society* **1955**, 51, 848

[121] P. J. Flory, L. Mandelkern, H. K. Hall, *J. Am. Chem. Soc.* **1951**, 73, 2532

[122] R. K. Eby, *J. Appl. Phys.* **1963**, 34, 2442

[123] I. C. Sanchez, R. K. Eby, *J. Res. Natl. Bur. Stand.* **1973**, 77, 353

[124] E. Helfand, J. I. Lauritzen *Macromolecules* **1973**, 6, 631

[125] M. Nagata, H. Goto, W. Sakai, N. Tsutsumi, *Polymer* **2000**, 41, 4373

[126] L. Wang, Z. Xie, X. Bi, X. Wang, A. Zhang, Z. Chen, J. Zhoub, Z. Fenga, *Polym. Degrad. Stabil.* **2006**, 91, 2220

[127] G. R. Strobl, M. Schneider, *J. Polym. Sci. Pol. Phys.* **1980**, 18, 1343

[128] B. Goderis, H. Reynaers, M. H. J. Koch, V. B. F. Mathot, *J. Polym. Sci. Pol. Phys.* **1999**, 37, 1715

[129] N. Stribeck, U. Nochel, S. S. Funari, T. Schubert, *J. Polym. Sci. Pol. Phys.* **2008**, 46, 721

[130] R. Yamadera, N. Murano, *Polym. Sci.* **1967**, 5, 2259

[131] U. Witt, R. J. Müller, W. D. Decker, *Macromol. Chem. Physic.* **1996**, 197, 1525

[132] U. Witt, R. J. Müller, W. D. Decker, *J. Environ. Polym. Degrad.* **1997**, 5, 81

[133] S. Kimata, T. Sakurai, Y. Nozue, T. Kasahara, N. Yamaguchi, T. Karino, M. Shibayama, J. A. Kornfield, *Science* **2007**, 316, 1014

[134] L. Fernandez-Ballester, D. W. Thurman, W. Zhou, J. A. Kornfield, *Macromolecules* **2012**, 45, 6557

[135] T. L. Bluhm, G. K. Hamer, R. H. Marchessault, C. A. Fyfe, R. P. Veregin, *Macromolecules* **1986**, 19, 2871

[136] B. Wunderlich, *in: Macromolecular Physics*, Vol. 1, *Academic Press, New York* **1973**, Chapt. 2-4

[137] M. Atfani, F. Brisse, *Macromolecules* **1999**, 32, 7741

[138] D. W. Van Krevelen, *Properties of polymers 4th ed., Elsevier* **2009**

[139] U. Alter, R. Bonart, *Colloid Polym. Sci.* **1976**, 254, 348

[140] F. Li, X. Xu, Q. Li, Y. Li, H. Zhang, J. Yu, A. Cao, *Polym. Degrad. Stabil.* **2006**, 91, 1685

[141] L. Mandelkern, R. G. Alamo, *Thermodynamic quantities governing melting in Physical properties of polymers handbook*, J. E. Mark, Ed., *Springer, New York* **2007**, p. 165

[142] X. H. Du, Ch. Sh. Zhao, Y. Z. Wang, Q. Zhou, Y. Deng, M. H. Qu, B. Yang, *Mater. Chem. Phys.* **2006**, 98, 172

[143] J. Karger-Kocsis, O. I. Benevolenski, E. J. Moskala, *J. Mater. Sci.* **2001**, 36, 3365

[144] A. Pawlak, A. Rozanski, A. Galeski, *Mech. Mater.* **2013**, 67, 104

[145] A. Toda, *Polymer* **1994**, 35, 3638

[146] T. Pakula, E. W. Fischer, *J. Polym. Sci. Pol. Phys* **1981**, 19, 1705

[147] Y. K. Godovsky, *Thermodynamic behavior of solid polymer in plastic deformation and cold drawing in: Thermophysical properties of polymers, Springer-Verlag, Berlin* **1992**, Chapt. 7

[148] S. H. Lee, K. Nakayama, H. H. Cho, *Fibers Polym.* **2008**, 9, 740

[149] K. Song, J. L. White, *Polym. Eng. Sci.* **1998**, 38, 505

[150] H. Li, J. L. White, *Polym. Eng. Sci.* **2000**, 40, 2299

[151] V. Warzelhan, BASF-Thermoplastic Research and Development, private communication, **2014**

[152] F. A. Bovey, G. V. D. Tiers, *J. Polym. Sci.* **1960**, 44, 173

[153] B. S. Hsiao, Z. Wang, F. Yeh, Y. Gao, K. C. Sheth, *Polymer* **1999**, 40, 3515

[154] Z. Gan, K. Kuwabara, M. Yamamoto, H. Abe, Y. Doi, *Polym. Degrad. Stabil.* **2004**, 83, 289

[155] P. R. Howard, B. J. Crist, *J. Polym. Sci. Pol. Phys.* **1989**, 27, 2269

[156] A. M. E. Baker, A. H. Windle, *Polymer* **2001**, 42, 651

[157] C. W. Bunn, *The Structure of Polyethylene in Polyethene*, 2^{nd} Ed., A. Renfrew, P. Morgan, Eds., *Interscience: New York* **1960**, Chapt. 5

[158] G. T. Davis, J. J. Weeks, G. M. Martin, R. K. Eby *J. Appl. Phys.* **1974**, 45, 4175

[159] S. Li, R. A. Register, *Crystallization in Copolymers in Handbook of Polymer Crystallization* E. Piorkowska, G. C. Rutledge, Eds., *John Wiley & Sons, Inc, Hoboken, New Jersey, Canada* **2013**, Chapt. 11

[160] W. O. Statton, *ASTM: International Symposium on Plastics Testing and Standarization* **1959**, 242

[161] J. Runt, D. M. Miley, X. Zhang, K. P. Gallagher, K. McFeaters, J. Fishburn, *Macromolecules* **1992**, 25, 1929

[162] I. Pillin, S. Pimbert, J. F. Feller, G. Levesque, *Polym. Eng. Sci.* **2001**, 21, 178

[163] A. Espinoza-Martinez, C. Avila-Orta, V. Cruz-Delgado, O. Olvera-Neria, J. González-Torres, F. Medellín-Rodríguez *Hindawi Publishing Corporation J. of Nanomaterials* **2012**, DOI: 10.1155/2012/189820

[164] W. Banks, M. Gordon, A. Sharples, *Polymer* **1963**, 4, 289

[165] A. Sharples, *Introduction to Polymer Crystallization, London* **1966**, p. 65-75

[166] J. H. Rayner, G. Brown, *Clays Clay Miner.* **1973**, 21, 103

[167] M. Lichocik, M. Owczarek, P. Miros, K. Guzińska, A. Gutowska, D. Ciechańska, I. Krucińska, P. Siwek, *Fibres Text. East. Eur.* **2012**, 20, 179

[168] PN-EN 14045: 2005: Packaging - Evaluation of the disintegration of packaging materials in practical oriented testes under defined composting conditions

[169] PN-EN 20200: 2007: Plastics - Determination of the degree of disintegration of plastics materials under simulated composting conditions in a laboratory -scale test

[170] PN-EN 14806: 2010: Packaging - Preliminary evaluation of the disintegration of packaging materials under simulated composting.

List of publications and patents connected with PhD thesis

Publications

- M. Wojtczak, S. Dutkiewicz, L. Pietrzak, A. Galeski, E. Piorkowska, *Nucleation and crystallization of random aliphatic-aromatic copolyester*, Polymer, In press
- M. Wojtczak, A. Galeski, S. Dutkiewicz, E. Piorkowska, *The influence of chemical composition of aliphatic-aromatic copolyesters on their properties*, *AIP Conference Proceedings* **2014**, 1599, 214
- M. Wojtczak, S. Dutkiewicz, A. Galeski, E. Piorkowska, *Structure and characterization of random aliphatic-aromatic copolyester*, *Eur. Polym. J.* **2014**, 55, 86
- M. Wojtczak, A. Galeski, S. Dutkiewicz, E. Piorkowska, *Krystalizacja kopoliestru alifatyczno-aromatycznego in: Modyfikacja polimerow stan i perspektywy w roku 2013*, R. Stellera, D. Żuchowskiej, Ed., *ISBN 978-83-86520-19-0, Wroclaw* **2013**, p. 495

Planed publications

- M. Wojtczak, S. Dutkiewicz, A. Galeski, E. Piorkowska, *The influence of chemical composition on aliphatic-aromatic copolyesters' crystallization*

Patents

- Polish patent application No. P 406 548. Date of application 16 December 2013, *Biodegradable copolyester composition and its manufacturing method*, K. Grzebieniak, S. Dutkiewicz, M. Szkopiecka, J. Wesolowski, A. Galeski, A. Pawlak, M. Wojtczak
- Polish patent application No. P 404 127. Date of application 29 May 2013, *Accelerated polycondensation polyesters' manufacturing method*, S. Dutkiewicz, Z. Mlodzikowski, J. Wesolowski, M. Wojtczak, A. Galeski, E. Piorkowska-Galeska

List of lectures and posters connected with PhD thesis

Invited lectures

- **2012 Fall Meeting European Materials Research Society, 17-21 September 2012**
  Properties of Polyhydroxybutyrate and its blends with copolyesters
  M. Wojtczak, A. Galeski, M. Pracella

- **Polymers for Advanced Technologies, 2-5 October 2011**
  Crystallization characteristics of random aromatic-aliphatic copolyesters
  M. Wojtczak, A. Galeski, S. Dutkiewicz, E. Piorkowska

Lectures

- **BIOMASA, Biodegradowalne Polimery, Kompozyty i Materialy Wlokniste, 13-14 November 2014, Lodz, Poland**
  Badania procesow przetwarzania PLA, IBPE oraz mieszanin PLA-IBPE
  A. Galeski, E. Piorkowska, M. Kowalczyk, M. Wojtczak, S. Dutkiewicz, A. Pawlak, K. Jurczuk, J. Morawiec, M. Pluta, P. Sowinski

- **6th International Conference on Polymer Behavior, 22-26 September 2014, Vienna, Austria**
  Aliphatic-aromatic copolyesters of various chemical composition
  M. Wojtczak, A. Galeski, S. Dutkiewicz, E. Piorkowska

- **7th International Conference Times of Polymers & Composites, 22-26 June 2014, Ischia, Italy**
  The influence of chemical composition of aliphatic-aromatic copolyesters on their properties
  M. Wojtczak, A. Galeski, S. Dutkiewicz, E. Piorkowska

- **22nd International Conference on Polymer Characterization, 7-11 April 2014, Stellenbosch, South Africa**
  The influence of chemical composition and nucleation on aliphatic-aromatic copolyesters' crystallization
  M. Wojtczak, A. Galeski, S. Dutkiewicz, E. Piorkowska

- **IXth International Conference on X-ray Investigations of Polymer Structure, 3-6 December 2013, Zakopane, Poland**
  The influence of chemical composition and nucleation on aliphatic-aromatic copolyesters' crystallization
  M. Wojtczak, A. Galeski, S. Dutkiewicz, E. Piorkowska

- **Modyfikacja Polimerow, 18-20 September 2013, Kudowa Zdroj, Poland**
  Krystalizacja kopoliestru alifatyczno-aromatycznego
  M. Wojtczak, A. Galeski, S. Dutkiewicz, E. Piorkowska

- **56th Zjazd Naukowy Polskiego Towarzystwa Chemicznego i Stowarzyszenia Inzynierow i Technikow Przemyslu Chemicznego, 16-20 September 2013, Siedlce, Poland**
  Biodegradowalne kopoliestry alifatyczno-aromatyczne. Synteza, wlasciwosci i zastosowania.
  S. Dutkiewicz, E. Piorkowska-Galeska, A. Galeski, M. Wojtczak, K. Twardowska-Schmidt, D. Chojnacki, K. Sulak, J. Wesolowski

- **5th International Conference on Polymer Behavior, 15-18 October 2012, Aveiro, Portugal**
  Crystallization of random aromatic-aliphatic copolyesters
  M. Wojtczak, A. Galeski, S. Dutkiewicz, E. Piorkowska

- **2ndWorkshop on Polymer Crystallization Under Conditions relevant to processing, 21-22 June 2012, Genua, Italy**
  Crystallization characteristics of biodegradable random aromatic-aliphatic copolyesters
  M. Wojtczak, A. Galeski, S. Dutkiewicz, E. Piorkowska

- **11th European Symposium on Polymer Blends, 25-28 March 2012, Donastia-San Sebastian, Spain**
  Crystallization of random aromatic-aliphatic copolyesters and their blends with polylactide
  M. Wojtczak, M. Kowalczyk, S. Dutkiewicz, E. Piorkowska, A. Galeski

Posters

- **3rd Workshop on Recent Advances and New Perspectives in Polymer Crystallization, 29-30 September 2014, Genova, Italy**
  The influence of chemical composition and nucleation on aliphatic-aromatic copolyesters' crystallization
  M. Wojtczak, A. Galeski, S. Dutkiewicz, E. Piorkowska

- **6th International Conference on Polymer Behavior, 22-26 September 2014, Vienna, Austria**
  Degradation of polyethylenes containing oxo-accelerating additives
  M. Wojtczak, A. Galeski, A. Krzan

- **11th European Symposium on Polymer Blends, 25-28 March 2012, Donastia-San Sebastian, Spain**
  Crystallization of random aromatic-aliphatic copolyesters
  M. Wojtczak, L. Pietrzak, S. Dutkiewicz, E. Piorkowska, A. Galeski

List of Figures

List of Tables